



**SRSF1-mediated gene  
therapy as a therapeutic  
approach for *C9ORF72*-  
related amyotrophic lateral  
sclerosis and fronto-temporal  
dementia (ALS-FTD).**

Submitted for the degree of Doctor of Philosophy (PhD)

December 2021

**Charlotte E. Mason, MSc 170147211**

Supervisors:

Dr Guillaume Hautbergue, Prof Dame Pamela Shaw & Prof Mimoun Azzouz

Department of Neuroscience  
Sheffield Institute for Translational Neuroscience,  
University of Sheffield

This PhD thesis is dedicated to my parents, Tracey and Peter Mason

Thank you for your constant support and for the sacrifices you have made throughout your  
lifetimes to allow me to succeed

## Acknowledgements

Firstly, I would like to thank my supervisors, Dr Guillaume Hautbergue, Professor Dame Pamela Shaw and Professor Mimoun Azzouz for all your advice, support and encouragement throughout my PhD. I am extremely grateful to Dr Hautbergue for giving me the opportunity to complete a PhD.

I would also like to express thanks to all past and present Azzouz and Hautbergue lab members for your various contributions to my PhD over the last 4 years. I could not have completed this PhD without your advice, expertise and input.

Thank you so much to Paul Barnes who has had unwavering confidence that I would complete this thesis. I cannot thank you enough for giving me the tools for success over the last 4 years and for having faith in my abilities even when I did not.

To my friends and colleagues at SITraN I cannot thank you enough for providing support in every imaginable way. You have laughed, cried, despaired, pranked, drank, picnic(ed), pandemic(ed) with me throughout these extraordinary few years, and I cannot imagine going through the trauma with anybody else. I would especially like to thank Emily, Amy, Lily, Ale, Toby, Matt, Mirinda, Joao, Michela and Joe. Thank you too, to all the research staff, technical staff and students in SITraN for your insight, hard work and friendship.

A big thank you to Amy Keerie who was always willing to try and save the world with me alongside our PhD's. We were always trying to "be the change we want to see" and I hope we made a difference in the time we were PhD students.

A huge thank you to Suzie, for taking me on adventures and reminding me that life is for living even in the greatest depths of my PhD (and Pandemic). And for always listening to my PhD woes, even if you didn't have a clue what I was talking about.

A final thank you to my family – for keeping me grounded and sane, without your encouragement and madness this PhD would not have been possible. Kathryn thank you for reading my thesis probably more than I have, I trust no one more with grammar and spelling. Unfortunately, we have lost people over the last few years, both in body and in mind, and I thank you all for your lifetime of support, until your very last breaths. I know this would have made you proud.

## Abstract

Amyotrophic lateral sclerosis (ALS) and frontotemporal dementia (FTD) form a spectrum of fatal adult onset diseases respectively characterised by progressive loss of upper/lower motor neurons and neurons in the frontal/temporal lobes of the brain. The most common genetic cause of these conditions involves polymorphic hexanucleotide repeat expansions in the first intron of the *C9ORF72* gene. Our groups have previously shown that Serine/Arginine-Rich Splicing Factor 1 (SRSF1) drives the nuclear export of pathological *C9ORF72* repeat transcripts, leading to the cytoplasmic production of toxic dipeptide repeat proteins (DPRs). Moreover, the partial depletion of SRSF1 or expression of an engineered SRSF1-m4 mutant (that binds *C9ORF72* repeat transcripts but has lost the ability to interact with the nuclear export machinery) efficiently inhibits the nuclear export of *C9ORF72* repeat transcripts and confer neuroprotection in *C9ORF72*-ALS/FTD cell models and *Drosophila*.

The objectives of this PhD were to evaluate the therapeutic safety and efficacy of the above neuroprotective strategies using two gene therapy approaches involving self-complementary adeno-associated virus (scAAV9) mediated depletion of SRSF1 or expression of SRSF1-m4 in wild type and *C9ORF72*-ALS/FTD mice. shRNAs directed against SRSF1 and SRSF1-m4 were cloned into scAAV9 plasmids to generate SRSF1-RNAi and SRSF1-m4 vectors respectively. SRSF1 depletion, SRSF1-m4 expression and DPR expression levels were analysed by western immunoblotting in transfected and transduced human HEK cell models of *C9ORF72*-ALS/FTD. Viral vectors were further administered to wild type mice via cisterna magna injection at post-natal day 1, and the mice were monitored to evaluate the safety of these interventions and the functionality of the virus at behavioural and molecular levels. The viruses were further administered to a *C9ORF72*-ALS/FTD mouse model to assess target engagement and the therapeutic potential of these approaches on DPR production in a disease model. We have found that scAAV9 viruses mediating SRSF1 depletion and SRSF1-m4 expression have been successfully produced. Moreover, both the viral plasmids and the viruses are functional *in vitro* leading to efficient inhibition of DPR production. Six-month old mice injected with the viruses do not exhibit visible side effects following the partial depletion of SRSF1 or the expression of SRSF1-m4. The findings also indicate that these two therapeutic strategies may significantly reduce DPR production 3 months post-administration.

## Table of Contents

Acknowledgements	iii
Abstract	iv
Abbreviations	x
List of Figures	xiv
List of Tables	xvii
CHAPTER 1: Introduction	1
1.1 Background	1
1.2 Amyotrophic Lateral Sclerosis (ALS)	1
1.3 Frontotemporal Dementia (FTD)	2
1.4 Genetic causes of ALS	3
1.4.1 <i>SOD1</i> -related ALS	4
1.4.2 TARDBP and FUS-related ALS	7
1.4.3 <i>C9ORF72</i> -linked ALS	9
1.4.4 SRSF1-dependent nuclear export of pathological <i>C9ORF72</i> repeat transcripts	15
1.4.5 <i>C9ORF72</i> -ALS/FTD mouse models	18
1.5 Current pharmacological treatments for ALS	21
1.5.1 Riluzole	21
1.5.2 Edaravone	21
1.5.3 Masitinib	22
1.6 Potential future treatments using gene therapy approaches	23
1.7 Gene therapy - viral vectors	24
1.7.1 Gene Therapy Vectors: Lentiviruses	24
1.7.2 Adenoviruses	26
1.7.3 Gene Therapy Vectors: Adeno – Associated Viruses	27
1.8 Non-viral gene therapy delivery systems	31
1.8.1 ASOs	31
1.9 Gene therapies currently at clinical trial stage	32
1.10 Current gene therapy developments for ALS	39

1.11 Current gene therapy developments for the specific treatment of C9ORF72 ALS/FTD	41
1.12 Introduction to the PhD	43
<b>CHAPTER 02: Materials and Methods</b>	<b>46</b>
2.1 Strains	46
2.2 Plasmids	46
2.2.1 Cloning	46
2.2.2 Gel Extraction	46
2.2.3 Annealing Oligonucleotides	47
2.2.4 Vector Preparation	48
2.2.5 Ligation	48
2.2.6 Sequencing	48
2.2.7 Transformation	48
2.2.8 Rough Mini-Preps	49
2.2.9 Spin-Preps	49
2.2.10 Midi-Preps	50
2.2.11 Mega-Preps	50
2.3 Western blot analysis	51
2.3.1 Transfection of plasmids into HEK Cells	51
2.3.2 Transfection of plasmids into N2A Cells	52
2.3.3 Protein Extraction from a 24-well plate	52
2.3.4 SDS-PAGE	52
2.3.5 Transferring and Imaging the Western Blots	53
2.3.6 Antibodies	54
2.4 Preparation of scAAV9 virus – small scale	55
2.4.1 Transfection of HEK cells for small AAV9 preparation	55
2.4.2 Harvesting AAV9 from transfected cells	55
2.4.3 Testing Viral Capsid Integrity	55
2.4.4 Transduction Assay	56
2.5 Large scale AAV preparation	56
2.5.1 Transfection	56
2.5.2 Harvesting and concentrating	57

2.5.3 AAV purification by iodixanol density gradient	57
2.5.4 Fraction analysis by SDS-PAGE	59
2.5.5 SYPRO RUBY Staining	60
<b>2.6 Titration of AAV virus</b>	<b>62</b>
<b>2.7 Titration of AAV via FACS (Fluorescence-activated cell sorting)</b>	<b>64</b>
<b>2.8 Animal work</b>	<b>65</b>
2.8.1 Ethics statement	65
2.8.1 Postnatal day 1 cisterna magna injections	65
2.8.2 Post-natal day 40 cisterna magna injections	65
2.8.3 Rotarod analysis	66
2.8.4 Weight analysis	66
2.8.5 Tissue collection	67
<b>2.9 Tissue preparation and histological analysis</b>	<b>67</b>
2.9.1 Tissue sectioning and staining	67
2.9.2 DNA Extraction	69
2.9.3 RNA Extraction	70
2.9.4 Protein Extraction	71
2.9.5 Poly-GP MSD ELISA Assay	71
<b>2.10 Statistical analysis</b>	<b>72</b>
 <b>CHAPTER 3 – Designing and Developing Viral Vectors for SRSF1-Targeted Gene Therapy</b>	
<b>Approaches in Mice</b>	<b>74</b>
<b>3.1 Aim</b>	<b>74</b>
<b>3.2 Therapeutic approach 1: Depletion of SRSF1</b>	<b>74</b>
3.2.1 Design of shRNAs for SRSF1 knockdown	75
3.2.2 Cloning of shRNA into scAAV9_KASPAR_Efs1 $\alpha$ _GFP	81
3.2.3 Effects on SRSF1-depletion on the production of DPRs in human HEK cell models of C9ORF72 ALS/FTD	84
3.2.4 Effects on SRSF1-depletion on the production of DPRs in mouse N2A cell models of C9ORF72 ALS/FTD	87
<b>3.3 Therapeutic approach 2: Expression of the point mutant protein SRSF1-m4</b>	<b>90</b>

3.3.1 Design of scAAV_AZ_CBh_SRSF1-m4	91
3.3.2 Cloning of the control scAAV_AZ_CBh_GFP plasmid	92
3.3.3 Cloning of SRSF1-m4 into scAAV_AZ_CBh	95
3.3.4 Effects of the SRSF1-m4 dominant mutant on the expression of DPRs in human HEK293 cell models of ALS/FTD	99
3.4 Summary of therapeutic plasmid production for <i>in vivo study</i>	101
3.5 Discussion	104
<b>CHAPTER 4 – Production of Functional Large-Scale SRSF1-Targeting Gene Therapy Viruses for Subsequent Investigation in Mouse Studies</b>	<b>108</b>
4.1 Aims	108
4.2 Viral vector choice and therapeutic construct	109
4.3 Overview of scAAV assembly	111
4.4 Small scAAV preparation of therapeutic constructs	112
4.5 Large scAAV9 preparation of therapeutic vectors	114
4.6 Determination of viral genome titres via qPCR	118
4.7 Determination of viral titres via FACS method	119
4.8 <i>In vitro</i> testing of the gene therapeutic vectors	126
4.9 Discussion	128
<b>CHAPTER 5 - Therapeutic Manipulation of SRSF1 in Mice: Pilot Safety and Efficacy Proof-of-principle</b>	<b>136</b>
5.1 Aims	136
5.2 Route of administration	137
5.3 <i>In vivo</i> proof-of-principle of functionality and safety of the therapeutic constructs in wild type C57Bl/6 mice	139
5.3.1 Biodistribution of the therapeutic constructs	139
5.3.2 Western Blot analysis of protein expression in C57Bl/6J mice 4-weeks and 6-months post injection	146
5.3.3 Body weight analysis in wild type C57Bl/6J mice 4-weeks post injection vs mice 6-months post injection	154
5.3.4 Overall Condition and Survival in C57Bl/6J mice	157
5.3.5 Rotarod Analysis in C57Bl/6J mice	158

<b>5.4 Histological analysis of the gene therapy interventions</b>	<b>160</b>
5.4.1 The effect of the therapeutic viruses on motor neuron cell count	160
5.4.2 The effect of the therapeutic viruses on SRSF1 expression in the spinal cord	165
<b>5.5 <i>In vivo</i> testing of the therapeutic scAAV9 viral vectors in a C9ORF72 ALS/FTD mouse model</b>	<b>168</b>
<b>5.6 Discussion</b>	<b>175</b>
<b>CHAPTER 6 – General Conclusions and Discussion</b>	<b>190</b>
<b>REFERENCES</b>	<b>198</b>
<b>APPENDIX - Cloning Strategies</b>	<b>229</b>
1. Cloning Strategy of scAAV AZ AmpR / CBh prom - GFP	229
2. Cloning of scAAV AZ AmpR / CBh prom - 3x FLAG SRSF1 11-196 m4	231

## Abbreviations

AAV	Adeno-Associated Virus
Ad	Adenovirus
AD	Alzheimer's disease
ADA-SCID	Adenosine Deaminase - Severe Combined Immunodeficiency
ALS	Amyotrophic Lateral Sclerosis
ALSoD	ALS online database
ANOVA	Analysis of variance
APS	Ammonium Persulfate
ASO	Antisense Oligonucleotides
ARRIVE	Animal Research: Reporting of <i>In vivo</i> Experiments
ATMP	Advanced Therapy Medicinal Products
ATP	Adenosine Triphosphate
AUC	Area Under the Curve
AZ	Azzouz
BAC	Bacterial Artificial Chromosomes
Bcl-2	B-cell Lymphoma 2
C9-500	500 C9ORF72 Repeat Transcripts
C9ORF72	Chromosome 9 Open Reading Frame 72
CBA	Chicken-beta-actin promoter
CBH	Chicken-beta-hybrid promoter
cDNA	Complementary DNA
CD8 <sup>+</sup> T Cells	Cluster of Differentiation 8 Thymus cells
CIP	Alkaline Phosphatase, Calf Intestinal
CMV	Cytomegalovirus
CNS	Central Nervous System
DAPI	4', 6-diamidino-2-phenylindole
DEPC	Diethyl Pyrocarbonate
DHT	Dihydrotestosterone
DMEM	Dulbecco's modified Eagle's medium
DNA	Deoxyribonucleic Acid
dNTPs	Deoxynucleotide Triphosphates
DPRs	Dipeptide-repeat Proteins
DPX	Distyrene Plasticizer Xylene
DTT	Dithiothreitol
EAAT2	Excitatory Amino Acid Transporter 2
ECL	Enhanced Chemiluminescence

<b>EDTA</b>	<b>Ethylenediamine Tetra acetic Acid</b>
<b>EtOH</b>	<b>Ethanol</b>
<b>FACS</b>	<b>Fluorescence-Activated Cell Sorting</b>
<b>fALS</b>	<b>Familial Amyotrophic Lateral Sclerosis</b>
<b>FDA</b>	<b>U.S. Food and Drug Administration</b>
<b>FIX</b>	<b>Human Clotting Factor IX</b>
<b>FLAG</b>	<b>Peptide Sequence DYKDDDDK</b>
<b>FTD</b>	<b>Frontotemporal Dementia</b>
<b>FUS</b>	<b>Fused in Sarcoma RNA-binding Protein</b>
<b>FVB</b>	<b>Friend Virus B-Type</b>
<b>G4C2</b>	<b>Sense GGGGCC expansion repeat</b>
<b>G2C4</b>	<b>Anti-sense CCGGGG expansion repeat</b>
<b>GFP</b>	<b>Green fluorescent protein</b>
<b>H1</b>	<b>Histone Protein 1</b>
<b>HAART</b>	<b>Highly Active Antiretroviral Therapy</b>
<b>HEK293T</b>	<b>Human Embryonic Kidney 293T Cells</b>
<b>HEPES</b>	<b>4-(2-hydroxyethyl)-1-piperazineethanesulfonic acid</b>
<b>HIV</b>	<b>Human Immunodeficiency Virus</b>
<b>HPLC</b>	<b>High-Performance Liquid Chromatography</b>
<b>hnRNP</b>	<b>Heterogeneous Nuclear Ribonucleoproteins</b>
<b>HuR</b>	<b>Hu Antigen R</b>
<b>HGF</b>	<b>Human Growth Factor</b>
<b>IgG</b>	<b>Immunoglobulin G</b>
<b>IMS</b>	<b>Industrial Methylated Spirit</b>
<b>ITRs</b>	<b>Inverted Terminal Repeats</b>
<b>IV</b>	<b>Intravenous</b>
<b>LB medium</b>	<b>Lysogeny Broth Medium</b>
<b>LV</b>	<b>Lentivirus</b>
<b>MCT1</b>	<b>Monocarboxylate transporter 1</b>
<b>MHC</b>	<b>Major Histocompatibility Complex</b>
<b>miRNA</b>	<b>MicroRNA</b>
<b>MND</b>	<b>Motor Neurone Disease</b>
<b>MOI</b>	<b>Multiplicity of infection</b>
<b>mRNA</b>	<b>messenger RNA</b>
<b>MSD</b>	<b>Meso Scale Discovery</b>
<b>N2A</b>	<b>Neuro2a cells</b>
<b>NaAC</b>	<b>Sodium Acetate</b>
<b>NaCl</b>	<b>Sodium Chloride</b>
<b>NAbs</b>	<b>Neutralising Antibody</b>

<b>NADPH</b>	<b>Nicotinamide Adenine Dinucleotide Phosphate</b>
<b>ns</b>	<b>Non-significant</b>
<b>NXF1</b>	<b>Nuclear RNA Export Factor 1</b>
<b>OPN</b>	<b>Optineurin</b>
<b>ORFs</b>	<b>Open Reading Frames</b>
<b>P1</b>	<b>Post-natal Day 1</b>
<b>P40</b>	<b>Post-natal Day 40</b>
<b>PBS</b>	<b>Phosphate buffered saline</b>
<b>PCI</b>	<b>phenol/chloroform/isoamyl alcohol</b>
<b>PCR</b>	<b>Polymerase Chain Reaction</b>
<b>PEI</b>	<b>Polyethylenimine</b>
<b>PFA</b>	<b>Paraformaldehyde</b>
<b>PIC</b>	<b>Protease Inhibitor Cocktail</b>
<b>PNK</b>	<b>Polynucleotide Kinase</b>
<b>POTS</b>	<b>Potential off-targeting score</b>
<b>PRRs</b>	<b>Pattern Recognition Receptors</b>
<b>qPCR</b>	<b>Quantitative polymerase chain reaction</b>
<b>rAAV</b>	<b>Recombinant Adeno-associated Virus</b>
<b>RAN Translation</b>	<b>Repeat-associated non-AUG (RAN) translation</b>
<b>RCA</b>	<b>Ras-Related C3 Botulinum Toxin Substrate 1</b>
<b>RNA</b>	<b>Ribonucleic Acid</b>
<b>RNAi</b>	<b>RNA interference</b>
<b>RRM1/2</b>	<b>RNA Recognition Motif 1 and 2</b>
<b>ROS</b>	<b>Reactive Oxygen Species</b>
<b>RPM</b>	<b>Revolutions Per Minute</b>
<b>RTU</b>	<b>Rapid Urease Test</b>
<b>scAAV</b>	<b>Self-complementary adeno-associated virus</b>
<b>siRNAs</b>	<b>Small interfering RNAs</b>
<b>siSPOTR</b>	<b>siRNA sequence probability of off-targeting reduction</b>
<b>SMA</b>	<b>Spinal muscular atrophy</b>
<b>SMN</b>	<b>Survival Motor Neuron Protein</b>
<b>SMN1</b>	<b>Survival of Motor Neuron 1</b>
<b>SOD1</b>	<b>Superoxide Dismutase 1</b>
<b>mSOD1</b>	<b>Mutant Superoxide Dismutase 1</b>
<b>SR-rich Proteins</b>	<b>Serine/Arginine-Rich Proteins</b>
<b>SRSF1</b>	<b>Serine/Arginine-Rich Splicing Factor 1</b>
<b>ssAAV</b>	<b>Single-stranded adeno-associated virus</b>
<b>SQSTM1</b>	<b>Sequestosome 1</b>
<b>SV40</b>	<b>Simian vacuolating virus 40</b>

<b>TAE</b>	<b>Tris-acetate-EDTA</b>
<b>TARDBP</b>	<b>TAR DNA-binding protein</b>
<b>TBS-T</b>	<b>Tris-Buffered Saline + 0.2% Tween 20</b>
<b>TEMED</b>	<b>N, N, N, N'-tetramethylethane-1,2-diamine</b>
<b>TDP-43</b>	<b>Transactive Response (TAR) DNA-binding protein of 43</b>
<b>tRNA</b>	<b>transfer RNA</b>
<b>UBQLN2</b>	<b>Ubiquitin 2</b>
<b>UTR</b>	<b>Untranslated region</b>
<b>VCP</b>	<b>Valosin Containing Protein</b>
<b>VEGF</b>	<b>Vascular Endothelial Growth Factor</b>
<b>VSV-G</b>	<b>Vesicular Stomatitis Virus</b>
<b>WT</b>	<b>Wildtype</b>
<b>X-SCID</b>	<b>X-linked severe combined immunodeficiency</b>

## List of Figures

<b>Description</b>	<b>Page no.</b>
Figure 1.1 Disease Mechanisms of ALS	6
Figure 1.2 Pathological nuclear export of C9ORF72 repeat transcripts	17
Figure 1.3 The two therapeutic strategies for the treatment of C9ORF72-ALS/FTD	45
Figure 2.1 Thermofisher DNA copy number calculator	63
Figure 3.1 SRSF1 alignment: Human vs Mouse	79
Figure 3.2 Cloning of shRNA into scAAV_KASPAR_EFs1 $\alpha$ _GFP results	82
Figure 3.3 Western blot image of shRNAs 9 and 10 co-transfected into HEK cells along with V5-tagged DPRs	83
Figure 3.4 Depicts a 24 well plate used to test the SRSF1 shRNA plasmids <i>in vitro</i>	85
Figure 3.5 Effects on SRSF1-depletion on the production of DPRs in human HEK cell models of C9ORF72 ALS/FTD	86
Figure 3.6 Effects on SRSF1-depletion on the production of DPRs in mouse N2A cell models of C9ORF72 ALS/FTD	89
Figure 3.7 Cloning of the control scAAV_AZ_CBh_GFP plasmid	94
Figure 3.8 Cloning of pAAV_AZ_CBh_SRSF1 m4	96
Figure 3.9 Cloning of scAAV_AZ_CBh_SRSF1-m4	98
Figure 3.10 Effects of the SRSF1-m4 dominant mutant on the expression of DPRs in human HEK293 cell models of ALS/FTD	100
Figure 3.11 scAAV9_SRSF1-RNAi (scAAV_KASPER_H1_shRNA 10_eGFP) Plasmid Map	101
Figure 3.12 scAAV9_GFP (scAAV_CBh_GFP) Plasmid Map	102
Figure 3.13 scAAV9_SRSF1-m4 (scAAV_CBh_SRSF1 m4) Plasmid Map	103
Figure 4.1 Overview of scAAV assembly and production	111
Figure 4.2 Western image depicting the expression of the capsid proteins, V1, V2 and V3 of the newly packaged viral vectors	113
Figure 4.3 Sypro Ruby staining of the scAAV9_SRSF1-m4 viral prep	115
Figure 4.4 Sypro Ruby staining of the scAAV9_GFP viral prep	116
Figure 4.5 Sypro Ruby staining of the scAAV9_SRSF1-RNAi viral prep	117

<b>Description</b>	<b>Page no.</b>
Figure 4.6 FACS Analysis of scAAV9_SRSF1 RNAi and scAAV9_GFP after transfection into HEK 293T cells – FACS analysis of untransfected and control GFP virus	<b>121</b>
Figure 4.7 FACS Analysis of scAAV9_SRSF1 RNAi and scAAV9_GFP after transfection into HEK 293T cells – FACS analysis of scAAV9_SRSF1-RNAi	<b>122</b>
Figure 4.8 FACS Analysis of scAAV9_SRSF1 RNAi and scAAV9_GFP after transfection into HEK 293T cells – FACS analysis of scAAV9_GFP	<b>123</b>
Figure 4.9 Western blot analysis of viral transduction in HEK293T cells	<b>127</b>
Figure 5.1 Biodistribution analysis of mice injected with PBS vs scAAV9_SRSF1-RNAi vs scAAV9_GFP	<b>143</b>
Figure 5.2 Biodistribution analysis of mice injected with PBS vs scAAV9_SRSF1-m4	<b>145</b>
Figure 5.3 Western blot analysis of mouse tissue	<b>149</b>
Figure 5.4 Cisterna magna delivery of scAAV9_SRSF1-RNAi and scAAV9_SRSF1-m4 at post-natal day 1 (P1) results in no significant difference in weight gain	<b>156</b>
Figure 5.5 Cisterna magna delivery of scAAV9_SRSF1-RNAi and scAAV9_SRSF1-m4 at post-natal day 1 (P1) results in no significant difference in rotarod performance	<b>159</b>
Figure 5.6 Counting motor neurons in nissl stained cervical spinal cord sections	<b>161</b>
Figure 5.7 Nissl stained cervical spinal cord sections 4-weeks post cisterna magna injection	<b>162</b>
Figure 5.8 Nissl stained cervical spinal cord sections 6-months post cisterna injection	<b>163</b>
Figure 5.9 Cisterna magna delivery of scAAV9 SRSF1-RNAi and scAAV9 SRSF1-m4 at post-natal day 1 (P1) results in no significant difference in average motor neurons per ventral horn at both 4-weeks and 6-months	<b>164</b>
Figure 5.10 SRSF1 DAB stained cervical spinal cord sections 4-weeks post cisterna magna injection	<b>166</b>

<b>Description</b>	<b>Page no.</b>
Figure 5. 11 SRSF1 DAB stained cervical spinal cord sections 6-months post cisterna magna injection	<b>167</b>
Figure 5. 12 MDS assay to assess the effect of scAAV9_SRSF1-RNAi on the expression of poly-GP DPRs in various tissue types	<b>170</b>
Figure 5. 13 MDS Assay to assess the effect of scAAV9_SRSF1-RNAi or scAAV9_SRSF1-m4 on toxic DPR levels in the brain cortex	<b>171</b>
Figure 5. 14 MDS Assay (normalised to a standard curve) to assess the effect of SRSF1 depletion or the expression of SRSF1-m4 on toxic DPR levels in the brain cortex	<b>172</b>

## List of Tables

<b>Description</b>	<b>Page no.</b>
Table 1.1 Summary of Transduction and optimal AAV serotypes in specific cell types	31
Table 1.2 Phase II/III ongoing gene therapy viral vector clinical trials	35
Table 2.1 Antibodies used during Western Blot analysis	54
Table 2.2 Viral transfection ratios and amounts	56
Table 2.3 Preparation of the Iodixanol Solutions	58
Table 2.4 qPCR plate design for the titration of scAAV	62
Table 3.1 Human SRSF1 shRNA (NM_006924.4)	75
Table 3.2 Mouse SRSF1 shRNA (NM_173374.4)	76
Table 3.3 shRNA targeting both human and mouse SRSF1 using Block-IT designer	77
Table 3.4 siSPOTR analysis of the most efficient shRNAs against Human and Mouse SRSF1 (Antisense)	78
Table 4.1 Viral Titres	118
Table 4.2 FACS results	124
Table 4.3 Summary of overall FACS calculations and concentrations (TU/ml)	125

## CHAPTER 1: Introduction

### 1.1 Background

Motor neuron disease (MND) describes a range of motor neuron disorders of which amyotrophic lateral sclerosis (ALS) is the most common. ALS is a life-limiting progressive neurodegenerative disease and the condition is interchangeably identified as Lou Gehrig's disease or Charcot's disease (Hardiman *et al.*, 2011; Kiernan *et al.*, 2011; Hardiman *et al.*, 2017). A French doctor, Jean-Martin Charcot, first described ALS in 1869. Since then, the understanding of the disease has greatly increased through genetic and molecular discoveries (Masrori and Van Damme, 2020).

### 1.2 Amyotrophic Lateral Sclerosis (ALS)

ALS is characterized by the selective deterioration and loss of both upper and lower motor neurons. This progressive neurodegeneration causes motor neurons to stop producing action potentials, resulting in progressive weakness and paralysis of voluntary muscles. As the muscle strength decreases, atrophy and muscle fasciculations occur, and the brain's ability to initiate and control voluntary muscle movement becomes progressively impaired. The disease has three recognised patterns of onset: limb (most common), bulbar, and respiratory onset. Patients with loss of motor neurons innervating the upper limbs often report an increase in dropping objects or difficulty manipulating objects with one hand; for instance, unlocking a door with a key or issues with handwriting. When motor neurons innervating the lower limbs are affected, symptoms can include foot drop, a sensation where there is heaviness in one foot/ leg with a tendency to trip. The symptoms have a gradual onset and are usually painless, with the first initial symptom experienced being muscle weakness, wasting or fasciculation. Other early symptoms can include abnormal fatigue of the arms and/or legs, slurred speech, dropping items and muscle twitches/cramps (McDermott and Shaw, 2008). The motor neurons which control the tongue, throat and respiratory muscles may also become affected, resulting in speech, swallowing and breathing difficulties. When the denervation eventually reaches the muscles in the diaphragm, the resulting respiratory failure is usually the main cause of death (Ji *et al.*, 2017). The respiratory muscles can be affected first, but this is the least common pattern of onset. Early symptoms of

neuromuscular respiratory failure include overnight hypoventilation, frequent waking, unrefreshing sleep and early morning headaches. Bulbar onset motor neurone disease also occurs in approximately 25-30% of patients, with the first sign being slurred speech, caused by weakness and/or spasticity of the tongue. This particular onset is also associated with emotional lability (McDermott and Shaw, 2008). The disease usually begins in adulthood (typically mid-later life) and rapidly advances, with death usually occurring within 2-5 years of symptom onset (Hardiman *et al.*, 2017).

### 1.3 Frontotemporal Dementia (FTD)

Some patients diagnosed with ALS also present with frontotemporal dementia (FTD). FTD is a common type of dementia, especially in patients <65 years old (Bang, Spina and Miller, 2015). Disease onset usually occurs between the ages of 50 and 60 years old and the hallmark features of FTD are the progressive but gradual decline in behaviour and language. FTD is most often characterised by the progressive degeneration of the temporal and frontal cortex (Rohrer *et al.*, 2015; Ji *et al.*, 2017). As the disease progresses, it becomes difficult for sufferers to behave appropriately in both social and work-related settings, to plan and organise activities, and eventually to even care for themselves (Hardiman, van den Berg and Kiernan, 2011).

There are three clinical variants of FTD: behavioural-variant frontotemporal dementia, semantic-variant primary progressive aphasia, and non-fluent variant primary progressive aphasia. Behavioural-variant frontotemporal dementia is associated with early behavioural and executive deficits. Semantic-variant primary progressive aphasia begins with the progressive disorder of semantic knowledge and naming, whilst non-fluent variant primary progressive aphasia involves progressive deficits in word output, speech and grammar. However, as FTD progresses over time, the three clinical variants often converge, as the initial focal degeneration spreads to affect larger regions of the frontal and temporal lobes. As time progresses further, FTD patients develop more global cognitive impairments and motor deficits and, in some patients, features of motor neuron disease. Patients in the final stages of FTD have difficulty swallowing, eating and moving, with death occurring approximately 8 years after symptom onset. Typically, the cause of death is pneumonia or other secondary infections (Bang, Spina and Miller, 2015).

Amyotrophic lateral sclerosis (ALS) and frontotemporal dementia (FTD) share many clinical and pathological features and are both known to be adult-onset progressive neurodegenerative diseases. The two conditions were once thought to be separate entities; however, a continuous FTD/ALS spectrum has been proposed following the identification of the *C9ORF72* gene (chromosome 9 open reading frame 72) (Gros-Louis, Gaspar and Rouleau, 2006; Majounie, Renton, *et al.*, 2012). A mutant form of the *C9ORF72* gene accounts for between 30% and 50% of all familial ALS cases (Renton *et al.*, 2011a; DeJesus-Hernandez *et al.*, 2011). It is also suggested that this mutation is involved in 25% of familial FTD and a small fraction of sporadic ALS-FTD (~5-7% each) (Majounie, Renton, *et al.*, 2012; van der Zee *et al.*, 2013). Up to 15% of ALS patients also have a diagnosis of FTD and around 50% of all ALS patients show some evidence of neuropsychological dysfunction if detailed evaluation is undertaken (Ringholz *et al.*, 2005).

#### 1.4 Genetic causes of ALS

There are over 25 genes that play a role in ALS. However, approximately 90% of cases are sporadic, while 10% of cases are inherited familial ALS (fALS) (Siddique and Ajroud-Driss, 2011). So far, it has been reported that most ALS mutations are inherited in an autosomal-dominant manner. The four most common autosomal-dominant mutations that cause inherited ALS are: SOD1 - involved in 20% of cases (Gaudette *et al.*, 2000), TARDBP (which encodes the protein TDP-43) - involved in 4% of cases (Sreedharan *et al.*, 2008), FUS - involved in 4% of familial ALS (Kwiatkowski *et al.*, 2009; Vance *et al.*, 2009) and *C9ORF72*, which is the most common known genetic cause as it is involved in 40% of inherited ALS cases (DeJesus-Hernandez *et al.*, 2011). These four mutations are also found in 5.1% (*C9ORF72*), 1.2% (SOD1), 0.8% (TARDBP) and 0.3% (FUS) of sporadic ALS cases in the European population according to Zou *et al.*, 2017.

---

### 1.4.1 *SOD1*-related ALS

---

*SOD1* and its implication in ALS has been widely studied, and researchers identified dominant mutations of *SOD1* over 25 years ago. It was the first genetic link to ALS (Rosen *et al.*, 1993). *SOD1* encodes the ubiquitously expressed cytoplasmic enzyme Cu-Zn superoxide dismutase, a free radical scavenging enzyme. Normal functioning *SOD1* catalyses the conversion of highly reactive superoxide radicals into oxygen and hydrogen peroxide. Superoxide free radicals are largely produced as a result of mitochondrial activity (Figure 1.1) *SOD1* is an antioxidant enzyme, and when mutated it acquires a toxic gain of function that contributes to ALS pathology in multiple ways (Bunton-Stasyshyn *et al.*, 2015).

So far, over 185 missense *SOD1* mutations have been reported (ALSoD, 2018). These are distributed across the whole length of the human *SOD1* protein of 154 amino acids. Research by Gurney in 1994 and by Wong in 1995 suggested that in mice, degeneration of motor neurons results from one or more toxicities of mutant *SOD1* (Gurney *et al.*, 1994; Wong *et al.*, 1995). It is suggested that a proportion of mutant *SOD1* protein fails to fold sufficiently, which could imply that the accumulation of this misfolded mutant *SOD1* (m*SOD1*) possibly contributes to ALS toxicity (Bruijn *et al.*, 1997). This misfolding can form the ubiquitinated cytoplasmic inclusions seen early on in ALS disease progression. Protein aggregation is seen in *SOD1* mutations with *SOD1* aggregates and *TARDBP* mutations with TDP-43 aggregates. Proteinopathy is also seen in patients with sporadic ALS: TDP-43 aggregates are present, highlighting an overall correlation between ALS and protein aggregation (Parone *et al.*, 2013). Mutant *SOD1* produces aggregates with HuR (stabilizes VEGF mRNA) reducing the amount of HuR available to stabilise VEGF mRNA, allowing the mRNA to decompose and resulting in decreased translation. This minimises angiogenesis and leads to poor neural vascularization and motor neuron cell death (Lu *et al.*, 2009; Storkebaum *et al.*, 2011)

Currently, the main therapeutic option in promising clinical trials is to knock down *SOD1* using antisense oligonucleotides (Miller *et al.*, 2013; Miller *et al.*, 2020). So far, we know that the misfolding of m*SOD1* is toxic to the cell, so by preventing this misfolding, cell toxicity and motor neuron death can be minimised. In a mouse model with mice carrying the *SOD1*-G93A mutation, an RNAi-mediated decrease in the level of both wild-type *SOD1* and mutant *SOD1* protein was observed. A lentiviral delivery system of shRNA targeting, in this case human *SOD1*, was shown to delay disease progression and extend survival in these mice

(Ralph *et al.*, 2005; Raoul *et al.*, 2005). Both models suggest that survival can be prolonged in an ALS model expressing mutant SOD1 when SOD1 is knocked down. The manipulation of these SOD1-related pathways could aid the discovery of new therapeutic strategies and prolong life in SOD1-related human disease (Iannitti *et al.*, 2018).

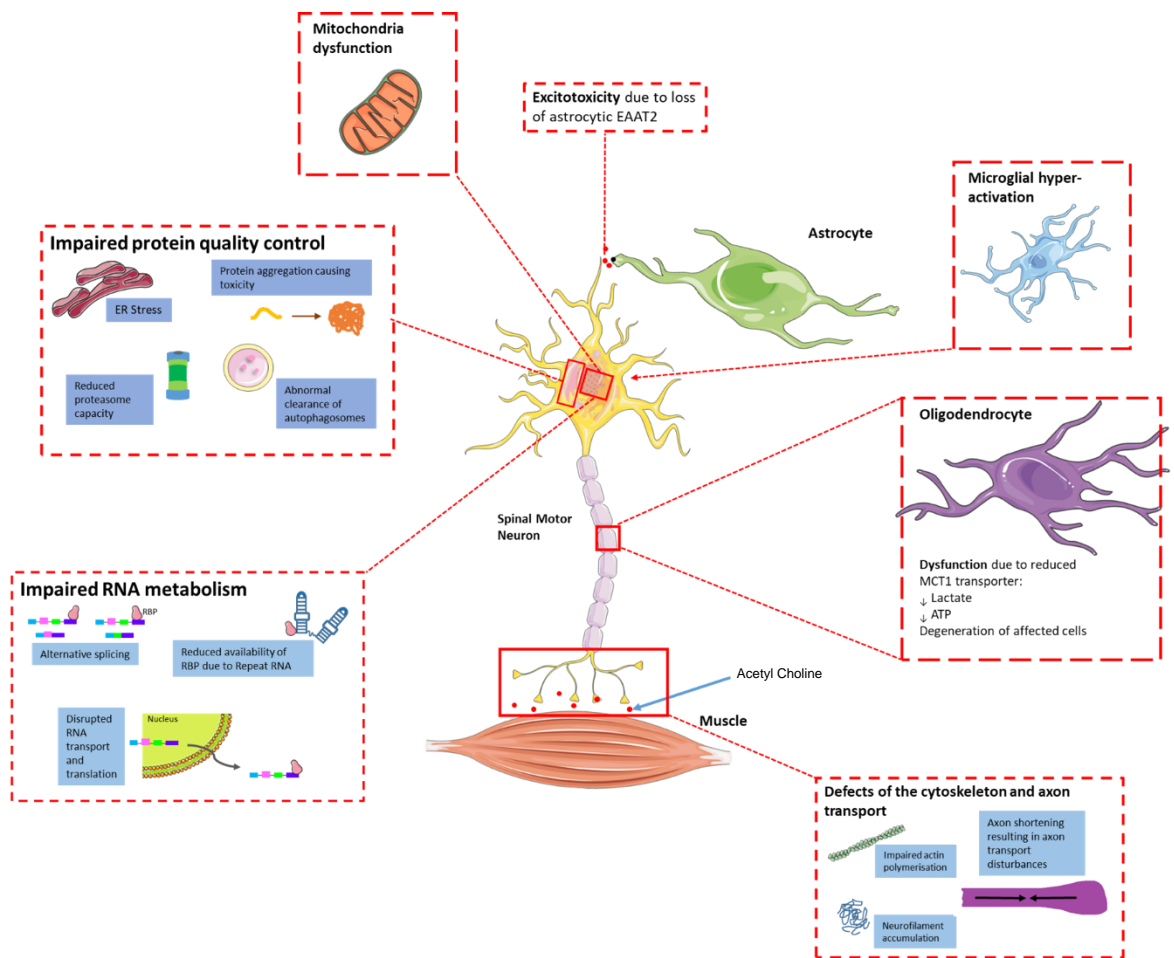


**Figure 1. 1 Disease Mechanisms of ALS** – The loss of the EAAT2 results in inefficient glutamate clearance by astrocytes, triggering the repetitive firing of motor neurons which results in excitotoxicity; Microglial hyper-activation involves the production of extracellular free radicals and inflammatory cytokines, resulting in inflammation and degeneration in motor neurons; Reduced MCT1 levels lessen energy levels supplied by the oligodendrocytes to the motor neurons; Defects of the cytoskeleton and disruption of axonal transport prevent the successful exchange of essential macromolecules and organelles between the neuronal cell body and the axon, which results in axonal retraction and the cell death of the neuron; Disturbances of RNA metabolism, such as RNA processing, utilization and transport, occur, which may result from impaired hnRNP function; familial ALS-associated mutations often affect genes that encode cellular components of the protein quality control system. Other mutations, including those in SOD1, affect protein folding; mitochondrial dysfunction due to interference with respiratory chain function within the mitochondria increases ROS and decreases ATP production, both eventually leading to apoptosis. Diagram adapted from Taylor *et al*, 2016.

---

## 1.4.2 TARDBP and FUS-related ALS

---

The accumulation of protein aggregate inclusions is a neuropathological hallmark of ALS, and TDP43-positive cytoplasmic inclusions and nuclear depletion of TDP-43 can be identified in >95% of all ALS sufferers (A. C. Ludolph and J. Brettschneider, 2015). Transactive Response DNA-binding Protein 43 (the gene that encodes the TDP-43 protein) mutations were linked to ALS in 2008 (Sreedharan *et al.*, 2008). Previously, it was recognized that TDP-43 cytoplasmic and nuclear inclusions were characteristic of both FTD and ALS. In FTD, the inclusions are found in the neocortex and dentate granule cells of the hippocampus (Neumann *et al.*, 2006; Davidson *et al.*, 2007). In ALS, there is cytoplasmic accumulation of TDP-43 in neurons and glia of the primary motor cortex, brainstem motor nuclei, and spinal cord motor neurons and glial cells (Bodansky *et al.*, 2010; Mackenzie, Rademakers and Neumann, 2010).

TDP-43 (TAR DNA-binding protein of 43) is ubiquitously expressed and is an initial target for ubiquitination. It is encoded by the gene *TARDBP* and is the main component of inclusions in the majority of ALS cases (Neumann *et al.*, 2006). Aggregated proteins (inclusions) accumulate in the cytoplasm (see Figure 1. 1). These are formed by compact or threadlike collections of proteins which are ubiquitinated. It is uncertain whether these cytoplasmic inclusions are toxic to the cell, which may result from sequestration of essential cellular proteins, or whether they may be beneficial by acting as a repository for misfolded and potentially toxic protein species (Vanden Broeck *et al.*, 2015; Ederle and Dormann, 2017).

Mutations in the *TARDBP* gene cause ALS in 1-2% of total cases, but 38 nonsynonymous missense mutations found in the glycine-rich C terminus of the encoded TDP-43 protein have been implicated in both familial and sporadic ALS. These mutations are dominantly inherited, which result in an autosomal-dominant form of ALS with the presence of TDP-43 positive inclusions. These TDP-43-positive aggregates have been suggested to be “aggresomes” that are later removed by autophagy. Aggregation of TDP-43 in the cytoplasm and its subsequent nuclear clearance in neurons has been suggested to cause a loss-of-function of this important protein in the nucleus, leading to neuronal injury. The aggregates are thought to spread from cell to cell in a prion-like manner (Nonaka *et al.*, 2013). Impairment of protein degradation pathways due to mutations in other ALS disease-related genes, such as *SQSTM1*, *VCP*, *UBQLN2*, and *OPTN*, may lead to high concentrations of TDP-43, TDP-43 aggregation, and TDP-43-positive inclusion formation. This would

explain why patients without TDP-43 mutations also show aggregation of TDP-43 in the cytoplasm. Thus, genetic mutations that alter protein homeostasis and induce stress in neurons may cause TDP-43 aggregation. Neuronal injury has been suggested to result in TDP-43 aggregation due to abnormal stress granule dynamics (Walker *et al.*, 2013; Liu-Yesucevitz *et al.*, 2014). Defects in RNA processing, which is a major function of TDP-43, have also been suggested as major drivers of neuronal injury, similar to observations of mutations in other RNA-binding proteins (RBPs) such as FUS (Vanden Broeck, Callaerts and Dermaut, 2014; Scotter, Chen and Shaw, 2015; Srinivasan and Rajasekaran, 2020).

Both *TARDBP* and *FUS* encode DNA/RNA-binding proteins involved in various aspects of gene expression regulation. This includes: biogenesis of miRNA (Ling *et al.*, 2010; Kawahara and Mieda-Sato, 2012; Morlando *et al.*, 2012), transcriptional control (Mackenzie and Rademakers, 2008; Honda *et al.*, 2014), alternative splicing of mRNA (Nakaya *et al.*, 2013), and in stressed conditions associated with stalled ribosomes and stress granules, as well as defects in the axonal transport of mRNA (Yoshimura *et al.*, 2006; Alami *et al.*, 2014; Chou *et al.*, 2018). Several thousand TDP-43 and FUS RNA-binding sites have been characterized on pre-mRNA molecules, including those that involved long pre-mRNA splicing functions, which are required for neuronal integrity and development. In TDP-43 and FUS -related ALS, alternative splicing of pre-mRNAs has been found to be extensively altered. This leads to the overall dysregulation of normal gene expression in neurons due to thousands of aberrantly spliced mRNAs (Lagier-Tourenne *et al.*, 2012; Rogelj *et al.*, 2012; Walsh *et al.*, 2015).

TDP-43 and FUS are both constituents of the hnRNP family of proteins (see Figure 1. 1) which shuttle between the nucleus and the cytoplasm of cells. Their composition involves two RNA Recognition Motifs (RRM) domains followed by carboxyl-terminal arginine/glycine regions (the prion domain,) which tend to aggregate due to lack of structure in the low complexity regions flanking the RRM domains. FUS specifically exhibits an RG-rich region within its amino terminus. It is in these RG-rich regions that the majority of ALS mutations are located, usually in exon 3-6 or 12-15. TDP-43 also has these regions, and ALS mutations cluster in exon 6. The precise consequences of the mutations have not yet been established, but they have been shown to alter interaction with Heterogeneous Nuclear Ribonucleoproteins (hnRNPs) A1, A2/B1, C1/C2 and A3, causing widespread alteration of splicing (Buratti *et al.*, 2005).

Transcriptome studies have indicated that pre-mRNA splicing alterations affect neurotrophic factor synthesis, synaptic function and RNA metabolism (Prudencio *et al.*, 2015; D'Erchia *et al.*, 2017; Castelli *et al.*, 2021). In TDP-43 transgenic mouse models (with specific alterations resulting from the Q331K ALS mutation), around one-third of the transcriptome is altered (Arnold *et al.*, 2013).

Two mechanisms were proposed to explain FUS-related neurodegeneration. The first mechanism suggests toxic gain-of-function, in which nuclear FUS aggregates in the cytoplasm spread in a prion-like manner throughout neuronal tissues (Armstrong, 2017). The second mechanism suggests that the depletion of FUS from the nucleus may result in impaired transcription, DNA repair and alternative splicing (Shang and Huang, 2016). There are reasonable amounts of evidence to support both mechanisms, and it would be reasonable to suggest that both loss of function and gain of function mechanisms may contribute to motor neuron injury in the presence of FUS mutations (Ishigaki and Sobue, 2018; An *et al.*, 2019). In mice, overexpression of FUS causes an ALS phenotype, resulting in the progressive degeneration and death of motor neurons occurring in an age- and dose-dependent manner (Mitchell *et al.*, 2013).

ALS-related mutations in these proteins can cause cytoplasmic mislocalisation and the formation of stress granules due to the alteration of transportin-mediated nuclear localisation import (Lagier-Tourenne and Cleveland, 2009; Lattante, Rouleau and Kabashi, 2013). It is still unclear whether motor neuron injury and loss is caused by a lack of normal nuclear function of TDP-43 and FUS and/or by toxic gain of functions through cytoplasmic mislocalisation of aggregates or soluble forms; however, it seems plausible that both of these mechanisms may be operating.

---

### 1.4.3 C9ORF72-linked ALS

---

The most common genetic cause of ALS/FTD is a hexanucleotide repeat expansion located in the first intron of the *C9ORF72* gene (Renton *et al.*, 2011; DeJesus-Hernandez *et al.*, 2011). The *C9ORF72* gene encodes the C9ORF72 protein that is abundantly found across neurons throughout the CNS. Globally, the expression of the C9ORF72 protein is mainly in the brain, spinal cord, the immune system, and at lower levels in other internal organs (lung, heart, liver, kidney, and skeletal muscle), which reflects the expression profile of the transcript. The 481-aa C9-long isoform is considered the most abundant (Frick *et al.*, 2018). In mouse tissues and the human brain, the C9ORF72 protein is cytoplasmic, along with punctate staining in

neurites suggesting that the protein resides in the neuron's presynaptic terminal, an area essential for sending and receiving signals between neurons (Atkinson *et al.*, 2015; Xiao *et al.*, 2015; Ferguson, Serafeimidou-Pouliou and Subramanian, 2016; Frick *et al.*, 2018; Laflamme *et al.*, 2019). Isoform-specific antibodies were developed by Xiao *et al.*, 2015 that showed that the C9ORF72 long isoform is present in the cytoplasm with some speckle-like structures in neurites, as previously reported. Meanwhile, the C9OF72 short isoform appeared to be localized at the nuclear membrane in post-mortem human brain tissue. C9ORF72 has 12 exons (10 of which are coding) and is regulated by two promoters (DeJesus-Hernandez *et al.*, 2011).

Nucleotide repeat expansions are short DNA sequences that are repeated many times in a row. C9ORF72-related ALS/FTD is caused by polymorphic repeat expansions (also called microsatellite repeat expansions), in this case the hexanucleotide GGGGCC (G4C2). These G4C2 repeat expansions are found in intron 1 of the C9ORF72 gene in mRNA. Around 50% of non-pathogenic alleles of C9ORF72 have only two G4C2 repeats, whilst the other 50% have between 2 and 25 G4C2 repeats. In pathogenic alleles seen in ALS patients, the number of repeats tends to vary between tens and thousands, and a repeat size of more than 30 is regarded as pathogenic (Renton *et al.*, 2011; DeJesus-Hernandez *et al.*, 2011). More than 95% of neurologically healthy individuals have less than 11 hexanucleotide repeats in their C9ORF72 gene (Rutherford *et al.*, 2012; M. B. Harms *et al.*, 2013; Van Mossevelde *et al.*, 2017). Despite the fact that the expanded repeats are found within the non-coding region of C9ORF72, the repetitive RNAs are translated in every reading frame to form 5 different dipeptide repeat proteins (DPRs) - poly-GA, poly-GP, poly-GR, poly-PA and poly-PR — via repeat-associated non-ATG (RAN) translation (Ash *et al.*, 2013; Gendron *et al.*, 2013; K. Mori *et al.*, 2013; Zu *et al.*, 2013).

The GGGGCC hexanucleotide repeat expansion in the C9ORF72 gene has been proven to be a major genetic factor in ALS and FTD patients, as it accounts for 40% of familial ALS (FALS), 30% of familial FTD, and 8% of sporadic ALS (SALS) cases in predominantly Caucasian populations (Majounie, Renton, *et al.*, 2012). The identification of C9ORF72 mutation in ALS/FTD led to the overall hypothesis that the mutation could play a role in other neurodegenerative disorders (Beck *et al.*, 2013). Given the clinical and pathological overlap between FTD and Alzheimer's disease, several studies were conducted to elucidate any possible association between the C9orf72 hexanucleotide expansion and the susceptibility to Alzheimer's disease (Majounie, Abramzon, *et al.*, 2012; M. Harms *et al.*, 2013). Majounie *et al.*, 2012 screened 342 families with members affected by late-onset alzheimers

disease for *C9ORF72* hexanucleotide repeat expansions. The hexanucleotide expansion was seen in 6 of 771 subjects (<1%) who had probable Alzheimer's disease, and the team concluded that the subjects had FTD which had been misdiagnosed. If this is the case, misdiagnosis of Alzheimer's disease is a likely to be a reasonable possibility across Alzheimer patient cohorts, and therefore testing for the *C9ORF72* genetic mutation may prevent the misclassification of FTD as Alzheimer's disease in future patients (Majounie, Abramzon, *et al.*, 2012). Harms *et al.*, 2013 found that *C9ORF72* repeat expansions do explain a small proportion of patients who display a clinical presentation indistinguishable from Alzheimer's disease. Overall, the study highlights the necessity of screening FTD genes in clinical Alzheimer cases with a strong family history of dementia (Harms *et al.*, 2013).

These repeat expansions are able to form stable parallel G-quadruplexes that avidly interact with RNA-processing factors (Fratta *et al.*, 2012; Reddy *et al.*, 2013; Haeusler *et al.*, 2014). A pathological hallmark of *C9ORF72*-related ALS is the presence of both sense (DeJesus-Hernandez *et al.*, 2011; Lee *et al.*, 2013) and antisense intra-neuronal RNA foci (Haeusler *et al.*, 2014). RNA foci are expanded RNA repeats that are largely retained in the nucleus, but may also be found in the cytoplasm, and fold into unusual secondary structures sequestering various RNA binding proteins; these may produce toxic loss and gain of function mechanisms.

The *C9ORF72* protein does not share homology with RNA-binding proteins and is not thought to play a direct role in the metabolism of mRNA. Three competing, but not exclusive, mechanisms for the neurotoxicity of the *C9ORF72* repeat expansions have been proposed: haploinsufficiency, toxic gain of function from sense and antisense *C9ORF72* repeat foci, and toxic gain/loss of function from DPRs. Each of these mechanisms is likely to contribute to disease progression, but the relative importance of each mechanism at various stages needs to be addressed to help develop therapeutic strategies.

## Haploinsufficiency

The pathological repeat expansions are found in intron 1 of the *C9ORF72* gene and are therefore not encoded into the protein. Introns are removed via splicing or alternative splicing, meaning that the protein encoded from the wild type allele or the spliced mutated allele is wild type. The large repeat expansions and their secondary structures are however hypothesised to alter transcription, thus leading to reduced expression levels of *C9ORF72* mRNA (by approximately a third) and potentially of the protein leading to haploinsufficiency. This mechanism has not yet been formally demonstrated in post-mortem human tissues and has only been identified in some *C9ORF72*-ALS/FTD cell and animal models (Renton *et al.*, 2011; DeJesus-Hernandez *et al.*, 2011; Ciura *et al.*, 2013; Zu *et al.*, 2013; Liu *et al.*, 2014; O'Rourke *et al.*, 2016). Haploinsufficiency appears to be variable and dependent on patient cell lines and samples, as other studies have not reported a reduction in the spliced *C9ORF72* mRNA (Tran *et al.*, 2015; Hautbergue, 2017). On the other hand, a full double allele knock-out of the *C9ORF72* gene does not cause neurodegeneration in mice, but rather produces immune response defects. Haploinsufficiency is therefore unlikely to be the mechanism causing ALS (Koppers *et al.*, 2015) yet it may contribute to disease progression and/or severity. Also, in *C9ORF72* knockout mouse models, autophagy substrate accumulation, including p62, has been observed (O'Rourke *et al.*, 2016). It maybe that haploinsufficiency of *C9ORF72* could be involved in disease progression due to its involvement in autophagy, which is essential for the removal of aggregates (Sellier *et al.*, 2016; Webster *et al.*, 2016). Less *C9ORF72* protein within the cell could make it increasingly difficult to clear misfolded proteins or aggregates from cells, leading to aggregate/protein build up. The hexanucleotide repeats found in *C9ORF72*-ALS/FTD can also lead to decreased *C9ORF72* mRNA expression levels, encoding a protein involved in vesicle trafficking (Farg *et al.*, 2014; Aoki *et al.*, 2017) and in the mouse immune response (Atanasio *et al.*, 2016; O'Rourke *et al.*, 2016) in both *in vivo* and *in vitro* model systems. Post-mortem tissue from patients with *C9ORF72*-ALS/FTD has shown that there is a significant decrease in *C9ORF72* transcript in comparison to healthy controls (DeJesus-Hernandez *et al.*, 2011; Van Blitterswijk *et al.*, 2015). However, it is still unclear how the direct contribution of reduced levels of *C9ORF72* protein impact on disease pathophysiology.

Research has indicated that small size expansions of approximately 50 repeats do not decrease the transcription of *C9ORF72*, (Cooper-Knock *et al.*, 2013) which is likely due to the fact that these smaller expansions do not result in hypermethylation in the promoter region of CpG island 5'-repeat sequence (Xi *et al.*, 2013, 2014). This further indicates that if

smaller repeats are pathogenic, then it is unlikely that haploinsufficiency is the sole responsible mechanism (Gómez-Tortosa *et al.*, 2013; Byrne *et al.*, 2014).

### **RNA Toxic Gain and Loss of Functions**

RNA toxic gain of function occurs via the sequestration of RNA binding factors onto RNA foci or processing transcripts (Figure 1. 1). It has been hypothesized that RNA toxicity is a likely pathophysiological mechanism of the G4C2 expansion repeats. These G4C2-repeat transcripts are accumulated in the form of nuclear RNA foci in the spinal cord and frontal cortex of patients with *C9ORF72* mutations. These accumulations are found predominantly in the nuclei of affected cells, and it has been observed that the bidirectional transcription of the G4C2 expansions results in the formation of sense and antisense RNA foci. However, RNA foci can also be located at lower levels in neuronal cytoplasm, as well as in peripheral blood leukocytes, skin fibroblasts, and patient iPSC-derived neurons (Donnelly *et al.*, 2013; Lagier-Tourenne *et al.*, 2013; Sareen *et al.*, 2013; Zu *et al.*, 2013; Cooper-Knock *et al.*, 2014) suggesting that RNA foci could serve as a significant disease biomarker.

In the majority of patient-derived cells, sense RNA foci have a greater abundance than antisense RNA foci. Recent research has tried to determine whether RNA-mediated toxicity is the main driver of disease, but it has been determined that there is a correlation between overall RNA foci burden and distribution with *C9ORF72* ALS/FTD clinical features. The results so far appear complex, but overall seem not to support that RNA foci are the predominant driver of neurodegeneration (Mizielinska *et al.*, 2013; Dejesus-Hernandez *et al.*, 2017).

The toxic gain of function that occurs is due to RNA foci sequestering RNA-binding proteins, which can alter the physiological function and cause neurotoxicity, which in turn can cause cell death. It has been proposed that RNA-mediated toxic gain of function is a contributing mechanism that prevents abnormally bound/sequestered RNA-processing factors from undertaking their normal function in the nucleus. It is suggested that in turn this leads to extensive alteration of *C9ORF72* gene expression in *C9ORF72*-related ALS (Ash *et al.*, 2013; Kohji Mori, Arzberger, *et al.*, 2013; Kohji Mori, Weng, *et al.*, 2013; Zu *et al.*, 2013).

## Protein Toxic Gain of Function

The locus of *C9ORF72* is transcribed bi-directionally, leading to both sense G4C2 transcripts and antisense G2C4 transcripts which form sense and antisense pre-mRNA repeat non-AUG translation (RAN translation) in the cytoplasm. This is an unconventional translation which involves translation of protein in all three coding frames and in absence of a canonical AUG start codon. As a result, G4C2 and G2C4 expansions will be translated into five sense and antisense dipeptide repeat proteins (DPRs) (Figure 2). It is these DPRs that are thought to be involved in protein toxic gain of function, and they are considered the main drivers of pathogenesis, at least in cell and animal models. From the sense transcript there are three DPRs: poly-glycine-arginine, poly-glycine-alanine and poly-glycine-proline. From the antisense RNA there are another three DPRs: poly-proline-glycine, poly-proline-arginine and poly-proline-alanine (Zu *et al.*, 2013). It is still unclear how each DPR contributes to the pathophysiology of ALS, but they have been demonstrated to be neurotoxic in both cell culture and animal models of disease. Star-shaped inclusions found within the cytoplasm are found in *C9ORF72*-mediated disease. They are negative for TDP-43 but are positive for p62 and the five DPR species that are products of unconventional RAN translation.

A potential treatment of *C9ORF72*-ALS/FTD could involve the prevention of DPR formation, therefore reducing the death of motor neurons (Freibaum and Taylor, 2017). Recent work in our lab (Hautbergue *et al.*, 2017) has shown that when DPRs are expressed in cells, this results in cell death and neurodegeneration. However, when nuclear export of the hexanucleotide repeats is manipulated, this prevents the production of DPRs resulting in an increase in cell survival and an overall neuroprotective effect. Initial findings have suggested that DPRs are the main driver of ALS/FTD pathogenesis. In *C9ORF72*-related ALS, DPRs are abundantly found in areas of the CNS both within the motor system and in extra-motor areas, including the cerebellum and hippocampus, and are thought to be responsible for the characteristic pathology of TDP-43-negative, p62 positive inclusions seen in the CNS of patients. This pathology has shown, in an *in vitro* model, that DPRs can alter RNA biogenesis and cause cellular toxicity (Kwon *et al.*, 2014) whilst also causing neurodegeneration in a *Drosophila* model (Mizielinska *et al.*, 2014).

---

#### 1.4.4 SRSF1-dependent nuclear export of pathological *C9ORF72* repeat transcripts

---

The functions of SRSF1 have been studied extensively in cancer immortalised cells, with the conclusion that SRSF1 overexpression leads to altered splicing functions linked to transformation and oncogenesis (Karni *et al.*, 2007; Anczuków *et al.*, 2015). However, the genome-wide functions of SRSF1 have not yet been investigated in the CNS, specifically in neurons. In proliferative cells, SRSF1 is involved in several RNA-processing functions including: alternative splicing (Cáceres and Krainer, 1993; Long and Cáceres, 2009); mRNA nuclear export (Müller-Mcnicoll *et al.*, 2016); RNA stability (Zhang and Krainer, 2004) and paused RNA polymerase II release from promoters (Ji *et al.*, 2013). It is known that SRSF1 plays an essential role in the tissue-specific splicing of the CaMKII $\delta$  (Ca<sup>2+</sup>/calmodulin-dependent kinase II $\delta$ ) transcript that is vital for successful embryonic development of the heart. Yet, it appears that SR proteins have a much more dispensable role in the viability of mature cardiomyocytes (Xu, Yang, J. H. Ding, *et al.*, 2005). Transcriptome results indicate that the individual depletion (> 90%) of each of the conserved SRSF1–7 proteins only affected the SRSF1-dependent nuclear export of 225 transcripts in immortalised cells and approximately 100–400 transcripts for the other SRSF2–7 factors, indicating that the NXF1-dependent nuclear export adaptor function involves redundancy and/or cooperation (Müller-Mcnicoll *et al.*, 2016). On the whole, further investigation is required to understand the genome-wide contribution of the function of SRSF1 in the neuronal context (Castelli *et al.*, 2021).

Usually, to prevent the deleterious consequences of SRSF1 loss/gain-of-function, the SRSF1 protein is tightly regulated inside the cell using multiple post-transcriptional and translational mechanisms, and its expression is negatively auto-regulated. SRSF1 regulates the splicing of its own transcript and prevents overexpression whilst promoting expression of premature termination codon-containing splice isoforms that are targeted to nonsense-mediated mRNA decay (Wu *et al.*, 2010; Das and Krainer, 2014).

Studies have shown that mice with a homozygous deletion of *SRSF1* do not continue past embryonic stage. Deletion of the *SRSF1* gene from heart tissue leads to heart failure and death within 6–8 weeks of birth (Xu, Yang, J. H. Ding, *et al.*, 2005). This is a potential concern when considering depleting SRSF1 for therapeutic purposes. However, SRSF1 and other SR-rich proteins are dispensable to the viability of mature cardiomyocytes, with Xu, Yang, J.-H. Ding, *et al.*, 2005 suggesting that the function of SRSF1 is only essential at the embryonic differentiating stage of the heart. However, other studies have suggested that SRSF1

overexpression in human mammary epithelial cells leads to increased proliferation and protection against apoptosis, therefore promoting breast cancer and potentially other cancers (Anczuków *et al.*, 2012, 2015). SRSF1 can act as an oncoprotein and could be implicated in tumour growth. Suppressing its overexpression could be another potential target for cancer treatment (Karni *et al.*, 2007). It is likely to be advisable that depletion of SRSF1 should not be a total knockdown of the protein, but rather a reduction to prevent any serious off-target effects of depletion, should this protein be used as a therapeutic approach.

In ALS, it has been reported that SRSF1 directly binds synthetic sense G4C2-repeat RNAs (Lee *et al.*, 2013; Cooper-Knock *et al.*, 2014). mRNA nuclear export adaptors interact with the RNA and the nuclear receptor NXF1, which they remodel into an open conformation alongside TREX complex subunits, increasing its affinity for mRNAs. This triggers the process of mRNA nuclear export. The selective remodelling of NXF1 also provides a mechanism for the retention of unprocessed transcripts within the nucleus (Hautbergue *et al.*, 2008; Viphakone *et al.*, 2012).

The sequestration of the mRNA nuclear export adaptor SRSF1 onto the repeat RNA sequences resulting from the pathological intronic expansion of the *C9ORF72* gene (Figure 1. 2) triggers the nuclear export of pathological sense and antisense *C9ORF72* repeat transcripts, leading to the subsequent RAN translation of DPRs in the cytoplasm, with resulting production of neurotoxic DPRs. This abnormal RAN translation results in five different DPRs: in the sense frames, glycine-alanine (GA), and glycine-arginine (GR); in the antisense frames, alanine-proline (AP) and proline-arginine (PR); and glycine-proline (GP) in both reading frames.

The involvement of SRSF1 in the nuclear export of sense and antisense *C9ORF72* repeat transcripts was investigated by our lab. During the investigation, transgenic ALYREF-RNAi and SRSF1-RNAi *Drosophila* lines were crossed with flies harbouring 36 uninterrupted G4C2 expansions and exhibited neurotoxicity induced by DPRs (Mizielinska *et al.*, 2014; Hautbergue *et al.*, 2017). The results indicated that a depletion of 70-80% of SRSF1 mRNAs inhibits nuclear export of G4C2 transcripts and the RAN translation of DPRs. The flies showed significant rescue of neurodegeneration and motor function (Hautbergue *et al.*, 2017). It was also reported, in the same paper, that the depletion of approximately 50% of SRSF1 also promotes the survival of *C9ORF72*-ALS motor neurons in co-cultures with astrocytes (Hautbergue *et al.*, 2017). Overall, this study identified SRSF1 as a promising therapeutic target for the treatment of *C9ORF72* ALS/FTD.

## Pathological nuclear export of C9ORF72 repeat transcripts

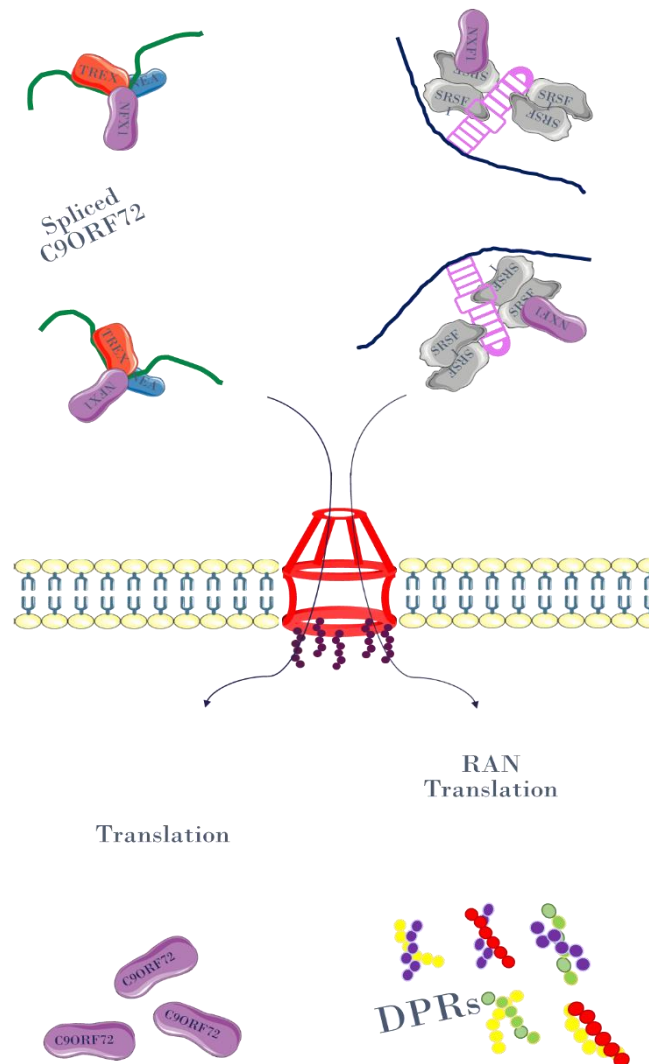


**Figure 1. 2** The protein SRSF1 can specifically bind to the pathogenic repeat expansions which are found in a G quadruplex structure. SRSF1 is then sequestered onto the repeat transcripts, allowing it to interact with the nuclear export machinery. This allows for the nuclear export and translation of the abnormal pre mRNA and the production of dipeptide repeat proteins (DPRs). SRSF1 does not bind the non-pathogenic repeat transcripts and is not involved in the nuclear export of the normal *C9ORF72* repeat transcripts. SRSF1 is therefore thought to be specific to the pathological species (Hautbergue *et al.*, 2017). *C9ORF72* RAN (non-ATG) translation occurs in all six antisense and sense reading frames. It results in five different DPRs: in the sense frames, glycine-alanine (GA), and glycine-arginine (GR); in the antisense frames, alanine-proline (AP) and proline-arginine (PR); and glycine-proline (GP) in both reading frames. These DPRs cause the formation of neuronal inclusions and all are found in patients with *C9ORF72*-related ALS-FTD. It has been suggested that these accumulated G4C2 repeats sequester RNA-binding proteins, whose role is involved in splicing, and that this ultimately leads to splicing dysfunction, therefore contributing to *C9ORF72* pathophysiology (Rohrer *et al.*, 2015). Diagram adapted from Hautbergue *et al.*; 2017.

---

#### 1.4.5 *C9ORF72*-ALS/FTD mouse models

---

The most common genetic cause of familial amyotrophic lateral sclerosis (ALS) and frontotemporal dementia (FTD) is the presence of polymorphic hexanucleotide repeat expansions (GGGGCC) ranging from 30-50 repeats to up to thousands in size in the first intron of the human *C9ORF72* gene (Renton *et al.*, 2011; DeJesus-Hernandez *et al.*, 2011). As research into the mechanism of *C9ORF72*-ALS/FTD continues, the need for a mouse model that replicates both the clinical and pathological features of ALS and FTD is crucial to help develop and test novel treatment options. The better the disease is modelled in mice, the more likely that the new therapeutic developments will be effective in human disease once they reach clinical trial. So far, several *C9ORF72*-ALS/FTD mouse models have been developed, all with varying degrees of success. The first G4C2-repeat expansion mouse model was published by Chew *et al.*, 2015. In this model, transgene delivery was mediated by an adeno-associated virus – serotype 2/9 (AAV2/9) that carried DNA encoding 66 G4C2 –repeats into the C57BL/6J mouse genome via the CNS. In the following section, I will review a number of current ALS mouse models and discuss the pros and cons of each, and why we have chosen to continue our research using the C9-500 BAC mice from the Ranum group described in Liu *et al.*, 2016 and Nguyen *et al.*, 2020.

In the model developed by Chew *et al.*, the DNA encapsulated within the viral vector is delivered via bilateral intra-cerebroventricular injection at post-natal day 1 to ensure widespread transduction across the brain. The transgene that is used in this model does not contain an ATG start codon allowing for the modelling of RAN translation of the (G4C2)<sub>66</sub> transcripts similar to what is seen in human *C9ORF72*-ALS patients. Six months after transgene delivery, the mice were tested for pathological, behavioural and biochemical abnormalities. The mice displayed increased anxiety levels, hyperactivity and reduced socialisation, and a significant motor coordination dysfunction was observed via the Rotarod test, yet no motor neuron loss was detected in the spinal cord. Unfortunately, this model did not show the characteristic symptoms seen in human ALS such as progressive paralysis. The aim of this paper was to show that the expression of repeat transcripts and DPR alone causes cognitive deficits (Chew *et al.*, 2015). This mouse model, although it reinforces that DPRs are a main driver of neurotoxicity in *C9ORF72*-ALS/FTD, is an overexpression model which does not recapitulate the pathophysiology of human *C9ORF72*-ALS/FTD disease. Another limiting factor of this model is that to induce the repeat expansions, an AAV virus

would have to be delivered which could interact with any potential AAV gene therapies or other therapeutics that have been designed as a potential treatment option.

Other *C9ORF72* ALS/FTD mouse models have all been BAC (bacterial artificial chromosome) transgenic models. Peter *et al.*, 2015 described using a BAC DNA containing the partial coding region of human *C9ORF72* gene (exon 1-6), along with a (G4C2)<sub>500</sub> region in an SJL/BL6 mouse strain. Jiang *et al.*, 2016, took a similar approach and used a BAC DNA containing a partial coding region of human *C9ORF72* gene (exon 1-5) but included a (G4C2)<sub>450</sub> repeat region in a C57BL6/C3H mouse strain. These mouse models did share some similar neuropathophysiology with human *C9ORF72* ALS/FTD; for example, neuronal poly GP aggregates were detected in both models, with the overall trend of older mice having larger aggregates present. However, no motor impairments were detected in either mouse model following behavioural tests for motor function at 12 months. Therefore, neither of these models mirror the human *C9ORF72* ALS/FTD disease trajectory (Peters *et al.*, 2015; Jiang *et al.*, 2016).

Another BAC mouse model has been constructed by O'Rourke *et al.*, 2015 which was devised by BAC DNA that contains the entire coding region of the human *C9ORF72* gene (exon 1-11) and includes a (G4C2)<sub>800</sub> region in a C57BL/6J mouse strain. Again these mice showed no distinct behavioural phenotype in keeping with *C9ORF72*-ALS/FTD human disease (O'Rourke *et al.*, 2015).

Hao *et al.*, 2019 have recently developed a mouse model that specifically produces the DPR poly-PR without the presence of RNA hexanucleotide repeats. Previous studies have indicated that poly-PR is toxic to cells *in vitro* (Wen *et al.*, 2014; Tao *et al.*, 2015). Both homozygous and heterozygous poly-PR mouse models were generated. The homozygous mice showed a significant reduction in body size, body weight and reduced survival in comparison to the heterozygous mice. The heterozygous mice showed motor deficits such as progressive gait and balance impairment, along with a reduced number of Purkinje cells in the cerebellum at 12 months. There was also activated microglia and astrocytes present in both the cerebellum and lumbar spinal cord of the heterozygous mice. However, there was no evidence of TDP-43 inclusions which is characteristic of *C9ORF72*-ALS/FTD in humans, suggesting that poly-PR is not the sole mechanism of disease in human *C9ORF72*-ALS/FTD. The difference between the phenotypes in homozygous and heterozygous mice suggests that poly-PR causes neurotoxicity in a dose dependent manner (Hao *et al.*, 2019). The model does appear to have a trackable motor deficit and could be used to develop

therapeutics that are specific to poly-PR DPRs. However, this model is still unable to truly reflect C9ORF72 ALS/FTD, especially without the presence of the G4C2 RNA repeat transcripts.

In this PhD project, the mouse model that was used was the C9-500 BAC transgenic mouse line, which currently displays most of the key features of human C9ORF72-ALS/FTD (Liu *et al.*, 2016). The C9ORF72 BAC (G4C2)<sub>500</sub> FVB/NJ mouse model was generated by integrating a BAC clone harbouring a human patient C9ORF72 gene containing (G4C2)<sub>1200</sub> repeat into the genome of an FVB/NJ mouse strain. As the repeat expansions from the human C9ORF72-ALS/FTD patient were highly unstable, the bacterial construct used to insert the gene into the mice was modified to contain ~500 or ~40 repeat expansions. The expression of the toxic expansion is driven by the human regulatory regions and therefore mirrors the human disease context. Phenotypes that produce anxiety-like behaviour, motor deficits/paralysis, and widespread neurodegeneration across the CNS, as well as overall decreased survival, were reported (Liu *et al.*, 2016; Nguyen *et al.*, 2020). The acute end-stage C9-500 BAC should display many of the key neuropathological features of both ALS and FTD which are consistent with the features of human C9ORF72 ALS/FTD disease. Novel therapeutic strategies can therefore be tested in this pre-clinical model of human C9ORF72-ALS/FTD disease.

Liu *et al.* have produced a mouse model that results in a heterogenous phenotype, with some mice developing severe motor deficits and others developing a slower progressive disease (as is often the case in human ALS disease). Unfortunately, this could be a severe disadvantage as there is no reliable way to assess which mice will develop the severe disease phenotype and which will develop the milder phenotype. The acute, rapidly progressive phenotype is characterized by paralysis, hindlimb weakness and a substantial decrease in survival compared to non-transgenic littermates. Mice that develop milder neurodegenerative changes have a longer lifespan than mice which develop the severe phenotype, which is characterised by reduced activity, kyphosis, clasp hyperactivity when provoked and intermittent seizures (Liu *et al.*, 2016). As it is difficult to predict which phenotype will occur in an individual mutant mouse, this may cause potential problems when administering treatments, as it could be unclear whether milder symptoms are a result of the delivered treatment or due to the slow progressive phenotype.

Along with the display of behavioural, molecular and neurodegenerative features of ALS/FTD, these mice also express C9ORF72 sense and antisense transcripts. Although this

mouse model is not perfect, currently this mouse model is the best fit for our project. An excellent capability of this mouse model is that it has been reported to provide trackable behavioural phenotypes that can be monitored throughout the mouse lifespan in a similar way to human *C9ORF72*-ALS/FTD disease, which was key for this study.

## 1.5 Current pharmacological treatments for ALS

Currently, there is no cure for ALS, and the treatments available to manage the condition are limited. The US has approved two treatments aiming to slow down disease progression: riluzole and edaravone. In contrast, in the UK and Europe only riluzole has been approved for the treatment of ALS, and edaravone has not obtained approval from the European Medicines Agency (EMA).

### 1.5.1 Riluzole

Glutamate is the major excitatory neurotransmitter within the CNS (Kvamme, Torgner and Roberg, 1991) and its excessive stimulation of glutamate receptors plays a role in the degeneration of neurons in MND (Van Den Bosch and Robberecht, 2000; Vanoni *et al.*, 2004). Riluzole inhibits this excessive pre-synaptic glutamate release and protects motor neurons via sodium channel blockade, but it does not reverse previous motor neurone damage. So far, it is the only ALS drug licenced in the UK and whilst it is thought to slow the progression of ALS, it is not a cure. The riluzole trial data indicated only a modest improvement in survival of approximately 3-4 months (Lacomblez *et al.*, 1996). However, a more recent analysis of the use of riluzole in the clinical setting has suggested that the survival effects of riluzole may be more substantial (Andrews *et al.*, 2020).

### 1.5.2 Edaravone

Edaravone is a promising drug and has recently been approved for clinical use in ALS by 6 countries: Japan, South Korea, US, Canada, Switzerland and China (Mitubishi Tanabe Pharma press release July 16 2020). Its mechanism of action remains to be fully elucidated, but it is considered an antioxidant. It is a free radical scavenger and it is suggested that it eliminates lipid peroxides and hydroxyl radicals. It works to lesson oxidative injury in motor neurons at risk of degeneration in ALS.

The drug was developed in Japan and was originally marketed as an intravenously administered treatment for stroke in 2001 (Rothstein, 2017). Evidence of reduced oxidative stress was observed in a Phase 2 study using intravenous administration of edaravone in ALS patients (Yoshino and Kimura, 2006). The use of edaravone was also shown to reduce motor neuron degeneration and motor symptoms in mice with the SOD1 mutant gene (Ito *et al.*, 2008) and may have potential protective effects on vascular endothelial cells (Sawada, 2017).

To date, long-term safety and efficacy has not been investigated. However, MT Pharma America presented 12-month edaravone and ALS data at ENCALS 2017 showing that, following 48 weeks of treatment, patients had less decline in physical function (measured by ALS functional scale-revised) compared with patients who were first given a 6 month placebo and then 6 months of edaravone (Al-Chalabi *et al.*, 2017) (Clinical Trial number: NCT01492686). Overall, evidence suggests that edaravone reduces the progression of disability (measured by the ALS functional rating scale (ALS-FRS-R)) at least over a short 6-month period and in a highly selected subset of patients. Unfortunately, the suggested treatment of 10-14 days of intravenous infusions, each taking approximately an hour, is onerous for the patients and costly for health care services.

Riluzole can be combined with edaravone, as each drug has different mechanisms of action. Edaravone, like riluzole, is not a cure, but may have some effect in slowing disease progression. Further investigation into the effects of this combined therapy is necessary and in addition, clinical trials are planned with an oral formulation of edaravone which would be less burdensome for patients compared to an IV preparation. If biomarkers could be identified, this would allow researchers to monitor drug efficiency.

---

### **1.5.3 Masitinib**

---

Masitinib, developed by AB Science in Paris, is a new drug which can also be combined with riluzole. The main mechanism of action of this drug is to inhibit enzymes involved in inflammation (Trias *et al.*, 2016). This is an attractive target for the treatment of ALS due to the significant neuroinflammation observed during the disease course. A recent phase 3 trial has estimated that 80% to 85% of patients (with normal disease progression) showed significant benefit from the masitinib treatment. Unfortunately, questions have been raised regarding these results and further scientific studies have been advised before the drug will be considered for approval. A double blind phase 3 trial to compare the efficacy and safety

of Masitinib compared with a placebo treatment began in September 2017 in Canada (*Home - ClinicalTrials.gov*, 09/01/2017) (clinical trial number: NCT03127267).

However, in June 2021, the drug had a setback following results from the Phase 3 study (clinical trial number: NCT03127267) that identified Masitinib as increasing the potential risk of ischaemic heart disease in patients. Further investigations will be required before approval will be considered.

## 1.6 Potential future treatments using gene therapy approaches

Gene therapy has recently been considered as a potential therapeutic option for C9ORF72-related ALS/FTD. It is an experimental technique first developed in 1972, but so far it has had limited success. Genetic material is used to prevent and treat disease in replacement of drug therapy using a variety of techniques: a mutant gene causing disease can be replaced with a healthy copy of the gene (gene replacement); a mutant gene that has improper function can be silenced (knocked down); or a new gene to help fight the disease can be introduced. Currently, gene therapy is only being considered for diseases that have no other cures and have limited treatment options.

For the successful delivery of gene therapy, there are several major challenges to overcome. It is essential that the new gene is delivered to the correct cell type. Delivery to the wrong cells/tissue would result in treatment inefficiency and is likely to cause off-target effects in the patient. Once the genes have reached their target they need to be turned on, but cells often shut down gene expression if they detect that genes are showing any unusual activity. It is also important to avoid triggering the immune response. When new genes are introduced by gene therapy, cells sometimes consider them as harmful intruders and trigger a protective immune response. Careful consideration is therefore required when choosing and designing vectors, in order to prevent triggering the immune response. The gene that is being delivered also needs to avoid interacting and disrupting the function of other genes.

The DNA encoding for a protein or RNAi (genetic material that is able to silence a particular gene) is packaged within a virus. The viral vector carries the gene of interest into the patient cells. Once inside, the idea is that the gene of interest or RNAi is expressed by the cell, leading to the production of the new therapeutic protein and/or deletion of a protein, restoring normal or near to normal protein function.

The aim of gene therapy is that the new gene will integrate itself into the patient's genome and will continue to replicate and function throughout the patient's life. There is a risk that the gene will insert itself elsewhere within the genome, disrupting the activity of another gene. For example, if the new gene interferes with an important cell division regulating gene, it may result in cancer. Another major hurdle is the cost of gene therapy. Genetic disorders that can be targeted are often extremely rare and require an individual, personalised medicine approach. This is effective but very expensive, as the therapy cannot be made in bulk or in advance. It also means that the treatment cannot be advertised and distributed to hospitals like traditional chemical drugs, and the process to create these gene therapies is long and arduous, meaning that it is difficult for companies to make a profit without a very high cost per patient treatment.

## 1.7 Gene therapy - viral vectors

Currently there are three viral vector strategies used for gene therapy: lentiviruses, adenoviruses and adeno-associated viruses.

### 1.7.1 Gene Therapy Vectors: Lentiviruses

Lentiviruses are retroviruses which are spherical, enveloped, single stranded RNA viruses that are approximately 100 nm in diameter (Campbell and Vogt, 1997). They are RNA viruses that are able to replicate their genomes using the viral encoded RNA-dependent RNA polymerase, allowing them to convert RNA into DNA which can then be successfully integrated into the host genome. Lentiviral particles enter the host cell via the interaction of glycoproteins, anchored to the outer envelope, and a specific cell receptor. The successful binding of the viral envelope to this cell surface receptor leads to a series of events that result in the fusion of the viral particle lipid bilayer and the host cell. Once fused, the virus can subsequently unload its viral genetic cargo into the host cell's cytoplasm, where it is integrated into the genome (Stein *et al.*, 1987; Sinangil, Loyter and Volsky, 1988).

The human immunodeficiency virus (HIV) is the most well-known lentivirus. One of their biggest assets, when used as a gene therapy vector, is that they can transduce both dividing and non-dividing cells, meaning that they are able to integrate into postmitotic cells e.g. neurons. However, initial gene therapy studies indicated that this strategy carries the risk of genotoxicity via insertional mutagenesis at the DNA integration site. This is likely caused by the disruption or inappropriate activation of a nearby host gene.

Lentiviruses are ideal gene therapy vectors as they permit long-term gene expression. They do have a much smaller packaging capacity of 9kb in comparison to adenoviruses (Naldini *et al.*, 1996). For certain diseases, high level expression of multiple genes may achieve the best therapeutic option, and lentiviral vectors have demonstrated that they have the ability to express multiple genes using a single vector (Zhu *et al.*, 2001; Yu *et al.*, 2003; Tian *et al.*, 2009). Lentiviral vectors are known to only elicit a relatively weak immune response (Abordo-Adesida *et al.*, 2005).

Lentiviral vector systems derived from the HIV-1 virus have had to evolve through the years to mitigate the potential risks associated with the virus. HIV is known to be a replication-competent provirus, which is obviously a major safety concern. To limit the formation of unintended replication-competent pro-virus, the most recent generation of lentivirus vectors has been created to have a vector packaging system that is self-inactivating. Lentivirus still has a bio-safety level of BSL-2, which is the same as an adenovirus, due to its ability to integrate into the genome of infected cells. However, this bio-safety level is higher than BSL-1, which is required when producing AAV.

First generation HIV-1-based vectors are composed mostly of the viral genome within the trans packaging construct, including the core of the virus, regulatory protein coding sequences, and accessory regulatory genes (Naldini *et al.*, 1996). In the three-plasmid design to generate lentiviral vectors, the env gene is replaced by the glycoprotein of vesicular stomatitis virus (VSV-G) and is separately provided in trans by a second plasmid. Pseudotyping the viral particle with VSV-G facilitates viral entry independent of its native host cell receptor. The third plasmid construct provides the therapeutic transgene along with the cis-acting elements that allow for viral encapsidation. Second generation lentiviral vectors are considered safer than first generation vectors as they are devoid of *vif*, *vpr*, *vpu*, and *nef* supporting genes, which are known to promote viral proliferation and infection (Zufferey *et al.*, 1997). To prevent unintended replication-competent pro-virus, the third generation of lentiviral vectors were produced to lack the regulatory genes, *tat* and *rev*, in the packaging construct (Dull *et al.*, 1998). The safety profile of these third-generation lentiviral systems is improved further by deleting a fragment of the 3'-LTR, which contains the transcription factor-binding sites and the TATA box; this therefore generates a self-inactivating vector packaging system (Zufferey *et al.*, 1997).

Unfortunately, it been reported that even these new self-inactivating lentiviral vectors, especially when carrying strong promoter and enhancer elements, can activate neighbouring

genes. In addition, integration of the vector genome can potentially form chimeric gene fusions made up of pro-viral and host sequences, which causes severe off-target effects (Moiani *et al.*, 2012), and could be implicated in certain cancers (Taniue and Akimitsu, 2021). Lentiviral vectors have been shown to cause aberrant splicing of cellular transcripts (Moiani *et al.*, 2012). Even though lentiviral vectors do have their shortfalls, they are still a common gene therapy tool in ALS studies and have been utilised to deliver short hairpin RNA (shRNA) targeting SOD1 (Ralph *et al.*, 2005; Raoul *et al.*, 2005) and to deliver motor neurons of the facial nucleus (Hottinger *et al.*, 2000) and neurotrophic factors to muscles (Azzouz *et al.*, 2004).

Lentiviral vectors are also used in many current gene therapy trials. Currently, lentiviral gene therapy clinical trials account for approximately 10.3% of total worldwide trials (Gene Therapy Clinical Trials Worldwide, 2021) and the vector is most often implicated in the development of treatments for autosomal recessive monogenic diseases (Fabry disease, Gaucher disease, Huntington disease etc.) and cancer diseases. There are also gene therapies in development for sickle cell disease, where the lentivirus is administered into the blood *ex vivo* before being transplanted back into the patient.

---

### 1.7.2 Adenoviruses

---

Adenoviruses (Ad) are non-enveloped viruses that are known to cause infections of the upper respiratory tract. Its capsid is composed of an icosahedral protein structure that has the capacity to accommodate a 26 to 45 kb linear double stranded DNA genome. The main advantages of using Ad vectors are: (1) they have a high transduction efficiency in both quiescent and dividing cells; (2) they provide epichromosomal persistence in the host cell; (3) they have broad tropism for different tissue targets; and (4) they can be used in scalable production systems (Lee *et al.*, 2017). The major objectives in Ad vector progression to the clinic are to overcome the challenges and disadvantages associated with the pre-existing viral immunity of the general population, their potential to cause life-threatening strong innate immune responses to its capsid proteins, and the robust human adaptive immune responses to new synthesized viral and transgene Ad derived products (Singh, Kumar and Agrawal, 2018). Since the first generation of E1A-deleted Ad vectors were established, various strategies have been developed to improve their tolerability by improving their efficacy, capacity, safety and gene transfer longevity.

Ad vectors have recently been utilised more frequently in human gene therapy research due to their practical advantages, such as their broad tropism profiles, lack of host genome integration, and large packaging capacities (>36 kb). Currently, Ad-based gene therapy clinical trials account for approximately 17% of total worldwide trials (Gene Therapy Clinical Trials Worldwide, 2021) and the majority of Ad gene therapies have been applied towards novel vaccines and cancer therapies (Leukaemia's, other Cancers, HIV and Cardiovascular Disease).

Adenoviruses are also used as genetic vaccines. Although immunogenicity is a disadvantage for using Ad as an efficient viral vector, it nevertheless has been exploited in the development of Ad-based vaccines (Lasaro and Ertl, 2009). In fact, the recent SARS-COV-2 vaccine, developed by Oxford University, is based on the chimp-derived ChAdOx1 capsid (Folegatti et al., 2020). Ad vectors can deliver foreign epitopes to boost the host immune response to invading pathogens by increasing pro-inflammatory cytokine production and effective adaptive humoral and cellular immune responses (Zhang and Zhou, 2016). These advantages have made Ad vectors an ideal vaccine carrier.

Ad vectors are also very useful in delivering gene therapies for the treatment of cancer, especially in the delivery of suicide genes. Some Ad vectors have been engineered to induce cell cycle arrest and apoptosis in tumour cells. Other engineered Ad vectors are able to deliver enzymes that can convert various pro-drugs into active drugs, resulting in tumour-cell killing. Unfortunately, due to the serious challenge of the high worldwide pre-existing immunity against common Ad serotypes and the small transgenes of interest, this viral vector was considered unsuitable for this PhD project.

---

### **1.7.3 Gene Therapy Vectors: Adeno – Associated Viruses**

---

Adeno-associated viruses (AAVs) are often the vector of choice when designing a gene therapy plasmid for delivery to the central nervous system (CNS). AAVs are small viruses with no envelope, used for the main reason that they are believed to be non-pathogenic in humans. They have a single-stranded genome 4.7 kb long, with the ability to insert genetic material onto a specific site on chromosome 19 with almost 100% certainty (Srivastava, Lusby and Berns, 1983). AAV does have some disadvantages as a gene therapy vector. It has a low packaging capacity, meaning that it has a limit on how big a gene it can carry (approximately 4.5kb) and it also has a complex procedure when being produced in an

academic laboratory setting. It takes 3-4 weeks to produce, concentrate and titrate each AAV before it can be used *in vitro* or *in vivo*.

When cloning transgenes into an AAV vector they must be engineered with the appropriate promoter, enhancer poly-(A) and splice signals to result in the optimal transgene expression. Natural AAV viruses integrate into the host's genome, while recombinant viruses produced for therapeutic use have been engineered and lack this capacity. These viruses are members of the parvoviridae family. They have a genome approximately 5kb long inside a T=1 icosahedron capsid (the viral capsid is composed of 60 asymmetric units made of one protein with a total of 60 capsid proteins) with a 25 nm diameter, making it extraordinarily stable. There are 2 open reading frames (ORFs), Rep and Cap, which, along with the packaged DNA/ therapeutic DNA insert, are inside the mature capsid. Therefore, recombinant AAV vectors are only small targets for the host immune system. The coding regions are flanked by inverted terminal repeats (ITRs) 145 base pairs long and have a T-shaped structure. ITRs are the start of the DNA replication/primary packaging signal. They are the only cis-active sequences required for the production of rAAV vectors and the only AAV-encoded sequences in AAV vectors. AAV ITRs plus Rep protein allow for enhancer activity, but without the Rep protein there is minimum promoter and enhancer activity (Pillay *et al.*, 2017).

The integrative wild-type AAV is not the form that is used in the development of gene therapeutics. Instead, recombinant AAV (rAAV) is used, which lacks viral DNA and is engineered to cross the cell membrane, allowing for the trafficking and delivery of its DNA cargo into the nucleus of targeted cells. rAAV is commonly called AAV in gene therapy applications and papers. Rep proteins are absent in rAAV, meaning that encoded transgenes can form circular concatemers than can persist as episomes within the nucleus of successfully transduced cells (Choi, McCarty and Samulski, 2006). The recombinant episomal DNA does not integrate into the host's genome, which provides a safety net, but also it is implied that after repeated rounds of replication the virus genomes will be diluted. Eventually, cell replication will result in the loss of the transgene/expression of the transgene, with the turnover rate depending on the transduced cell type. Multiple injections of AAV are then needed, depending on targeted cell type. This is not as much of a problem for diseases of the CNS, as the majority of neurons do not divide; however, astrocytes and glia do. Multiple administrations of AAV would likely cause an immune reaction due to repeated exposure to the virus, which could then result in the destruction of the virus before it is able to transduce its target cells.

The packaging size of 4.7kb of the rAAV vector is a considerable challenge, as the expression cassette remains between and includes the two ITRs. Single stranded AAV vectors deliver the transgene to the nucleus, where it undergoes conversion into a double-stranded transgene. This process limits the onset of transgene expression and so an alternative is to use a self-complementary vector. When delivered to the nucleus, the single stranded packaged genome of the scAAV is able to complement itself to form a double stranded genome, bypassing the limiting step that occurs when using a single stranded AAV. Although transcription expression has a more rapid onset, self-complementary vectors have a reduced packaging capacity of 2.2kb (McCarty, Monahan and Samulski, 2001; McCarty, 2008).

Gene therapies being developed to target ALS usually use an adeno-associated virus as a therapeutic vector. Different virus serotypes of AAV are chosen depending on the target tissue and disease. The most common serotypes used as gene therapy vectors are: 2, 5, 6, 9 and 10. Each serotype has a different rate of transduction depending on the target tissue/organ (Table 1. 1). AAV infects post-mitotic (non-dividing) cells such as neurons and has high tropism for the central nervous system. Therefore, the virus can deliver genetic material to the brain and CNS which is advantageous for the treatment of ALS (Samulski and Muzyczka, 2014). For AAV to produce an effective viral infection, it must be co-infected with a helper virus, a safety feature which prevents the spread of recombinant AAV after clinical application. In the wild, Ad is the natural helper virus, but in cell culture, herpes virus and baculovirus can be used as a helper (Daya and Berns, 2008).

Wild-type AAV infection is widely disseminated among the human population, but it has not been associated with any particular disease or clinical pathology, and many people are seropositive for a number of AAV serotypes. This is down to the exposure of wild-type AAV in early childhood, often as early as 2 years old, where humans develop antibodies against the viral capsids (Calcedo *et al.*, 2011). Both innate and adaptive immunity can be activated after the administration of rAAV, as the AAV capsid protein is highly similar to that of wild type AAV. The innate immunity is the body's first barrier against pathogens and its response depends on the recognition of the pathogen-associated molecular patterns expressed via pattern recognition receptors (PRRs) expressed by immune cells. The molecular recognition of viral nucleic acids, membrane glycoproteins, or chemical messengers by PRRs results in the translocation of nuclear KB and IRF. These translocation factors play an essential role in pro-inflammatory cytokines and IFNs expression (Trinchieri, 2007). In the context of rAAV gene therapy, preclinical studies have supported the important role of type I IFNs in the induction of CD8<sup>+</sup> T cell responses. It has been shown that blocking the activation of

innate immune responses prevented both cytotoxic (Rogers *et al.*, 2017; Shirley *et al.*, 2020) and humoral anti-capsid responses *in vivo* (Nathwani *et al.*, 2011). Both the capsid and the DNA may cause the activation of the innate immune response, and even the production and purification of AAV can lead to the presence of empty AAV capsids and DNA and protein contaminants in the final AAV preparation, further increasing the risk of activation. Unfortunately, it is difficult to predict whether an immune response will occur following administration, even after thorough *in vivo* testing in animals (Wang *et al.*, 2007; Li *et al.*, 2009a; Li *et al.*, 2009b).

The adaptive immune system takes considerably longer to activate but is another barrier to pathogens. T and B lymphocytes are activated after molecular recognition of a specific antigen APC (Abbas *et al.*, 2009). Following the activation of the adaptive immune system, lymphocytes expand and differentiate into effector cells that inactivate and clear antigens using humoral and cytotoxic responses. Once the circulating antigens have been reduced by the immune response, memory and T and B cells are produced with the ability to respond to any successive antigen stimulation faster and more efficiently (Abbas *et al.*, 2009). Following the administration of rAAV, both transduced cells and professional APCs present capsid-derived epitopes to cytotoxic CD8<sup>+</sup> T cells via MHC class I (Pien *et al.*, 2009; Hui *et al.*, 2015; Rogers *et al.*, 2017). These activated CD8<sup>+</sup> T cells could clear rAAV-transduced cells, inducing inflammation in the target organ and affecting the gene transfer outcome/efficiency (George *et al.*, 2017; Palaschak *et al.*, 2017). Indeed, experience from clinical trials indicates that rAAV vector administration leads to the development of anti-AAV antibodies (IgG and Nabs) (Murphy *et al.*, 2009), which indicates that vector re-administration would result in the activation of the immune response. It is thought that up to 60% of the population is seropositive for AAV2, and often there is a high degree of cross-reactivity of anti-AAV antibodies with other AAV serotypes. To combat this problem, most gene-therapy trials screen for seropositive subjects and exclude them from their studies (Wang *et al.*, 2010). However, this does also limit large portions of the population who may not be able to be successfully treated using AAV gene therapy.

**Table 1. 1** Summary of Transduction and optimal AAV serotypes in specific cell types (Kwon and Schaffer, 2007; Mori *et al.*, 2008; Hammond *et al.*, 2017). Adapted from Addgene: Adeno-associated virus (AAV) Guide, 2017

AAV Serotype	Tissue
<b>AAV1</b>	CNS, Heart, Retinal Pigment Epithelium, Skeletal muscle
<b>AAV2</b>	CNS, Kidney, Photoreceptor cells, Retinal Pigment Epithelium
<b>AAV4</b>	CNS, Lung, Retinal Pigment Epithelium
<b>AAV5</b>	CNS, Lung, Photoreceptor cells, Retinal Pigment Epithelium
<b>AAV6</b>	Lung, Skeletal Muscle
<b>AAV7</b>	Liver, Skeletal Muscle
<b>AAV8</b>	CNS, Heart, Liver, Pancreas, Photoreceptor cells, Retinal Pigment Epithelium
<b>AAV9</b>	CNS, Heart, Liver, Lung, Skeletal Muscle
<b>AAV10</b>	Bone Marrow, Heart, Liver, Ileum, Kidney, Adrenal gland, Lymph nodes

## 1.8 Non-viral gene therapy delivery systems

### 1.8.1 ASOs

Oligonucleotides are short sequences of single stranded RNA or DNA and ASOs (Anti-Sense Oligonucleotides) are synthetically made oligonucleotide-based therapies. ASOs alter gene expression via two mechanisms:

1. They are designed to target sequence specific transcripts through complementary base pairing (Kaczmarek, Kowalski and Anderson, 2017). They are an oligonucleotide DNA sequence that anneal and are reverse complementary to mRNAs and promote their degradation by RNase-H within a cell (Bennett *et al.*, 2017), thus silencing gene expression.
2. They are designed to bind and are reverse complementary to the target pre-mRNA or mRNA and physically block splicing and/or translation protein interactions. Modulation of splicing can allow for the selective inclusion or exclusion of introns and exons from pre-mRNA, resulting in the production of non-functional mRNA.

ASOs have been in development for over 30 years and yet very few ASOs are available as approved treatments due to multiple challenges. Administration can be an issue, as ASOs are

difficult to get to the target organ or cells. Unlike viral vectors that can target specific cell types, ASOs have a localised and general effect. Older generation ASOs degrade very quickly, sometimes before they can start their therapeutic effects, and so a large concentration and volume of therapies may be required. The treatments are required to be administered more than once, often every few months, or even every week, depending on the rate of degradation of the ASO *in vivo*. It is therefore more comparable to a small molecule drug rather than a gene therapy vector, which would be expected to be administered once rather than repeatedly.

There are also safety concerns, especially regarding on or off target effects: on-target effects are unintended consequences of the modification of gene expression of the target RNA, while off-target effects are due to the sequence used in the ASO not being specific to just one target, meaning multiple genes are affected. However, this issue is shared with gene therapy viral vectors.

## 1.9 Gene therapies currently at clinical trial stage

Gene therapy is a relatively new approach and currently there are very few approved gene therapies in the UK. Current approved gene therapy drugs include GSK Strimvelis for Adenosine deaminase deficient severe combined immunodeficiency (ADA-SCID) “bubble boy syndrome,” which was approved by the FDA in June 2016. In January 2018, the NICE final draft guidance recommended Strimvelis treatment in the UK (NICE, 2018). The most recent approved gene therapy drug is Zolgensma® (Novartis) which is an AAV derived gene therapy designed to treat SMA (spinal muscular atrophy). SMA is a rare genetic neurological disease which is characterised by progressive motor neuron degeneration and muscle weakness, paralysis and in the most severe form (type 1 SMA or Werdnig-Hoffman disease) leads to permanent ventilation usually by the time the patient is 2 years old. Zolgensma® is designed to treat the genetic root cause of SMA by using an AAV9 to deliver a functional *SMN1* gene and replace the defective *SMN1* gene, with the intention to halt disease progression with a single infusion of the drug. The gene therapy is approved for the treatment of patients under the age of 2 who have SMA, including patients who are pre-symptomatic. The UK’s first patient was treated with the drug in June 2021.

Fomivirsen used to be an approved gene therapy drug for cytomegalovirus retinitis (eye disease) in 1998; however, it was withdrawn due to the development of highly effective antiretroviral drug-based therapy HAART. A gene therapy for treatment of familial

hypercholesterolemia, mipomersen, was approved by the FDA in Jan 2013 (Kastelein *et al.*, 2006; Akdim *et al.*, 2011). There are, however, numerous studies progressing into clinical trials in the UK. Gene therapies are classed as advanced therapy medicinal products, as defined by EC ATMP regulation 1394/2007. Clinical trials involving ATMP products continue to increase yearly, and in the UK, there are 154 trials reported as ongoing in 2020, which is a 20% increase when compared to the previous year. This increase has occurred even with the interruptions of Covid-19. This number accounts for 12% of all ongoing ATMP clinical trials globally, demonstrating that the UK is a key player in the developments of novel gene therapies (C. and G. T. C. A. clinical trials report, 2020).

The majority of clinical trials are using lentiviral vectors, retrovirus vectors and AAV (Table 1. 2) Adeno-associated virus vectors have many serotypes, each one able to target various tissues. However, many of the trials taking place are treating eye disorders and haemophilia. Using viral vectors in the eye has several advantages. First, it is a small organ, making transfection easier and much more efficient. It is also an isolated organ, making transfection in other areas of the body unlikely, since the ocular cells being targeted do not divide, and therefore the risk of an immune response is greatly diminished.

Haemophilia is another disease being treated by AAV gene therapies, and it is the focus of various ongoing clinical trials (Table 1. 2). Unlike the eye, the blood is a complicated target as a build-up of AAV vector in other organs would be undesirable. In a recent study, investigators showed that a single intravenous administration of a serotype 8 based adeno-associated virus (AAV8) vector encoding the human clotting factor IX (FIX) gene resulted in a stable (>6 years) therapeutic expression of FIX without long-lasting toxicity. This is a positive development, as it indicates that a single administration of an AAV viral vector can express its gene of interest over a long time period and does not result in any serious adverse effects. This represents an exciting progression in the gene therapy field (Nathwani *et al.*, 2014a). Similar gene therapy techniques are also being trialled for the treatment of haemophilia A. A Phase 1/2, Dose-Escalation Safety, Tolerability and Efficacy Study of BMN 270, an adenovirus-associated virus vector-mediated gene transfer of human factor viii in patients with severe haemophilia A, is currently being undertaken at the Queen Elizabeth Hospital Birmingham (NCT03370913).

So far, only one gene therapy trial targeting a neurological disease and featuring AAV has been accepted in the UK, as of November 2021, which is Zolgensma®. Previous potential neurological gene therapy treatments have used lentiviral vectors. There is a definite gap in

the field regarding potential AAV targets in the CNS, which can be observed when reviewing current ongoing Phase III trials (Table 1. 2), especially considering the sheer amount of research currently being undertaken in cell and animal models in neuroscience.

It is evident that gene therapy research is finally getting the recognition it deserves and is progressing into the clinical stage after decades of pre-clinical research. With the Strimvelis treatment approved in 2016, and Zolgensma® approved in 2021, this is just the beginning of gene therapy success and we can look forward to further approved treatments in the future.

Table 1. 2 Phase II/III ongoing gene therapy viral vector clinical trials (adapted from www.catapult.org.uk)

Title	Clinical Database numbers	Trial status	Type of viral vector used	Disease Area	Year Trial Began
<b>A Phase II/III Study of the Efficacy and Safety of Hematopoietic Stem Cells Transduced with Lenti-D Lentiviral Vector for the Treatment of Cerebral Adrenoleukodystrophy (CALD)</b>	NCT01896102 2011-001953-10	In follow-up	<b>Lentivirus</b>	Adrenoleukodystrophy (Adrenomyeloneuropathy/Schilder-Addison Complex)	2013
<b>Long-term Follow-up of Subjects with Cerebral Adrenoleukodystrophy who were Treated with Lenti-D Drug Product</b>	NCT02698579 2015-002805-13	Recruiting	<b>Lentivirus</b>	Adrenoleukodystrophy	2015
<b>A Randomized, Open Label, Outcomes-assessor Masked, Prospective, Parallel Controlled Group, Phase III Clinical Trial of Retinal Gene Therapy for Choroideremia Using an Adeno-associated Viral Vector (AAV2) Encoding Rab Escort Protein 1 (REP1)</b>	NCT03496012 2015-003958-41	In follow-up	<b>AAV</b>	Choroideremia	2016
<b>A Dose Escalation (Phase I), and Dose Expansion (Phase II/III) Clinical Trial of Retinal Gene Therapy for X-linked Retinitis Pigmentosa Using an Adeno-Associated Viral Vector (AAV8) Encoding Retinitis Pigmentosa GTPase Regulator (RPGR)</b>	NCT03116113 2016-003852-60	Recruiting	<b>AAV</b>	Retinitis Pigmentosa (Retinitis)	2017
<b>A Phase III Open-Label, Single-Arm Study To Evaluate The Efficacy and Safety of BMN 270, an Adeno-Associated Virus Vector Mediated Gene Transfer of Human Factor VIII in Hemophilia A Patients With Residual FVIII Levels &lt;= 1 IU/dL Receiving Prophylactic FVIII Infusions</b>	NCT03370913 2017-003215-19	In follow-up	<b>AAV</b>	Haemophilia A	2017
<b>A Phase III Single Arm Study Evaluating the Efficacy and Safety of Gene Therapy in Subjects with Transfusion-dependent <math>\beta</math>-Thalassemia, Who Do Not Have a <math>\beta^0/\beta^0</math> Genotype, by Transplantation of Autologous CD34+ Stem Cells Transduced Ex Vivo with a Lentiviral <math>\beta</math>A-T87Q-Globin Vector in Subjects &lt;=50 Years of Age</b>	NCT02906202 2015-004122-33	In follow-up	<b>Lentivirus</b>	$\beta$ -Thalassemia	2017
<b>A Phase III Single Arm Study Evaluating the Efficacy and Safety of Gene Therapy in Subjects with Transfusion-dependent B-thalassemia by Transplantation of Autologous CD34+ Stem Cells Transduced Ex Vivo with a Lentiviral Ba-T87Q-globin Vector in Subjects &lt;=50 Years of Age</b>	NCT03207009 2016-003611-35	Recruiting	<b>Lentivirus</b>	$\beta$ -Thalassemia	2017
<b>European, Phase III, Open-label, Single-arm, Single-dose Gene Replacement Therapy Clinical Trial for Patients with Spinal Muscular Atrophy Type 1 with One or Two SMN2 Copies Delivering AVXS-101 by Intravenous Infusion</b>	NCT03461289 2017-000266-29	In follow-up	<b>AAV</b>	Spinal Muscular Atrophy	2018

<b>A Global Study of a Single, One-time Dose of AVXS-101 Delivered to Infants with Genetically Diagnosed and Pre-symptomatic Spinal Muscular Atrophy with Multiple Copies of SMN2</b>	NCT03505099 2017-004087-35	In follow-up	<b>AAV</b>	Spinal Muscular Atrophy	2018
<b>A Long-term Follow-up Study to Evaluate the Safety and Efficacy of Retinal Gene Therapy in Subjects with Choroideremia Treated Previously with Adeno-associated Viral Vector Encoding Rab Escort Protein-1 (AAV2-REP1) in an Antecedent Study</b>	NCT03584165 2017-003104-42	Recruiting	<b>AAV</b>	Choroideremia	2018
<b>Phase III Study To Evaluate Efficacy/Safety of Valoctocogene Roxaparvovec an AAV Vector-Mediated Gene Transfer of hFVIII at a Dose of 4E13vg/kg in Hemophilia A Patients with Residual FVIII Levels &lt;=1IU/dL Receiving Prophylactic FVIII Infusions</b>	NCT03392974 2017-003573-34	In follow-up	<b>AAV</b>	Hemophilia A (Factor VIII Deficiency)	2018
<b>A Global Randomized Multicenter Phase III Trial of JCAR017 Compared to Standard of Care in Adult Subjects with High-risk, Second-line, Transplant-eligible Relapsed or Refractory Aggressive B-cell Non-Hodgkin Lymphomas (TRANSFORM)</b>	NCT03575351 2018-000929-32	Recruiting	<b>Lentivirus</b>	B-cell Non-Hodgkin Lymphomas	2018
<b>An Open-label, Multicentre, Long-term Followup Study to Investigate the Safety and Durability of Response Following Dosing of a Novel Adeno-associated Viral Vector (FLT180a) in Patients with Haemophilia B</b>	NCT03641703 2017-005080-40	Recruiting	<b>AAV</b>	Haemophilia B	2018
<b>Long-term Follow-up of ND4 LHON Subjects Treated with GS010 Ocular Gene Therapy in the Rescue or Reverse Phase III Clinical Trials</b>	NCT03406104 2017-002153-11	In follow-up	<b>AAV</b>	Leber Hereditary Optic Neuropathy	2018
<b>Efficacy and Safety of Bilateral Intravitreal Injection of GS010: A Randomized, Doublemasked, Placebo-controlled Trial in Subjects Affected with G11778A ND4 Leber Hereditary Optic Neuropathy for up to One Year</b>	NCT03293524 2017-002187-40	In follow-up	<b>AAV</b>	Leber Hereditary Optic Neuropathy	2018
<b>A Phase III, Randomized, Open-label Study Evaluating Efficacy of Axicabtagene Ciloleucel Versus Standard of Care Therapy in Subjects with Relapsed/Refractory Diffuse Large B Cell Lymphoma</b>	NCT03391466 2017-002261-22	In follow-up	<b>Retrovirus</b>	B-Cell Lymphoma	2018
<b>Phase III, Open-label, Single-dose, Multi-center, Multinational Trial Investigating a Serotype 5 Adeno-associated Viral Vector Containing the Padua Variant of a Codon-optimized Human Factor IX Gene (AAV5-hFIXco-Padua, AMT061) Administered to Adult Subjects with Severe or Moderately Severe Hemophilia B</b>	NCT03569891 2017-004305-40	In follow-up	<b>AAV</b>	Haemophilia B	2018
<b>A Phase II/III Study of Lenti-D Drug Product After Myeloablative Conditioning Using Busulfan and Fludarabine in Subjects &lt;=17 Years of Age with Cerebral Adrenoleukodystrophy (CALD)</b>	NCT03852498 2018-001145-14	Recruiting	<b>Lentivirus</b>	Adrenoleukodystrophy	2019

<b>A Phase III, Multicenter, Randomized, Openlabel Study to Compare the Efficacy and Safety of Bb2121 Versus Standard Regimens in Subjects with Relapsed and Refractory Multiple Myeloma (RRMM) (KarMMa-3)</b>	NCT03651128 2018-001023-38	In follow-up	<b>Lentivirus</b>	Multiple Myeloma	2019
<b>Long-Term Follow-up Protocol for Subjects Treated With Gene-Modified T Cells</b>	NCT03435796 2017-001465-24	Recruiting	<b>Lentivirus</b>	Oncology	2019
<b>Open-label, Single-arm, Multi-center Study of Intracerebral Administration of Adeno-associated Viral (AAV) Serotype rh.10 Carrying Human N-sulfoglucosamine Sulfohydrolase (SGSH) cDNA for Treatment of Mucopolysaccharidosis Type IIIA</b>	NCT03612869 2018-000195-15	In follow-up	<b>AAV</b>	Mucopolysaccharidosis Type IIIA	2019
<b>Tisagenlecleucel Versus Standard of Care in Adult Patients with Relapsed or Refractory Aggressive B-cell Non-hodgkin Lymphoma: A Randomized, Open Label, Phase III Trial (BELINDA)</b>	NCT03570892 2016-002966-29	Recruiting	<b>Lentivirus</b>	Non-Hodgkin Lymphoma	2019
<b>An Observational Long-term Follow-up Study for Patients Previously Treated with Autologous ex Vivo Gene Therapy for Severe Combined Immunodeficiency Due to Adenosine Deaminase Deficiency (ADA-SCID)</b>	NCT04049084	Recruiting	<b>Lentivirus</b>	Adenosine Deaminase (ADA) Deficiency Related SCID	2019
<b>A Phase III, Open-label, Randomized, Parallel Group Study to Evaluate the Efficacy and Safety of Intrapleural Administration of Adenovirusdelivered Interferon Alpha-2b (rAd-IFN) in Combination with Celecoxib and Gemcitabine in Patients with Malignant Pleural Mesothelioma</b>	NCT03710876 2017-003169-82	Recruiting	<b>Adenovirus</b>	Malignant Pleural Mesothelioma	2019
<b>Longterm Follow-up of Subjects With Hemoglobinopathies Treated With Ex Vivo Gene Therapy Using Autologous Hematopoietic Stem Cells Transduced With a Lentiviral Vector</b>	NCT02633943 2013-002245-11	Recruiting	<b>Lentivirus</b>	Sickle Cell Disease $\beta$ -Thalassemia	2020
<b>A Phase II/III Study Evaluating Gene Therapy by Transplantation of Autologous CD34+ Stem Cells Transduced Ex Vivo With the LentiGlobin BB305 Lentiviral Vector in Subjects With Sickle Cell Disease</b>	NCT04293185 2019-000331-63	In Planning/ Set-up	<b>Lentivirus</b>	Sickle Cell Disease	2020
<b>A Phase III Randomized Study Comparing JNJ-68284528, a Chimeric Antigen Receptor T Cell (CAR-T) Therapy Directed Against BCMA, Versus Pomalidomide, Bortezomib and Dexamethasone (PVd) or Daratumumab, Pomalidomide and Dexamethasone (DPd) in Subjects with Relapsed and LenalidomideRefractory Multiple Myeloma</b>	NCT04181827 2019-001413-16	Recruiting	<b>Lentivirus</b>	Multiple Myeloma	2020
<b>Phase III, Open Label, Single Arm Study to Evaluate Efficacy and Safety of Fix Gene Transfer with PF-06838435 (RAAV-SPARK100- HFIX-PADUA) in Adult Male Participants with Moderately Severe to Severe Hemophilia B (Fix:C <math>\leq</math>2%) (BENEGENE-2)</b>	NCT03861273 2018-003086-33	Recruiting	<b>AAV</b>	Hemophilia B (Factor IX Deficiency)	2020

<b>A Phase III, Multicenter, Randomized, DoubleBlind, Placebo-Controlled Study to Evaluate the Safety and Efficacy of PF-06939926 for the Treatment of Duchenne Muscular Dystrophy</b>	NCT04281485 2019-002921-31	In Planning/ Set-up	<b>AAV</b>	Duchenne Muscular Dystrophy	2020
<b>A Randomized, Controlled, Double-arm, Double-blind, Multi-center Study of Ofranergene Obadenovec (Vb-111) Combined with Paclitaxel Vs. Paclitaxel Combined with Placebo for the Treatment of Recurrent Platinum-resistant Ovarian Cancer</b>	NCT03398655 2019-003884-23	In Planning/ Set-up	<b>AAV</b>	Ovarian Cancer	2020

## 1.10 Current gene therapy developments for ALS

Other than investigations and phase III trials using Zolgensma® to treat SMA, currently in the UK there are no clinical trials involving the use of gene therapy viral vectors to treat motor neuron disease. However, a phase 3 trial has recently been completed, as of October 2021, evaluating an antisense oligonucleotide (ASO) drug to treat SOD1 ALS following promising results reported from a phase 2 trial (Miller *et al.*, 2020).

As previously discussed, at least some patients with sporadic ALS have been shown to have misfolded SOD1 in their affected tissues. Astrocytes and motor neurons derived from sporadic ALS patients show lower toxicity levels when synthesis of SOD1 is reduced (Haidet-Phillips *et al.*, 2011). Due to these promising preliminary results, Foust and team have used two transgenic ALS mouse models to evaluate a single peripheral injection of AAV9 which encodes an shRNA to reduce the synthesis of mSOD1. Delivery of the AAV9 with shRNA to mice who had not yet developed the disease extended their overall survival by delaying disease onset and slowing its progression. When delivered after the onset of symptoms, the treatment still markedly slowed ALS progression and extended survival significantly. Moving forward with this promising technique, when delivered intrathecally to normal non-human primates or SOD1 mice, SOD1 suppression is evident throughout the spinal cord, in motor neurons and glia (Foust *et al.*, 2013; Iannitti *et al.*, 2018). Similar results were also seen in a rat model of ALS (Thomsen *et al.*, 2014). The antisense drug tofersen (Biogen) has recently been evaluated in phase III clinical trial. Tofersen is an anti-sense oligonucleotide which binds to SOD1 mRNA, allowing for the degradation of the protein via RNase-H to reduce SOD1 protein production. The patients were followed for 28 weeks post-administration. Trends were found to favour tofersen across multiple secondary and exploratory measures of clinical function and biologic activity, such as motor and respiratory function, and overall quality of life in comparison to the placebo groups. In addition, SOD1 proteins levels were reduced in CSF, and CSF and plasma levels of neurofilament light (a biomarker of axonal degeneration) were significantly reduced in the group receiving active tofersen therapy. However, statistical significance was not reached for the primary end-point of the trial (change in the ALS-FRS-R)(Miller *et al.*, 2020; Biogen, 2021). A phase III trial that will further this investigation (ATLAS) started recruiting in April 2021 and will seek to determine the optimal time points for tofersen administration in pre-symptomatic carriers of SOD1 ALS (NCT04856982).

Another recent development in gene therapy for ALS comes as a Phase I/II study into the safety of VM202 intramuscular injections (Sufit *et al.*, 2017). VM202 is a DNA plasmid containing novel cDNA hybrid human HGF (Hepatocyte Growth Factor). It induces angiogenesis and cell migration in a more effective manner than a plasmid vector that only expresses a single isoform. It is thought that once the plasmid has been injected into the patient's muscle, the DNA is taken up by the cell and produces the HGF protein, which is then released from the cell, inducing the formation of new blood vessels by activating a number of signalling pathways. The aim is for VM202 to promote the microvascular system of the nerve cells and hopefully encourage their regeneration in patients with ALS (NCT02039401 - *ClinicalTrials.gov*).

The VM202 DNA plasmid expresses both wild-type HGF – HGF<sub>723</sub> and HGF<sub>728</sub>. Transgenic overexpression of HGF in the nervous system of SOD1-G93A mice (ALS Model) attenuates motor neuron death and prolongs lifespan (Ishihara *et al.*, 2005). A similar effect has also been seen in SOD1-G93A rats (Pasinelli *et al.*, 1998)

During the study, 18 ALS patients were treated with VM202 administrated intramuscular injections on days 0, 7, 14 and 21. They were evaluated for adverse effects at 9 months. Twelve patients reported mild-moderate injection site reactions. Three patients experienced 5 serious adverse effects unrelated to VM202. One patient died from ALS progression. Multiple intramuscular injections of VM202 appears safe in ALS subjects, but retreatment will determine whether or not VM202 can alter the progression of ALS (Sufit *et al.*, 2017).

Due to these positive findings, Helixmith have launched a REViVALS-1A Phase 2a trial which will evaluate the safety and effectiveness of VM202 (aka Enggenesis) against a placebo in 18 adults with ALS who have displayed motor symptoms in their limbs for <4 years. Participants will receive an injection of the placebo or Enggenesis into their arm and leg muscles. The treatment cycle will be 128 injections each, every 2 weeks for 3 cycles. The main goal of this trial is to assess the gene therapy's safety, but secondary goals include reviewing changes in survival, quality of life, disability, motor function, strength and respiratory function (NCT04632225).

Mueller *et al.*, 2020 treated two fALS patients, with SOD1 mutations, with a single intrathecal infusion of adeno-associated virus (AAV10) encoding a microRNA targeting SOD1. Patient 1 had had an immune response to the AAV10 capsid throughout the experiment which had to be treated with prednisone. Unfortunately, due to the numbers of patients the treatment

was administered to, no clinical conclusions could be made about the treatment effects. Additional studies are required to determine the results of this strategy in a larger cohort of patients with fALS with SOD1 mutations (Mueller *et al.*, 2020).

The challenge is progressing the animal and cell models that provide proof of concept into clinical trials. So far, very few therapies have reached pre-clinical stage, but over the next few years we will see these coming to clinical trial and it will be interesting to see how the human body reacts. If gene therapy can be successful and become a safe alternative to drugs, its application in other diseases could be immense.

### 1.11 Current gene therapy developments for the specific treatment of C9ORF72 ALS/FTD

Gene therapy is a relatively new therapeutic approach compared to the use of drug molecules and so far, is only considered for progressive life limiting diseases. This is mainly due to the high risks associated with gene therapy approaches, which involve either the depletion of a specific protein/RNA or the overexpression of a protein of interest into the hosts' cells. Unfortunately, it is often difficult to predict or measure how these alterations of gene expression may potentially affect other cellular processes. It is therefore difficult to assess the long-term safety of these approaches. There are currently no licenced gene therapy options for C9ORF72-ALS/FTD; however, there are several strategies under trial. As of November 2021, there were only 2 registered gene therapy C9ORF72-ALS/FTD specific clinical trials.

An ASO has recently been developed for the treatment of C9ORF72-ALS/FTD (BIIB078). There is currently an active phase I double blind trial to evaluate the safety, tolerability and pharmacokinetics of the study drug when administered in repeated doses to adult patients with C9ORF72-ALS. The antisense drug targets the C9ORF72 expansion containing transcripts and induces RNase H mediated degradation (NCT03626012).

Another ASO being developed by Wave Life Sciences has been specifically designed to treat C9ORF72-ALS/FTD (WVE-004). WVE-004 is a stereopure antisense oligonucleotide which has been designed with controlled placement of Sp and Rp linkages in the backbone. The position of Sp and Rp linkages can alter oligonucleotide activity and, in this case, allows the ASO to yield more efficient RNase H mediated knockdown of the target proteins (Liu *et al.*, 2021). C9ORF72 contains 3 sets of RNA instructions to produce the C9ORF72 protein.

The three different types are called V1, V2 and V3. Mutations in *C9ORF72* can result in faulty V1 and V3 leading to the toxic build-up of DPRs. WVE-004 has been designed to target the faulty V1 and V3 RNA and mark for RNase H mediated degradation, leaving the functional V2 RNA to produce the healthy *C9ORF72* protein. There is currently a Phase 1/2a study (FOCUS-C9) in the recruitment phase, designed to assess safety and tolerability of dose dependent administration in *C9ORF72*-ALS/FTD patients (EudraCT Number: 2020-005193-94).

Only a couple of years ago, there were no genetic therapy treatments for *C9ORF72*-ALS/FTD at clinical trial stage. In fact, there were very few treatments in the pipeline for this genetic ALS variant even outside of the gene therapy field. But the research in this area is rapid and there are new strategies being uncovered to speed up the development of potential treatments for *C9ORF72*-ALS/FTD. Again, the biggest hurdle in getting primary research into clinical trials is the lack of a solid *C9ORF72*-ALS/FTD mouse model with a phenotype that mimics the disease in humans. Without a reliable mouse model, there will be an inevitable delay before some of the newest strategies can even be tested in patients, and time is not something MND patients have spare.

## 1.12 Introduction to the PhD

Due to the recent identification of *C9ORF72* and its genetic role in ALS and FTD, its mechanism of pathophysiology is not yet fully understood. Previous work in our lab has identified the selective driving mechanism of the SRSF1-dependent nuclear export of pathological *C9ORF72* repeat transcripts as a potential therapeutic approach using patient-derived neurons and *Drosophila* models (Hautbergue *et al.*, 2017). The group has shown that inhibiting the nuclear export of *C9ORF72* repeat transcripts via partial depletion of SRSF1 (approximately 50%) or expression of an engineered protein that blocks the nuclear export of repeat transcripts (a point mutant of SRSF1 which does not interact with the nuclear export machinery) subsequently inhibits the RAN translation. Consequently, there is reduced production of toxic DPRs in the cytoplasm which confers neuroprotection, rescuing locomotor deficits *in vivo* in *C9ORF72*-ALS *Drosophila* (Hautbergue *et al.*, 2017). Previously, the lab has also used this intervention in a patient-derived co-culture system and has found that this method increases the survival of motor neurons when co-cultured with astrocytes derived from *C9ORF72*-ALS patients.

My project aims to evaluate the therapeutic safety and potential efficacy of these neuroprotective strategies previously used in *Drosophila* and cell models, in a *C9ORF72*-ALS/FTD mouse model. I will be using two gene-therapy approaches based on adeno-associated virus (AAV9) vectors in a pre-clinical mouse model of *C9ORF72*-linked ALS. I will assess whether the partial depletion of SRSF1 using shRNA designed against SRSF1 or the expression of an SRSF1 point mutant (therapeutic SRSF1-m4) that is sequestered onto *C9ORF72* repeat transcripts (but fails to interact with the nuclear export machinery) is safe in wild type mice and leads to DPR reduction in *C9ORF72*-ALS/FTD mice (Ranum model). My project initially involved investigating the effects of the SRSF1 depletion and SRSF1-m4 expression on the behaviour (motor/cognitive phenotypes) of the treated *C9ORF72*-ALS/FTD mice. However, I was unable to perform this 12-month study due to the covid-19 related closure of the labs and the subsequent half-day shift pattern.

We hypothesise that the partial depletion of SRSF1 will lead to reduced sequestration of the protein onto the pathogenic pre-mRNA containing pathological repeat expansions in *C9ORF72*-ALS/FTD reporter cell models and mouse brains, further inhibiting the interaction of the SRSF1:*C9ORF72*-repeat RNAs with the nuclear export machinery and the nuclear export of the pathological transcripts. Consequently, less DPRs will be produced in the cytoplasm of the cell and will prevent neurotoxicity. We also hypothesise that the mutant

SRSF1-m4 protein, which retains the ability to bind repeat RNAs, will be sequestered onto the repeat transcripts instead of the wild-type SRSF1 (Figure 1. 3), further inhibiting the interaction with NXF1, nuclear export and RAN translation.

My aims were:

1. To generate adeno-associated virus 9 which carries shRNA against SRSF1 or the SRSF1-m4 point mutant.
2. To validate whether the viruses are functional in cell models by observing their ability to deplete SRSF1 or express m4 *in vitro* and lead to a reduction in DPR production.
3. To inject wild-type mice with the SRSF1-RNAi and SRSF1-m4 mutant viruses to evaluate the safety of the knockdown or expression of SRSF1 mutant in wild-type mice. Injected mice will be maintained for either 4 weeks or 6 months and motor function will be monitored using rotarod test. Mice from each treatment will be sacrificed one-month post-vector delivery to evaluate gene transfer efficiency.
4. To inject *C9ORF72*-ALS/FTD mice with the SRSF1-RNAi and SRSF1-m4 mutant viruses to evaluate the ability of the 2 strategies to reduce DPR production *in vivo* as a proof-of-principle efficacy for future larger and longer studies.

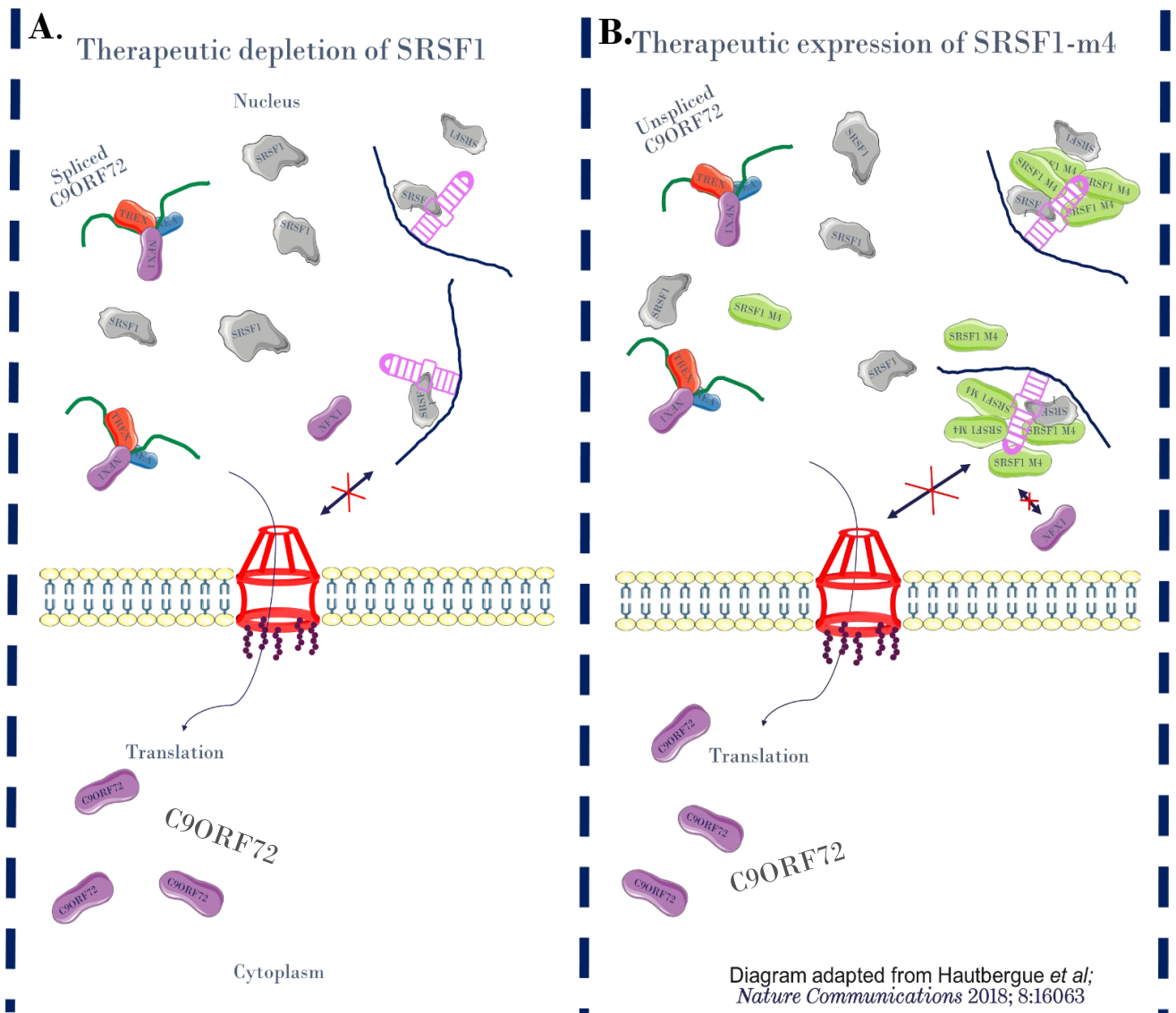


**Figure 1. 3** The two therapeutic strategies for the treatment of C9ORF72-ALS/FTD (A) Therapeutic SRSF1 depletion: the depletion of SRSF1 partially within a cell will lead to a reduction in the sequestration of SRSF1 onto the pathogenic RNA. Therefore, this will inhibit the interaction with the nuclear export machinery and the overall export of the pathogenic transcripts. Consequently, less DPRs will be produced in the cytoplasm of the cell, preventing neurotoxicity. (B) Therapeutic expression of SRSF1-m4: The mutant SRSF1 M4 protein is a mutant that has been engineered to have the property of being able to interact with the pathogenic repeat RNA but cannot interact with RNA export machinery. SRSF1-m4 has a higher affinity for binding the pathogenic RNA transcripts compared to wild-type SRSF1, and once bound prevents the transcripts from exiting the nucleus. Diagram adapted from Hautbergue *et al*; *Nature Communications* 2017; 8:16063.

## CHAPTER 02: Materials and Methods

### 2.1 Strains

During this project human embryonic kidney cells (HEK293T cells) and mouse neuroblastoma Neuro-2A cells were used. For viral preparation, human kidney cells (HEK 293T cells) were used. DH5 $\alpha$  E. coli cells have been used during transformations of the experimental plasmids.

### 2.2 Plasmids

#### 2.2.1 Cloning

The polymerase chain reaction was used to amplify target DNA sequences (in this case SRSF1 wild-type and SRSF1 m4). First, the oligonucleotides for the respective DNA sequences were resuspended in a 1:10 dilution. A number of reagents were then added to a PCR tube: 26.5  $\mu$ l dH<sub>2</sub>O, 10  $\mu$ l 5 x Herculase Buffer (*Agilent*), 8  $\mu$ l dNTPs (*Bioline*), 1  $\mu$ l NMSO, 1.25  $\mu$ l Primer 1, 1.25  $\mu$ l Primer 2, 1  $\mu$ l Herculase (*Agilent*) and then either 1  $\mu$ l of p 3 X-FLAG-SRSF1 or p 3 X-FLAG-SRSF1 m4 template DNA. The samples then underwent a standard PCR protocol: an initial denaturation of 1 minute at 95°C followed by a 30 times cycle of denaturation (20 minutes at 95°C), annealing (20 minutes at 54°C), extension (2 minutes at 68°C) and finishing off with 4 minutes at 68°C.

#### 2.2.2 Gel Extraction

A 1.5% agarose gel was used (3 g of Agarose + 200ml of TAE Buffer + 4  $\mu$ l ethidium bromide) with a 10 well comb. For the ladder, 5  $\mu$ l of Generuler DNA Ladder (ThermoFisher Scientific) Mix was loaded into the well. 10  $\mu$ l of DNA loading dye (ThermoFisher Scientific) was added into 50  $\mu$ l of SRSF1 and into 50  $\mu$ l of SRSF1 m4. SRSF1 and SRSF1 m4 were then loaded onto adjacent gels and run using a BioRad PowerPac™ Basic Power Supply at 80 volts for 30 minutes. The band was removed using a blade and a UV-transilluminator to visualise the expected band. The Qiagen gel extraction kit was then used to extract the DNA. First, the band within the agarose gel was weighed and three volumes of buffer QG were added to 1 volume of gel (100 mg – 100  $\mu$ l). This mix was then incubated for 10 minutes, until the gel has dissolved at 50 °C. The sample was vortexed every 2-3 minutes to aid the dissolving process. Once the band had dissolved completely, the mixture turned yellow. At

this point, 1 gel volume of isopropanol was added to the sample and mixed. A QIAquick column was placed in a collection tube and the sample was applied and centrifuged at 13,000 rpm for 1 minute; after which the flow through was discarded and the collection tube was replaced. Buffer QG was added (0.5 ml) and the sample was centrifuged again for 1 minute at the same speed. Again, the flow through was removed and the collection tube was replaced for the washing step. For this, 0.75 ml of buffer PE was added to the column and centrifuged for 1 minute at 13,000rpm. Flow through was again discarded and the column was centrifuged for an additional minute at 13,000 rpm. The column was then placed into a 1.5 ml microcentrifuge tube, 50 µl of Buffer EB was added to the centre of the column to elute the DNA. This was centrifuged at 13,000 rpm for 1 minute.

The extracted DNA then underwent an overnight restriction at 37 °C: 50 µl of newly extracted DNA, 30µl distilled H<sub>2</sub>O, 10µl restriction buffer (10 x), 5 µl of XhoI and 5 µl of EcoRI.

To clean up the DNA, the following day 100µl of PCI (phenol/chloroform/isoamyl) was added to the restricted DNA. This was then vortexed for 1 minute and then centrifuged for 3 minutes at 13,000 rpm. Next, 90µl of this clean DNA had 10 µl of 3 M NaAC added to it and was vortexed, after which 300µl EtOH was added. Tubes were then inverted and placed in the -20 °C freezer for 20 minutes. Next, samples were centrifuged at 13,000rpm for another 20 minutes before the supernatant was removed to allow the pellet to air dry. Purified DNA was then resuspended in 16µl of distilled H<sub>2</sub>O.

---

### 2.2.3 Annealing Oligonucleotides

---

In order to resuspend oligonucleotides to 100mM, they were placed in a new microtube and 6µl of the forward and reverse oligonucleotide was added, along with 38 µl of annealing buffer. This was heated for 4 mins at 90 °C, then 10 minutes at 70 °C using a PCR machine. This was allowed to slowly cool to room temperature before keeping it at 4 °C for 15 minutes. The oligonucleotides were then phosphorylated by adding 4µl of annealed oligonucleotides to a new 1.5 ml tube along with 3 µl of distilled water, 1 µl 10x forward PNK buffer (*Biolabs*), 1 µl 10mM ATP and 1 µl PNK (*Biolabs*). This reaction then underwent heat inactivation for 5 minutes at 90 °C, before being allowed to cool to room temperature on the bench.

---

### 2.2.4 Vector Preparation

---

The vector was added to a microtube (10 µl) along with 2 µl of Enzyme 1 and 2 µl of Enzyme 2 (*FastDigest ThermoFisher Scientific*). Then, the 5 µl of 10 x restriction buffer (*ThermoFisher Scientific*) and 31 µl distilled H<sub>2</sub>O was added. This was left on the heat block for 2 hours at 37 °C. After the incubation period, the sample was dephosphorylated by adding 1 µl of CIAP and replacing on the heat block for a further 15 minutes at 37 °C. Following this, 50 µl of distilled water and 100 µl of PCI was added and the dephosphorylated vector solution was vortexed for 1 minute. This was then centrifuged for 3 minutes at 13,000 rpm at room temperature. Next, 90 µl of this clean DNA had 10 µl of 3M NaAC added to it and was vortexed, after which 300 µl EtOH was added. Tubes were then inverted and placed in the -20 °C freezer for 20 minutes. After this, the samples were centrifuged at 13,000 rpm for another 20 minutes, before the supernatant was removed to allow the pellet to air dry. Purified DNA was then resuspended in 25 µl of distilled H<sub>2</sub>O.

---

### 2.2.5 Ligation

---

Vectors and inserts were ligated together by adding 16 µl of the insert, 1 µl of vector, 2 µl 10x ligation buffer (*BioLabs*) and 1 µl T4 DNA ligase (*BioLabs*). The ligation was then incubated for 2-4 hours at room temperature or overnight at 16 °C. For annealed oligonucleotides, 10 µl of phosphorylated oligonucleotides was added instead of 16 µl.

---

### 2.2.6 Sequencing

---

Plasmids were sent for sequencing at the University of Sheffield Medical School. The machine they used was an Applied Biosystems' 3730 DNA Analyser. We supplied 10 µl of plasmid DNA in water >100 ng/µl and a single direction primer supplied at HPLC purification levels.

---

### 2.2.7 Transformation

---

To transform the plasmids, 10 µl of plasmid was combined with 80 µl of DH5 alpha cells which was left on ice for 10 minutes. The sample then underwent a heat shock by placing the sample at 37 °C for 5 minutes, and then returning the cells back to the ice for a further 2 minutes. Lysogeny broth (950 µl) was added to the cells which was then incubated at 37°C for 1 hour, following which the sample was centrifuged at 7000 rpm for 1 minute. The

supernatant was poured off and the pellet was resuspended by pipetting up and down. Then, whilst working aseptically, the resuspended pellet was pipetted onto an agar (amoxicillin) plate and was spread across the plate until the agar was dry. The plate was incubated at 37 °C whilst on a shaker.

---

### 2.2.8 Rough Mini-Preps

---

To prepare and purify the plasmids, a rough mini prep (*Qiagen*) was first undertaken to ensure that the DNA insert had successfully integrated into the plasmid. For this 1.5 ml of the overnight *E. coli* culture, including the plasmid, was centrifuged in a microtube for 1 minute at 13,000 rpm. The resulting supernatant was discarded, and the cell pellet was resuspended in 200 µl of P1 buffer solution and vortexed. Next, P2 buffer (200 µl) was added and the sample was inverted slowly 5 times, before being incubated at room temperature for 3-5 minutes. S3 buffer solution was then added (300 µl) then inverted 10 times after which they were centrifuged at 13,000 rpm. The supernatant was then removed and added to fresh 1.5 ml microtubes, which were inverted 5 times following the addition of 700 µl of propranolol-2-ol being added to the supernatant. Tubes were then incubated at room temperature for 10 minutes, before being centrifuged for 10 minutes at 13,000 rpm. The supernatant was then carefully removed taking care to prevent dislodging the pellet, using a P1000 pipette. The sample was then re-centrifuged for 1 minute and a double pipette tip was used to remove the last of the supernatant. The pellet was then air dried for 10 minutes. Once dry, 50 µl of buffer EB or distilled H<sub>2</sub>O was used to resuspend the pellet.

---

### 2.2.9 Spin-Preps

---

For the extraction and purification of the shRNA 6, 9 and 10, the Qiagen QIAprep Spin Miniprep Kit was used. A pellet was obtained by centrifuging 2 ml of the bacterial overnight culture at 13,100 rpm for 3 minutes at room temperature. The pellet was then resuspended in 250 µl of buffer P1 and transferred to a microcentrifuge tube. Buffer P2, 250 µl, was then added and mixed thoroughly by inverting until the solution became clear. The lysis reaction was not allowed to proceed for more than 5 minutes. Following this, 350 µl of buffer N3 was added and mixed immediately and thoroughly by inverting 4-6 times and centrifuged for 10 mins at 13,000 rpm. The supernatant was then poured into a QIAprep 2.0 spin column and a vacuum was applied to the manifold to draw the solution through. The QIAprep 2.0 spin column was then washed through with 0.5 ml of buffer PB and the vacuum was applied again. The spin column was then washed with 0.75 ml of Buffer PE, using the vacuum to

discard the flow through. Next, the QIAprep 2.0 spin column was transferred into the collection tube and centrifuged for 1 minute at 13,000 rpm to remove any residual wash buffer. After disposing of any flow through, the spin column was inserted into a 1.5ml microtube. To elute the DNA, 50 µl of EB buffer was added to the centre of the spin column and left to stand for 1 minute, after which it was centrifuged at 13,100 rpm for 1 minute.

---

### 2.2.10 Midi-Preps

---

The midi-prep (*Qiagen*) was used to produce a high yield of plasmid. Overnight culture was harvested by centrifuging at 6000 g for 15 minutes at 4 °C in 50 ml falcon tubes. The pelleted bacteria were then completely resuspended in 4ml buffer P1. Next, 2 ml of buffer P2 was added and gently mixed by inverting the tubes several times. Once the lysate appeared viscous, the solution was incubated at room temperature for 3 minutes. A QIAfilter cartridge was placed into a new universal tube, making sure to leave space for the addition of buffer BB. Prior to this, buffer S3 had been added to the lysate and mixed thoroughly by inverting 5 times. At this point, the lysate was transferred to the QIAfilter cartridge and incubated at room temperature for 10 minutes. During this incubation period, tube extenders were inserted into each column. Once the incubation period was over, the plunger was inserted into the QIAfilter cartridge and the cell lysate was filtered into the tube. 2 ml of buffer BB was then added to the cleared lysate and was inverted 5 times to mix. Lysate was then transferred into a QIAGEN plasmid plus spin column, and tube extenders were added before attaching to the vacuum. An approximate -300 mbar vacuum was applied to the lysate until it had been completely drawn through the columns. Once this had been completed, 0.7 ml of buffer ETR was added to wash the DNA, and the column was attached underneath to allow for centrifugation at 13,000 rpm for 1 minute. The DNA was then washed again, this time with 0.7 ml of buffer PE, and was centrifuged again at 13,000 rpm for 1 minute. To ensure all the liquid had run through the column, it was then centrifuged using the previous settings and any flow through was discarded. The final step involved placing the QIAGEN plasmid plus spin column into a clean 1.5 ml tube and adding 200 µl buffer EB to the centre of the spin column to elute the DNA. This was allowed to stand for over 1 minute and was then centrifuged at 13,000 rpm for 1 minute.

---

### 2.2.11 Mega-Preps

---

A mega prep kit (QIAGEN-tip 2500) with an overall expected yield of 1.5-2.5 mg of high-copy plasmid was used to increase our plasmid yield. First, a single colony from a freshly

streaked plate was selected and used to inoculate a starter of 5-10 ml LB medium containing, in this case, ampicillin as the selection antibiotic. This was then incubated for 8 hours at 37 °C on a shaker. The starter culture was then diluted to 1/500 into a selective LB medium. A 500 ml flask of this selective LB medium was then inoculated with 500-1000µl of the starter culture and was left to grow at 37 °C for 12 to 16 hours on the shaker. Following this incubation period, the bacterial cells were harvested by centrifugation at 6000 x g for 15 minutes at 4 °C, before being resuspended in 50 ml of buffer P1. To ensure successful resuspension of the pellet, the sample was thoroughly vortexed and shaken until the whole pellet had been resuspended. 50 ml of buffer P2 was then added and mixed thoroughly by vigorous inversion 5 times, before being incubated at room temperature for 5 minutes. Next, 50 ml of buffer P3 was added and thoroughly mixed by inverting 5 times. This was then incubated on ice for a further 30 minutes. After the full incubation, the solution was centrifuged at a speed greater than 20,000 x g for 30 minutes at 4 °C and it was ensured that the supernatant was removed promptly after centrifugation. The supernatant was then centrifuged again at a speed greater than 20,000 x g for 15 minutes at 4 °C and again the supernatant was removed promptly. During the centrifugation process, a QIAGEN-tip 2500 was equilibrated by the application of 35 ml of buffer QBT, allowing the column to empty by gravity flow. The supernatant collected from the last centrifugation was then applied to the QIAGEN-tip and allowed to flow through the resin via gravity. The QIAGEN-tip was then washed using 200ml of buffer QC. Once this wash had completely flowed through, the DNA was eluted with 3 5ml of buffer QF and precipitated out by adding 24.5 ml room-temperature isopropanol. This was mixed and centrifuged immediately at a speed greater than 15,000 x g for 30 minutes at 4°C, following which the supernatant was carefully decanted. The remaining DNA pellet was then washed with 7 ml of room-temperature 70% ethanol and further centrifuged at a speed greater than 15,000 x g for 10 minutes. Again, the supernatant was carefully decanted to avoid disturbing the DNA pellet. The pellet was air dried for 10-20 minutes and re-dissolved in a suitable volume of buffer. The concentration of the DNA was measured using a nano-drop spectrophotometer (*Thermo Fisher Scientific*).

## **2.3 Western blot analysis**

### **2.3.1 Transfection of plasmids into HEK Cells**

HEK293 cells were maintained by following the manufacturer's recommendations and were seeded onto 24-well plates at a density of 50,000 cells per well. Approximately 24 hours post-plating, the cells were co-transfected with 350 ng of each plasmid and 350 ng of either sense

or antisense V5 (DPRs) using PEI as a transfection reagent (1.75 ng/ well). Opti-MEM (50  $\mu$ l/well) was used to maintain the cells in reduced serum conditions to help prevent reduced transfection efficiency. The cells were harvested 48 hours after transfection and the protein was extracted.

---

### 2.3.2 Transfection of plasmids into N2A Cells

---

N2A cells were maintained by following the manufacturer's recommendations and were seeded onto 24-well plates at a density of 75,000 cells per well. Approximately 24 hours post-plating, the cells were co-transfected with 350 ng of each plasmid and 350 ng of either sense or antisense V5 (DPRs) using PEI as a transfection reagent (2.1 ng/ well). Opti-MEM (50  $\mu$ l/well) was used to maintain the cells in reduced serum conditions to help prevent reduced transfection efficiency. The cells were harvested 48 hours after transfection and the protein was extracted.

---

### 2.3.3 Protein Extraction from a 24-well plate

---

First, all media was removed from the cells and discarded in a virkon pot and 200  $\mu$ l of sterile PBS was added to each well to wash the cells. Next, the cells were lysed with cell lysis buffer (150 mM NaCl, 1 mM EDTA, 1 mM DTT, 0.5% Triton x 100, 50 mM HEPES, 10% Glycerol, pH 7.5) and filtered, before 20  $\mu$ l of PIC (protease inhibitor cocktail, *Roche*) per 1 ml of cell lysis buffer was added. 50  $\mu$ l of the cell lysis buffer was added to each well. Following this, the cells were scraped using a P-200 pipette tip, combining wells with the same lysate into one well and making sure to pipette over the whole well several times. Once all the lysate was transferred into one well, it was transferred into its own microtube tube. Once all the different lysates had been transferred into their own microtubes, they were incubated on ice for 5 minutes. The microtubes were then centrifuged at 13,000 rpm at 4°C to pellet the cell debris. The supernatant, now containing the protein extract, was then transferred into a fresh microtube. Samples (2  $\mu$ l) were added to a 1 ml 1 x Bradford reagent and their absorbance was recorded. From this, their concentrations were calculated.

---

### 2.3.4 SDS-PAGE

---

Using a Bio-Rad Mini-PROTEAN® Tetra Cell System, the cassette was set up. Before use, the glass plates were cleaned with 70% IMS then wiped, ensuring that they were flipped and cleaned on both sides. The process was then repeated with water. The glass plates were then

placed together and clamped into the cassette, and the edges were checked to ensure that there were no leakages. Then, 12% resolving gels were prepared: 3.5 ml of distilled H<sub>2</sub>O, 2.5 ml resolving lower buffer, 4 ml of 30% acrylamide (protogel, *National Diagnostics*), 50 µl of 10% APS (10% ammonium persulphate solution) and 20 µl of TEMED (*Sigma-Aldrich*). These solutions were mixed together before adding 4.5ml of the gel solution to each cassette. 200 µl of isopropanol was then used to top off the resolving gel. The gels were left to set for approximately 10-15 minutes to polymerase. During this time, the stacking gel was prepared: 5.7 ml of distilled H<sub>2</sub>O, 2.5 ml stacking upper buffer, 1.8 ml of 30% acrylamide (protogel, *National Diagnostics*), 50 µl of 10% APS and 20 µl of TEMED (*Sigma-Aldrich*). Before adding the gel to the cassette, it was ensured that the isopropanol was removed from the resolving gel with filter paper. Next, the stacking was added (ensuring it was filled to the top of the glass plates) and the appropriate comb was inserted before the gel set. Samples were prepared by adding 5.5 µl of 4 x Laemmli buffer to each and leaving them to denature for 5 minutes at 100 °C, before adding them to the wells of the gel. The samples were then run at 150 V for 1.5 hours.

---

### **2.3.5 Transferring and Imaging the Western Blots**

---

After samples had been run, the gels were first transferred to a nitrocellulose membrane, then to a Biometra Fastblot™ analytic jena, in accordance with the manufacturer's protocol. Following the 1-hour transfer process, the membrane was transferred into block (5% Milk in TBST solution) for 1 hour. After this, it was placed into the primary antibody for overnight incubation. The following day, the membrane was washed for 5 minutes in TBST. This step was repeated 5 times, and then the membrane was placed in the secondary antibody for 1 hour. After the 1 hour incubation period, the membrane was washed for 5 minutes in TBST. This was again repeated 5 times. The membranes were then exposed to ECL (enhanced chemiluminescence) for 1 minute and imaged using a G: BOX Chemi XX6/XX9 - (High resolution gel imaging for fluorescence and chemiluminescence).

### 2.3.6 Antibodies

Table 2. 1: Antibodies used during Western Blot analysis

Primary Antibody	Company and product code	Dilution	Secondary Antibody	Company and product code	Dilution
<u><math>\alpha</math>Tubulin</u>	Santa Cruz sc-32293	1:2000	Anti-Mouse HRP conjugate	Promega W4028	1:5000
<u><math>\alpha</math>V5</u>	Invitrogen R96025	1:1000	Anti-Mouse HRP conjugate	Promega W4028	1:5000
<u><math>\alpha</math>FLAG</u>	Sigma	1:5000	Anti-Mouse HRP conjugate	Promega W4028	1:5000
<u><math>\alpha</math>SRSF1</u>	Cell signalling 8241S/ 14902S	1:1000	Anti-Rabbit HRP conjugate	Promega W4018	1:5000
<u><math>\alpha</math>GFP</u>	Abcam ab13970	1:2000	Anti-Chicken HRP conjugate	Promega G135A	1:5000
<u><math>\alpha</math>V1 V2 V3</u>	American Research Products, Inc Product #: 03-61084	1:1000	Anti-Rabbit HRP conjugate	Promega W4018	1:5000

## 2.4 Preparation of scAAV9 virus – small scale

The HEK293T cells were passed into two T175 flasks (per virus) so that flasks could be transfected the next day. A confluent T175 flask was used and was split 1:3. The cells were kept in full DMEM media before being transfected 24 hours later.

### 2.4.1 Transfection of HEK cells for small AAV9 preparation

Two 15ml falcon tubes were labelled as DNA and PEI, respectively, and 3ml of serum free medium was added to each of the tubes. 40 µg of pHelper, 20 µg 2-9 packaging plasmid and 10 µg plasmid of interest were added into the 'DNA' tube (which already contained 3 ml serum free media.) 240 µl of PEI (1 mg/ml) was then added to the 'PEI' tube (which already contained 3 ml serum free media.) Each tube was then mixed well and incubated at room-temperature for 5 minutes. The contents of the DNA tube were then added to the PEI tube, and the two components were then vortexed immediately for 10 seconds. An incubation of 15 minutes at room-temperature followed. 3 ml of the transfection complex was added to each T175 flask. The virus was then collected 48 hours later.

### 2.4.2 Harvesting AAV9 from transfected cells

Media was removed 48 hours later, and 20 ml of PBS was added to each T175 flask. The cells were then scraped off into the PBS and resuspended, before being transferred into a microtube tube. These lysates were then spun down at 500 g for 5 minutes, after which the supernatant was removed, and the pellet was resuspended in 500 µl of PBS and transferred into a new microtube tube. The lysates were vortexed and snap-frozen on dry ice (or placed in -80 °C freezer for 2-3 minutes,) then thawed in a water bath between 37 °C and 50 °C. These two steps were repeated three times overall, making sure lysates were vortexed after each thawing stage. The lysate was also passed through a 19-gauge needle to help the lysis process. The lysates were then spun down in a microtube centrifuge at maximum speed at 4 °C for 15 minutes. The supernatant was removed and transferred into a new tube. This resulting small-scale AAV virus was stored at 4 °C.

### 2.4.3 Testing Viral Capsid Integrity

Using the hood, 10 µl of the viral prep was added to 10 µl of 2 x Laemmli sample buffer and heated on a heat block at 95 °C for 5 minutes. The protocol then continued as a normal SDS-

PAGE using a 10-12% gel. Following the transfer, the primary antibody used was anti-AAV VP1+VP2+VP3 (American Research Products, Inc – Product #: 03-61084) and the secondary antibody used was anti-rabbit.

#### 2.4.4 Transduction Assay

A 12 well plate was seeded and transduced with increasing amounts of viral sample; 25  $\mu$ l, 50  $\mu$ l and 100  $\mu$ l were used per well. The transduced cells were then used 48 hours later to perform an SDS-PAGE and western blot, which indicated whether the vector was functional and whether the transgene had been packaged successfully.

## 2.5 Large scale AAV preparation

### 2.5.1 Transfection

At 16-20 hours before transfection, HEK-293 cells were seeded into 30 T175 flasks using 30 ml DMEM (10% FBS, 1% pen/strep, *Gibco*) per flask. Two confluent T175 flasks were split into a further 15 T175 flasks and their condition was visually monitored daily. The day before transfection, the 15 confluent flasks were split into 30 T175 flasks, resulting in around 80-90% confluent cells the following day. Using the table below, the required plasmids were scaled up to the amounts required for 30 flasks and the DNA aliquots were mixed.

Table 2. 2: Viral transfection ratios and amounts

Plasmid	Ratio	Amount per plate ( $\mu$ g)	Amount per 30 plate transfection ( $\mu$ g)
Helper plasmid (pHelper)	2	26	780
Packaging plasmid (pAAV2/9)	1	13	390
AAV transgene (scAAV_...)	1	13	390

15.5 ml of SF-DMEM was aliquoted into six 50 ml falcon tubes. Three tubes were marked 'DNA,' whilst the other three were marked 'PEI'. The DNA mixture of the three plasmids was then divided equally between each tube marked 'DNA'. PEI 1 mg/ml (1560  $\mu$ l) was added to each of the 'PEI' tubes (which already contained 15.5 ml of SF-DMEM) and mixed, so that the PEI to DNA ratio was maintained at a ratio of 3:1 (w/w). Contents of the 'DNA'

tubes were combined with contents from the 'PEI' tubes and the combined components were vortexed immediately for approximately ten seconds. Complexes of DNA and PEI were then left for 15 minutes at room temperature. Each of the 3 tubes of DNA-PEI complexes contained an approximate total volume of 34 ml; this depended on the volume of the DNA mix, which in turn depended on plasmid concentration. The 34 ml was enough to sufficiently transfect 10 T175 flasks. Approximately 3.3 ml of the DNA-PEI complexes was added to a flask and well distributed by gentle agitation. This was repeated for the remaining 29 flasks. Transfected flasks were transferred to the incubator. For plasmids where a transgene was used, the efficiency of transfection was monitored 24 hours later. Otherwise cells were left to produce AAV for 5 days/120 hours.

---

### **2.5.2 Harvesting and concentrating**

---

At the end of the 5-day incubation period, the supernatant was collected and transferred into clean media bottles. The total volume was equal to just under 700 ml. Benzonase (*Sigma*, 250 unit/ $\mu$ l) was added to each bottle to create a final concentration of 12.5 unit/ml, before the bottles were incubated in the 37°C incubator for 2-3 hours (mixing by inversion every 30 minutes.) The cell debris was clarified by a short centrifugation (3850 x g/ 3-5 min, Sigma 3-16PK, rotor 11180) in eight 50 ml Falcon tubes. The supernatant was transferred to the top of a Nalgene filtering unit (the protocol required two: 0.22  $\mu$ m vacuum filter – *Thermo Scientific* Nalgene Rapid-Flow filter unit) and a vacuum was applied. The clarified supernatant was then concentrated using Amicon Ultra-15 Centrifugal 100K Filters (*Millipore*). The supernatant was added onto the filter in 15 ml batches and centrifuged at 3800 g at 4°C until a volume of 27-28 ml was achieved. Six filter tubes per 30 dishes were used, starting with 10-15-minute spins which were then extended to 30-minute, 40 minute and 1-hour spins. The overall volume was subsequently split between 2 ultracentrifuge tubes for the gradient spin. This stock of the viral supernatant remained refrigerated or kept on ice throughout this entire procedure.

---

### **2.5.3 AAV purification by iodixanol density gradient**

---

The viral supernatant, which had been concentrated, was further purified using an iodixanol density gradient. For the iodixanol gradient ultracentrifugation, Quick-Seal 39 ml tubes (Beckman Coulter #344326) were used and the solutions (described in Table 2. 2) were added slowly, from the bottom upwards. This was to prevent the mixing of the gradient layers and the formation of bubbles.

Table 2. 3: Preparation of the Iodixanol Solutions

Percentage Iodixanol	Iodixanol ( <i>Optiprep-Sigma</i> ) 60% stock	5M NaCl	5 x PBS-MK (1x phosphate buffered saline (PBS), 1 mM MgCl <sub>2</sub> , and 2.5 mM KCl)	H <sub>2</sub> O	Phenol Red ( <i>Sigma Aldrich</i> )
15%	12.5ml	10ml	10ml	17.5ml	-
25%	20.8ml	-	10ml	19.2ml	100µl
40%	33.3ml	-	10ml	6.7ml	-
54%	45ml	-	-	5ml	100µl

Before setting up the gradient, the centrifuge was set to 18 °C and a falcon tube with sterile PBS was prepared, along with a tube with 70% IMS and a tube with distilled water. The iodixanol solutions were then layered using disposable syringes in the following order:

14ml concentrated virus (from the 30 plates)

1. 4 ml of 15% iodixanol
2. 9 ml of 25% iodixanol in PBS-MK buffer containing Phenol Red (slightly pink)
3. 9 ml of 40% iodixanol in PBS-MK buffer
4. 5 ml of 54% iodixanol containing Phenol Red (slightly yellow)

To ensure the tubes were completely full, they were filled up to the rim of the neck with PBS using either a 10 µl fine pipette tip or a syringe with a small gauge needle, ensuring that no bubbles were created. After this, the tubes were securely sealed using the recommended heat-sealing device so as to prevent leakage during centrifugation. The tubes were then transferred to the type 70Ti rotor (*Beckman Coulter*) and centrifuged at 69,000 RPM for 1 hour 20 minutes at 18 °C using maximum acceleration and no brake. When using the no brake option, it took approximately 3 hours for the centrifuge to stop; however, once the RPM had reduced to 10000, the soft brake option was utilised.

After centrifugation, it was the clear fraction of the 40% layer that contained the virus. To isolate these fractions, the tubes were clamped in a retort stand and a 19-gauge needle was inserted into the top of the tube to introduce air. Then, in order to extract the pure virus sample and separate it from debris and empty capsids, a standard 19-gauge (or slightly thinner) syringe needle was inserted approximately 1cm from the bottom of the tube. It was

pushed halfway into the tube with the bevel pointing upwards. The placing of the needle was such that it was towards the upper portion of the 60% iodixanol layer. It was vital to puncture the top of the tube first to allow the liquid to flow. Placing the needle in this manner thus caused slow leakage of the solution through the needle in a drop-wise fashion. The drops were collected in samples of approximately 250-500  $\mu$ l in 1.5 ml microtube. An adequate number of collection tubes (approximately 14-16) was prepared and labelled in advance. The samples collected included the entire 40% layer of the gradient and the first half of the 25% layer of the gradient. This fraction isolation process was then repeated for the second tube, which contained the second half of the viral prep. The collected fractions were then stored short term (approximately 1 month) at 4°C, until further analysis was required.

---

#### 2.5.4 Fraction analysis by SDS-PAGE

---

SDS-PAGE and SYPRO Ruby staining were used to analyse how much purified virus was in each of the fractions collected. A high concentration of purified virus was required for *in vivo* experiments to ensure the fraction was clean, with no other proteins that could interact with the biochemistry of the *in vivo* model to which it was administered. Each of the fractions was diluted with water in a 1:1 ratio (6  $\mu$ l of fraction with 6  $\mu$ l of water) and combined with 4 times Laemmli loading buffer (3  $\mu$ l,) before being boiled and resolved by SDS-PAGE on a 10% polyacrylamide gel. The capsid proteins of the AAV were then visualized via SYPRO Ruby staining, and fractions containing pure virus were pooled together for *in vivo* experiments.

Pooled AAV fractions were concentrated and desalted by centrifuging through a BIOMAX 100 Ultrafree 15 centrifugal filter device (*Millipore* UFV2BHK 10 or 40) or Amicon Ultra centrifugal filter device (*Millipore* UFC910008). The decision on which fractions to pool was made based on the analysis of the fraction resolution results seen using SDS-PAGE and SYPRO ruby staining. “High quality” fractions (containing no high molecular weight bands) were pooled into one tube, and “Low quality” fractions (dirty fractions which do contain high molecular weight bands) were pooled together in another tube.

The filter devices were placed into 50 ml falcon tubes, and 15 ml of PBS+35 mM NaCl (filtered and sterile) was added. The falcon tubes were then centrifuged at 3000 g for 15 minutes. After 1 minute, the amount of PBS that had been filtered was observed, in order to check the speed at which the solution went through the filter. It was expected that approximately 500  $\mu$ l of liquid would remain in the device.

1 x PBS + 35 mM NaCl was used as the final formulation buffer (final NaCl was 172mM). The pooled fractions were added to the top of the column which were filled to 15 ml with PBS + 35 mM NaCl. They were then spun for 15-20 mins, ensuring that the low quality and high-quality fractions remained in separate filters. After 3 minutes, the speed of filtration was checked. It was expected that the fractions should have concentrated 10-fold and that no more than 300-500  $\mu$ l should remain.

Once there was only 500  $\mu$ l in each ultrafiltration unit, the solution was pipetted up and down onto the side of the filter device whilst being careful not to pierce or touch the filter. This was done 5 times on each side of the filter. The step was required to ensure that no viral particles had become stuck to the filter.

A further 15 ml of PBS+35 mM NaCl buffer was added to the fractions and then they were spun again. This time, the spin time was increased by approximately 10 minutes, since the spin would take successively longer to reduce the sample. After 3-5 minutes, the speed of filtration was checked. The final volume needed to be under 700  $\mu$ l (generally 200-500  $\mu$ l).

PBS+35 mM NaCl buffer was added at 15 ml increments until the original volume of fractions was exchanged at least 10 times and until the desired volume of the vector in the final formulation buffer was achieved. After the final volume was achieved, the solution was pipetted up and down the filter device several times to resuspend the AAV particles. The fractions were then stored in aliquots of 20  $\mu$ l at -80 °C for storage to avoid freeze thawing of the virus. It was ensured that one aliquot was left at -20 °C for analysis.

To analyse the vector purity and its identity, SDS-PAGE and western blotting were used. The purified, concentrated and desalted vector was resolved on a 10% SDS-PAGE gel run at 150 volts for 1 hour, in duplicate. The proteins on one of the 10% gels were stained by SYPRO® Ruby dye; the other was transferred to the nitrocellulose paper and incubated with antibodies against AAV capsid proteins, before being incubated with a secondary antibody conjugated to HRP.

---

### **2.5.5 SYPRO RUBY Staining**

---

The SYPRO® Ruby protein gel stain is an ultrasensitive, luminescent stain for the detection of proteins separated by polyacrylamide gel electrophoresis. The first step of this protocol was to prepare the solutions.

## **Fix Solution**

A 500 ml fix solution was prepared: 50% methanol, 7% acetic acid.

## **Wash solution**

A 500 ml of wash solution was prepared using 10% methanol, 7% acetic acid.

The first step of the staining process was to fix the 10% acrylamide gel. Following electrophoresis, the gel was placed into a clean container, along with 100 ml of fix solution, and agitated on an orbital shaker for 30 minutes. This fix solution was then removed, and a further 100 ml of fresh fix solution was added and placed on the orbital shaker for a further 30 minutes. Following this, the used solution was poured away and 60 ml SYPRO® Ruby gel stain was added to the gel. This was then left to agitate on an orbital shaker overnight. Next, the gel was transferred to a clean container and 100 ml of wash solution was added, before leaving on the orbital shaker for 30 minutes. This transfer step was used to minimise the background staining irregularities and stain speckles on the gel. Before imaging, the gel was rinsed with ultrapure water for 5 minutes, twice, to prevent possible corrosive damage to the imager.

The gels were imaged using a G: BOX to assess the 12 viral fractions purified from the AAV production. The decision on which fractions to pool was made based on the analysis of the fraction resolution results seen using SDS-PAGE and SYPRO ruby staining. “High quality” fractions (containing no high molecular weight bands) were pooled into one tube, and “Low quality” fractions (dirty fractions which do contain high molecular weight bands) were pooled together in another tube.

## 2.6 Titration of AAV virus

The titre of an AAV virus was established using qPCR. The PCR reaction per well was as follows:

5  $\mu$ l of SYBR buffer, from small blue kit for fast PCR (*Agilent Technologies Brilliant III Ultra-Fast SYBR Green QPCR Master Mix*).

1. 1  $\mu$ l of 10  $\mu$ M Fwd primer
2. 1  $\mu$ l of 10  $\mu$ M Rev primer
3. 2  $\mu$ l of H<sub>2</sub>O
4. 1  $\mu$ l of DNA/virus sample

For the titration, a standard curve, using a linearized version of the plasmid packaged in the virus, was used by preparing 8 dilutions:  $10^{-1}$ ,  $10^{-2}$ ,  $10^{-3}$ ,  $10^{-4}$ ,  $10^{-5}$ ,  $10^{-6}$ ,  $10^{-7}$ ,  $10^{-8}$ . Three dilutions of the virus were also required:  $10^{-2}$ ,  $10^{-3}$  and  $10^{-4}$ . These viral dilutions were prepared in a hood. Next, a master mix was prepared which depended on the number of wells required. In each well, 1  $\mu$ l of each DNA dilution was pipetted, making sure to use the duplicates depicted in Table 2. 4. In two wells, water was pipetted to act as a non-template control. The plate was then taken to the hood, where 1  $\mu$ l of each virus dilution was added in accordance with the following table.

**Table 2. 4 qPCR plate design for the titration of scAAV**

<b>Standard curve (linearized plasmid)</b>		<b>Virus samples</b>									
$10^{-1}$	$10^{-1}$	$10^{-2}$	$10^{-2}$								
$10^{-2}$	$10^{-2}$	$10^{-3}$	$10^{-3}$								
$10^{-3}$	$10^{-3}$	$10^{-4}$	$10^{-4}$								
$10^{-4}$	$10^{-4}$										
$10^{-5}$	$10^{-5}$										
$10^{-6}$	$10^{-6}$	H <sub>2</sub> O (NTC)	H <sub>2</sub> O (NTC)								
$10^{-7}$	$10^{-7}$										
$10^{-8}$	$10^{-8}$										

Once the DNA/Virus was on the plate, 9  $\mu\text{l}$  of the master mix was added to each well that contained a sample. Once completed, the lid was placed onto the plate which was subsequently spun at 1750 x g for 1 minute. It was then placed in the BioRad qPCR machine (CFX96 real-time system C1000 thermal cycler,) which ran using the following programme:

1. 95°C for 5 minutes
  2. 95°C for 10 seconds
  3. 60°C for 30 seconds
  4. Plate read
  5. Go to 2 (39 x)
- 
1. 65°C for 31 seconds
  2. 65°C for 5 minutes +0.5°C/cycle, Ramp 0.5°C/s
  3. Plate read
  4. Go to 7 (60 x)

Once the programme was completed, the results were exported and BioRad CFX manager was used to view the results and to check duplicates and melting curves for simple amplification.

This calculator provides instructions on how to dilute a DNA stock solution to obtain specific DNA copy number per  $\mu\text{L}$ .

1. If you know that the weight of your DNA (molar mass per bp) is different from the average weight of DNA basepair, change the value. Otherwise just use the default value.
2. Choose the organism your DNA originates from, or choose "Custom DNA fragment". If you choose a custom fragment, fill in the length of the fragment.
3. Fill in the measured concentration of your stock solution.
4. Fill in the desired concentration (copies/ $\mu\text{L}$ ) and volume.

The application will automatically calculate the pipetting volumes required for the desired dilution.

Molar mass per base pair:  (g/mol)/bp

Custom DNA fragment

Fragment length (nt):

Molar mass(g/mol):

Copies/ng:

*Escherichia coli*  
 Bacteriophage lambda  
 *Drosophila melanogaster*  
 *Homo sapiens* (human)  
 Custom DNA fragment

---

Stock solution

Measured concentration (ng/ $\mu\text{L}$ ):

Copies/ $\mu\text{L}$  in stock:

Molarity of stock:  nM

**Figure 2. 1:** Thermofisher DNA copy number calculator

To do this, the ThermoFisher DNA copy number calculator (ThermoFisher, 2018) was used (Figure 2. 1). The “Custom DNA fragment” option was highlighted and the size of the plasmid (in bp) was inserted into the fragment length box. The measured concentration (ng/μl) was also inserted into the online form. The copy number was copied into excel and converted into a scientific number, then used in the CFX software (settings -> plate set up -> view/edit plate). All the standard wells were selected, and in the “sample type” box, “standard” was selected. In the 10<sup>-1</sup> wells of the standard, in the box “number of replicates”, “load” was selected, and the scientific number was pasted and divided by 10 (because it was 10 X diluted). For example, if the number was 4.32 x 10<sup>9</sup>, 4.32 x 10<sup>8</sup> was introduced. This method was repeated for each of the standard replicates, decreasing the exponential one by one: 4.32 x 10<sup>8</sup>, 4.32 x 10<sup>7</sup>, etc. Once completed, “Apply changes” was selected.

At this point, the standard curve was reviewed to ensure that the R<sup>2</sup> value was at least 0.98. The data were then exported (export -> export all data sheets -> excel 2007) and saved into several Excel files in the location of choice. The file “Quantification plate view results” was opened and the mean was calculated for each replicate in the viral sample wells. The results, in VGs/μl, were multiplied by 1000 for VGs/ml. Next, each of the 3 viral samples was multiplied by their corresponding dilution factor (x 100 for the 10<sup>-2</sup>, x 1000 for the 10<sup>-3</sup>, x 10,000 for the 10<sup>-4</sup>). The mean of these 3 values was calculated to give the overall AAV titre.

This q-PCR method was also used for analysing the bio-distribution of each virus within different tissues of virus treated mice.

## **2.7 Titration of AAV via FACS (Fluorescence-activated cell sorting)**

The specialised type of flow cytometry, fluorescence-activated cell sorting (FACS), is a method of sorting heterogeneous mixtures of cells into two or more containers, cell by cell. In this case, it was used to separate GFP labelled cells and non-labelled cells. The procedure is based upon the fluorescent characteristics and specific light scattering of each cell, providing fast, objective and quantitative analysis of fluorescent signals from individual cells, as well as physical separation of cell types. The individual cells pass a laser beam in a single file, allowing the fluorescence of each cell to be measured. A nozzle then forms small droplets using vibration, each of which contains a single cell. This is given a positive or negative charge, depending on whether the cell is fluorescing (for example expressing GFP.) A strong electric field then defects the variously charged droplets into separate containers, so that each container has a homogeneous population of cells.

## 2.8 Animal work

### 2.8.1 Ethics statement

All animal *in vivo* experiments were approved by the University of Sheffield Ethical Review Sub-Committee, the UK Animal Procedures Committee (London, UK) and performed according to the Animal (Scientific Procedures) Act 1986, under the Project License P31C8CC9D. Both the C57bl/6 and the C9-500 (Liu *et al.*, 2016) mice were maintained in a controlled facility in a 12h dark/12h light photocycle (on at 7am/ off at 7pm) with free access to food and water. The ARRIVE (Animal Research: Reporting of *In vivo* Experiments) guidelines have been followed in reporting this study (Kilkenny *et al.*, 2013).

### 2.8.1 Postnatal day 1 cisterna magna injections

On the day of birth, the pups were tattooed to allow for identification during the *in vivo* mouse study. To promote survival of the pups in the study it was ensured that they were of a large enough size. The pups were first removed from the mother and placed on the warming plate to ensure that their temperature did not drop throughout the procedure. Before starting the procedure, the Hamilton 700RN syringe was filled with just over 5µl of virus/PBS. The induction chamber was filled with isoflurane by setting the oxygen flow rate to 4L/min and isoflurane to 5%. The mouse pup receiving the injection was then placed inside the chamber until unconscious. Before removing the pup from the chamber, isoflurane was reduced to 1.5L/minute with a flow of 0.5% through the face mask. The pup was then transferred to the face mask and positioned over an infrared light (to visualize the cisterna magna through the skin.) The pup was kept secure with the right hand, while the left hand was used to manoeuvre the needle into the cisterna magna. The virus/PBS was then injected into the mouse at a rate of 1µl/ minute. Once the injection was finished, the needle remained in the cisterna magna for approximately 30 seconds. After completion, breathing was monitored for a few minutes before returning the pup to its mother.

### 2.8.2 Post-natal day 40 cisterna magna injections

Adult mice were first anaesthetised by placing them in an induction chamber and setting the oxygen flow rate to 4L/min and isoflurane to 5%. Once the breathing of the mouse had reduced to 30 breaths/ minute, it was affixed to a stereotaxic frame. Oxygen flow rate was

then reduced to 0.5L/min and isoflurane to 2% and switched over to the output mask. Around 10 µl lignocaine (a local anaesthetic) was injected subcutaneously between the mouse's ears. A 1 cm vertical incision was made in the skin and muscle between the ears and a colibri was inserted to hold back the muscle and skin layers. The Virus/PBS was loaded into a Hamilton syringe, which was moved into position, before 10µl of the virus/PBS was injected at a rate of 2 µl/minute into the cisterna magna of the mouse. After the injection had been completed, a wait of 1 minute was required to allow the substance to disperse from the injection site. The needle was then slowly withdrawn, and the skin and muscle layers were sutured back together. The mouse was then allowed to recover in an incubator at 35 °C and monitored until it was fully ambulatory.

---

### **2.8.3 Rotarod analysis**

---

#### **C57Bl/6**

Mice in the 6-month cohort had one training session on three consecutive days at postnatal day 60. Rotarod performance was assessed once every two weeks from post-natal day 70 until the animals were sacrificed. Mice were placed on the rotarod for up to 5 mins as the machine accelerated from 3 to 37 revolutions per minute. Performance was measured by observing how many seconds the mouse could remain on the rotarod.

#### **FVB/NJ-Tg (C9orf72) 500Lpwr/J**

Mice had one training session on three consecutive days at postnatal day 60. During these training sessions, mice were placed on the Rotarod for 3 minutes at a constant speed of 5 rpm. Rotarod performance was then assessed weekly from postnatal day 67 until the animals were sacrificed at postnatal day 90. Mice were placed on the Rotarod, which first accelerated from 15 to 33 rpm in 10 seconds, then 33 rpm to 15 rpm in 10 seconds. The direction of the rod was then inverted, and the procedure repeated (15 to 33 rpm in 10 seconds; 33 to 15 rpm in 10 seconds.) The direction was reversed again, and so on. The trial ended after 110 seconds. Each animal ran 3 trials. The animals were left to rest for 3 minutes in their home cage with water in between the trials.

---

### **2.8.4 Weight analysis**

---

All mice were weighed weekly throughout the experiment to measure overall condition following their treatment.

---

### **2.8.5 Tissue collection**

---

The mice were sacrificed via terminal anaesthesia with pentobarbital and then perfused with sterile PBS. Once the mouse was successfully perfused, the following tissues were harvested: brain, spinal cord, liver, spleen, gastrocnemius muscle and heart. The organs were dissected, placed in sterile 1.5ml microtubes and directly frozen in liquid nitrogen. Half of the animals in each treatment group had their brains and cervical spinal cords removed and post-fixed in 4% PFA for further histological analysis. These tissues were kept in 4% PFA for 24 hours, before placing in a 30% sucrose solution for a further 24 hours. The brains and spinal cords were then mounted in OCT, frozen on dry ice and kept at -20 °C until they were required for sectioning.

## **2.9 Tissue preparation and histological analysis**

---

### **2.9.1 Tissue sectioning and staining**

---

Frozen cervical spinal cords and whole mouse brains were sectioned into 20 µm thick slices using a cryostat at -20 °C. The slices were directly fixed onto charged slides using a 5-slide series method, with 6 spinal cord sections on each slide. When sectioning the brain, 6 brain sections were also placed on each slide.

#### **Nissl Staining**

Slides were first placed in 95% ethanol for 5 minutes, then moved into 70% ethanol for 1 minute, then rinsed in water. Filtered 1% cresyl fast violet was used to cover the slides for 15 minutes, after which sections were differentiated in 0.25% acetic acid for 4 seconds. The slides were then rinsed in 100% ethanol and fixed in Xylene for 1 minute. DPX mounting media was used to mount the slides, which were then placed in the oven overnight at 40 °C. The slides were then scanned using a Hamamatsu NanoZoomer S60 digital slide scanner. Motor neurons were counted using the NDP.view2 viewing software.

#### **Fluorescence Staining**

Tissue sections were first warmed to room temperature. The sections were then fixed in 95% alcohol for 5mins before being washed in water for 1 minute. Another wash in TBS for 5mins was then required. A pressure cooker (Antigen Access Unit A. Menarini Diagnostics) antigen retrieval step was then used using a pH 6 citrate buffer. Following the antigen

retrieval step, the tissue sections were washed in water for 2 minutes and were then placed in 0.2% glycine in PBS for 15 minutes. A stock of normal serum was made up by adding 3 drops stock normal serum (*VECTASTAIN® Elite ABC-HRP Kit, Peroxidase*) to 10 ml TBS. The sections were then incubated in normal serum (*VECTASTAIN® Elite ABC-HRP Kit, Peroxidase*) for 30 minutes. The sections were drained by wiping around the edges of the section, but the normal serum was not washed off. The sections were then incubated with 300 µl primary GFP antibody (*Invitrogen GFP Polyclonal Antibody #A-11122, Abcam ab13970, Sigma-Aldrich Monoclonal ANTI-FLAG® M2 antibody F1804*) diluted in TBS for 1 hour at room temperature. Once completed, slides were washed in TBS for 2 times 5 minutes. Sections were then incubated in Vector RTU biotinylated secondary antibody for 30 minutes. After the secondary antibody step, the sections were washed in TBS for 5 minutes. Streptavidin conjugated 488 was then prepared to the required fluorochrome and sections were incubated for 1 hour in the dark. The sections were then washed one last time in TBS (with a quick wipe around the sections) before being mounted in Vectashield with DAPI. Images were viewed using the Nikon microscope and the IN-CELL 2000 (GE).

### **DAB staining**

Tissue sections were first warmed to room temperature. The sections were then fixed in 95% alcohol for 5mins before being washed in water for 1 minute. Another wash in TBS for 5mins was then required. The sections were then blocked in endogenous peroxidase in 3% H<sub>2</sub>O<sub>2</sub>/methanol for 20 minutes. A pressure cooker (*Antigen Access Unit A. Menarini Diagnostics*) antigen retrieval step was then used using a pH 6 citrate buffer. Following the antigen retrieval step the tissue sections were washed in water for 2 minutes whilst a stock of normal serum was made up by adding 3 drops stock normal serum (*VECTASTAIN® Elite ABC-HRP Kit, Peroxidase*) to 10 ml TBS. The sections were then incubated in normal serum (*VECTASTAIN® Elite ABC-HRP Kit, Peroxidase*) for 30 minutes. The sections were drained by wiping around the edges of the section, but the normal serum was not washed off. The sections were then incubated with 300 µl primary SRSF1 antibody (*Cell signalling 8241S/ 14902S*) diluted in TBS for 1 hour at room temperature at a 1:1000 dilution. Once completed, slides were washed in TBS for 2 times 5 minutes. Sections were then incubated in anti-rabbit Vector RTU biotinylated secondary antibody (*VECTASTAIN® Elite ABC-HRP Kit, Peroxidase*) for 30 minutes. After the secondary antibody step, the sections were washed in TBS for 2 times 5 minutes. Sections were then incubated in ABC reagent for 30 minutes and again washed in TBS twice for 5 minutes. The reaction was then visualized using DAB and incubated for 10 minutes. Sections were then rinsed with distilled water followed

by 5 minutes in tap water and counter stained with Harris haematoxylin for 1 minute. Again, the tissue was washed in tap water for 1 minute and then placed in Scott's tap water for 10 seconds. The sections were then washed one last time in tap water before being dehydrated through 70%, 95% and 100% alcohols. The sections were then placed in xylene and mounted using DPX mounting media and then placed in the oven overnight at 40°C. The slides were then scanned using a Hamamatsu NanoZoomer S60 digital slide scanner. Tissue was then analysed using the NDP.view2 viewing software.

A negative control was prepared for each batch of SRSF1 staining in the same way but instead of adding a primary antibody TBS was added for this step. The positive control in this case was the PBS treated tissue.

### **Haematoxylin and Eosin (H&E) staining**

Tissue sections were rehydrated through the graded alcohols, each for 2 minutes: 100% twice, 95% and 70% and then into water. The slides were then placed into Harris haematoxylin for 2 minutes and then washed with tap water. The sections were then differentiated in 1% acid/alcohol for approximately 10-15 seconds, using a microscope to review differentiation. Again, the sections were washed in tap water for 2 minutes and then put to 'Blue' in Scott's Tap water for 2 mins. Once again, the sections were washed in tap water for 2 minutes and then stained in 1% eosin for 5 minutes. Finally, the sections were briefly washed in tap water and dehydrated through the graded alcohols, 70%, 95%, 100% twice, each for 2 minutes. The sections were then placed into xylene and mounted using DPX mounting media. The slides were then scanned using a Hamamatsu NanoZoomer S60 digital slide scanner. Tissue was then analysed using the NDP.view2 viewing software.

---

### **2.9.2 DNA Extraction**

---

To extract the DNA from the mouse tissue, the SIGMA GenElute Mammalian Genomic DNA miniprep kit was used. We used the mammalian tissue preparation protocol to prepare our tissue samples. Once the DNA was extracted, the Nanodrop was used to review how much DNA was extracted from the tissue samples. These samples were then diluted to a concentration of 10 ug/ $\mu$ l.

---

### 2.9.3 RNA Extraction

---

The tissue samples were lysed in 200 µl purezol (trizol) and ground until homogenized. The samples were then incubated at room temperature for 10 minutes, before being centrifuged at 12000 g for 10 minutes at 4 °C. The trizol was transferred to a fresh tube and 40 µl chloroform was added, after which the samples were shaken for 15 seconds. The samples were then incubated at room temperature for another 10 minutes. After this, they were centrifuged at 12000g for 10 minutes at 4 °C and the upper layer was transferred to a new tube. An equal volume of isopropanol, plus 1 µl glycogen, was then added and the sample was incubated for 20 minutes at room temperature. Following this incubation period, the samples were then centrifuged for 15 minutes at 13100 g at 4°C and then the isopropanol layer was removed. 500 µl of 70% ethanol (using DEPC water) was added and samples were then centrifuged once more at 13100g for 10 minutes at 4°C. The supernatant was removed and then the sample was pulsed once again in the centrifuge so that any supernatant residue was also removed. The samples were then left to air dry for 10 minutes. The samples were then made up into a 25 µl reaction using: 22 µl DEPC water, 2.5 µl 10 x buffer (*Thermo Fisher Scientific*) and 0.5 µl enzyme (*FastDigest Thermo Fisher Scientific*). These reactions were then incubated first for 30 minutes at 37 °C, then for 10 minutes at 75 °C. Once completed, the RNA concentration was measured using the Nanodrop.

### Reverse transcription and cDNA Preparation

To synthesise the RNA into cDNA, we used the following: 2 ug RNA, 1 µl dNTPs (*Agilent*), 1 µl of 40 µM dN6 (*Sigma*) plus 13 µl of DEPC water. This reaction was prepared in duplicate to allow for the preparation of a -RT reaction and a +RT reaction. The -RT reaction included: 13 µl of cDNA, 4 µl 5 x FS buffer (*Invitrogen*), 2 µl 0.1M DTT (*Invitrogen*) and 1 ul M-MLV reverse transcriptase (*Invitrogen*). The +RT reaction included: 13 µl of cDNA, 4 µl 5 x FS buffer (*Invitrogen*), 2 µl 0.1M DTT (*Invitrogen*) and 1 µl DEPC water. These 2 reactions were carried out in a thermal cycler under the following conditions:

- |         |                 |
|---------|-----------------|
| 1. 25°C | 10:00 (min:sec) |
| 2. 42°C | 60:00           |
| 3. 85°C | 5:00            |
| 4. 10°C | ∞               |

Following the reaction, 40 µl of DEPC water was added to the cDNA, which was then stored in the freezer at -20 °C.

---

#### 2.9.4 Protein Extraction

---

To lyse the harvested tissue, a 1 x working reporter lysis buffer was prepared by diluting 5 x reporter lysis buffer (*Promega*) with a protease inhibitor cocktail (20  $\mu$ l per ml) and PMSF (with a final concentration of 1-2 mM). The tissue, which had been snap frozen in liquid nitrogen, was immersed in 600  $\mu$ l of 1 x working reporter lysis buffer and 7-10 1.4mm Zirconium Oxide beads (*Precelly* P000927-LYSK0-A.0) and homogenized in a *Precelly* Evolution Homogenizer at 5500 rpm for 2 x 30 seconds. The samples were then left on ice for 10 minutes before again being homogenized at 5500 rpm for 2 x 30 seconds. The tissue, along with the beads, was then centrifuged at 17,000 g for 10 minutes at 4 °C. The cell lysate (supernatant) was then transferred to a new tube and the protein concentration was determined using a Bradford assay.

---

#### 2.9.5 Poly-GP MSD ELISA Assay

---

Mouse tissue was prepared for the MSD DPR (dipeptide repeat) assay by extracting the protein at a concentration of 2  $\mu$ g/ $\mu$ l. First the organ tissue was lysed using 1 x working reporter lysis buffer. The buffer was prepared by diluting a 5 x reporter lysis buffer (*Promega*) with a protease inhibitor cocktail (20  $\mu$ l per ml) and PMSF (with a final concentration of 1-2 mM). The tissue, which had been snap frozen in liquid nitrogen, was immersed in 600  $\mu$ l of 1 x working reporter lysis buffer and 7-10 1.4mm Zirconium Oxide beads (*Precelly* P000927-LYSK0-A.0) and homogenized in a *Precelly* evolution homogenizer at 5500 rpm for 2 x 30 seconds. The samples were then left on ice for 10 minutes before again being homogenized at 5500 rpm for 2 x 30 seconds. The tissue, along with the beads, was then centrifuged at 17,000 g for 10 minutes at 4 °C. The cell lysate (supernatant) was then transferred to a new tube and the protein concentration was determined using a Bradford assay. In this case the protein concentration was diluted to 2  $\mu$ g/ $\mu$ l ready for the MSD DPR assay.

Dr Adrian Higginbottom completed the following MSD DPR assay protocol using the prepared tissue. First, a poly GP Capture antibody was used to detect dipeptide repeat proteins in mouse tissue. The amount of capture antibody solution was calculated based on the number of wells required during the experiment. In each well, 30  $\mu$ l of capture antibody was added to each experimental well in a 96-well plate. The plate was then sealed with adhesive sealing sheets and wrapped in foil to protect the bottom of the plate. The plate was then placed on a shaker at 1250 rpm for 15 seconds, ensuring that the bottom of each well was coated evenly. The shaker plate speed was reduced to 600 rpm for 15 minutes and the

plate was incubated overnight at 4 °C in the fridge. Following overnight incubation, the antibody solution was removed, and the plate was tapped dry. The wells were washed three times with 150 µl wash buffer (TBS – Tween 0.2%) per well, ensuring not to leave the wash buffer on for longer than 5 min. The wash buffer was removed, and the plate was tapped dry. 150 µl blocking buffer was then added per well using a multi-channel pipette and the plate was sealed with adhesive sealing sheets and wrapped in foil to protect the bottom and incubated for 2 hours shaking at 600 rpm at room temperature. The blocking buffer was then removed. The plate was then washed three times with 150 µl wash buffer per well, after each round the wash buffer was removed and the plate was tapped dry. 25 µl of EC buffer was then added to each well and 50 µl of the prepared 2 µg/µl protein samples were added to each of the experimental wells. The plate was then sealed with adhesive sealing sheets, wrapped in foil to protect the bottom and incubated overnight shaking at 600 rpm at 4 °C.

The detector antibody solution was then made up by adding detector antibody to the blocking buffer and mixed by vortexing for 5 seconds at a low speed. The protein samples were then removed from the plate and the plate was washed three times with 150 µl wash buffer and after each round it was removed immediately. 25 µl of detection antibody was then added per well. The plate was again sealed, wrapped in foil and incubated for 2 hours, shaking at 600 rpm at room temperature. Again, the antibody was removed, and the plate was washed three times with 150 µl of wash buffer per well. After each round, the wash buffer was removed immediately. Each well was then incubated with 25 µl of streptavidin sulfotag per well and the plate was sealed, wrapped in foil and incubated for 1 hour shaking at 600 rpm at room temperature.

After incubation, the streptavidin sulfotag was removed. The plate was washed three times with 150 µl of wash buffer per well. After each round, the wash buffer was removed immediately and tapped dry. Finally, 150 µl of 1 x read buffer was added per well and the plate was read immediately on the MSD plate reader.

## 2.10 Statistical analysis

Syngene: Gene Tools was used to quantify the western blot images and then GraphPad Prism was used to analyse the quantification. Data underwent a 1-way ANOVA and samples were compared to the mean of each other before being plotted on a bar graph. [NS = Nonsignificant; \* =  $p < 0.05$ ; \*\* =  $p < 0.01$ ; \*\*\* =  $p < 0.001$ ; \*\*\*\* =  $p < 0.0001$ ].

Rotarod and weight data were analysed using GraphPad Prism software ®, as was the biodistribution and Nissl staining data.

## CHAPTER 3 – Designing and Developing Viral Vectors for SRSF1-Targeted Gene Therapy Approaches in Mice

### 3.1 Aim

Amyotrophic lateral sclerosis (ALS) is an adult onset disease characterised by the selective process of motor neuron cell death, leading to progressive paralysis that is eventually fatal, usually within 2-5 years. It is accepted that hexanucleotide repeat expansions in the non-coding region of the *C9ORF72* gene are the most common cause of ALS and frontotemporal dementia (FTD). Previously, the team has identified that the nuclear export factor SRSF1 selectively drives the nuclear export of *C9ORF72* repeat transcripts, leading to the production of toxic dipeptide repeat proteins (DPRs) in the cytoplasm. Partial depletion of SRSF1 or expression of a point mutant of SRSF1 (an engineered protein that retains the ability to bind the *C9ORF72* repeat transcripts but fails to interact with NXF1, which drives the nuclear export of mRNAs through nucleopores) has been shown to promote *C9ORF72*-ALS patient-derived neuron survival *in vitro* and prevent neurodegeneration-associated locomotor deficits *in vivo* in *C9ORF72*-ALS *Drosophila* (Hautbergue *et al.*, 2017).

The aims of the work described in this chapter were to evaluate the therapeutic safety and efficacy of the above neuroprotective strategies using two gene-therapy approaches involving either depletion of SRSF1 or expression of the SRSF1-m4 point mutant using self-complementary adeno-associated virus serotype 9 (scAAV9), and to test their functionality *in vitro* before producing large amounts of virus for delivery into mice.

### 3.2 Therapeutic approach 1: Depletion of SRSF1

During this study we used two different therapeutic approaches to manipulate the expression of the nuclear export protein SRSF1. First, I will describe the therapeutic strategy in which SRSF1 is partially depleted using an shRNA. For this part of the project, we inserted shRNA into an scAAV-KASPAR plasmid prior to producing scAAV9 viruses which had previously been used in SOD1 ALS studies (Iannitti *et al.*, 2018) and the efficacy in driving transgene expression in several mouse models was already known. The dose and route of administration of scAAV9 virus produced using this plasmid was also already investigated, and toxicology studies had already been undertaken (Iannitti *et al.*, 2018). Below, I will describe how the shRNA targeting SRSF1 was designed and cloned, and how its functionality and overall effects on DPR production were tested.

---

### 3.2.1 Design of shRNAs for SRSF1 knockdown

---

The overall aim of this project was to design shRNA that would silence the expression of endogenous SRSF1 and therefore disrupt the nuclear export of the pathological *C9ORF72* repeat expansions in the central nervous system. To achieve this, the initial shRNA design was conducted using the Invitrogen Block-it RNAi designer (*Invitrogen Block-it RNAi designer*, 2021). The input sequence was collected from the NCBI database using accession number 'NM\_006924.4,' which corresponds to the human transcript variant 1 sequence of the SRSF1 mRNA. We used the shortest variant to ensure that we targeted all SRSF1 isoforms. The Open Reading Frame (ORF) was selected as the target design region, whilst the GC content was set at the default values of 35-55%. The output sequence strand orientation was set to sense-loop-antisense and the selected loop sequence was set to CGAA.

BLOCK-iT™ RNAi Designer is a web tool that was used to design and order custom synthetic siRNA, Stealth RNAi™ siRNA, shRNA, or miR RNAi oligonucleotides from nucleotide target sequences. Once the target sequence is entered and the design parameters set, the designer generates several RNAi designs ranked by their probability of successful gene knockdown. The top 8 output sequences for the human transcript, ranked by likelihood of off-target efficiency, are provided in Table 3. 1.

**Table 3. 1: Human SRSF1 shRNA (NM\_006924.4)**

Number	Target Sequence	Region	GC %	Rank (out of 5)
1	GCTGATGTTTACCGAGATG GC	ORF	52.39	3.5
2	GTGGAGTTTGTACGGAAA GAA	ORF	42.86	3
3	GGAGTTTGTACGGAAAGA AGA	ORF	42.86	4.5
4	GAGTTTGTACGGAAAGAA GAT	ORF	38.1	3
5	GGAAAGAAGATATGACCT ATG	ORF	38.1	3.5
6	GAAAGAAGATATGACCTA TGC	ORF	38.1	3.5
7	GATCTCATGAGGGAGAAA CTG	ORF	47.62	3
8	AGGGAGAAACTGCCTACA TCC	ORF	52.39	3

The mouse transcript variant 1 of SRSF1, accession number NM\_173374.4, was then used and the same parameters were applied to the sequence (Table 3. 2).

**Table 3. 2: Mouse SRSF1 shRNA (NM\_173374.4)**

Number	Target Sequence	Region	GC %	Rank (out of 5)
1	AGGGAGAAACTGCCTACAT CC	ORF	52.39	3.5
2	GCCTACATCCGGGTAAAG TT	ORF	47.62	3
3	GGGCCCAGAAGTCCAAGTT AT	ORF	52.39	4.5
4	GGCCCAGAAGTCCAAGTTA TG	ORF	52.39	3
5	GCCCAGAAGTCCAAGTTAT GG	ORF	52.39	3.5
6	GGAAGATCTCGATCTCGAA GC	ORF	52.39	3.5
7	GAAGCCGTAGCAGAAGCA ACA	ORF	52.39	3
8	GCAGAGGATCACCACGCTA TT	ORF	52.39	3

The highlighted sequences indicate the sequences that were found in both the human and mouse SRSF1 transcripts. As can be seen from Table 3. 1 and Table 3. 2, there is only one sequence common to both mouse and human variants. Using a sequence that is common to both species is ideal, as the aim is to target both human and mouse SRSF1. In anticipation of the *in vivo* investigation being successful, it is expected that the shRNAs will not need to be redesigned to be effective in a non-human primate model and in human clinical trials.

As only one common sequence was found, additional sequences were searched for. The highly conserved region of human *SRSF1* 448-750 (3' end of the coding region) was taken and used in the same program again (Table 3. 3):

5'-

GCTGATGTTTACCGAGATGGCACTGGTGTCTGAGTTTGTACGGAAAGAAGATATGA  
 CCTATGCAGTTCGAAAAGTGGATAACACTAAGTTTAGATCTCATGAGGGAGAAAAGTGC  
 CTACATCCGGGTTAAAGTTGATGGGCCAGAAAGTCCAAGTTATGGAAGATCTCGATCT  
 CGAAGCCGTAGTCGTAGCAGAAGCCGTAGCAGAAGCAACAGCAGGAGTCGCAGTTAC  
 TCCCAAGGAGAAGCAGAGGATCACCACGCTATTCTCCCCGTCATAGCAGATCTCGCTC  
 TCGTACATAA-3'

**Table 3. 3: shRNA targeting both human and mouse SRSF1 using Block-IT designer**

Number	Target Sequence	GC %	Rank (out of 5)
1	GCTGATGTTTACCGAGATG GC	52.39	3.5
2	GGAGTTTGTACGGAAAGA AGA	42.86	4.5
3	GAAAGAAGATATGACCT ATG	38.1	3.5
4	GAAAGAAGATATGACCTAT GC	38.1	3.5
5	GCCTACATCCGGGTTAAAG TT	47.62	3.5
6	GGGCCAGAAAGTCCAAGTT AT	52.39	4.5
7	GGCCAGAAAGTCCAAGTTA TG	52.39	3.5
8	GCCAGAAAGTCCAAGTTAT GG	52.39	4
9	GGAAGATCTCGATCTCGAA GC	52.39	4.5
10	GCAGAGGATCACCACGCTA TT	52.39	5.0

The Block-IT RNA designer (Table 3. 3) indicates that, of these 10 shRNAs, shRNAs 1, 2, 5, 6, 9 and 10 (highlighted) are conserved and most common to both human and mouse SRSF1 and are predicted to be the most efficient. shRNA 10 is fully conserved in both mouse

and human SRSF1 and has the highest score with 5.0. We took this shRNA as one of our three choices, along with 9 and 6.

These sequences were then used to create their complementary antisense sequences to confirm that our shRNA choices would be the most effective. siSPOTR analysis was used, which is an RNAi design tool that produces candidate siRNAs and shRNAs with the lowest off-targeting potential for a given target transcript. siSPOTR contains a function enabling the design of minimal off-targeting shRNA sequences irrespective of potential efficacy (Boudreau *et al.*, 2013). Again, we used the region h*SRSF1* 448-747 (3' end CDS) which is highly conserved within mouse SRSF1 and design shRNA.

**Table 3. 4: siSPOTR analysis of the most efficient shRNAs against Human and Mouse SRSF1 (Antisense)**

shRNA	Anti-Sense Strand	POTS (MOUSE)	POTS (HUMAN)	Seed Sequence
1	GCCATCTCGGTAACATCAGC	355.351	463.716	CCATCTC
2	TCTTCTTCCGTACAACTCC	501.411	588.488	CTTCTTT
3	CATAGGTCATATCTTCTTCC	96.137	149.126	ATAGGTC
4	GCATAGGTCATATCTTCTTTC	140.373	167.649	CATAGGT
5	AACTTTAACCCGGATGTAGGC	390.256	526.984	ACTTTAA
6	ATAACTTGGACTTCTGGGCC	221.397	339.052	TAACTTG
7	CATAACTTGGACTTCTGGGCC	237.138	351.458	ATAACTT
8	CCATAACTTGGACTTCTGGGC	159.58	215.339	CATAACT
9	GCTTCGAGATCGAGATCTTCC	41.326	41.3938	CTTCGAG
10	AATAGCGTGGTGATCCTCTGC	21.324	22.5396	ATAGCGT

In siSPOTR, shRNA sequences are given a potential of off-targeting score (POTS), a score of  $\leq 30$  is considered ideal. Higher scores suggest a high likelihood of an off-target effect. This method gave only one sequence with a POTS score lower than 30, which was shRNA 10 (Table 3. 4).

Here is the siSPOTR analysis of shRNAs 1, 2, 5, 6, 9 and 10 (common human/ mouse SRSF1 and predicted most efficient). The results were compared between Table 3. 3 and Table 3. 4 to create our final shortlist. Table 3. 4 shows that shRNA sequences 1 and 2 have very high POTS scores and are therefore likely to have a greater potential of causing off-target effects and so were excluded from our shortlist. Sequences 9 and 10 had the lowest POT scores and so were used as two of our final shRNA sequences. shRNA 6 was chosen as the third choice due to its higher rank (Table 3. 3) and its lower POTS score (Table 3. 4) when compared with shRNA 5. The human-mouse *SRSF1* alignment was used to visualise where the designed shRNAs were positioned on the gene (Figure 3. 1).

### Alignment human (NM\_006924.4) and mouse (NM\_173374.4) SRSF1

```

hSRSF1  ATGTCGGGAGGTGGTGTGATTCGTGGCCCCGCAGGGAACAACGATTGCCGCATCTACGTG  60
|||||
mSRSF1  ATGTCGGGAGGTGGTGTGATCCGTGGCCCCGGGGGAACAACGACTGCCGCATCTACGTG  60

hSRSF1  GGTAACCTACCTCCAGACATCCGAACCAAGGACATTGAGGACGTGTTCTACAAATACGGC  120
|||||
mSRSF1  GGTAACCTACCTCCGATATCCGAACCAAGGACATCGAGGACGTGTTTACAAATACGGC  120

hSRSF1  GCTATCCGCGACATCGACCTCAAGAATCGCCGCGGGGGACCGCCCTTCGCCTTCGTTGAG  180
||
mSRSF1  GCCATCCGCGACATCGACTGAAGAACCGCCGCGGGGGACCGCCCTTCGCCTTCGTTGAG  180

hSRSF1  TTCGAGGACCCGCGAGACGCGGAAGACGCGGTGTATGGTCGCGACGGCTATGATTACGAT  240
|||||
mSRSF1  TTCGAGGACCCGCGAGACGCGGAAGATGCGGTGTACGGTCGCGACGGCTACGACTACGAC  240

hSRSF1  GGGTACCGTCTGCGGGTGGAGTTTCTCGAAGCGGCCGTGGAACAGGCCGAGGCGCGGC  300
||
mSRSF1  GGCTACCGCTGCGGGTAGAGTTTCCCCGAAGCGCCGCGGGACCGGCCGAGGCGCGGC  300

hSRSF1  GGGGGTGGAGGTGGCGGAGCTCCCCGAGGTGCTATGGCCCCCATCCAGGCGGTCTGAA  360
|||||
mSRSF1  GGGGGTGGAGGCGCGGCCGCCGAGAGGCCGCTATGGCCCCCGTCCAGGCGGTCCGAG  360

hSRSF1  AACAGAGTGGTGTCTCTGGACTGCCTCCAAGTGAAGTTGGCAGGATTTAAAGGATCAC  420
|||||
mSRSF1  AACAGAGTGGTGTCTCTGGACTGCCTCCGAGTGAAGCTGGCAGGACTTAAAGGATCAC  420

hSRSF1  ATGCGTGAAGCAGGTGATGTATGTTATGCTGATGTTTACCGAGATGGCACTGGTGTCTGT  480
|||||
mSRSF1  ATGCGTGAGGCAGGTGATGTATGTTACGCTGATGTTTACCGAGATGGCACTGGTGTCTGT  480

hSRSF1  GAGTTTGTACGGAAGAAGATATGACCTATGCAGTTCGAAAACCTGGATAACACTAAGTTT  540
|||||
mSRSF1  GAGTTTGTACGGAAGAAGATATGACGTATGCAGTTCGAAAACCTGGATAACACTAAGTTT  540

hSRSF1  AGATCTCATGAGGGAGAACTGCCTACATCCGGGTTAAAGTTGATGGGCCAGAAAGTCCA  600
|||||
mSRSF1  AGATCTCACGAGGGAGAACTGCCTACATCCGGGTTAAAGTTGATGGGCCAGAAAGTCCA  600

hSRSF1  AGTTATGGAAGATCTCGATCTCGAAGCCGTTAGTTCGTAGCAGAAGCCGTAGCAGAAGCAAC  660
|||||
mSRSF1  AGTTATGGAAGATCTCGATCTCGAAGCCGTTAGTTCGTAGCAGAAGCCGTAGCAGAAGCAAC  660

hSRSF1  AGCAGGAGTCGCAGTTACTCCCCAAGGAGAAAGCAGAGGATCACCACGCTATTCTCCCCGT  720
|||||
mSRSF1  AGCAGGAGTCGCAGTTACTCCCCAAGGAGAAAGCAGAGGATCACCACGCTATTCTCCCCGT  720

hSRSF1  CATAGCAGATCTCGCTCTCGTACATAA  747
|||||
mSRSF1  CATAGCAGATCTCGCTCTCGTACATAA  747

```

shRNA	Antisense sequence	POTS	POTS	Seed sequence
6	ataacttgacttctggccc	221.397 (mouse)	339.052 (human)	TAACTTG
9	gcttcgagatcgagatctcc	41.326 (mouse)	41.3938 (human)	CTTCGAG
10	aatagcgtggtgatcctctgc	21.324 (mouse)	22.5396 (human)	ATAGCGT

**Figure 3. 1:** SRSF1 alignment: Human vs Mouse – Shows where on the gene alignment the designed shRNAs were located.

The forward and reverse oligonucleotides were then designed to create the chosen three shRNAs:

shRNA\_6\_fwd:

GATCC GGGCCCAGAAGTCCAAGTTAT TTCAAGAGA ATAACCTGGACTTCTGGGCC C TTTTTT GGA A

shRNA\_6\_rev:

AGCTT TCC AAAAAA G GGGCCCAGAAGTCCAAGTTAT TCTCTTGAA ATAACCTGGACTTCTGGGCC G

shRNA\_9\_fwd:

GATCC GGAAGATCTCGATCTCGAAGC TTCAAGAGA GCTTCGAGATCGAGATCTTCC C TTTTTT GGA A

shRNA\_9\_rev:

AGCTT TCC AAAAAA G GGAAGATCTCGATCTCGAAGC TCTCTTGAA GCTTCGAGATCGAGATCTTCC G

shRNA\_10\_fwd:

GATCC GCAGAGGATCACCACGCTATT TTCAAGAGA AATAGCGTGGTGATCCTCTGC C TTTTTT GGA A

shRNA\_10\_rev:

AGCTT TCC AAAAAA G GCAGAGGATCACCACGCTATT TCTCTTGAA AATAGCGTGGTGATCCTCTGC G

Once designed, the oligonucleotides were ordered from Sigma.

.

---

### 3.2.2 Cloning of shRNA into scAAV9\_KASPAR\_Efs1 $\alpha$ \_GFP

---

The three shRNAs, designed to target and silence the SRSF1 gene, were cloned into the scAAV-KASPAR\_EFs1 $\alpha$ \_GFP plasmid between the BamHI and HindIII restriction sites (Figure 3. 2A shows the restriction sites of the “scAAV\_KASPAR\_EFs1 $\alpha$ \_GFP” plasmid). The EFs1 $\alpha$  promoter, which is a weaker promoter, was used to allow for the co-expression of GFP along with the shRNA to monitor viral distribution *in vivo*. The weaker promoter was used to prevent the toxic over expression of GFP. DH $\alpha$  cells were transformed onto agar plates selective against ampicillin and three colonies of each of the shRNA’s were picked. A spin mini prep was undertaken to produce a small-scale isolation of the plasmid from *E. coli* bacteria. Following that, a digest with BamHI and KpnI using a 3% agarose gel was undertaken to test whether the shRNA had successfully integrated into the plasmid. An expected band just under 200bp was observed, indicating that the insertion of the shRNA into the plasmid had been successful (see Figure 3. 2B). It was decided from this result that clone #1 of each of the shRNAs would be used to progress with the project, and these clones were subsequently used to prepare midi-preps of the plasmids. Following the midi-prep, to purify the shRNA and produce a high-yield of plasmid, the nano-drop spectrophotometer was used to ensure that we had at least 500ng/ul of plasmid. Once completed, we re-digested using BamHI and KpnI and ran the samples on a 3% agarose gel. Figure 3. 2C shows a clear band just under 200bp, again indicating that our shRNA has been successfully inserted into our plasmid. Following the production of the shRNA against SRSF1, these shRNA containing plasmids were then transfected into HEK and N2A cells to assess how effective they are *in vitro*. To ensure that the eGFP would successfully express following transfection, HEK cells were transfected to confirm (Figure 3. 3).

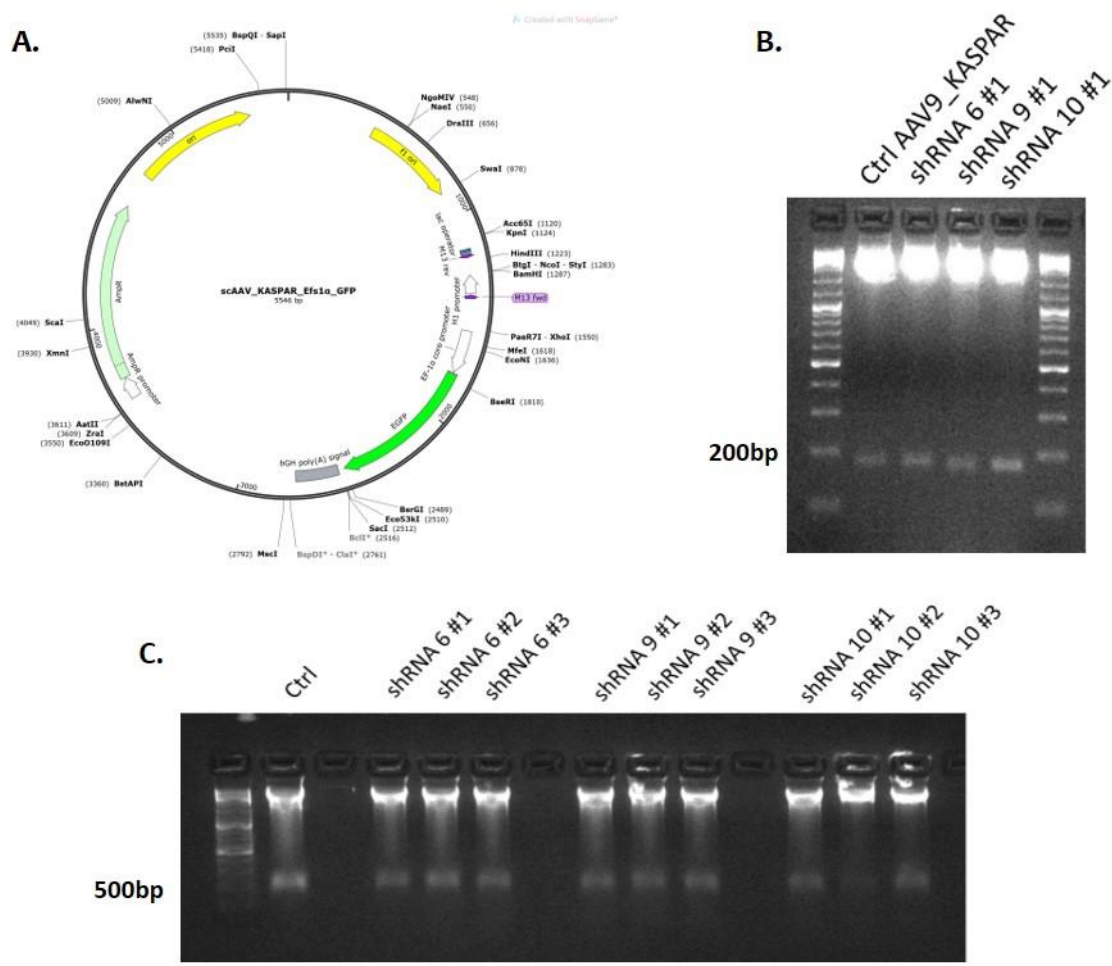


**Figure 3. 2 (A)** Plasmid map of scAAV\_KASPAR\_EFs1 $\alpha$ \_GFP. **(B)** shRNA 6, 9 and 10 mini-prep digests with BamH1 and Kpn1. The Bottom band (163 bp = Cntrl and 184 bp = shRNAs) visualises the shRNA insert. **(C)** Digest of the shRNA midi-prep using BamH1 and Kpn1. The bottom bands of 184bp indicate that the shRNA insert has been excised out of the vector.

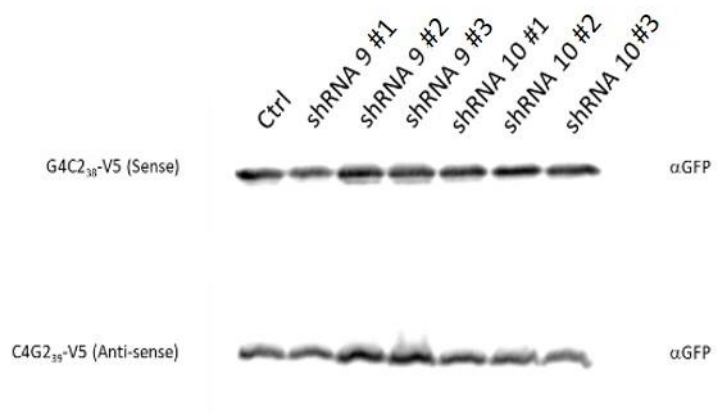


**Figure 3. 3** Western blot image of shRNAs 9 and 10 clones to ensure they are able to successfully express GFP (24kDa).

---

### 3.2.3 Effects on SRSF1-depletion on the production of DPRs in human HEK cell models of C9ORF72 ALS/FTD

---

Once the designed shRNA 6, 9 and 10 against SRSF1 were cloned into the scAAV\_KASPAR\_EFs1 $\alpha$ \_GFP vector, the functionality of the constructs was tested. The aim was to test whether these plasmids could lead to the depletion of SRSF1 and subsequent inhibition of the RAN translation of V5-tagged DPRs in human HEK293T and mouse N2A reporter cell models of C9ORF72-ALS/FTD (Hautbergue *et al.*, 2017). The DPR expressing plasmids (either sense or antisense) were co-transfected along with the recently designed constructs.

Control plasmids were transfected alongside the shRNA, again co-transfected with v5 sense or antisense DPRs. We used a control scAAV-KASPAR plasmid bearing just the H1 promoter (empty plasmid) and another control scAAV-KASPAR plasmid expressing a scrambled shRNA sequence driven from the H1 promoter (Figure 3. 4).

The western blot results indicated that in comparison with the control plasmids, the three-designed shRNA led to reduced SRSF1 expression, indicating that they successfully knocked down SRSF1 protein (Figure 3. 5A). This was evident in both the sense and antisense western blot images.

A V5 antibody was used to identify the expression of the V5 tagged DPRs. The western blot image (Figure 3. 5A) shows a clear reduction in DPR expression. SRSF1-shRNA-treated samples showed both reduced expression levels of SRSF1 and sense or antisense V5-tagged DPRs. This indicated that all 3 transfected shRNA plasmids are functional *in vitro* with the depletion of SRSF1 successfully leading to efficient inhibition of the RAN translation of DPRs.

Western blots from three independent biological repeats of the transfection experiments were then quantified. As expected, no significant difference in SRSF1 expression could be seen between the untransfected and the control shRNA plasmid. On the other hand, a significant difference was observed between the plasmid expressing the scrambled shRNA and the three designed SRSF1-shRNAs. When the shRNA that knocks down SRSF1 was expressed, there was an obvious reduction in SRSF1 expression, indicating that the shRNAs were successfully down-regulating the expression of the SRSF1 protein. This trend occurs when shRNA is co-transfected with both sense and antisense DPRs (Figure 3. 5 B and C).

Cells were co-transfected with a plasmid expressing V5 tagged DPRs to observe the effect that the shRNA against SRSF1 has on DPRs. When we looked at the DPR level, we could see that the shRNA treated cells showed an obvious reduction of DPR expression compared to control cells when viewing the western blot images (Figure 3. 5A).

Quantification of the three repeats of the western blot analysis indicated that there was a significant difference [\*\*\*\* =  $p < 0.0001$ ] between the control plasmids (empty and expressing a scrambled shRNA) and the shRNAs against SRSF1. The significant difference between the untransfected and the control plasmids [\*\*\*\* =  $p < 0.0001$ ] could be explained by the fact that the untransfected cells had no V5 tagged DPRs transfected into them and so did not express V5. Overall, a significant reduction in DPR expression was observed in cells that have been treated with shRNA 6, 9 and 10 compared with cells that have been treated with the control plasmids [\*\*\*\* =  $p < 0.0001$ ]. This indicated that these shRNA were able to inhibit RAN translation (Figure 3. 5 B and C). Again, there was a similar trend that was obvious in both sense and antisense experiments. From Figure 3. 5 it can also be noted that the tubulin in both the sense and antisense experiments demonstrated equal loading of protein extracts across lanes.

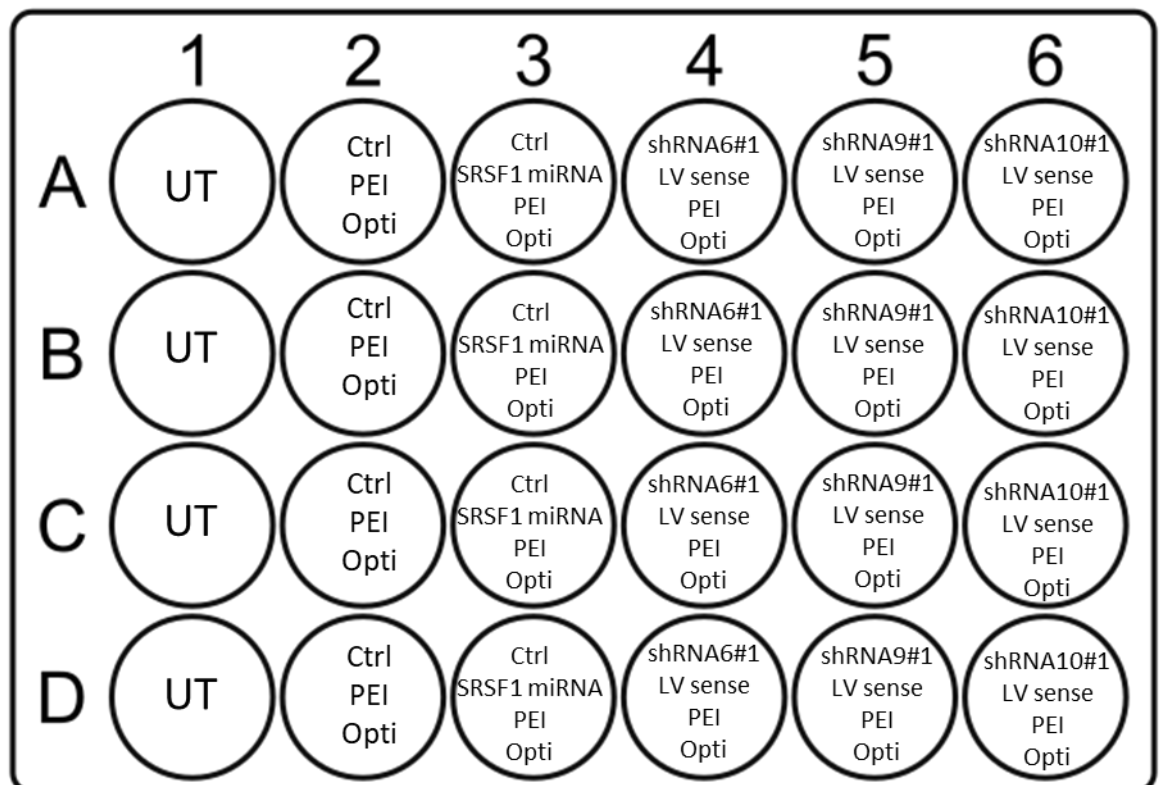


**Figure 3. 4** Depicts a 24 well plate used to test the SRSF1 shRNA plasmids *in vitro*. UT = untransfected, Ctrl = control, LV sense = Lenti-virus plasmid expressing sense DPRs, PEI = gene delivery system, Opti = Opti-MEM which is a reduced serum medium.

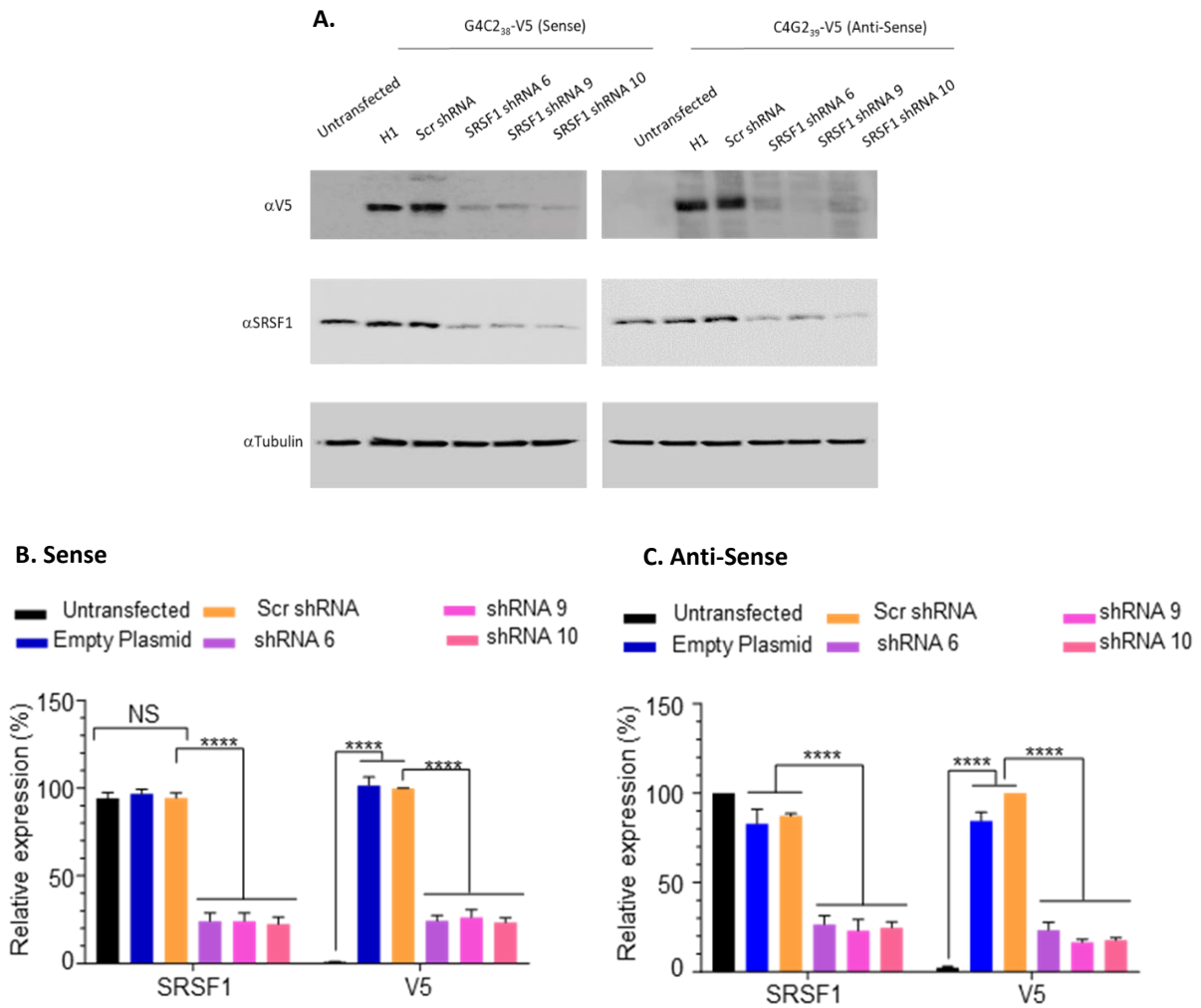


**Figure 3. 5 (A)** Western Blot images visualising the effect of shRNA 6, 9 and 10 on the expression of DPRs (V5 – 23 kDa) and the expression of SRSF1 (SRSF1 – 33 kDa) in respect to the expression of tubulin (tubulin – 55 kDa) 48hrs post transfection into HEK cells. **(B)** Quantification of three repeated western blots of shRNA 6, 9 and 10 co-transfected with V5 sense into HEK cells. Analysed using a 1-way ANOVA [NS = No significance; \* =  $p < 0.05$ ; \*\* =  $p < 0.01$ ; \*\*\* =  $p < 0.001$ ; \*\*\*\* =  $p < 0.0001$ ]. **(C)** Quantification of three repeated western blots of shRNA 6, 9 and 10 co-transfected with V5 anti-sense into HEK cells. Analysed using a 1-way ANOVA [NS = No significance; \* =  $p < 0.05$ ; \*\* =  $p < 0.01$ ; \*\*\* =  $p < 0.001$ ; \*\*\*\* =  $p < 0.0001$ ].

---

### 3.2.4 Effects on SRSF1-depletion on the production of DPRs in mouse N2A cell models of C9ORF72 ALS/FTD

---

The recently designed constructs with the inserted shRNAs against SRSF1 were co-transfected along with either V5 tagged sense or antisense DPRs into N2A cells. The dipeptide repeat proteins (DPRs) play an integral role in the pathogenesis of C9ORF72 ALS/FTD. These DPRs were co-transfected along with the recently designed constructs to observe how the shRNA against SRSF1 would affect DPR expression in a neuronal mouse cell line. The idea was that reducing DPR expression would result in reduced neurodegeneration. A mouse cell line was used to ensure that a similar effect would be observed when the treatment strategy was applied to a mouse model.

N2A cells were transfected with the control constructs (scAAV-KASPAR-H1-empty and scAAV-KASPAR-H1-scrambled-shRNA) and the 3 scAAV-KASPAR-shRNA against SRSF1. Figure 3. 6A depicts the western blot results from this transfection. They clearly show reduced expression of SRSF1 in shRNA-treated cells compared with control plasmid-treated cells [\*\*\* =  $p < 0.001$ ; \*\*\*\* =  $p < 0.0001$ ]. Similarly, we also saw that the DPR expression in shRNA-treated cells showed an obvious reduction in DPR expression compared to control cells, indicating that the shRNAs were functioning well and were able to inhibit DPR production. The reduced DPR expression appeared more obvious in the sense images compared with the antisense images but the trend remained the same in both experimental conditions [\*\*\* =  $p < 0.001$  vs \*\*\*\* =  $p < 0.0001$ ].

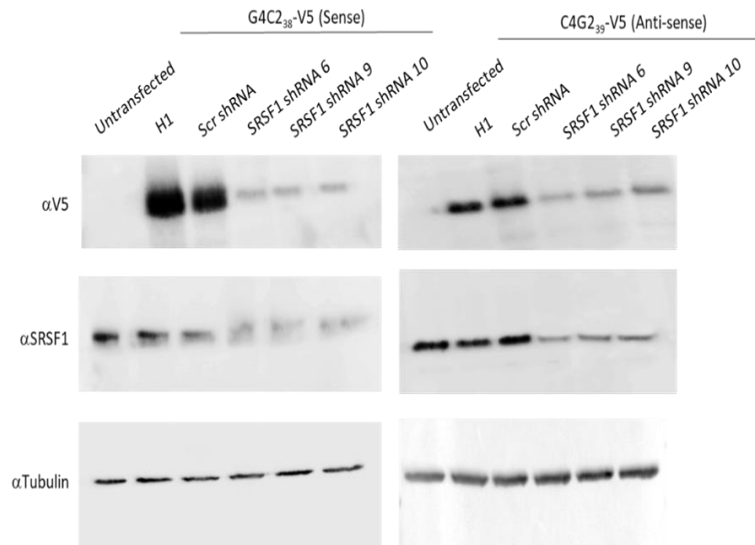
Tubulin was used as our loading control and the western blot images clearly show that equal protein loading was achieved across all six wells. As expected, quantification of three repeated transfection western blot images showed no significant difference in SRSF1 expression between the untransfected and the control plasmids. However, there was significantly reduced expression of SRSF1 between the control plasmids and the shRNA, similar to the result seen in HEK cells (Figure 3. 6 B and C).

Again, for the HEK cells, it was observed that when we expressed the shRNA against SRSF1, a definite reduction in SRSF1 expression was seen, strongly indicating that all three shRNAs were able to knock down the SRSF1 protein in N2A mouse cells.

The quantification of the DPR results showed a strong significant reduction in DPR expression in cells treated with the shRNAs compared with cells treated with control plasmids. No significant difference was witnessed between the control plasmids. The

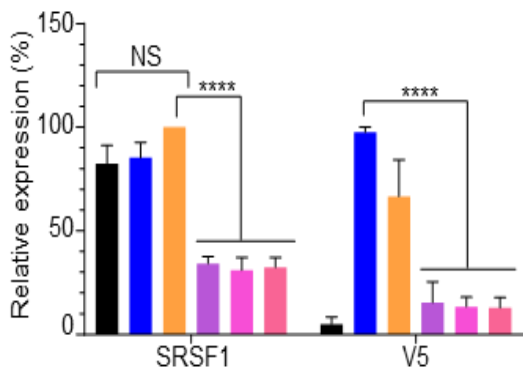
untreated cells showed no DPR expression, as these cells were not transfected with V5 tagged DPRs. This highlights the overall indication given from the images that the shRNAs were functional and were able to inhibit RAN translation in N2A cells. Following the results in the last two sections we conclude that we will use shRNA 10 in future experiments. The final plasmid that will be used *in vivo* to deplete SRSF1 is depicted in Figure 3. 10.

**A.**



**B. Sense**

■ Untransfected    ■ Scr shRNA    ■ shRNA 9  
 ■ Empty Plasmid    ■ shRNA 6    ■ shRNA 10



**C. Anti-Sense**

■ Untransfected    ■ Scr shRNA    ■ shRNA 9  
 ■ Empty Plasmid    ■ shRNA 6    ■ shRNA 10

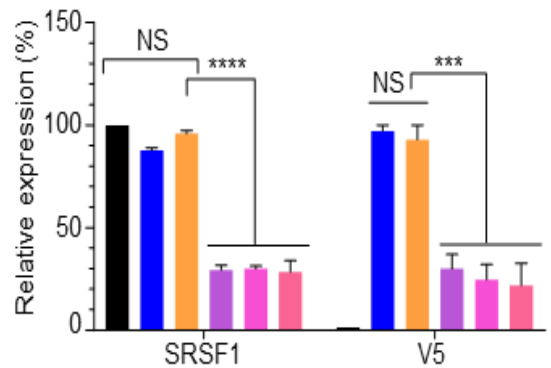


**Figure 3. 6 (A)** Western Blot images visualising the effect of shRNA 6, 9 and 10 on the expression of DPRs (V5 – 23 kDa) and the expression of SRSF1 (SRSF1 – 33 kDa) 48hrs post transfection into N2A cells in respect to the expression of tubulin (tubulin – 55 kDa). **(B)** Quantification of three repeated western blots of shRNA 6, 9 and 10 co-transfected with V5 sense into N2A cells. Analysed using a 1-way ANOVA [NS = No significance; \* =  $p < 0.05$ ; \*\* =  $p < 0.01$ ; \*\*\* =  $p < 0.001$ ; \*\*\*\* =  $p < 0.0001$ ]. **(C)** Quantification of three repeated western blots of shRNA 6, 9 and 10 co-transfected with V5 anti-sense into N2A cells. Analysed using a 1-way ANOVA [NS = No significance; \* =  $p < 0.05$ ; \*\* =  $p < 0.01$ ; \*\*\* =  $p < 0.001$ ; \*\*\*\* =  $p < 0.0001$ ].

### 3.3 Therapeutic approach 2: Expression of the point mutant protein SRSF1-m4

During this study we used two different therapeutic approaches to manipulate the expression of the nuclear export protein SRSF1. Here, I will describe the therapeutic strategy in which we reduced wild-type endogenous SRSF1 binding to the *C9ORF72* repeat transcripts by expressing an SRSF1 mutant protein which carries amino-acid substitution of 4 residues involved in the interaction with the nuclear export machinery. SRSF1 is known to mediate nuclear export through its interaction with NXF1. Our lab has previously shown that four arginine residues that lie in the unstructured linker region between the two RNA recognition motifs of SRSF1 (RRM1 and RRM2 aka RNA Recognition Motif 1 and 2) are required for interaction with RNA. The linker between RRM1 and RRM2 (amino-acid 89-120) is required for the interaction with NXF1. It was found that the quadruple mutations of the four arginine residues R90, 93, 117, 118A into alanine severely impairs the co-immunoprecipitation of NXF1 and the nuclear export and RAN translation of the reporter *C9ORF72*- repeat transcripts which are used in my studies (Hautbergue *et al.*, 2017). This mutant, called SRSF1-m4 with amino-acid 11.196, behaves as a dominant negative mutant of the SRSF1-dependent nuclear export and RAN translation of *C9ORF72*-repeat transcripts. The C-terminal RS-rich region of the SRSF1 protein (aa197-248) was removed in SRSF1-m4, as it is phosphorylated during splicing prior to being dephosphorylated for coupling to the nuclear export machinery via interaction with NXF1 (Tintaru *et al.*, 2007). In order to not risk altering splicing-dependent function, we therefore retain the smallest dominant negative mutant that can bind RNA via the RRM domains but has lost its property to interact with NXF1 due to the 4-arginine substitutions in the linker region.

The mutant can therefore bind to expanded hexanucleotide repeats such as those seen in *C9ORF72*-ALS/FTD, but should be unable to bind NXF1. It has been suggested that the SRSF1-m4 protein is sequestered onto the pathogenic hexanucleotide repeats found in the *C9ORF72* gene instead of the endogenous SRSF1. The arginine mutations prevent the interaction between the expanded repeat transcripts and NXF1, thus interrupting the overall nuclear export of the expanded repeat transcripts and therefore interrupting the production of toxic DPRs. Nuclear export of non-pathogenic repeats does not depend on SRSF1 and is not affected by the therapeutic SRSF1 m4 (Hautbergue *et al.*, 2017; Castelli *et al.*, 2018).

---

### 3.3.1 Design of scAAV\_AZ\_CBh\_SRSF1-m4

---

For this part of the project, we inserted the p3xFLAG SRSF1 m4 protein into a pAAV plasmid with a strong CBh promotor to drive the expression of the protein following transfection. A wild type p3xFLAG SRSF1 11-196 plasmid was created using the same method as a control for the *in vitro* study. Once the pAAV plasmid had been constructed, the p3xFLAG SRSF1 m4 protein was then inserted into an scAAV plasmid to increase transduction efficiency *in vivo*.

Below is the design of the FLAG-tagged SRSF1-m4 and SRSF1 WT sequences that will be used for the cloning into scAAV are demonstrated:

#### **p3xFLAG SRSF1-m4 (aa11-196 R90,93,117,118A)**

3x FLAG            AAG CTT: HindIII            GCG GCC GC: NotI

SRSF1 aa11-196            TCT AGA: XbaI

c-Myc                    **TGA**: stop

ATG GAC TAC AAA GAC CAT GAC GGT GAT TAT AAA GAT CAT GAC  
ATC GAT TAC AAG GAT GAC GAT GAC AAG CTT GCG GCC GCG CCA  
AAA AAG AAG AGA AAG GTC GAA GCA GGG AAC AAC GAT TGC CGC  
ATC TAC GTG GGT AAC TTA    CCT CCA GAC ATC CGA ACC AAG GAC  
ATT GAG GAC GTG TTC TAC AAA TAC GGC GCT ATC CGC GAC ATC  
GAC CTC AAG AAT CGC CGC GGG GGA CCG CCC TTC GCC TTC GTT  
GAG TTC GAG GAC CCG CGA GAC GCG GAA GAC GCG GTG TAT GGT  
CGC GAC GGC TAT GAT TAC GAT GGG TAC CGT CTG CGG GTG GAG  
TTT CCT **GCT** AGC GGC **GCT** GGA ACA GGC CGA GGC GGC GGC GGG  
GGT GGA GGT GGC GGA GCT CCC CGA GGT CGC TAT GGC CCC CCA  
TCC **GCG GCG** TCT GAA AAC AGA GTG GTT GTC TCT GGA CTG CCT  
CCA AGT GGA AGT TGG CAG GAT TTA AAG GAT CAC ATG CGT GAA  
GCA GGT GAT GTA TGT TAT GCT GAT GTT TAC CGA GAT GGC ACT  
GGT GTC GTG GAG TTT GTA CGG AAA GAA GAT ATG ACC TAT GCA  
GTT CGA AAA CTG GAT AAC ACT AAG TTT AGA TCT CAT GAG GGA  
GAA ACT GCC TAC ATC CGG GTT AAA GTT GAT GGG TCT AGA GAA  
CAA AAA CTC ATC TCA GAA GAG GAT CTG **TGA**

### p3xFLAG SRSF1 WT (aa11-196)

3x FLAG            AAG CTT: HindIII            GCG GCC GC: NotI  
SRSF1 aa11-196            TCT AGA: XbaI  
c-Myc                    **TGA**: stop

ATG GAC TAC AAA GAC CAT GAC GGT GAT TAT AAA GAT CAT GAC  
ATC GAT TAC AAG GAT GAC GAT GAC AAG CTT GCG GCC GCG CCA  
AAA AAG AAG AGA AAG GTC GAA GCA GGG AAC AAC GAT TGC CGC  
ATC TAC GTG GGT AAC TTA    CCT CCA GAC ATC CGA ACC AAG GAC  
ATT GAG GAC GTG TTC TAC AAA TAC GGC GCT ATC CGC GAC ATC  
GAC CTC AAG AAT CGC CGC GGG GGA CCG CCC TTC GCC TTC GTT  
GAG TTC GAG GAC CCG CGA GAC GCG GAA GAC GCG GTG TAT GGT  
CGC GAC GGC TAT GAT TAC GAT GGG TAC CGT CTG CGG GTG GAG  
TTT CCT CGA AGC GGC CGT GGA ACA GGC CGA GGC GGC GGC GGG  
GGT GGA GGT GGC GGA GCT CCC CGA GGT CGC TAT GGC CCC CCA  
TCC AGG CGG TCT GAA AAC AGA GTG GTT GTC TCT GGA CTG CCT  
CCA AGT GGA AGT TGG CAG GAT TTA AAG GAT CAC ATG CGT GAA  
GCA GGT GAT GTA TGT TAT GCT GAT GTT TAC CGA GAT GGC ACT  
GGT GTC GTG GAG TTT GTA CGG AAA GAA GAT ATG ACC TAT GCA  
GTT CGA AAA CTG GAT AAC ACT AAG TTT AGA TCT CAT GAG GGA  
GAA ACT GCC TAC ATC CGG GTT AAA GTT GAT GGG TCT AGA GAA  
CAA AAA CTC ATC TCA GAA GAG GAT CTG **TGA**

---

### 3.3.2 Cloning of the control scAAV\_AZ\_CBh\_GFP plasmid

---

For the project to be successful *in vivo*, a control plasmid was required to ensure that the biodistribution of the virus could be tracked. The same vector as our therapeutic scAAV9 SRSF1 m4 vector was used, except instead of expressing the SRSF1 m4 protein, it was designed to express a GFP protein. The GFP protein allows for the visualisation of the virus post-delivery and allows for the biodistribution of the virus to be tracked throughout multi-organ systems. First, we took the previously made pAAV\_AZ\_CBh\_GFP control plasmid and restricted the CBh promoter – GFP from the plasmid using MluI and XbaI enzymes. The CBh promoter – GFP was extracted from a 1.5% agarose gel (Figure 3. 7A). The plasmid scAAV AZ AmpR / CMV prom - SMN was then digested with MluI/XbaI and treated with CIP and the restricted vector band corresponding to scAAVAZ AmpR MluI/XbaI + CIP was extracted from a 1% agarose gel (Figure 3. 7B) and was sub-cloned into an scAAV plasmid expressing SMN (Valori *et al*, 2010), scAAV / CMV promoter – SMN, using the same MluI and XbaI restricted sites and treated with CIP. The CBh promoter – GFP MluI/XbaI was then ligated into the scAAV\_AZ\_MluI/XbaI + CIP to generate

scAAV\_AZ\_CBh\_GFP. The plasmid was checked to ensure that the ligation was successful by running a MluI / XbaI digest on a 1% agarose gel to check for cloning of the CBh promoter – GFP insert. Bands were expected at 3217 bp + 1603 bp and from Figure 3. 7C it is evident that all the clones are correct. A small digest was undertaken using SmaI (Figure 3. 7D) to check the integrity of the ITRs in the plasmid and the expected bands were as follows: 2724bp, 1000bp, 997bp, 77bp and 11bp. The control lane containing scAAV\_AZ\_CMV\_SMN has an extra insert as it contains an extra SmaI site in the CMV promoter region. From the gel image, all clones appear to be correct. As such, we decided to use clone #1 to progress the development of a midi-prep. ITRs and the insert were checked again using the methods described previously and the clone was found to be correct. SRSF1 /SRSF1 m4 were further cloned under the CBh promoter using this scAAV\_AZ\_CBh\_GFP as a template. The final plasmid that will be used for the *in vivo* can be reviewed in Figure 3. 12. Full cloning strategy explained in the Appendix.

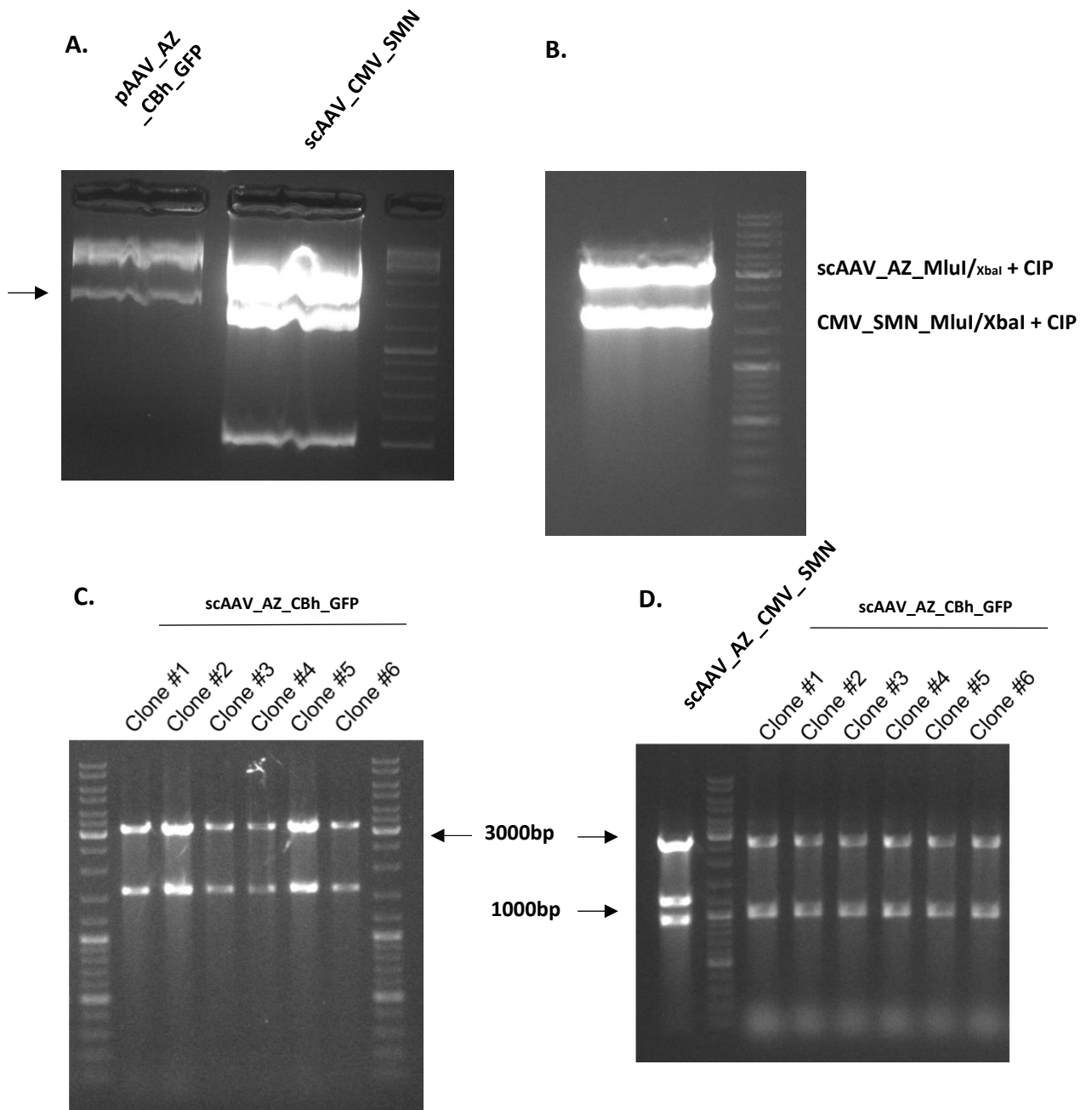


**Figure 3. 7 (A)** Insert preparation: CBh prom- GFP MluI/XbaI was restricted from pAAV\_AZ\_CBh\_GFP. Arrow depicts band that was extracted from the 1.5% agarose gel. **(B)** Vector preparation: the plasmid scAAV\_AZ\_CMV\_SMN was digested with MluI/XbaI and treated with CIP and the restricted vector band corresponding to scAAV\_AZ\_MluI/XbaI + CIP was extracted from a 1% agarose gel. **(C)** scAAV\_AZ\_CBh\_GFP clones #1-6. MluI / XbaI digest run on 1% agarose gel to check for cloning of CBh\_GFP insert. **(D)** scAAV\_AZ\_CBh\_GFP clones #1-6. SmaI

---

### 3.3.3 Cloning of SRSF1-m4 into scAAV\_AZ\_CBh

---

#### Cloning of pAAV\_AZ\_CBh\_SRSF1 m4

To create a therapeutic construct that would be able to express the SRSF1 m4 mutant and interact with the nuclear export machinery in cell models, we needed to clone the SRSF1 m4 protein into a therapeutic construct, which in this case will be: pAAV\_AZ\_CBh\_3x FLAG-SRSF1-m4. The CBh promoter was used in this study after previous research suggested results that “the CBh promoter is a strong and ubiquitous promoter for CNS applications” (Gray et al; 2011). A strong promoter is required to drive the expression of the SRSF1 and SRSF1 m4 proteins following transfection/transduction. However, the CBh promoter that was required could not be efficiently amplified by PCR due to its pure GC rich region. Therefore, sub cloning was needed, which was described previously (3.3.2) when cloning scAAV\_AZ\_CBh\_GFP. Accuzyme PCR was used to amplify and prepare both the SRSF1 WT and the mutant SRSF1-m4 for cloning into the plasmid scAAV\_AZ\_CBh\_GFP. Primers with 5' EcoRI and 3' XbaI sites were used. Following the PCR, a 1.5% agarose gel was run for gel extraction (Figure 3. 8A).

The vector was prepared by digesting pAAV\_AZ\_CBh by EcoRI and XbaI + CIP which underwent phenol precipitation and the dried pellet was resuspended. 3X FLAG SRSF1-m4 EcoRI/XbaI was then ligated into pAAV\_AZ\_CBh EcoRI/XbaI + CIP to obtain pAAV\_AZ\_CBh\_SRSF1-m4. A digest using EcoRI and XbaI on a 1% gel was undertaken to check whether the insert had been successfully inserted into the plasmid. Bands were expected at 4278bp + 672bp and, as can be seen in Figure 3. 8B, all clones were found to be correct.

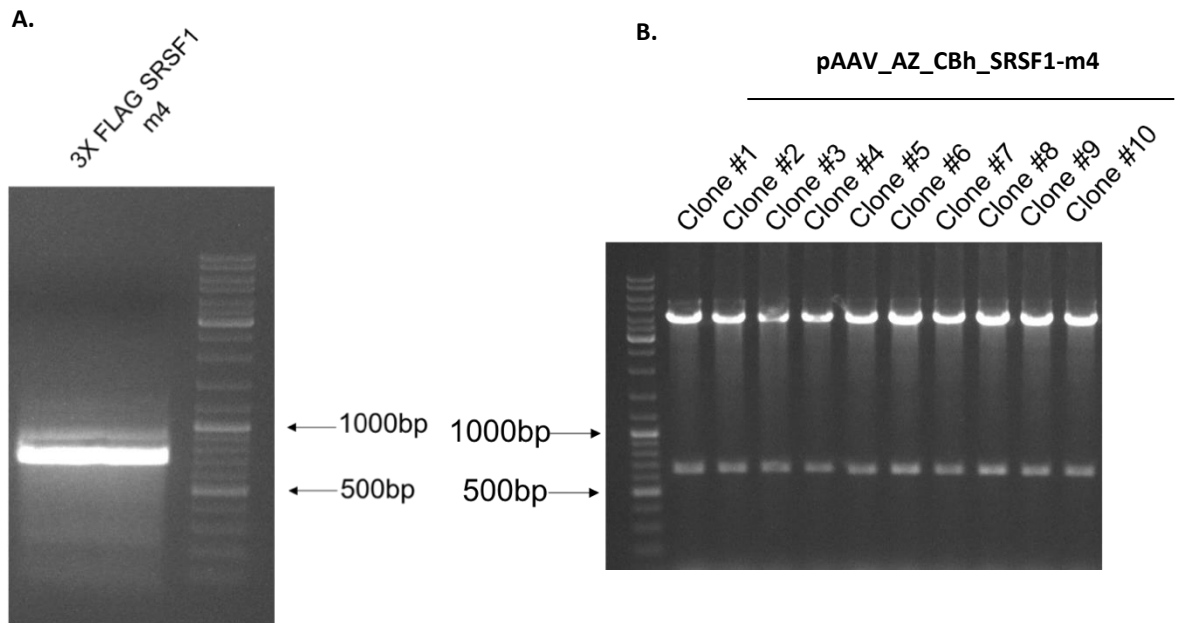


**Figure 3. 8 (A)** Insert preparation: Accuzyme PCR to amplify SRSF1-m4 from p3X-FLAG / SRSF1 11-196 m4 plasmid using primers with 5' EcoRI and 3' XbaI sites. Digest with EcoRI and XbaI and run a 1.5% agarose gel and gel extract. **(B)** Vector Preparation: Ligation of 3XFLAG SRSF1-m4 EcoRI/XbaI into pAAV\_AZ\_CBh EcoRI/XbaI + CIP to obtain pAAV\_AZ\_CBh\_SRSF1-m4. EcoRI/XbaI digest run on 1% agarose gel.

## Cloning of scAAV\_AZ\_CBh\_SRSF1-m4

The SRSF1 proteins were then packaged into self-complimentary AAV (scAAV) vectors. Previously, the SRSF1 proteins were inserted into pAAV single stranded vectors, which are hindered by their need to convert the single-stranded DNA genome into double-stranded DNA prior to expression. This step can be entirely avoided by instead using self-complementary vectors. scAAV vectors can package an inverted repeat genome that can fold into double stranded DNA without requiring DNA synthesis or base-pairing between multiple vector genomes. The efficiency of viral transduction of scAAV is therefore much greater than pAAV.

First, the insert was prepared; pAAV\_AZ\_CBh\_SRSF1-m4 was digested with MluI and XbaI and extracted CBh\_3X FLAG SRSF1-m4 from a 1% agarose gel (Figure 3. 9A). Then the vector was prepared using the method above (Figure 3. 9B) and scAAV\_AZ\_MluI/XbaI + CIP was restricted and extracted from scAAV\_AZ\_CBh\_GFP using a 1% agarose gel.

CBh\_3X FLAG SRSF1-m4 MluI/XbaI was then ligated into scAAV\_AZ\_MluI/XbaI + CIP, resulting in the plasmid scAAV\_AZ\_CBh\_SRSF1-m4. A digest was then undertaken using MluI and XbaI enzymes on a 1 % agarose gel to check for the successful cloning of CBh\_3X FLAG SRSF1-m4 insert (Figure 3.8B). The expected band sizes were 3217bp and 1493bp and from Figure 10B we established that all of the clones showed the correct band size. We then digested scAAV\_AZ\_CBh\_SRSF1-m4 with SmaI to check the integrity of its ITRs (Figure 3. 9C). The expected band sizes were 2734bp, 1000bp, 997bp, 77bp, 11bp and 11bp, and after reviewing the digest results, scAAV\_AZ\_CBh\_SRSF1-m4 clone #1 was selected to undergo a midi-prep. Following the midi-prep, the plasmid was checked again using a MluI/XbaI digest and a SmaI digest and again the bands that were seen were those that were expected (Figure 3. 9D). The final plasmid that will be used for the *in vivo* study is shown in Figure 3. 13. Full cloning strategy explained in the Appendix.

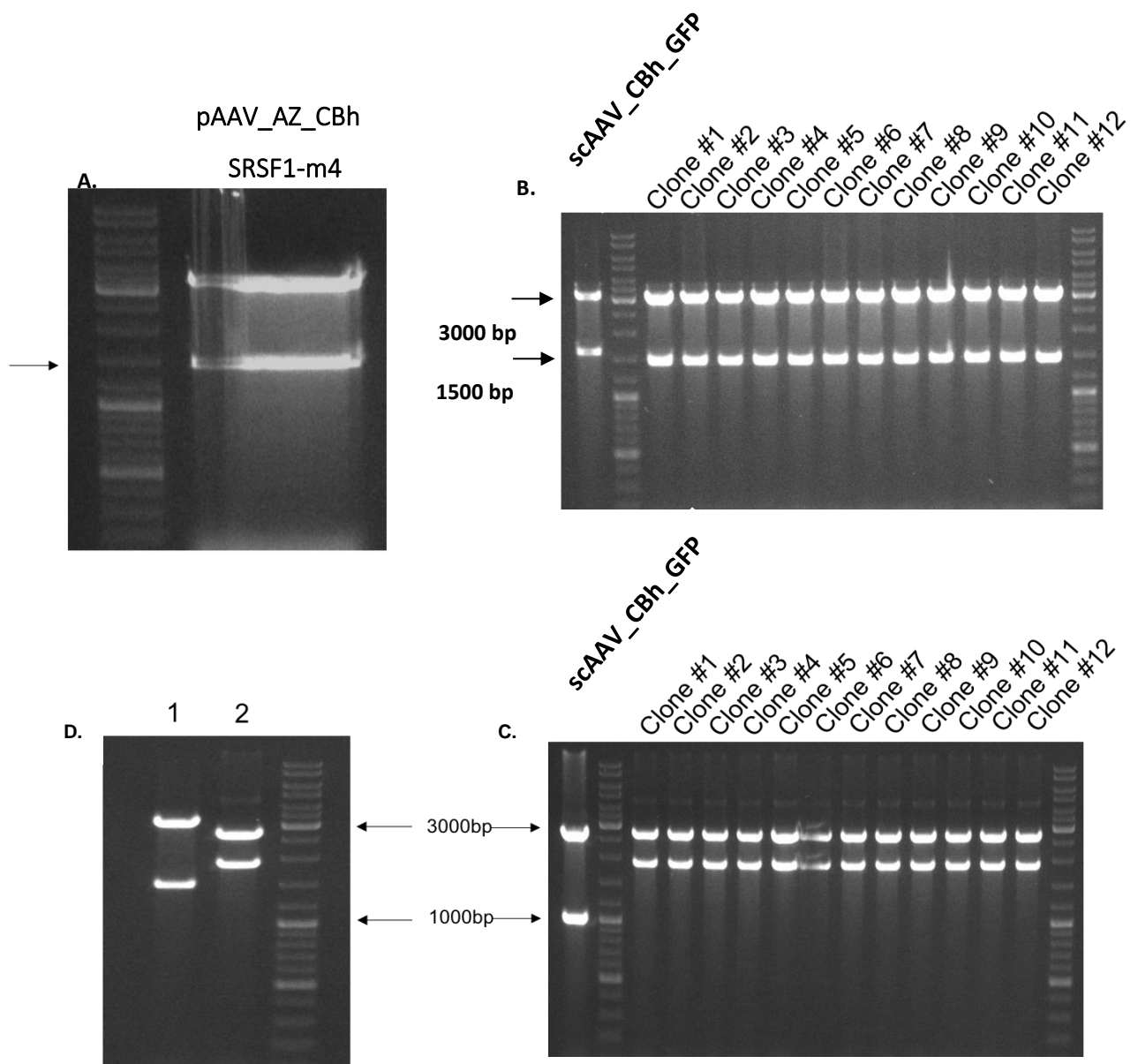


**Figure 3. 9** (A) Insert prep: CBh\_3x FLAG SRSF1-m4 fragment was digested from pAAV\_AZ\_CBh\_3xFLAG SRSF1-m4 using MluI and XbaI and extracted from a 1% preparative agarose gel. Arrow indicates band that was extracted. (B) Ligation of CBh\_3x FLAG SRSF1-m4 MluI/XbaI into scAAV\_AZ MluI/XbaI+CIP to obtain scAAV\_AZ\_CBh\_3x FLAG SRSF1-m4. MluI / XbaI digest run on a 1% agarose gel to check for cloning of CBh\_3x FLAG SRSF1-m4 insert. (C) SmaI digest run on a 3% agarose gel to check the integrity of the ITRs in the scAAV\_AZ\_CBh\_3x FLAG SRSF1-m4 plasmid. (D) scAAV\_AZ\_CBh\_3x FLAG SRSF1-m4 clone #1 was selected for a midi-prep and checked with a MluI/XbaI digest (Lane 1) and a SmaI digest (Lane 2), both of which indicate that the plasmid is functioning well.

---

### 3.3.4 Effects of the SRSF1-m4 dominant mutant on the expression of DPRs in human HEK293 cell models of ALS/FTD

---

To review the effect that SRSF1 m4 could have on the expression of toxic dipeptide repeat proteins in C9ORF72 ALS/FTD, HEK cells were co-transfected with either scAAV-CBh-SRSF1 or scAAV-CBh-SRSF1-m4 along with a plasmid expressing sense or antisense V5 tagged DPRs. For the control plasmids we used: a 3XFLAG plasmid which expresses only a FLAG tag protein; a non-AAV expression SRSF1 (Hautbergue *et al.*, 2017); and a non-AAV expression SRSF1 m4 plasmid previously used in Hautbergue *et al.*, 2017. The western blot image showed that, compared to the control 3XFLAG plasmid, each of the SRSF1/SRSF1 m4 plasmids expressed the FLAG protein, suggesting that the insert and the plasmid successfully integrated into the host cells and that the plasmid was working sufficiently *in vitro*. The result showed the same trend in both sense and antisense co-cultures (Figure 3. 10A).

There was an observable difference between DPR expression in cells treated with SRSF1 containing plasmids and cells treated with SRSF1 m4 containing plasmids in both the sense experiment and the anti-sense experiments. There was a definite reduced expression of V5 seen in the western blot images in cells treated with both the control m4 and the new therapeutic SRSF1 m4 when compared with endogenous SRSF1 using both sense and anti-sense DPRs. It could also be easily extrapolated from Figure 3.9A that all SRSF1/SRSF1 m4 plasmids expressed FLAG in comparison to untransfected and the control plasmid treated cells.

Three repeats of this co-transfection were then quantified using their western blot images. No significant difference in FLAG expression could be seen between the original SRSF1-shRNA/SRSF1 m4 plasmids and the newly designed SRSF1-shRNA/SRSF1 m4 plasmids [NS = No significance]. The quantification provides evidence that cells treated with therapeutic SRSF1 m4 show a significant reduction in DPR expression compared with cells treated with SRSF1 in both sense and antisense co-cultures (Figure 3. 10 B and C) [\*\*\*\* =  $p < 0.0001$ ]. This indicates that therapeutic SRSF1 m4 can reduce DPR expression when used to treat cells and is able to successfully inhibit RAN translation, which was similarly reported with the non-AAV expressing SRSF1-m4 plasmid in Hautbergue *et al.*, 2017.

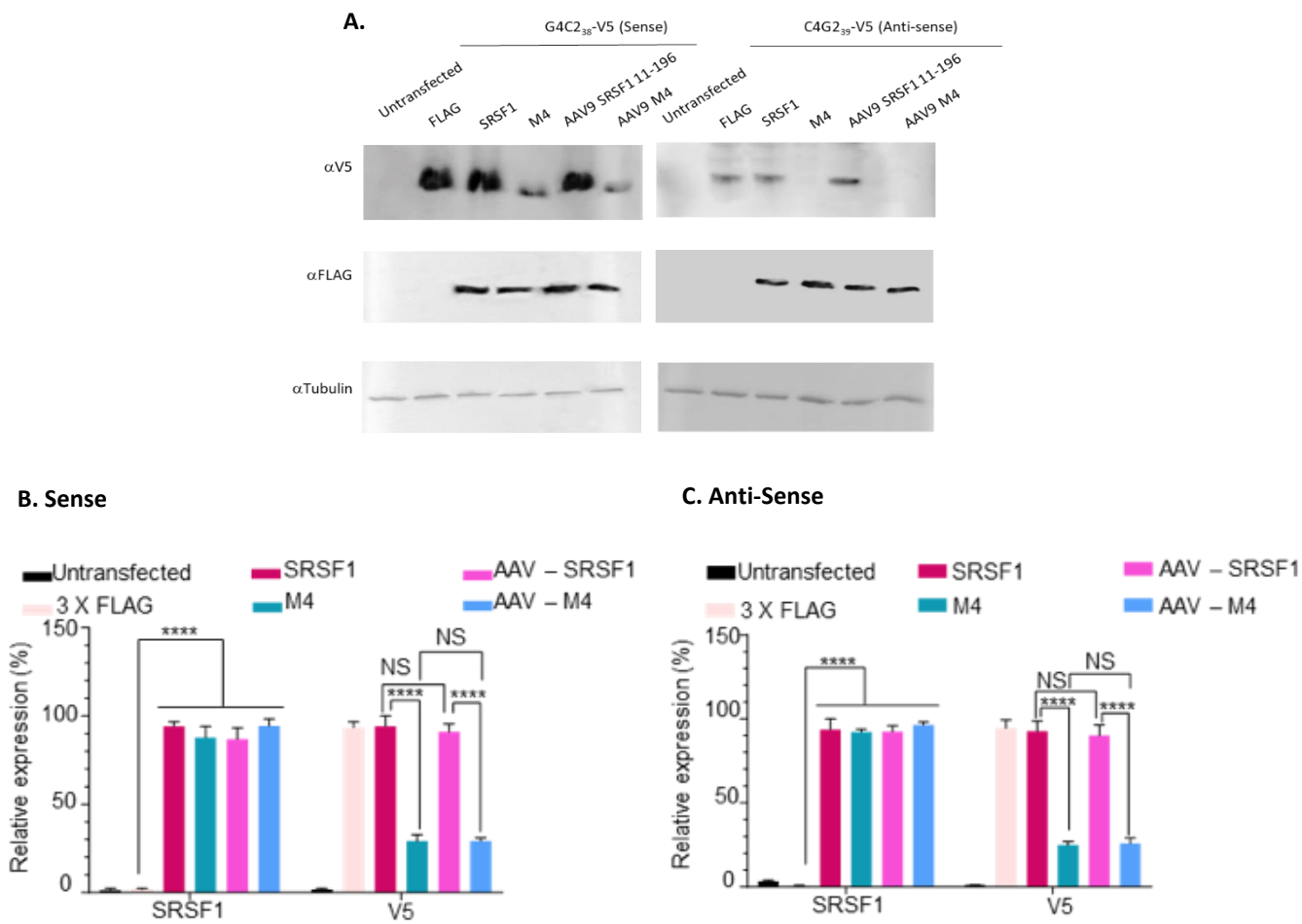


**Figure 3. 10 (A)** Western Blot images visualising the effect of SRSF1/SRSF1 m4 on the expression of DPRs (V5 – 23 kDa) and the expression of FLAG (FLAG – 27 kDa) in respect to tubulin (tubulin – 55 kDa) 48hrs post transfection into HEK cells **(B)** Quantification of three repeated western blots of SRSF1/SRSF1 m4 co-transfected with V5 sense into HEK cells. Analysed using a 1-way ANOVA [NS = No significance; \* =  $p < 0.05$ ; \*\* =  $p < 0.01$ ; \*\*\* =  $p < 0.001$ ; \*\*\*\* =  $p < 0.0001$ ]. **(C)**. Quantification of three repeated western blots of shRNA 6, 9 and 10 co-transfected with V5 anti-sense into HEK cells. Analysed using a 1-way ANOVA [NS = No significance; \* =  $p < 0.05$ ; \*\* =  $p < 0.01$ ; \*\*\* =  $p < 0.001$ ; \*\*\*\* =  $p < 0.0001$ ].

### 3.4 Summary of therapeutic plasmid production for *in vivo* study

Overall, 3 scAAV plasmids were produced to be packaged into therapeutic scAAV9 viruses: scAAV9-eGFP, scAAV9 SRSF1 m4 and scAAV9 SRSF1 RNAi. Below are the final plasmids following all cloning.

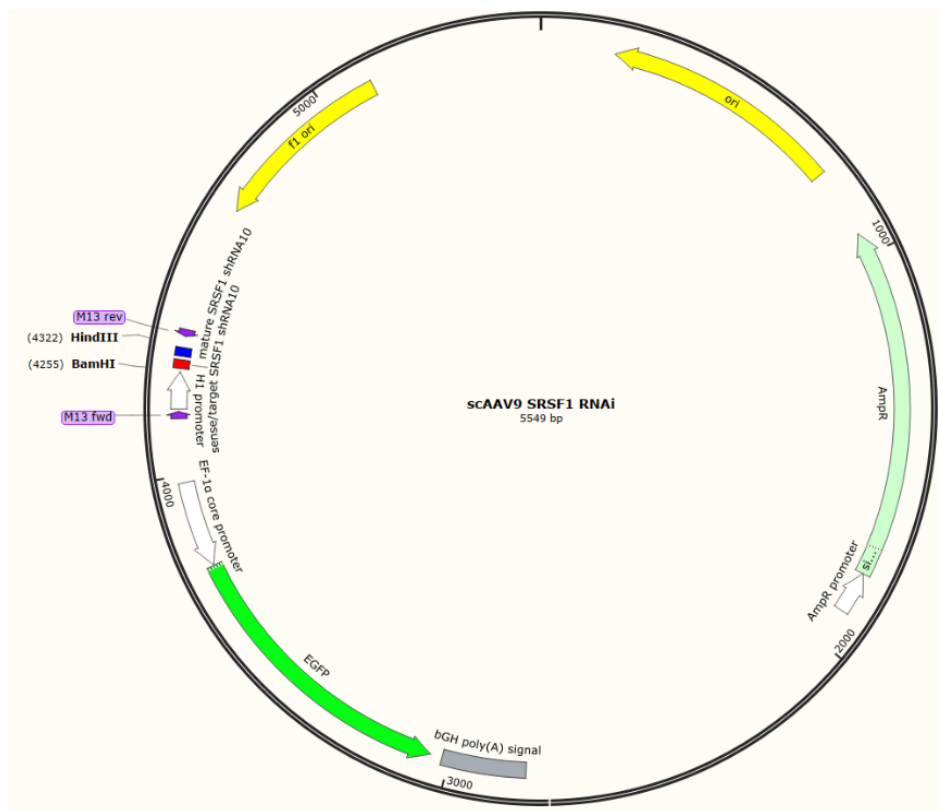


Figure 3. 11 scAAV9\_SRSF1-RNAi (scAAV\_KASPER\_H1\_shRNA 10\_eGFP). The shRNA 10 construct was cloned between HindIII and BamHI restriction sites. The construct also contains an Efs1 $\alpha$  – eGFP construct. Full cloning procedure in 3.2.2-5 pages 6-14.

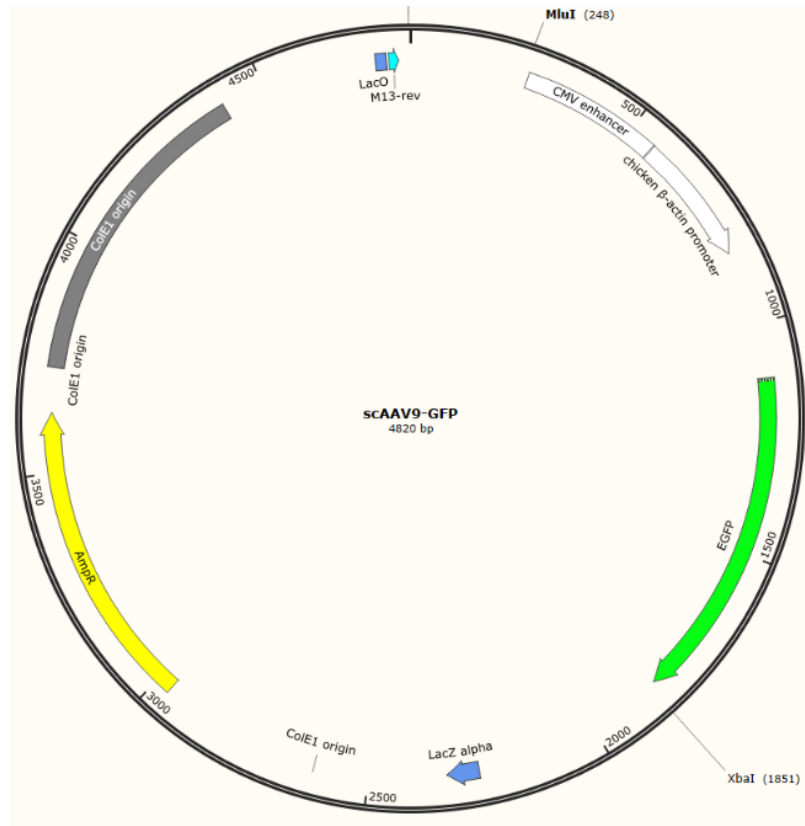


Figure 3. 12 scAAV9\_GFP (scAAV\_CBh\_GFP). The CBh promotor and eGFP sequence is cloned between MluI and XbaI restriction sites. Full cloning procedure in 3.3.2 page 18.



### 3.5 Discussion

This project focuses on *C9ORF72*-ALS/FTD which is caused by polymorphic pathogenic repeat expansions (GGGGCC) in intron 1 of the *C9ORF72* gene. In ALS/FTD patients, these intron-containing *C9ORF72* repeat transcripts (pre-mRNAs) are exported into the cytoplasm in an SRSF1-dependant manner where they subsequently undergo RAN translation. This results in the formation of toxic dipeptide repeat proteins (DPRs) which constitute an important pathophysiological component of motor neuron injury and cell death. Previous studies in my lab have indicated that the SRSF1 protein is sequestered onto these pathogenic repeat transcripts, which allows it to interact with the nuclear export machinery resulting in its export into the cytoplasm. The transcripts subsequently undergo RAN translation, leading to the formation of DPRs. My lab has also shown that the partial depletion of SRSF1, using two chained miRNAs against SRSF1, reduces inhibits the interaction with NXF1 and the nuclear export machinery. This inhibits overall nuclear export of the pathogenic repeat transcripts and reduces RAN translation and therefore the formation of DPRs in reporter cell models, patient-derived neurons and *Drosophila* models of disease. My lab has also used a mutated SRSF1 (SRSF1 m4) which was engineered to bind to the pathogenic repeat transcripts but does not interact with NXF1 and the nuclear export machinery. It was found that the expression of SRSF1-m4 also inhibited the nuclear export of the pathogenic repeat transcripts into the cytoplasm preventing RAN translation, resulting in an overall reduction in toxic DPRs in the cytoplasm in reporter cell models (Hautbergue *et al.*, 2017).

Due to the promising therapeutic benefit of targeting the SRSF1 function in patient-derived neurons and *Drosophila*, the aim of my project is to test both partial depletion of SRSF1 and the expression of therapeutic SRSF1-m4 in mice in order to test the therapeutic proof-of-concept of these gene therapy approaches in one of the closest animals to man. If successful, the longer-term aim would be to move on to larger cohort to validate safety and efficacy in mice and non-human primate studies prior to eventually designing human clinical trials. For this to occur, we had to move from using miRNA against SRSF1 to using shRNA against SRSF1 which are approved by the FDA for gene therapy trials. This is because miRNAs are potentially less specific than shRNAs and could target multiple mRNAs at the same time. Therefore, miRNAs are less useful when trying to target a single gene. Here we have inserted our newly designed shRNA into a plasmid that has successfully been used in previous SMA type 1 clinical trials (Mendell *et al.*, 2017). This approach gives confidence that the plasmid

has the potential to be administered successfully as a clinical trial vector in both mice (Iannitti *et al.*, 2018) and human trials.

My overall project aims are to evaluate the therapeutic efficiency and safety of two neuroprotective strategies in a mouse model. I will assess whether the partial depletion of SRSF1 using shRNA designed against the protein or the expression of a SRSF1 point mutant (therapeutic SRSF1 m4), that is sequestered onto C9ORF72 repeat transcripts (but fails to interact with the nuclear export machinery), can produce a significant neuroprotective effect at molecular, neuronal and motor functional levels.

To achieve these aims our objective throughout the work described in this chapter was to produce functional shRNA plasmids that were able to partially deplete the expression of SRSF1 *in vitro*. And also produce a functional plasmid capable of expressing an SRSF1 point mutant (therapeutic SRSF1 m4) that is sequestered onto C9ORF72 repeat transcripts (but fails to interact with the nuclear export machinery) *in vitro*.

Here, the shRNA constructs against SRSF1 were designed and cloned into a plasmid backbone of a scAAV9 vector. The SRSF1 m4, along with a GFP control, was also constructed and again inserted into a plasmid backbone of an scAAV9 transfer vector. These 3 main constructs were then validated *in vitro* to ensure that they exhibited the expected effects on SRSF1 and DPR expression after transfection in different cell types.

During the co-transfection of both HEK293T and N2A cells with our shRNA plasmids (6, 9 and 10) alongside sense or antisense DPR plasmids, the cells were harvested 48 hours post transfection and a significantly reduced expression of SRSF1 was observed. This suggests that the shRNA is being successfully expressed by the plasmid which then binds to and silences the mRNA of SRSF1 and downregulates the overall expression of the SRSF1 protein. Since the cells were co-transfected with V5-tagged DPRs the reduced expression of V5 protein in cells treated with the shRNA can be explained by this reduction of DPR production. By reducing the expression of SRSF1 this reduces the amount of C9ORF72 repeat transcripts (expressed by the DPR plasmid) that are able to be transported into the cytoplasm, reducing the amount of pathological repeat transcripts that undergo RAN translation and therefore reducing the amount of toxic dipeptide repeat proteins (DPRs) produced within the cytoplasm of the cells (Cooper-Knock, *et al.*, 2014b; Lee *et al.*, 2016).

In comparison to HEK293T cells, there was a slight reduced significance in SRSF1 expression when co-transfecting in N2A cells in the anti-sense experiment which could be due to differing expression levels of SRSF1 in murine cells in comparison to humans. N2A

cells only have a transfection efficiency 25-30% in our lab compared to >95% transfection efficiency observed in HEK cells. There could also be different rectifying mechanisms in each species. Mouse cells may be able to compensate for SRSF1 knockdown more effectively than human cells. However, the reduction of DPR expression appears to be just as effective even when SRSF1 expression is not reduced to the same extent. It can therefore be concluded that the newly designed shRNA constructs against SRSF1 are working as expected. The reason that the shRNAs have been tested in both human cells and in mouse cells is to ensure that the treatment is transferable and that the shRNAs will be able to target both the human mRNA and the mouse mRNA *in vivo*. The results from these experiments suggest that the shRNAs can target both species and successfully deplete SRSF1 in both mouse and human cells.

For the second therapeutic approach we used the SRSF1 mutant (m4) construct and transfected it into HEK293T cells along with V5-tagged DPRs. The quantification indicates that the expression of SRSF1 significantly impacts and decreases the expression of V5. This indicates that the plasmid is able to successfully enter the nucleus of the cell and express the SRSF1 m4 which has a higher affinity for the C9ORF72 hexanucleotide repeats compared to endogenous SRSF1. Once sequestered onto SRSF1 m4, the complex is unable to interact with the export machinery in the nucleus meaning that the pathological repeats are unable to undergo nuclear export and therefore do not undergo RAN translation. With RAN translation unable to occur, the production of toxic DPRs would be severely hindered therefore reducing the expression of V5-tagged DPRs (Freibaum *et al.*, 2015; Zhang *et al.*, 2015). We compared the labs previously published plasmid with our newly developed plasmid. Both plasmids behave in a similar manner and both significantly reduce the expression of the V5-tagged plasmids which produce DPRs. However, the expression of endogenous SRSF1 remains at a similar level to that of untransfected cells. This indicates that SRSF1 m4 does not affect the production and expression of endogenous SRSF1 even though it is able to significantly affect the production of toxic DPRs. It is therefore unlikely that the role of endogenous SRSF1 is hindered in any way and it should be able to carry out its physiological functions within the cell. In conclusion, these constructs also behave as anticipated and align with the results observed in Hautbergue *et al.*, 2017.

In summary, the results of this study suggest that all the newly designed constructs (scAAV\_SRSF1\_shRNA6\_eGFP, scAAV\_SRSF1\_shRNA 9\_eGFP and scAAV\_SRSF1\_shRNA 10\_eGFP) are fully functional vectors capable of mediating SRSF1 protein knockdown and reduced DPR expression *in vitro* (in the case of SRSF1-targeting

constructs), or acting as suitable negative controls (in the case of control constructs, scAAV\_KASPAR\_H1\_Efs1 $\alpha$ \_eGFP). The constructs have been validated in two different cell models, HEK and N2A. The results of this study also indicate that our newly designed constructs (scAAV9\_CBh\_SRSF1 and scAAV9\_CBh\_SRSF1-m4) are fully functional vectors capable of expressing either SRSF1 or SRSF1 m4 *in vitro*, in both HEK and N2A cells. The scAAV\_SRSF1\_shRNA 10\_eGFP was chosen due to its knockdown performance *in vitro* to progress into *in vivo* studies. This validation allows the constructs to be carried forward and packaged into scAAV9 virus' gene therapy vectors which will be the focus of the next chapter. From now on the therapeutic plasmids will be referred to as follows: scAAV\_AZ\_CBh\_SRSF1-m4 will be referred to as **scAAV9\_SRSF1-m4**; scAAV\_AZ\_CBh\_GFP will be referred to as **scAAV9\_GFP**; scAAV\_KAS\_H1-SRSF1\_shRNA10\_GFP will be referred to as **scAAV9\_SRSF1-RNAi**; and scAAV\_KAS\_H1\_scrambled-shRNA\_GFP will be referred to as **scAAV9\_Ctrl-RNAi**.

## CHAPTER 4 – Production of Functional Large-Scale SRSF1-Targeting Gene Therapy Viruses for Subsequent Investigation in Mouse Studies

### 4.1 Aims

C9ORF72-linked ALS and FTD forms a spectrum of fatal neurodegenerative diseases, ALS being characterised by the death of motor neurons and progressive paralysis, while degeneration of neurons in the frontal and temporal lobes of the brain leads to altered personality features and psychological disinhibition in FTD. C9ORF72-ALS/FTD is the most common genetic cause of motor neuron disease and involves polymorphic hexanucleotide repeat expansions in the proximal non-coding region of the *C9ORF72* gene. Our group has previously shown that SRSF1 drives the nuclear export of pathological *C9ORF72* repeat transcripts leading to the cytoplasmic production of toxic dipeptide repeat proteins (DPRs). Moreover, the partial depletion of SRSF1 or expression of an engineered SRSF1-m4 mutant (that binds *C9ORF72* repeat transcripts but has lost ability to interact with the nuclear export machinery) efficiently inhibits the nuclear export of *C9ORF72* repeat transcripts and confers neuroprotection in *C9ORF72*-ALS/FTD cell models. Depletion of SRSF1 also showed rescue of neurodegeneration-associated locomotor deficits in a *C9ORF72* ALS/FTD *Drosophila* model (Hautbergue *et al.*, 2017). The previous chapter further confirms that the recently designed scAAV9 compatible plasmids successfully result in the expression of the engineered SRSF1-m4 protein or partial depletion of SRSF1. In the previous chapter, I showed that scAAV\_SRSF1-RNAi depletion of SRSF1 expression and the expression scAAV\_SRSF1-m4 inhibits the RAN translation of DPRs in reporter cell models of *C9ORF72*-ALS/FTD.

In this chapter the experimental plasmids (scAAV\_SRSF1-RNAi, scAAV\_SRSF1-m4, scAAV\_GFP) were packaged into adeno associated serotype 9 viruses (AAV9). Their ability to infect cells will be tested both *in vitro* and *in vivo*. The functionality of these viruses will also be tested to ensure that the viral particles act in a similar manner resulting in the inhibition of the RAN translation of DPRs as shown in the previous chapter for the unpackaged plasmids.

The overall goal of the work described in this chapter was to test the efficacy of the SRSF1 manipulating self-complementary adeno associated viruses in a mouse model. The mouse studies require large amounts of virus to be produced, with a final dosage of  $1 \times 10^{10}$  vg

delivered in a 5µl intra-thecal injection. This chapter describes the large volume production of the three experimental scAAV9 in preparation for the *in vivo* experiments.

## 4.2 Viral vector choice and therapeutic construct

For this study, adeno-associated virus 9 (AAV9) has been chosen as the gene therapy delivery system because of its tropism for the CNS (Akache *et al.*, 2006; Shen *et al.*, 2011; Bell *et al.*, 2012; Castle *et al.*, 2016). AAVs are usually single stranded viruses but in this case a self-complementary AAV has been used. The DNA genome of self-complementary AAV (scAAV) is double stranded therefore increasing the efficiency of the virus, as cell machinery is not required to provide the second strand to express the transgene of interest. scAAV is packaged as a single-stranded inverted repeat, which folds into double-stranded DNA (dsDNA) without the requirement for DNA synthesis, leading to more efficient transduction than standard single stranded AAV. The use of scAAV should reduce the time in which the gene therapy becomes effective and potentially less virus would be required to produce a greater effect than if using single stranded pAAV (McCarty *et al.*, 2003; Yokoi *et al.*, 2007; McCarty, 2008).

AAV is made up of two genes *Rep* and *Cap* which are both flanked by 2 inverted terminal repeats. The *Rep* gene encodes 4 proteins which are vital for genome replication and virion assembly: Rep40, Rep52, Rep68 and Rep78. The *Cap* gene encodes for three capsid proteins, Virion protein 1 (VP1), VP2 and VP3. Additionally, *Cap* also encodes for an assembly-activating protein (AAP) which is involved in capsid assembly. AAV virions are composed of 60 virion protein subunits at a ratio of VP1:VP2: VP3. There are 9 variable regions on each subunit on the virion surface (Xie *et al.*, 2002; Govindasamy *et al.*, 2006). These variable surface regions determine the primary tropism and intra-cellular trafficking of the AAV vector, and it is these particular regions that are recognized by neutralizing antibodies. When these variable regions are genetically modified this can change the transduction efficiency and the ability of neutralizing antibodies to bind to the surface of the AAV virion (Büning *et al.*, 2015; Kotterman *et al.*, 2015).

It has been shown that C9ORF72-ALS/FTD dipeptide repeat proteins (DPRs) are present within motor neurons, found in the CNS, and that reducing their amounts confers neuroprotection in *Drosophila*, reporter cell models and patient-derived neurons (Mizielinska *et al.*, 2014; Hautbergue *et al.*, 2017). The gene therapy strategies that we have designed will be delivered to the CNS as the production of DPRs, that are the pathological response in

C9ORF72 ALS/FTD, are our main target and principal readout for efficacy and target engagement. The overall aim is to deliver the therapeutic AAV9 constructs successfully into the CNS without resulting in major off target effects. The AAV9 variant that was chosen targets the cells in the CNS and has been shown to be able to cross the blood brain barrier (a major hurdle when designing a successful gene therapy vector for the CNS). We know that AAV9 is also able to target the heart, but it has been shown that AAV9 has a high tropism for the CNS which suggests that the majority of the virus will remain within the CNS if directly delivered to the CSF (Lukashchuk *et al.*, 2016; Saraiva, Nobre and Pereira de Almeida, 2016). AAV9 also has a tropism for muscle and if there is an off-target effect found in the muscle, it is predicted that this will increase the efficiency of the virus (Gao *et al.*, 2004; Bey *et al.*, 2020). Neurons connecting with the muscles are often most affected with the neurodegenerative effects of motor neuron disease. Reducing dipeptide repeat proteins in both the CNS and the muscle could be a valuable therapeutic strategy.

scAAV9\_SRSF1-RNAi is based on the vector, used in Iannitti *et al.*, 2018, which included an shRNA against the SOD1 protein. The results from this paper were very encouraging and so the same backbone plasmid was used to create the scAAV\_SRSF1-RNAi plasmid. The AAV in the SOD1 study was a single stranded AAV and in this study we subcloned into an scAAV to increase transduction efficiency.

Overall, we have reason to believe scAAV9 to be effective as a gene therapy for neurological diseases especially due to promising evidence resulting from the new Zolgensma® drug. In May 2019 the FDA approved the gene therapy Zolgensma® designed to treat type 1 Spinal Muscular Atrophy which is a severe form of childhood motor neuron disease. Zolgensma® is delivered via an AAV9 viral vector and the results from this new treatment are very encouraging with the main side effects reported being vomiting and increased serum aminotransferases (Mendell *et al.*, 2017).

As AAV9 has been involved in the main studies above, treating other types of motor neuron disease with little off-targeting effects, this gives confidence that this serotype would be the most appropriate for our gene therapy designed for C9ORF72-ALS/FTD.

### 4.3 Overview of scAAV assembly

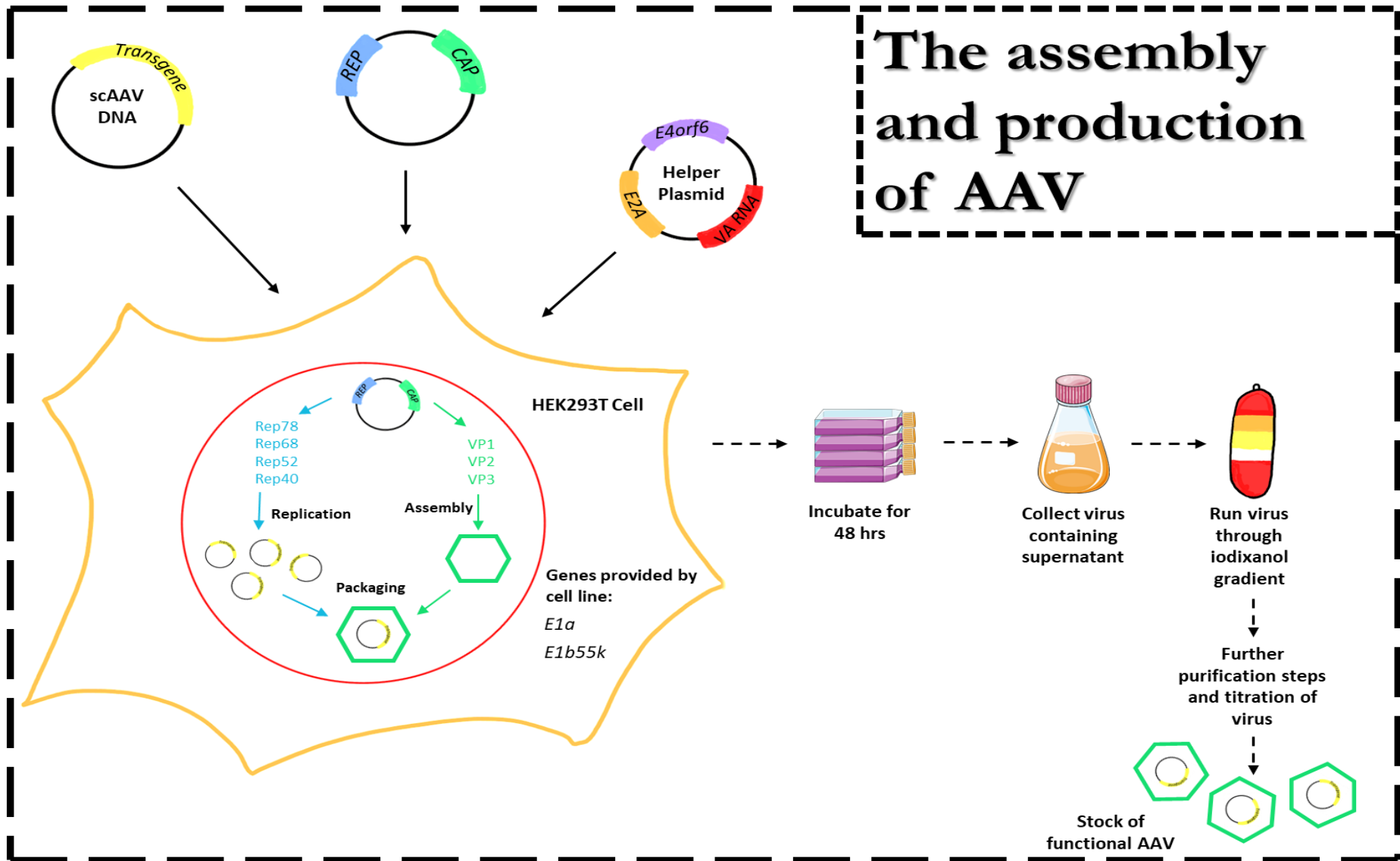


**Figure 4. 1 Overview of scAAV assembly and production.** To generate the large scale production scAAV vectors, four key components are required: A cassette to provide the transgene enclosed by two inverted terminal repeats (ITRs), a plasmid to provide the scAAV Rep and Cap genes that are required for capsid formation and replication, a plasmid that provides the adenovirus helper genes E4orf6, E2a, VA RNA, and a viral packaging cell line provides the helper genes E1a and E1b55k. Once the virus is assembled it can travel outside the cell and remains in the supernatant which is harvested after a 48-hour incubation period. The supernatant then undergoes various filtration, purification, de-salting and finally titration to produce a stock of functional scAAV with the correct transgene successfully integrated into the DNA.

#### 4.4 Small scAAV preparation of therapeutic constructs

It can be concluded from the results discussed in chapter 3 that SRSF1-m4 expressed from the scAAV plasmid is effective at reducing the expression of DPRs and is therefore functional *in vitro*. The results also indicate that the newly designed SRSF1-shRNA cassette reduces SRSF1 expression whilst also inhibiting the expression of DPRs, therefore allowing the study to move on to the *in vivo* testing of both of these constructs. For these plasmids to work therapeutically and be effective throughout the nervous system during *in vivo* experimentation, they need to be enveloped into a viral vector. We have chosen scAAV9 as our viral vector. A small-scale viral prep was used to ensure that the plasmids would be effective once packaged into the scAAV9 vector before attempting large scale production.

To be able to track where the therapeutic vectors can distribute themselves following administration, a control virus expressing GFP was designed with the same backbone as the FLAG-tagged SRSF1-m4 construct under a strong promoter, chicken  $\beta$ -actin (CBA) hybrid promoter (CBh). The recently prepared plasmids scAAV9\_GFP (is the control), scAAV9\_SRSF1-WT (used in *in vitro* experiments in chapter 3), scAAV9\_SRSF1-m4 and scAAV9\_SRSF1-RNAi were then packaged into an scAAV9 virus. Each of the plasmids were co-transfected with a helper and rep/cap plasmid to produce a small volume preparation of each therapeutic virus. Once the small scAAV preparation was completed, the viruses underwent SDS-PAGE and western blot analysis using the antibodies targeting V1, V2 and V3 to detect the capsid proteins in order to assess whether the plasmid had been successfully encapsidated. Figure 4. 2A showed that the three proteins (V1, V2 and V3) were expressed by each of the viral vectors and confirmed that the capsid had formed successfully. The viral vectors were then transduced into 293T HEK cells to ensure that the control viral vector was able to express GFP once it was packaged within the capsid. Both the scAAV9\_GFP and scAAV9\_SRSF1-RNAi showed expression of GFP in the western blot suggesting that these vectors were functional, and that the constructs had been packaged successfully.

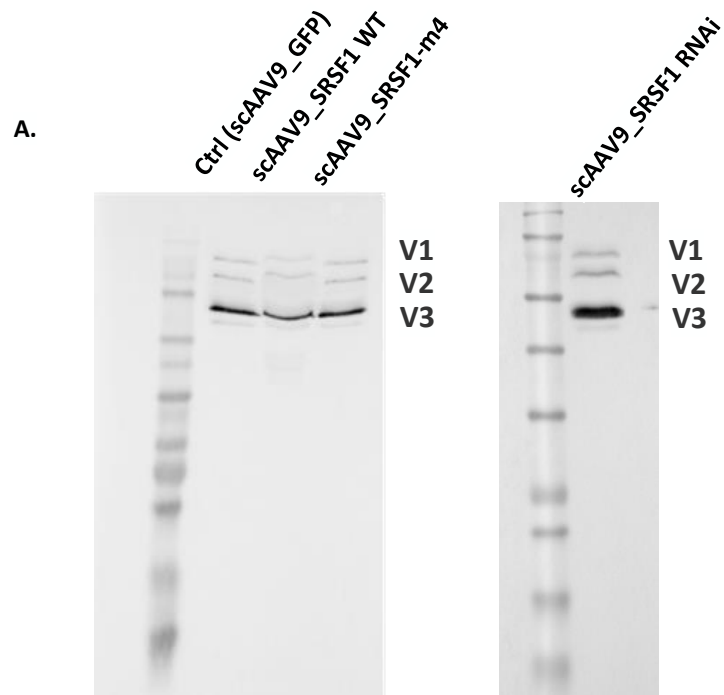
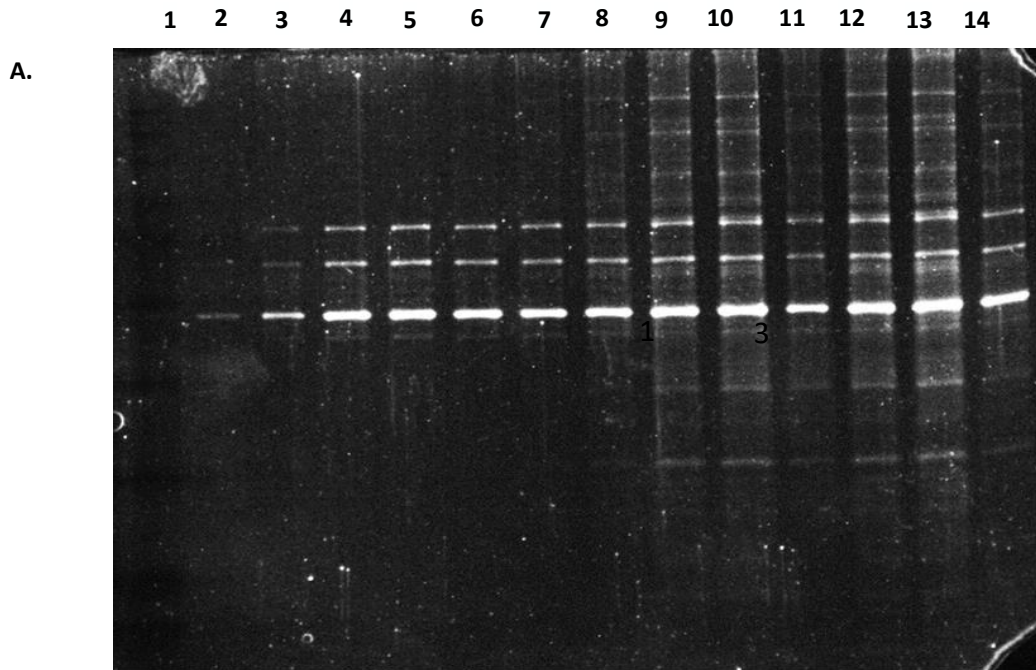


**Figure 4. 2 (A)** Western image depicting the expression of the capsid proteins, V1 (87 kDa), V2 (73kDa) and V3 (62kDa) of the newly packaged viral vectors.

## 4.5 Large scAAV9 preparation of therapeutic vectors

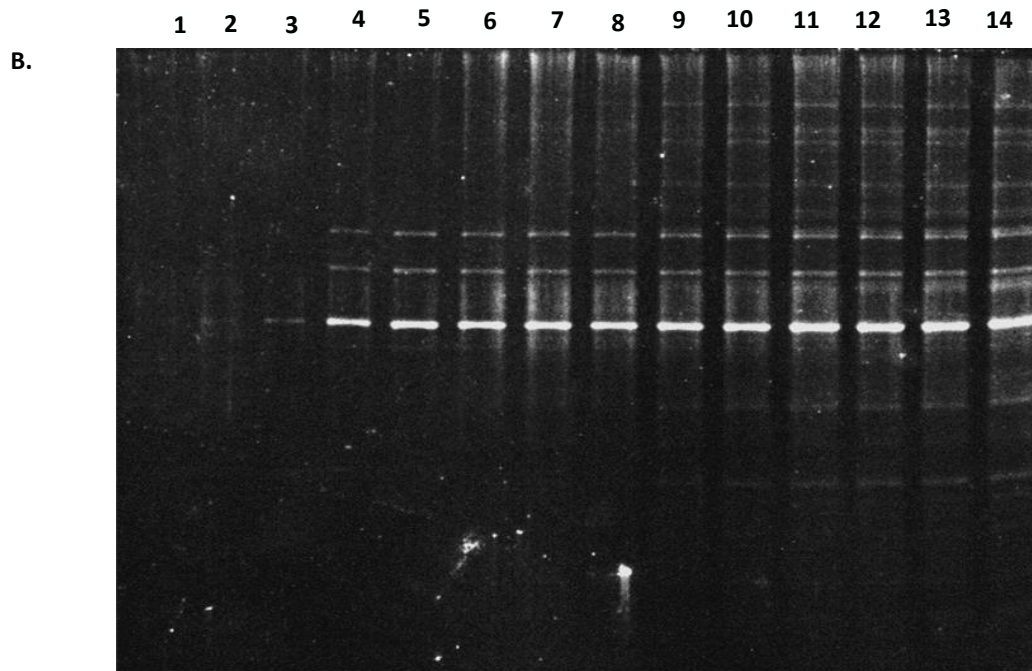
The small scAAV preparation of the three constructs (scAAV9\_CBh\_eGFP, scAAV9 CBh\_SRSF1-m4 and scAAV9 SRSF1 RNAi) indicated that they were able to be successfully encapsidated whilst still maintaining their function. Previous studies within the lab indicate that a functional scAAV9-H1-ctrl shRNA virus has already been created and utilised in previous projects (Ianitti et al, 2018). The control scAAV9 H1 shRNA virus was produced externally and so this virus did not undergo a large-scale preparation in our laboratory.

The constructs then underwent a large scAAV preparation to produce an increased yield of virus (Figure 4. 1). The plasmids were co-transfected with a helper plasmid and rep/cap plasmid into 15 T175 flasks of HEK293T cells. The supernatant/virus from the flasks was harvested 48 hours post transfection and purified and concentrated (materials and methods). Once each of the viruses had been concentrated the collected fractions were run on a 12% acrylamide gel using SDS-PAGE. The gel was then stained with Sypro Ruby, which is used to visualise the total protein within the concentrated fractions. The fractions with the most purified virus have three distinct bands to represent the three capsid proteins V1, V2 and V3. Any fractions that have other bands indicate that the fractions have other proteins contaminating the virus and are not considered to be as pure. The purest fractions of each virus were pooled together to produce the high-quality virus and the least pure fractions were pooled together to produce the low-quality virus (Figure 4. 3, Figure 4. 4 and Figure 4. 5). The high-quality virus will be used for the *in vivo* study as contamination by other proteins had been minimised, reducing the risk of off target effects. The low-quality virus was used for further *in vitro* experiments to ensure that the high-quality virus could be utilised during the *in vivo* study.



**Tube 1 Fractions**

**High Quality – 1-11**  
**Low Quality – 12 & 13**



**Tube 2 Fractions**

**High Quality – 1-6**  
**Low Quality – 7-10**

**Figure 4. 3 (A)** Sypro Ruby staining of the scAAV9\_SRSF1-m4 viral prep (tube 1 fractions). **(B)** Sypro Ruby staining of the scAAV9\_SRSF1-m4 viral prep (tube 2 fractions). Lanes 1 to 11 of the fractions isolated from tube 1 and lanes 1 to 6 of the fractions isolated from tube 2 were combined to produce the high quality scAAV9\_SRSF1-m4 virus. Lanes 12 and 13 from the fraction isolated from tube 1 and lane 7 to 10 from the fraction isolated from tube 2 were combined to produce the low quality scAAV9\_SRSF1-m4.

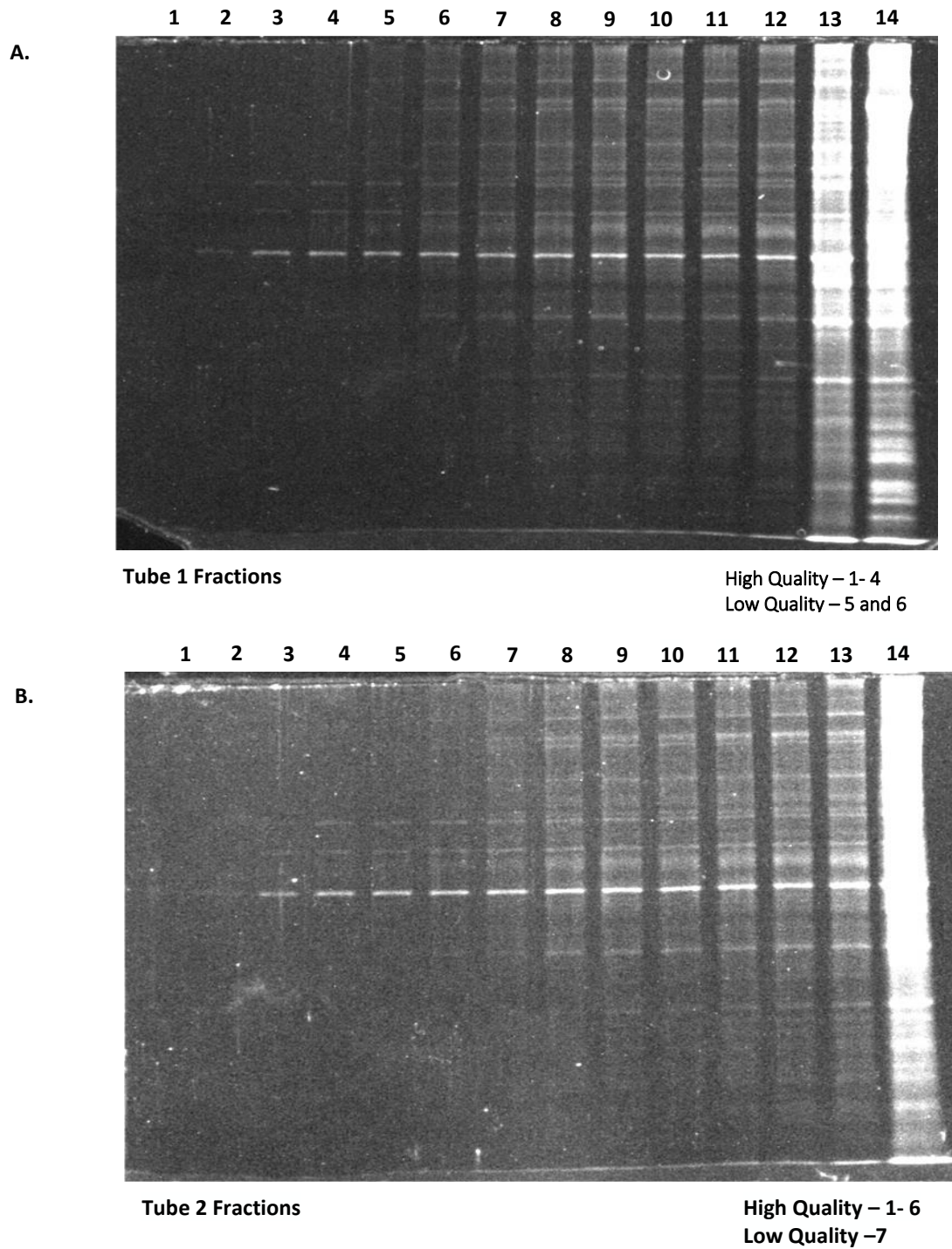


**Figure 4. 4** (A) Sypro Ruby staining of the scAAV9\_GFP viral prep (fractions from centrifuge tube 1). (B) Sypro Ruby staining of the scAAV9\_GFP viral prep (fractions from centrifuge tube 2). Lanes 1 to 4 of the fraction isolated from tube 1 and lanes 1 to 6 of the fraction isolated from tube 2 were combined to produce the high quality scAAV\_GFP virus. Lanes 5 and 6 from the fraction isolated from tube 1 and lane 7 from the fraction isolated from tube 2 were combined to produce the low quality scAAV9\_GFP.

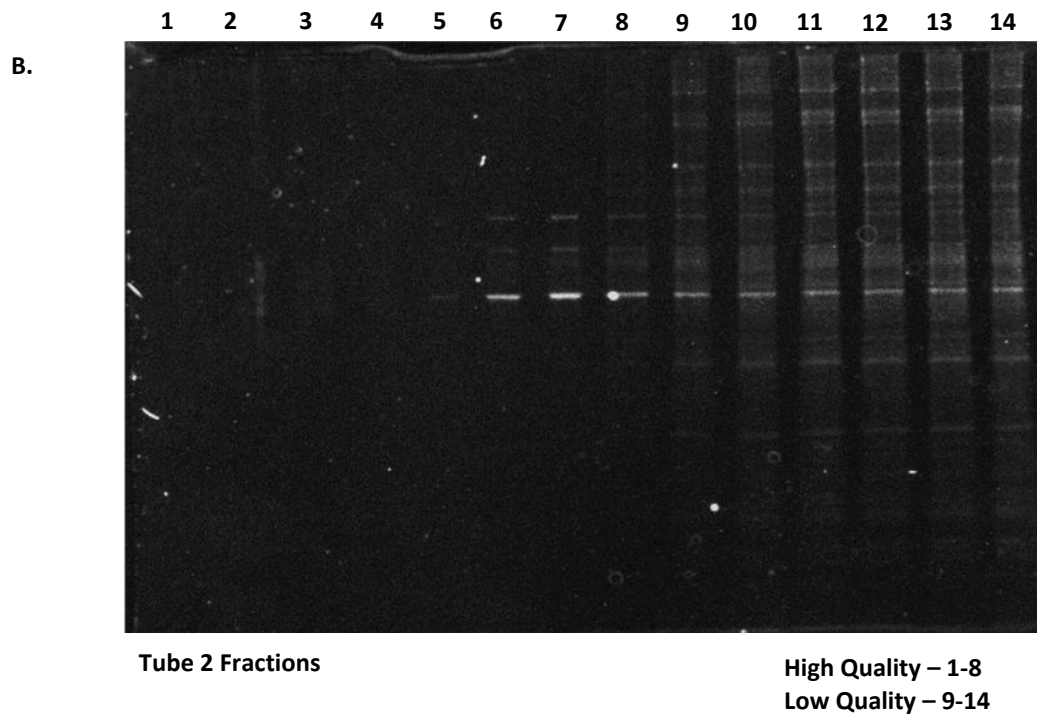
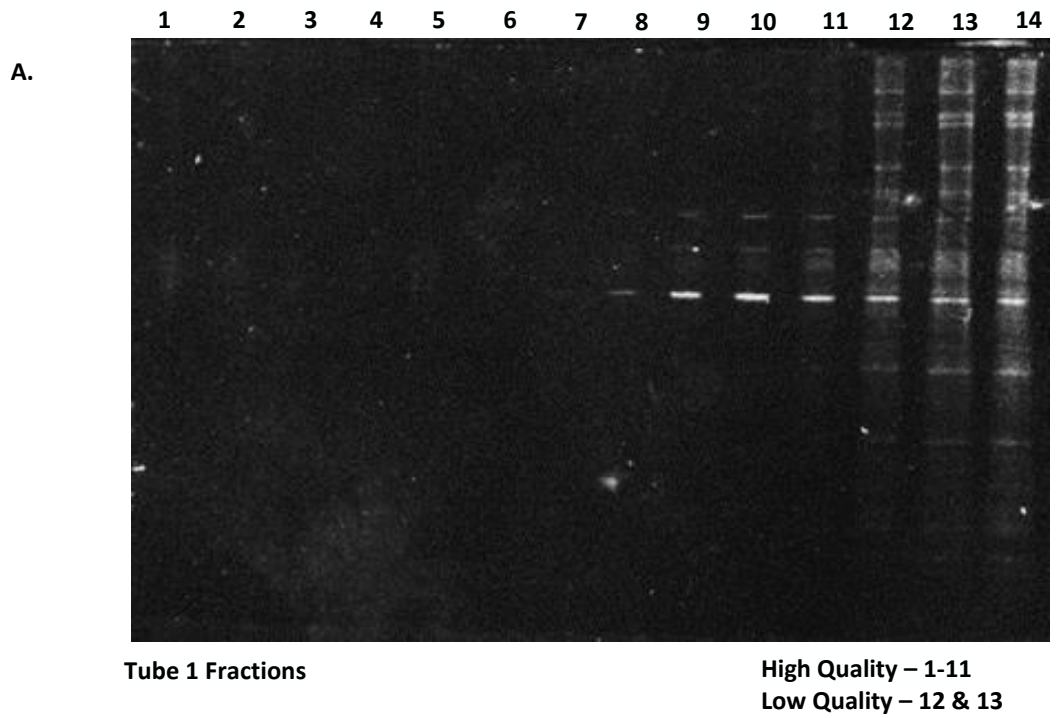


**Figure 4. 5 (A)** Sypro Ruby staining of the scAAV9\_SRSF1 RNAi viral prep (tube 1 fractions). **(B)** Sypro Ruby staining of the scAAV9\_SRSF1 RNAi viral prep (tube 2 fractions). Lanes 1 to 11 of the black fraction and lanes 1 to 8 of the blue fraction were combined to produce the high quality scAAV9\_SRSF1 RNAi virus. Lanes 12 and 13 from the black fraction and lane 9 to 14 from the blue fraction were combined to produce the low quality scAAV9\_SRSF1-m4.

## 4.6 Determination of viral genome titres via qPCR

Once the large scAAV preparation of scAAV9\_SRSF1-m4, scAAV9\_SRSF1-RNAi and scAAV9\_GFP had been completed and high-quality virus of each construct had been successfully obtained, we calculated the physical titre of each virus by quantifying the viral genome copy numbers using qPCR (Chapter 2: Materials and Methods).

Clinical dosing of recombinant AAV (rAAV) therapeutics is based on the physical vector genome (vg) titre and requires quality control methods that can accurately determine the amount of vector being administered. To standardize therapeutic vector doses used by different investigators, there was a need for a well-characterized rAAV reference standard of materials. The most common method for quantification of packaged AAV vector genomes is the quantitative polymerase chain reaction (qPCR) assay that uses a standard curve prepared with a linearized plasmid DNA as a reference (U.-P. Rohr *et al.*, 2002).

Using the AAV titration protocol, indicated in the materials and methods, scAAV9 CBh\_GFP, scAAV9 CBh\_SRSF1-m4 and scAAV9 SRSF1 RNAi had their physical concentrations calculated in vg/ml using qPCR (Table 4. 1).

**Table 4. 1:** Viral Titres – Viruses were titered and their concentrations were calculated using qPCR data. There was no low-quality virus available for control pAAV9 CBh\_GFP as it was created by a different lab and only the high-quality virus was used in their studies.

Virus	High Quality Virus Titre	Low Quality Virus Titre
Control pAAV9_GFP	7.9 x 10 <sup>12</sup> vg/ml	N/A
scAAV9_GFP	3.5 x 10 <sup>11</sup> vg/ml	2.19 x 10 <sup>11</sup> vg/ml
scAAV9_SRSF1-m4	1.91 x 10 <sup>12</sup> vg/ml	1.98 x 10 <sup>12</sup> vg/ml
scAAV9_SRSF1-RNAi	2.68 x 10 <sup>11</sup> vg/ml	1.2 x 10 <sup>11</sup> vg/ml

The the physical titres would be expected to be higher than what was calculated, at least  $1 \times 10^{12}$  vg/ml and closer  $1 \times 10^{13}$  vg/ml. Therefore, the titres of scAAV9 CBh\_GFP and scAAV9 SRSF1 RNAi are considerably lower than would be expected following this large preparation protocol. It was then checked whether or not these lower physical titres directly correlated with a decrease in biological titre and infectivity.

The difference between a physical and infectious titre is that a physical titre is a measurement of the quantity of virus present and expressed as viral genomes per ml (vg/ml), whereas the infectious titre is the measurement of how much of the virus is able to infect the target cells and is expressed as transduction units per ml (TU/ml).

#### 4.7 Determination of viral titres via FACS method

Once the large preparations of scAAV9\_CBh\_SRSF1\_m4, scAAV9\_SRSF1\_RNAi and scAAV9\_CBh\_GFP had been completed and high-quality virus of each construct had been successfully obtained, the biological titre of each virus was calculated using FACS.

FACS stands for fluorescence-activated cell sorting (FACS) which is a specialized type of flow cytometry. It is a method that is able to sort a heterogeneous mixture of biological cells into two or more groups, one cell at a time, by the observation of light scattering and fluorescent characteristics of each individual cell. The method provides fast, objective and quantitative recording of fluorescent signals from individual cells. It also provides physical separation of cells of interest.

FACS was used to test infectivity of our scAAV large scale viral preparations to determine a biological titre in transducing units (TU). Transduction requires the entry of scAAV vectors into the cells, the translocation of vector genomes (vg) to the nucleus and their eventual conversion into double stranded DNA, and, in addition, transcription of the transgene. The readout is the detection of the fluorescent transgene encoded protein.

The number of GFP positive cells was calculated in our viral transduced 293T HEK cells. These cells were transduced with either scAAV9 CBh\_GFP or scAAV9 SRSF1 RNAi virus that was diluted to either  $10^{-2}$ ,  $10^{-3}$ ,  $10^{-4}$  using DMEM media and harvested 72 hours later. The cells were processed (as described in the material and methods) then fixed in 4% paraformaldehyde in their individual dilutions

The processed cell suspension was then inserted into the centre of a rapidly flowing, narrow stream of liquid. The flow of the liquid stream is arranged so that there is a large separation between cells relative to their diameter. There is a vibrating mechanism which causes the stream of cells to break into individual droplets. The system is designed and adjusted so that there is a high probability that there is only one cell per droplet. Before the liquid stream breaks the flow into droplets, the flow passes through a fluorescence measuring station where the fluorescent character of interest of each cell is measured (in this case GFP). Where the stream breaks into droplets there is an electrical charging ring. Immediately prior to the fluorescence intensity measurement, a charge is placed on the ring and the opposite charge is trapped on the droplet as it breaks free from the stream. These oppositely charged droplets then fall through an electrostatic deflection system that diverts droplets into containers based upon their charge. The amount of fluorescence present is then calculated depending on the charged particles in the containers.

For this experiment a 12 well plate was used with four groups: untransfected, transduced with a control pAAV9 GFP virus (titre already known), scAAV9\_GFP or scAAV9\_SRSF1 RNAi. Cells were collected following a 48-hour incubation period and prepared for FACS analysis.

Using the amount of fluorescence detected from our GFP transduced cells using this FACS flow cytometry method, the infectious titre of the two scAAV9 viruses was calculated (page 17-19). These calculations were used to deduct the GFP containing viruses predicted qPCR concentrations would be using both the FACS and qPCR concentration of a previously known virus. Usually when using FACS analysis a known MOI of the virus is used. However, during this study the qPCR concentrations of our viruses appeared unusually low compared to previously prepared viruses. It was hypothesised that any differences were likely due to the fact that the viruses were scAAV9 rather than pAAV9 which was more commonly used in previous studies. Instead of using known MOI's to transduce the cells virus dilutions ( $10^{-1}$ ,  $10^{-2}$ ,  $10^{-3}$ ) were used. The limiting factor of this method is that the transduction efficiency of the scAAV9\_SRSF1-m4 virus was unable to be assessed as it does not express GFP. However, as the scAAV9\_SRSF1-m4 virus had the same back bone as the control scAAV9\_GFP, it was anticipated that they would behave and transduce with similar efficiency.

A.

BD FACSDiva 8.0.1

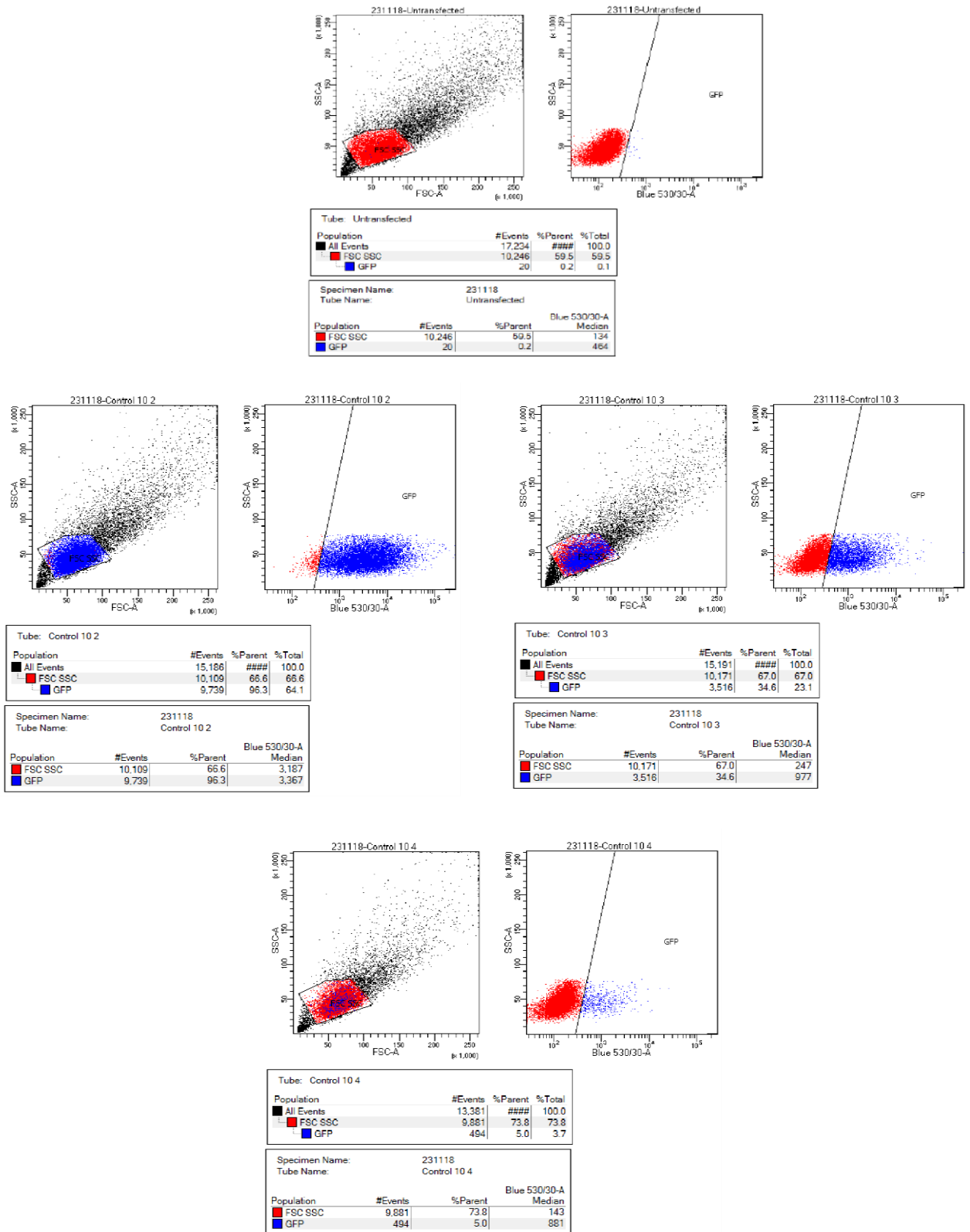


Figure 4. 6 FACS Analysis of scAAV9\_SRSF1 RNAi and scAAV9\_GFP after transfection into HEK 293T cells (A) FACS analysis of untransfected cells and a control GFP virus. In the left-hand side scatter graph for each concentration of the control virus the gate represents live cells (red). The right-hand side scatter graph for each concentration of control virus represents what population of those live cells are GFP positive (blue).

B.

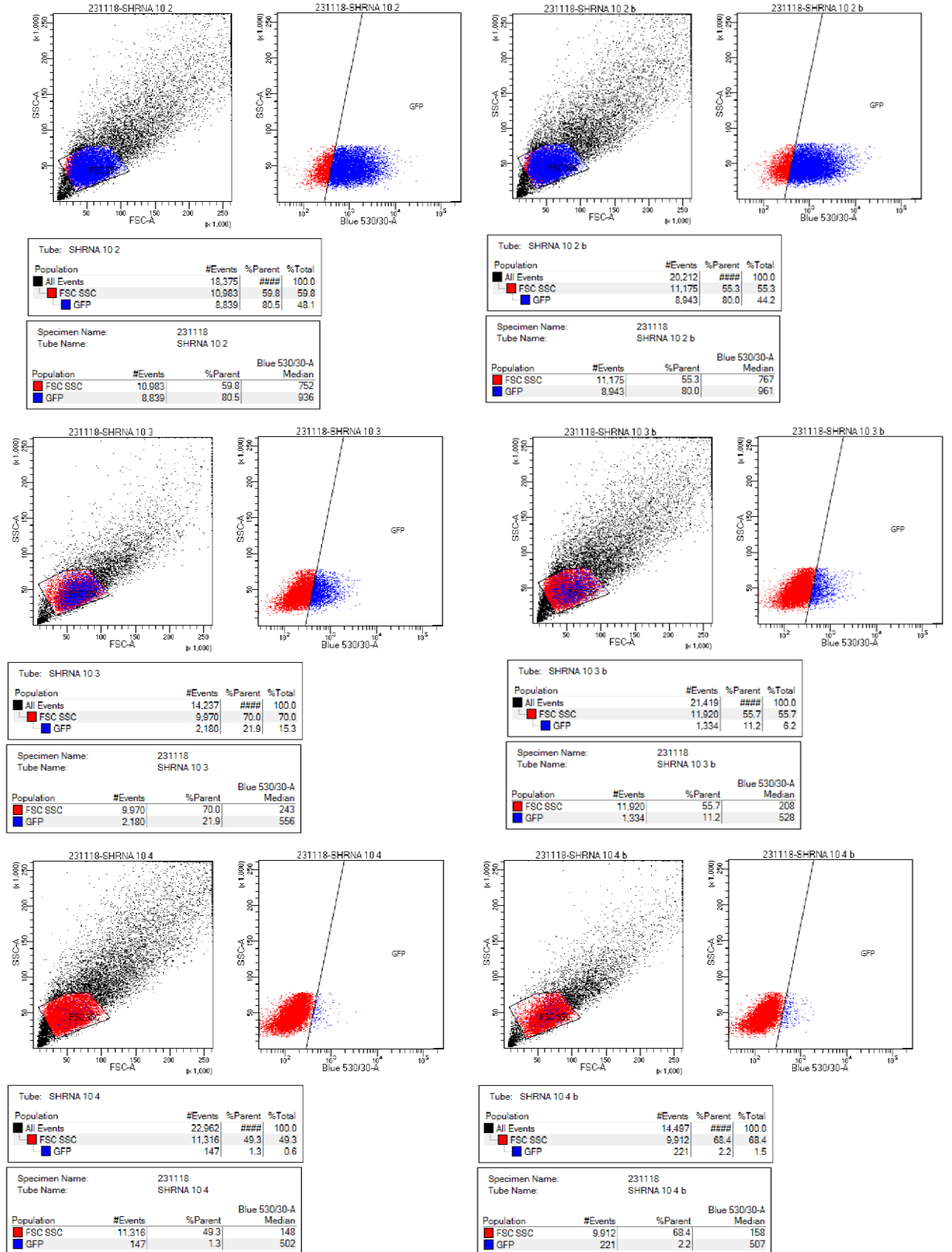


Figure 4. 7 FACS Analysis of scAAV9\_SRSF1 RNAi and scAAV9\_GFP after transfection into HEK 293T cells. (B) FACS analysis of scAAV9\_SRSF1 RNAi. On the left-hand side scatter graph for each concentration of scAAV9\_SRSF1-RNAi, the gate represents live cells (red). The right-hand side scatter graph for each concentration of scAAV9\_SRSF1-RNAi represents what population of those live cells are GFP positive (blue).

C.

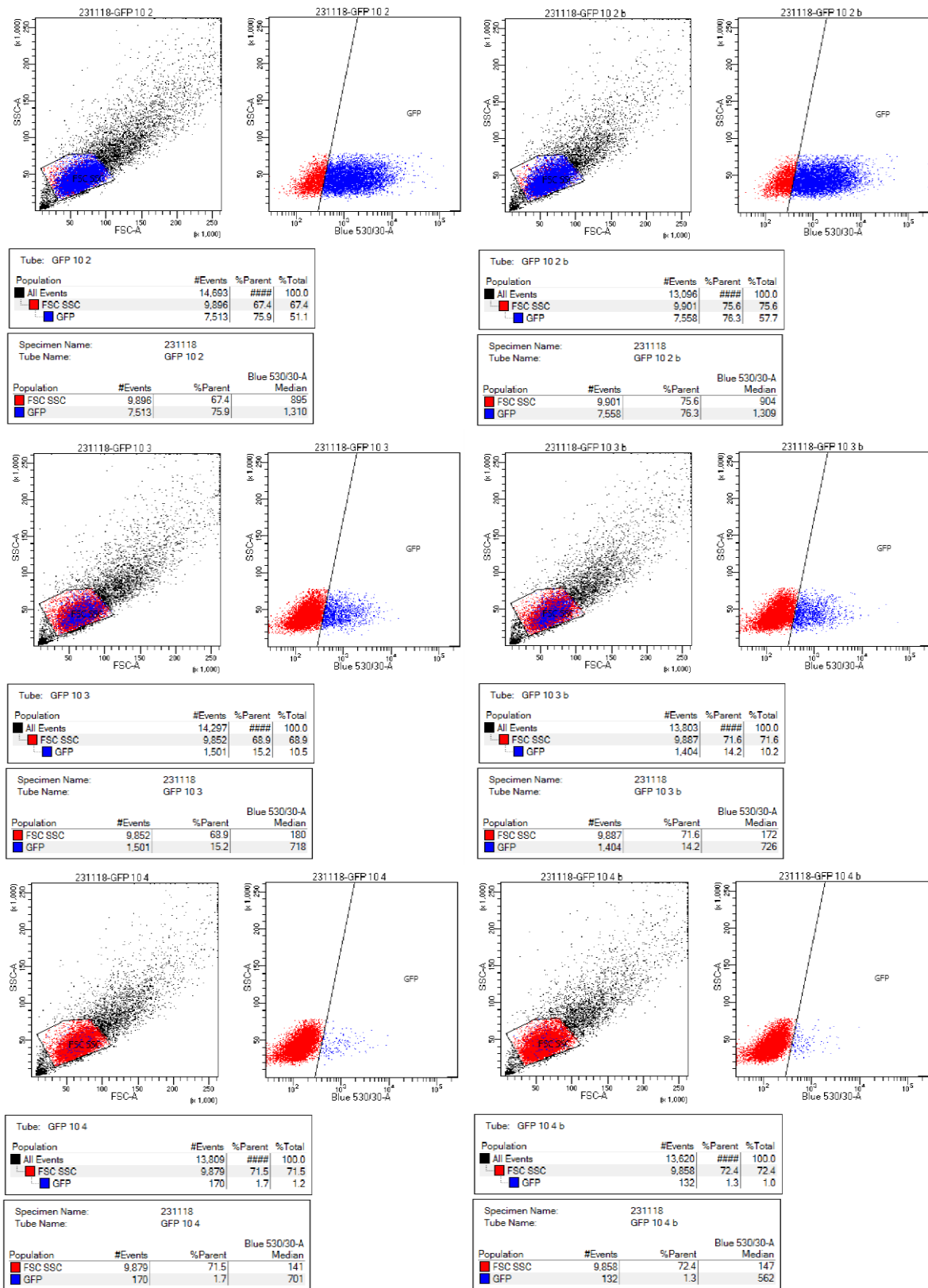


Figure 4. 8 FACS Analysis of sAAV9\_SRSF1 RNAi and sAAV9\_GFP after transfection into HEK 293T cells (C) FACS Analysis of sAAV9\_GFP. On the left-hand side scatter graph for each concentration of sAAV9\_GFP, the gate represents live cells (red). The right-hand side scatter graph for each concentration of sAAV9\_GFP represents what population of those live cells are GFP positive (blue).

**Table 4. 2: FACS results** – percentage of fluorescent GFP positive cells in each population of live cells treated with either the control GFP virus, scAAV\_GFP, scAAV9\_SRSF1-RNAi or untransfected cells.

<b>Dilution</b>	<b>Control/ %</b>	<b>scAAV9 GFP/ %</b>	<b>scAAV9 SRSF1-RNAi/ %</b>	<b>Untransfected/ %</b>
10 <sup>-2</sup>	96.3	80.3	76.1	0.2
10 <sup>-3</sup>	34.6	16.6	14.7	0.2
10 <sup>-4</sup>	5.0	1.75	1.5	0.2

Table 4. 2 consolidates our FACS results (Figure 4. 6, Figure 4. 7 and Figure 4. 8) comparing the four experimental groups. The untransfected cells, as anticipated, have a very low percentage population of GFP positive cells. The untransfected cells were not transfected or transduced with any GFP expressing plasmid or virus and therefore any GFP signal recorded is expected to be background. The control GFP virus of known titre shows the highest percentage of GFP positive cells in the live cell population compared to both experimental viruses. scAAV9\_GFP has a higher percentage population of GFP positive cells in comparison to scAAV9\_SRSF1-RNAi which was expected as scAAV9\_GFP has a stronger promoter to drive the expression of the inserted transgene. Even though there is a difference in promoters, the percentage population of GFP cells in both groups is similar however due to the promoter differences this may not necessarily suggest similar titres. It is known that the CBh promoter is stronger than the H1 promoter used to express the RNAi. The percentages obtained from the FACS analysis were then used to calculate the biological titre of each GFP expressing virus. The calculations were as follows:

**Example - Control GFP virus – pAAV CBh GFP FACS Titration**

$$\begin{aligned}
 & \mathbf{10^{-2}}(0.963 \times 70,000) - (0.002 \times 70,000) \\
 & = 67410 - 140 = 67,270 \\
 & \text{TU/ml} = (67,270 \times 1000)/0.1 \\
 & = 6.727 \times 10^7 / 0.1 = \mathbf{6.727 \times 10^8 \text{ TU/ml}}
 \end{aligned}$$

$$10^{-3} (0.346 \times 70,000) - 140 = 24,080$$

$$\text{TU/ml} = (24,080 \times 1000)/0.01$$

$$= 2.4080 \times 10^7/0.01 = \underline{\underline{2.4080 \times 10^9 \text{ TU/ml}}}$$

$$10^{-4} (0.05 \times 70,000) - 140 = 3360$$

$$\text{TU/ml} = (3360 \times 1000)/0.001$$

$$= 3.36 \times 10^6/0.001 = \underline{\underline{3.36 \times 10^9 \text{ TU/ml}}}$$

$$\text{Average of } 10^{-2}, 10^{-3} \text{ and } 10^{-4} = \underline{\underline{2.1469 \times 10^9 \text{ TU/ml}}}$$

**Table 4. 3.** Summary of overall FACS calculations and concentrations (TU/ml)

<u>Concentration</u>	<u>Control GFP virus – pAAV CBh GFP/ TU/ml</u>	<u>scAAV9 GFP/ TU/ml</u>	<u>scAAV9 SRSF1- RNAi/ TU/ml</u>
<u>10<sup>-2</sup></u>	6.727 x 10 <sup>8</sup>	5.313 x 10 <sup>8</sup>	5.6 x 10 <sup>8</sup>
<u>10<sup>-3</sup></u>	2.4080 x 10 <sup>9</sup>	1.15 x 10 <sup>9</sup>	1.15 x 10 <sup>9</sup>
<u>10<sup>-4</sup></u>	3.36 x 10 <sup>9</sup>	1.085 x 10 <sup>9</sup>	9.10 x 10 <sup>8</sup>
<u>Overall Concentration</u>	<b>2.1469 x 10<sup>9</sup></b>	<b>9.24 x 10<sup>8</sup></b>	<b>8.28 x 10<sup>8</sup></b>

Once the overall FACS titres were calculated (Table 4. 3) for the 3 scAAV9 viruses the *in vitro* testing in HEK cells commenced.

## 4.8 *In vitro* testing of the gene therapeutic vectors

Each of the therapeutic viruses were tested *in vitro* following the large scAAV preparation, to ensure that packaging the plasmids into an scAAV9 virus resulted in the same response and therapeutic benefit, with no off-target effects. Each of the viruses (scAAV9\_GFP, scAAV9\_SRSF1-m4 and scAAV9\_SRSF1-RNAi) was transduced at an MOI of 300,000 into HEK 293 cells. The cells were then harvested 72 hours post-transduction and analysed via SDS-PAGE and western blot analysis. In Chapter 3 one it was observed that the SRSF1 RNAi plasmid was able to reduce the expression of SRSF1 whilst also reducing the production of toxic DPR proteins. During the viral *in vitro* cell experiments there was no evidence to suggest that any of the viruses increased cell death or affected cell growth during the 72 hours before harvest. As is shown in Figure 4. 9, it can be confirmed that the scAAV9\_SRSF1-RNAi virus is also able to reduce the expression of SRSF1 and the production of V5 tagged DPRs. HEK 293 cells that have been treated with scAAV9\_SRSF1-RNAi can be seen to have a reduced expression of SRSF1 in comparison to the UT and control treated cells suggesting that SRSF1 RNAi, in viral form, is able to achieve knockdown of SRSF1 expression. It can also be confirmed that scAAV9\_SRSF1-RNAi successfully transduced into the HEK 293T cells by the expression of GFP, which was also the case for scAAV9\_GFP (Figure 4. 9). The *in vitro* results indicated that scAAV9\_SRSF1-m4 had successfully transduced the HEK293 cells as they were clearly expressing the flag tag fused to the SRSF1-m4 protein. Again, the scAAV9\_SRSF1-m4 expressed both the endogenous SRSF1 and the lighter SRSF1-m4, as well as reducing the expression of the toxic dipeptide repeat proteins, as expected. Each of the therapeutic constructs that underwent a large scAAV preparation were considered functional following these *in vitro* results. Following transduction into the HEK293 cells, the treatments also appeared safe as cells grew normally compared to controls.

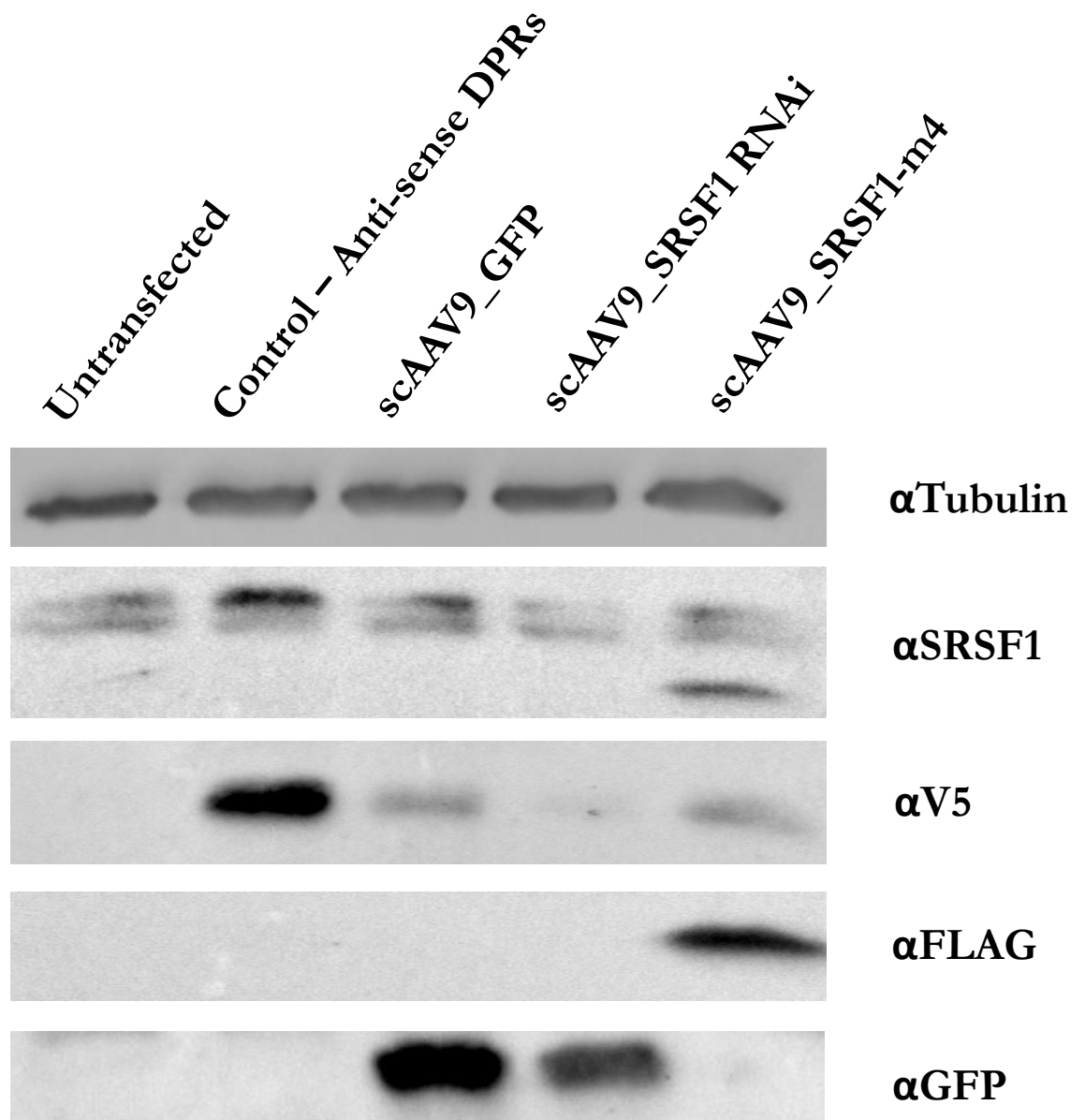


**Figure 4. 9** Western blot analysis of viral transduction in HEK293T cells– each of the viruses (scAAV9\_GFP, scAAV9\_SRSF1-m4 and scAAV9\_SRSF1-RNAi) that had undergone the large scAAV preparation protocol were tested *in vitro* at an MOI of 300,000 in HEK293T cells as well as co-transfected with an LV anti-sense DPR plasmid. Here we visualise the effect these viruses have on the expression of SRSF1/ SRSF1-m4 ( $\alpha$ SRSF1 – 33 kDa) and V5 tagged anti-sense DPRs ( $\alpha$ V5 – 23kDa) in comparison to our loading control ( $\alpha$ Tubulin – 55 kDa). The use of  $\alpha$ GFP (24 kDa) and  $\alpha$ FLAG (27 kDa) was used to evaluate whether the viruses had successfully assembled and were expressing their DNA sequences.

## 4.9 Discussion

This section of the chapter aims to provide a thorough discussion of the results shown in Chapter 4 (Production of Functional Large-Scale SRSF1-Targeting Gene Therapy Viruses for Subsequent Investigation in Mouse Studies). In Chapter 3, it was shown that two novel therapeutic vectors, scAAV9\_SRSF1-m4 and scAAV9\_SRSF1 RNAi, are capable of SRSF1 manipulation *in vitro* resulting in the reduced expression of toxic dipeptide repeat proteins (DPRs). Further studies are required to determine whether these therapeutic viruses have the capabilities to manipulate SRSF1 expression levels *in vivo*, but before that is achievable the viruses must undergo large scale preparation and purification. In this chapter, three scAAV9 viral vectors, one expressing an shRNA construct targeting SRSF1 mRNA, one expressing a mutant SRSF1 transgene (m4) and one control vector expressing GFP under a CBh promoter both underwent small volume and large volume viral preparation procedures.

The small scale scAAV preparation showed that all the therapeutic constructs could be successfully encapsidated and are able to express the 3 capsid proteins V1, V2 and V3 (Figure 4. 2) when triple transfected with HEK293T cells and the relevant packaging plasmids (Figure 4. 1). The small-scale vectors were then shown to successfully produce competent viral vectors when transduced into HEK293T cells. Both scAAV9\_GFP and scAAV9\_SRSF1-RNAi infected HEK293T cells were able to express GFP, suggesting that the viruses are functional and can successfully transduce the host cells. This confirmation of success allowed for the large scale scAAV production to be prepared with confidence. Large scale high titre viruses are required for the future *in vivo* study that will follow on from the previous *in vitro* experiments presented in chapter 3. Each mouse would be dosed at  $1 \times 10^{12}$ - $1 \times 10^{13}$  vg/kg which would require each mouse recipient to be injected with 5  $\mu$ l of the virus, and treatment groups would ideally have 24 or more mice in each subsequent study. Each 5 $\mu$ l injection would provide  $1 \times 10^9$  –  $1 \times 10^{10}$  vg of treatment. The objective was that each large preparation should provide enough concentrated virus for all subsequent *in vivo* studies encompassing this project.

The large-scale production of scAAV in an academic lab is a major issue. The lead time for preparing cell lines can take 2-3 weeks before the production of the virus even begins. The transduction and harvesting of the virus take at least 5 days following which numerous purification and titration steps need to be undertaken. It takes approximately 6 weeks to create a new scAAV if the plasmid has been designed and tested previously. In this project at least 3 large scAAV preparations were made (scAAV9\_GFP, scAAV9\_SRSF1 RNAi,

scAAV9\_SRSF1-m4). An extra 2 preparations of scAAV9\_GFP had to be repeated due to low viral concentrations, excessive impurities and centrifuge failure. scAAV9\_SRSF1-m4 had to be remade due to the product having less volume than required, and scAAV9\_SRSF1-RNAi had to be remade due to low concentration. Overall, throughout this project I undertook 9 large volume AAV productions. I had to repeat the production of 2 of the therapeutic viruses (scAAV9\_SRSF1-m4 and scAAV9\_SRSF1 RNAi) as the project advanced, due to additional virus being required due to an increase in the number of animals treated with the therapeutic vector. Creating these scAAV viruses in house is approximately £1400 (as of August 2021) which is cheaper than outsourcing the production to a company (approximately £3000) but if the repeated preparations of scAAV due to numerous issues that can and do occur are considered then the cost is likely similar, if not more, when considering the wasted consumables. However, the experience that is gained by producing scAAV's in house is invaluable as a gene therapy PhD student and I was able to learn the technology. The experience gave us a deeper understanding of the overall production process allowing for the more efficient design of future viruses, whilst also giving vital experience to those PhD students or Post-Docs who may want to move into the gene therapy industry.

The time implications of repeating the large-scale production is also immense. The numerous purification and titration steps required during a large-scale production of scAAV are the reason the procedure is so time consuming. Each of these AAV purification steps has the potential to go awry and there is the potential to lose virus at every stage in the process, especially with inexperience. As the project progressed, vital experience and knowledge was gained with every large preparation. Had I had this experience at the beginning of the project significant time would have been saved. After several failures, a sample was taken at the end of each step in the process to review at which steps viral loss could be an issue. These results gave us vital insight on how each step of the purification process relates to the overall concentration and purification of scAAV.

Between each large viral preparation there was a lot of variation. Both scAAV9\_SRSF1-m4 and scAAV9\_SRSF1-RNAi had 17 and 19 high quality fractions respectively, however the control scAAV9\_GFP only had 10 high quality fractions. All the viruses underwent the same large preparation procedure and yet differences in purity can be seen in Figure 4. 3, Figure 4. 4 and Figure 4. 5. The Sypro ruby gel results from each virus indicate that some of the fractions have numerous impurities, with many more bands than fractions containing just bands indicating VP1 VP2 and VP3. These extra bands represent impurities in scAAV stocks. It is well known that residual impurities from AAV production can impact the safety and

efficacy of the gene therapy in question. The most commonly found impurities in AAV stocks include: defective particles (AAV capsids that are not infective or do not contain the therapeutic gene), illegitimate DNA from plasmids, cells, or helper viruses that may be encapsidated into scAAV particles and residual proteins from helper viruses and host cells. These impurities may play a role in immunotoxicity (Penaud-Budloo et al, 2018). AAV capsids are known to encapsidate not only the designed recombinant DNA, but they also encapsidate illegitimate DNA during AAV production in HEK293T cells. In the US the FDA (Food and Drug Administration) have a limit of residual DNA in AAV stocks, especially those used in a clinical setting, to limit the genotoxic risk. It is recommended that the level of residual cellular DNA is below 10 ng per parenteral dose and a median DNA fragment size of less than 200 bp (FDA briefing document: vaccines and related biological products advisory committee meeting: cell lines derived from human tumours for vaccine manufacture). Gene therapy products also have supplementary quality controls regarding DNA contaminants. qPCR quantification of potential hazardous sequences, such as antibiotic-resistance genes and E1 and E4 adenoviral genes are required before these products can be used in humans.

It has recently come to light that there is a potential risk that prokaryotic antibiotic resistance sequences from the transfection plasmids can be transferred following gene therapy treatment, resulting in antibiotic resistance sequences in the receiver (Chadeuf *et al.*, 2005). For the transient transfection preparation method (the method that was used in this project), using antibiotic-resistance gene-targeted qPCR, residual plasmid DNA must be less than 100 ng per  $1 \times 10^{12}$  vg in the overall purified AAV product (Wright and Zeleniaia, 2011). It has been shown that AAV2 stocks produced by transfection with pAAV-GFP and pDG plasmid 14 contained  $1.5 \times 10^9$  copies/ml of kanamycin resistance in  $3.8 \times 10^{10}$  copies of GFP/ml, representing 3.9% of the total vector genomes. Recently, studies have shown that in pAAV2-gfp and AAVrh8R-FVIII stocks, following benzonase treatment, 0.5-3% of vector genomes were ampicillin-resistant gene sequences, caused by suboptimal encapsidation. The suboptimal encapsidation of plasmid sequences, such as antibiotic resistance, is dependent on plasmid backbone size, type of AAV vector and AAV genome sequence. In scAAV, the level of residual suboptimal encapsidated plasmid DNA can be up to 26% of the amp antibiotic resistance sequence detected in scAAV-GFP stocks (Schnödt *et al.*, 2016). Careful consideration should be made when designing vector plasmids, the bacterial selection marker should be carefully chosen to avoid the spread of antibiotic resistance in humans. In the USA, the FDA recommends not using plasmids with  $\beta$ -lactam antibiotic resistance genes in therapeutics destined for clinical usage to reduce the risk of transferring antibiotic resistance

sequences to the patient (Food and Drug Administration, 2016). However, this advice has yet to be specifically recommended the European Medicines Agency (EMA). Yet it is appropriate that gene therapies are designed for use in all countries and so the FDA advice should be taken into consideration when designing new gene therapies. In this study, although these impurities should have been measured and reviewed before considering *in vivo* work, it was decided to use a plasmid with ampicillin antibiotic resistance genes. The FDA did not advise against the use of B- lactam antibiotic resistance genes use until after this project commenced in 2017. In future work it is likely that a different antibiotic resistance gene, such as kanamycin, will be cloned into the therapeutic constructs described in this study before moving on to further *in vivo* work in preparation for clinical testing.

Impurities involving rep-cap sequences and the generation of replication-competent AAV is also a real risk. Replication-competent particles comprise of all the genetic elements required for the propagation of AAV in the presence of a helper virus. AAV is considered non-pathogenic, and so replication-competent particles are unfavourable, especially because cap expression may trigger an immune response and rep proteins can induce nicks in DNA. However, several optimizations added to the purification process have reduced the chance of these types of recombinants forming. Recombination events that can arise between the homologous sequences in the ITRs and adjacent sequences and the rep/cap cassette were thought to be the main cause of replication competent AAV. These events were avoided with the use: of heterologous promoters (Flotte, 1995; Grimm *et al.*, 1998). Separating the *rep* and *cap* sequences into two different cassettes and manufacturing an oversized cap sequence by adding an intronic sequence were all proposed to limit rep-cap encapsidation (Halbert, Allen and Miller, 2001). When using the above optimisations for the design of AAV plasmids, the level of replication competent AAVs (when preparing via HEK293-derived vector batches) with sequences derived from the and rep-cap plasmid (Figure 4. 1) are present at a lower level of 0.02%–1% of vector genomes (Halbert *et al.*, 2011; Martin *et al.*, 2013).

Overall, although numerous steps were taken to extensively purify the scAAV viruses within this project, should these therapeutics be used clinically, further steps will need to be taken to ensure that the purity is acceptable in a clinical setting. As the field of gene therapy advances, so do the scAAV purification methods. Good manufacturing practice (GMP) facilities, used for AAV production, currently use different methods. They use affinity chromatography, where the resin and column size are selected based on the predicted virus load. The scAAV capsids bind to antibody fragments on the affinity chromatography resin, but the affinity resin also binds empty capsids, lacking the vector genome which do not

provide a therapeutic benefit. These empty AAV capsids are undesirable due to the risk of an increased immune response during clinical use. To reduce these unwanted empty capsids, anion exchange chromatography is used as the next step in AAV purification. Empty capsids are removed based on the difference in charge between the two populations. Anion exchange chromatography also effectively removes host cell proteins and host cell DNA contaminants. To further purify AAV an additional step using cation exchange chromatography, can be added if required. The purification steps within GMP facilities result in the removal of more potentially hazardous impurities than the methods we have used in this project. In the future, once the scAAV has passed the *in vitro* testing steps, it may be more cost and time effective to outsource the production of rAAVs to a GMP facility to ensure optimized production, which may enhance the overall transduction efficiency and potentially the effectiveness of the AAV vector *in vivo* studies.

Once the therapeutic scAAV's were purified, the next step was to assess their titres. FACS is not commonly used to evaluate titration of AAV viruses when produced at industry level, but it is well described in the literature to assess AAVs biological titre (Rohr *et al.*, 2002; Stender *et al.*, 2007; François *et al.*, 2018). The biological titre measures the ability of the virus to transduce cells and express its transgene *in vitro*. FACS can only be used to quantify how many cells in a population of cells are able to express a fluorescent tag, in this case GFP. The biological titre depends on the type of promoter used within the viral DNA which is used to drive the expression of the fluorescent tag. It is therefore difficult to compare different viruses unless they have the same DNA background and the same promoter. For example, a virus with a strong promoter may need a lower physical titre to produce the same biological titre as a virus with a weaker promoter. The two therapeutic viruses designed for this study, scAAV9\_SRSF1-m4 and scAAV9\_SRSF1-RNAi have different promoters, which is due to them having different roles. The role of the CBh promoter in scAAV9 CBh\_SRSF1-m4 is to drive the expression of a transgene (SRSF1-m4) whilst the role of the H1 promoter in scAAV9\_SRSF1-RNAi is to silence SRSF1 using an shRNA. These roles require different promoters. Promoters are essential to control the expression of the therapeutic gene and provide the specific genetic region required for the binding of RNA polymerase (RNAP) to initiate transcription of the therapeutic gene. The promoter present in the plasmid backbone must to be compatible with the type of RNA that needs to be made: for mRNA (for gene expression) an RNAP II promoter is required, whereas small RNAs (such as shRNA) are transcribed from the RNAP III promoters (Zheng and Baum, 2008). In this case each of the viruses require a different type of promoter and therefore a direct comparison is not possible their function and therefore their abilities to produce GFP may differ.

FACS was used in this case because the viruses that had been produced had low physical titres when titered via qPCR, but this did not seem to affect their overall *in vitro* function. We wanted to know if their low physical titres resulted in a similarly low biological titre. The physical titre of an AAV is the concentration of viral particles that contain viral genomes. They are measured by quantifying the concentration of viral genomes, in this case by qPCR, since each viral particle typically contains only one viral genome. This type of titre gives a theoretical maximum value, but a physical titre does not necessarily give any indication of the infectious/ biological titre (Lock *et al.*, 2010). Therefore, the virus's biological titre was compared with a different control pAAV-GFP virus with a known biological and physical titre and that was successful *in vivo* and *in vitro*. The results indicate that, although the physical titre is low in both designed GFP scAAV viruses, the biological titres of scAAV9\_GFP and scAAV9\_SRSF1-RNAi appear very similar even though the low quality scAAV9\_SRSF1-RNAi is half that of scAAV9\_GFP. This suggests that scAAV9\_SRSF1-RNAi has a greater transduction efficiency when compared to scAAV9\_GFP. This outcome was not predicted. scAAV9\_GFP has a much stronger promoter (CBh) when compared to the H1 promoter within the scAAV9\_SRSF1-RNAi virus which would suggest that more GFP positive cells would be present in cells treated with the same amount scAAV9\_GFP compared with cells treated with the same amount of scAAV9\_SRSF1-RNAi. However, it may be that the scAAV9\_GFP is able to infect more cells but due to its very strong promoter, the cells produce so much GFP that it has a toxic effect resulting in the cells expressing GFP undergoing apoptosis prematurely (Liu *et al.*, 1999; Detrait *et al.*, 2002; Howard *et al.*, 2008). This would mean that the GFP positive cells would die prematurely and would not be present when the cells are harvested for FACS analysis. The eGFP can be toxic to cells especially when the transgene is driven by a strong promoter such as CBh. It has been suggested that GFP is involved in the initiation of the apoptosis cascade which would explain its toxicity and role in cell death (Liu *et al.*, 1999).

The FACS results (Figure 4. 6, Figure 4. 7 and Figure 4. 8 and Table 4.2 and Table 4. 3) indicate that a lower qPCR titre of an scAAV9 may not be detrimental to its transduction efficiency when compared to a pAAV9 with a greater qPCR/physical titre. The biological titre of the control pAAV GFP virus was only 2.3 – 2.5 times higher than that of the scAAV9 viruses to which it was compared. Considering that the qPCR titre of the pAAV9 virus was measured 10-fold higher than the scAAV9 viruses, this suggests that scAAV9 viruses overall may have greater transduction efficiency at a lower concentration. At a manufacturing level, this would be ideal as less scAAV would be required per patient in comparison to

manufacturing a similarly functioning single stranded pAAV. Even in smaller *in vivo* studies, the reduced volume required per mouse reduces the manufacturing time.

It has been confirmed that scAAV9\_GFP, scAAV9\_SRSF1-RNAi and scAAV9\_SRSF1-m4 are all functional and the results do not provide any evidence that they are toxic or unsafe when delivered *in vitro*. In cells treated with scAAV9\_SRSF1-RNAi, reduced SRSF1 expression is evident along with an obvious reduction in DPR expression. However, the results indicate that there is a reduction in DPR expression even in scAAV9\_GFP and scAAV9\_SRSF1-m4 treated cells, but to a lesser extent when compared to scAAV9\_SRSF1-RNAi treated cells. This could suggest that the treatment of using scAAV, regardless of the transgene could impact upon DPR expression. The mechanism by which scAAV enters or is cleared from the cell could affect DPR expression.

The cells that were treated with scAAV9\_SRSF1-m4 express the lighter SRSF1-m4 band indicating that the transgene was successfully transduced and was successfully expressed in the host cells. SRSF1-m4 treated cells also express the flag tag, again producing evidence that the AAV has been successfully built and reproduced during the large-scale production and is able to transfect and express the SRSF1-m4 protein.

The aim of the work described in this chapter was to package the experimental plasmids (scAAV9\_SRSF1 RNAi, scAAV9\_SRSF1-m4, scAAV9\_GFP) into functional and live adeno associated viruses that can infect cells both *in vitro* and *in vivo*. Enough virus was produced to carry out the initial *in vivo* safety and efficacy study which was approximately 200µl per virus. Once the plasmids had been packaged into these functional viruses, their concentration and their ability to infect cells *in vitro* was assessed. The viral concentrations were assessed using qPCR to report the physical titre and FACS was then used to review the biological titre of the GFP producing viruses. The functionality of these viruses, once packaged, was tested in 293T HEK cells to ensure that their behaviour *in vitro*, when packaged, had remained the same as the unpackaged designed plasmids (Chapter 3 - Designing and developing viral vectors for SRSF1-targeted gene therapy approaches in mice).

The results described in this chapter indicate that the experimental viruses scAAV9\_SRSF1 RNAi, scAAV9\_SRSF1-m4 and scAAV9\_GFP, are fully functional *in vitro*, following large scale preparation and purification. The next step is to evaluate these novel therapeutic viruses *in vivo* to test the efficacy of the SRSF1 manipulating self-complementary adeno associated viruses in a mouse model. The overall aim of the *in vivo* study will be to assess the biodistribution, short and long-term transduction efficiency and stability of viral-mediated transgene expression using scAAV9 gene therapy vectors as treatments for C9ORF72-linked

amyotrophic lateral sclerosis and frontotemporal dementia (C9ORF72-ALS/FTD). The first *in vivo* study will use wild-type C57bl/6 mice to review the overall safety of the novel therapeutic gene therapy viruses before we move on to reviewing the effect these gene therapy viruses have in a C9ORF72 ALS/FTD mouse model.

## CHAPTER 5 - Therapeutic Manipulation of SRSF1 in Mice: Pilot Safety and Efficacy Proof-of-principle

### 5.1 Aims

The overall aim of this *in vivo* study was to assess the biodistribution, short and long-term transduction efficiency and stability of viral-mediated transgene expression from two self-complementary adeno-associated virus 9 (scAAV9) gene therapy vectors. The gene therapy vectors have been developed for the testing the proof-of-principle safety and efficacy in wild type and *C9ORF72*-linked ALS/FTD mice. The three designed viruses that were designed and produced as described in Chapters 3 and 4 were used in this study: one control expressing green fluorescent protein (scAAV9 GFP), one expressing a modified SRSF1 protein (scAAV9 SRSF1-m4) and one co-expressing an shRNA targeting SRSF1 and GFP (scAAV9 SRSF1-RNAi).

Previous work in our lab has shown that the expression of the dominant negative mutant protein SRSF1-m4 or the partial depletion of SRSF1 inhibits the pathological nuclear export of *C9ORF72*-repeat transcripts and the subsequent RAN translation of neurotoxic DPRs, conferring neuroprotection in patient-derived neurons and *Drosophila* models of *C9ORF72*-ALS/FTD (Hautbergue *et al.*, 2017).

Adeno-associated virus serotype 9 (AAV9) effectively transduces neural cells, is not known to be pathogenic in humans and presents a suitable vector candidate for viral administration of therapeutic transgenes. This study was used to assess the ability of the three vectors to mediate both short and long-term transgene expression in the central nervous system (CNS) of wild type C57bl/6 mice after injection via the cisterna magna. It also allowed the assessment of viral biodistribution at 2 time-points: 4-weeks and 6-months post injection. Once completed, the results of the study were used to inform the design of a subsequent study whereby the gene therapy viral vectors were used to test target engagement through DPR reduction in a *C9ORF72*-ALS/FTD mouse model (Liu, *et al.*, 2016). This BAC transgenic mouse model of *C9ORF72*-ALS/FTD was reported to develop decreased survival, anxiety-like behaviour, motor deficits from 4 months, muscle denervation, motor neuron loss and cortical and hippocampal neurodegeneration. This mouse model expresses *C9ORF72* sense transcripts and upregulated antisense transcripts whilst RAN dipeptide repeat proteins accumulate with age from 3 months old (Liu *et al.*, 2016).

## 5.2 Route of administration

To ensure the scAAV9 viruses could reach their therapeutic target, in this case the CNS, the route of administration was crucial to the success of these novel therapeutic strategies. A safe and effective route to achieve global scAAV9 distribution across the CNS was required.

Previously, intraparenchymal injection has been a commonly used route of AAV administration to the CNS, (Hocquemiller *et al.*, 2016; Choudhury *et al.*, 2017) and even used in many clinical studies. Direct delivery into the brain parenchyma circumvents the blood-brain barrier (BBB) and requires a much lower dose of viral vector in comparison to other administration methods. However, injecting directly into the brain can lead to poor vector distribution, resulting in transgene expression that is limited to the injection site, this is more effective for brain diseases that are restricted to particular brain areas such as the substantia nigra in Parkinson's disease (Leone *et al.*, 2012; Tardieu *et al.*, 2014). This is a major limitation for the treatment of many neurodegenerative disorders that affect large regions of the CNS, such as lysosomal storage disorders, Alzheimer's disease and motor neuron disease. Intraparenchymal injection is an invasive procedure requiring a craniotomy and general anaesthetic, with the associated risk of pathogen contamination, cerebral injury and haemorrhaging.

Intravenous administration (IV) of AAV9 has been studied, with promising results due to AAV9s capacity to cross the BBB (Foust *et al.*, 2009). Proof of concept has been shown in a variety of studies and the recent Zolgensma drug to treat spinal muscular atrophy used IV administration in human patients with great efficiency and few off target effects (NCT02122952). It is a minimally invasive procedure when administering IV which is one of its major benefits. However, the main reason this administration method was not chosen was due to larger viral volumes required for systemic delivery. As this is a preliminary study, increased viral volumes for intravenous (IV) delivery would have increased the study cost considerably. Another issue was that the laboratory work conducted previously along with the *in vitro* testing (Chapter 3 - Designing and developing viral vectors for SRSF1-targeted gene therapy approaches in mice) focused on the effect of SRSF1 manipulation in neuronal models, patient derived cells and a *Drosophila* model. We were therefore unsure of the off-target effects the systemic delivery of our designed viruses might cause in a complex mammalian animal model. Although this delivery method was not used, if no serious off target issues occur after SRSF1 manipulation, IV administration may be considered as a future option.

Due to concerns discussed above, in this study it was decided that cisterna magna injection would be used to administer scAAV9\_GFP, scAAV9\_SRSF1-RNAi and scAAV9\_SRSF1-m4 into the cerebrospinal fluid (CSF) of mice. The cisterna magna is one of three principal openings in the subarachnoid space between the arachnoid and pia mater layers of the meninges surrounding the brain. It is located between the cerebellum and the dorsal surface of the medulla oblongata and contains the CSF produced in the fourth ventricle which drains into the cisterna magna. The CSF is vital for the transport of nutrients, proteins and molecules throughout the CNS and by directly injecting the viruses into the CSF, the approach, avoids the issue of crossing the blood brain barrier. The blood brain barrier (BBB) protects the CNS from invasion of pathogens and circulating toxins that could cause disease of the CNS, whilst still allowing vital nutrients to reach the brain. scAAV9 has been shown to be able to cross the BBB, however, by injecting directly into the CSF via the cisterna magna this obstacle is removed and therefore increase the overall concentration of the viral vector within the CNS. Previous studies in our department have administered AAV9 via cisterna magna injections which have resulted in an improved outcome in a SOD1 ALS mouse model, and the absence of significant off-target effects (Iannitti *et al.*, 2018).

The cisterna magna injection was administered between post-natal day 1 and 2 and was minimally invasive, since the cisterna magna is visible through the translucent skin of the mouse pup. The pup is only required to be anaesthetised for a short amount of time (<10 minutes) with no need for invasive surgery, sutures or a prolonged recovery period. In summary, for the purposes of this study, a direct CSF delivery of viral vector by intra-cisternal administration was chosen, for the following reasons: (1) smaller viral volumes required compared to using systemic delivery (Bevan *et al.*, 2011; Nathwani *et al.*, 2014b); (2) direct CSF delivery mediates widespread CNS transduction in numerous animal models and multiple cell types, and circumvents the need to traverse the blood brain barrier (Federici *et al.*, 2012; Bey *et al.*, 2017; Hinderer *et al.*, 2018); (3) delivery direct to the CSF reduces peripheral organ transduction, potentially avoiding both a harmful immune response and reduced transgene expression due to circulating neutralising antibodies (Gray *et al.*, 2013); (4) cisterna magna delivery is less invasive and results in a broader transduction compared to intraparenchymal injection (although considerably more invasive than IV delivery) (Bey *et al.*, 2020); (5) cisterna magna delivery results in widespread transduction in the brain, along with transduction throughout the spinal cord in both rodents and large animals (Lukashchuk *et al.*, 2016).

### 5.3 *In vivo* proof-of-principle of functionality and safety of the therapeutic constructs in wild type C57Bl/6 mice

The C57Bl/6 mouse strain was used during this safety and efficacy study. There were two experimental time points: 4-weeks and 6-months. At each of these time points there were 4 treatment groups: PBS treated, scAAV9\_GFP, scAAV9\_SRSF1-m4 and scAAV9\_SRSF1-RNAi with 6 mice per group. The mice were injected via the cisterna magna between post-natal day 1 and post-natal day 2 with 5  $\mu$ l of virus/treatment at a rate of 1  $\mu$ l per minute. The viral vectors were diluted into a vehicle solution of sterile phosphate-buffered saline plus 35 mM sodium chloride (PBS + 35 mM NaCl). Mice in the control (PBS) group received an injection of 5  $\mu$ l of PBS+35mM NaCl at a rate of 1  $\mu$ l per minute. The final dosages of each virus were as follows: scAAV9\_GFP =  $1.75 \times 10^{12}$  vg/kg ( $1.75 \times 10^9$  vg/ mouse); scAAV9\_SRSF1-RNAi =  $1.3 \times 10^{12}$  vg/kg ( $1.3 \times 10^9$  vg/ mouse); and scAAV9\_SRSF1-m4 =  $5.75 \times 10^{12}$  vg/kg ( $1 \times 10^{10}$  vg/ mouse).

Each mouse litter consisted of a mixture of both control and virus treated pups to account for litter differences and litter environment. The mice were observed daily for the first week to ensure that their condition was stable and then every few days thereafter. Three weeks post injection all mice were weighed weekly and their overall condition was monitored until the end of the study.

---

#### 5.3.1 Biodistribution of the therapeutic constructs

---

Tissue was harvested from the mice at both the 4 week and the 6-month time point. The tissue was used to assess the biodistribution of each of the therapeutic constructs. To first prepare the tissue for the biodistribution analysis, approximately a quarter of each organ underwent homogenisation followed by DNA extraction. qPCR was used to review how many viral copies of the therapeutic constructs were present per genome in 100 ng of DNA extracted from each tissue type (brain, heart, liver, spleen, muscle) using a standard curve of known dilutions and concentrations of the original plasmids. Primers were designed to anneal to GFP DNA in both scAAV9\_GFP and scAAV9\_SRSF1-RNAi viruses for the biodistribution analysis. For scAAV9\_SRSF1-m4 we designed primers to anneal to the CMV enhancer region of the plasmid but unfortunately, we could not find primers that were specific enough to efficiently pick out the viral DNA. We tried to design primers that spanned the 3 x FLAG region but again the qPCR results were inconsistent and non-specific. Eventually, we used primers that could anneal to SRSF1. It is known that SRSF1 is also

expressed endogenously in the host genome and so an increase in the steady state levels of SRSF1 transcripts was looked for in the presence of the virus expressing the SRSF1 transgene. It was assumed that any increase from that seen in PBS mice in comparison to scAAV9\_SRSF1-m4 treated mice would be the result of the viral DNA of the scAAV9\_SRSF1-m4-virus.

### **Biodistribution of scAAV9 SRSF1-RNAi and scAAV9 CBh\_GFP**

Figure 5. 1 shows the viral genome biodistribution of scAAV9\_GFP and scAAV9\_SRSF1-RNAi quantified by qPCR across 6 tissue types: brain, spinal cord, liver, spleen, heart and muscle. At 4-weeks post injection, the greatest distribution of scAAV9\_SRSF1-RNAi is found in the brain and spinal cord, which is to be expected as the tropism of the viral vector is the central nervous system (CNS). The virus remaining within the CNS in the weeks immediately following injection is a positive outcome, as this is the area of interest and where we would like the treatment to reduce SRSF1 expression. It was observed that there was an off-target distribution in the heart, again this was expected. It is known that during development of the heart SRSF1 is essential and is found in abundance within the organ. The viral tropism of scAAV9 means that the heart is one of its targets, but considering the abundance of SRSF1 and the distribution shown there were no side effects observed in the mice, behaviour or health wise, that could have been attributed to this off-target distribution. There was also a considerable distribution of scAAV9\_SRSF1-RNAi within the muscle tissue (gastrocnemius) (Figure 5. 1) which would be an ideal off-target effect. MND results in the neurodegeneration of motor neurons therefore resulting in the eventual paralysis of muscles. If the therapeutic constructs can target the motor neurons within and around the muscles along with the CNS, the hope is that this could result in a more effective treatment. Further research into how other muscles are targeted will be required to understand the overall distribution across the body following injection.

scAAV9\_GFP shows a similar distribution pattern across all tissues compared with scAAV9\_SRSF1-RNAi (Figure 5. 1). However, there is much less GFP DNA found in the brain and spinal cord in scAAV9\_GFP treated animals [ $p < 0.001$  (\*\*\*)]. The main target of scAAV9\_GFP is the brain and the spinal cord. Yet, it has fewer viral copies per genome when compared with scAAV9\_SRSF1-RNAi. This is likely the consequence of scAAV9\_GFP having a stronger promoter. This experiment reviews the amount of GFP DNA that is present within 100ng of tissue rather than the expression of GFP within each tissue type. Therefore, the level of GFP expression, when comparing both GFP viruses,

could show a different result to that observed in the biodistribution data. The CBh promoter in scAAV9\_GFP is much stronger than the EFS-1 $\alpha$  promoter in scAAV9\_SRSF1-RNAi consequentially different dosages of each virus may be required to result in the same transgene expression, in this case GFP. Another reason that scAAV9\_GFP treated mice have fewer viral copies within the CNS, is that large amounts of GFP can be toxic to cells. The strong CBh promoter may be driving GFP expression within the CNS, causing a build-up of toxic GFP in cells successfully transduced by the virus, resulting in cell death. The outcome of this build-up of GFP would be that fewer living cells in the CNS would have GFP DNA present. Again, there is very little distribution of scAAV9\_GFP in the spleen and liver but a similar distribution in the heart and muscle when compared to scAAV9\_SRSF1-RNAi. The similar pattern in distribution at 4-weeks in both scAAV9 viruses is indicative of the tropism of the scAAV9 virus.

In the 6-month cohort, biodistribution data (Figure 5. 1) across all tissues was similar to the data observed at the earlier 4 week time point, except in the spleen which had the least distribution of both viral DNA. Both scAAV9\_SRSF1-RNAi and scAAV9\_GFP show a marked reduction of viral copies per genome within the CNS at 6-months compared with 4-weeks. This marked reduction could be due to the clearance and metabolism of the virus via the liver resulting in the excretion of the viral DNA via faeces and urine. The increase in distribution in the liver of animals treated with scAAV9\_SRSF1-RNAi could also be due to the clearance of the virus from the CNS throughout the 6-months post injection. As there was less viral DNA in the CNS of scAAV9\_GFP treated animals, the liver would not have been under as much pressure to clear the virus and therefore would clear it more effectively compared to the livers of mice treated with scAAV9\_SRSF1-RNAi.

The dramatic reduction between 4-weeks and 6-months in viral GFP DNA present across the various tissues was unexpected (Figure 5. 1). The reduction in GFP viral DNA could be due to the low viral concentration injected into the cisterna magna which may not have been high enough to avoid total clearance via excretion, from the system after one dose. These results indicate that more than one dose may be more appropriate. However, research as to whether a second dose would elicit an immune response should be undertaken in the first instance. The results could also indicate that this dosage scAAV9\_GFP =  $1.75 \times 10^{12}$  vg/kg ( $1.75 \times 10^9$  vg/ mouse); scAAV9\_SRSF1-RNAi =  $1.3 \times 10^{12}$  vg/kg ( $1.3 \times 10^9$  vg/ mouse); and scAAV9\_SRSF1-m4 =  $5.75 \times 10^{12}$  vg/kg ( $1 \times 10^{10}$  vg/ mouse) could be given if unsure whether the treatment would be tolerated by the patient. If the virus was not well tolerated it would have the ability to be cleared within 5 to 6-months of administration but this would

only be appropriate if the side effects were manageable or if the therapeutic construct did not appear to be producing a therapeutic effect.

Unexpectedly, there is more GFP DNA present in the PBS treated animals at 6-months than was found at 4-weeks (Figure 5. 1). It was hypothesised that this could be due to shedding of the virus in treated animals sharing a cage with PBS treated animals. The GFP distribution of PBS animals follows the same trend as the treated animals just with lower viral copies per genome present, suggesting that the viruses have somehow been administered. It could be that the mice injected with scAAV9\_SRSF1 RNAi and scAAV9\_SRSF1 m4 are shedding the virus through their urine and faeces throughout the 6-months. Mice are coprophagic animals and are known to ingest their own and each other's faeces. Further research will be required to assess how much virus is shed in treated animals' faeces and whether the virus can be passed on in this way to untreated animals.

It was considered that the increase in GFP DNA in PBS treated animals maybe due to the cleaning method of the injection needle between treatment groups. However, the PBS treated mice were always treated first therefore ruling out this hypothesis. It was also considered whether this could have resulted after the tissue harvest with contaminated surgical equipment, but we would have anticipated seeing this issue also in the 4-week cohort, which was not the case. Contamination of GFP could have also occurred in the process of setting up the qPCR experiments, but to eliminate this possibility the plates, pipette and pipette tips were placed under UV for at least 30 minutes before plate preparation.

## Biodistribution of scAAV9\_SRSF1-RNAi and scAAV9\_GFP 100ng

4-weeks vs 6-months

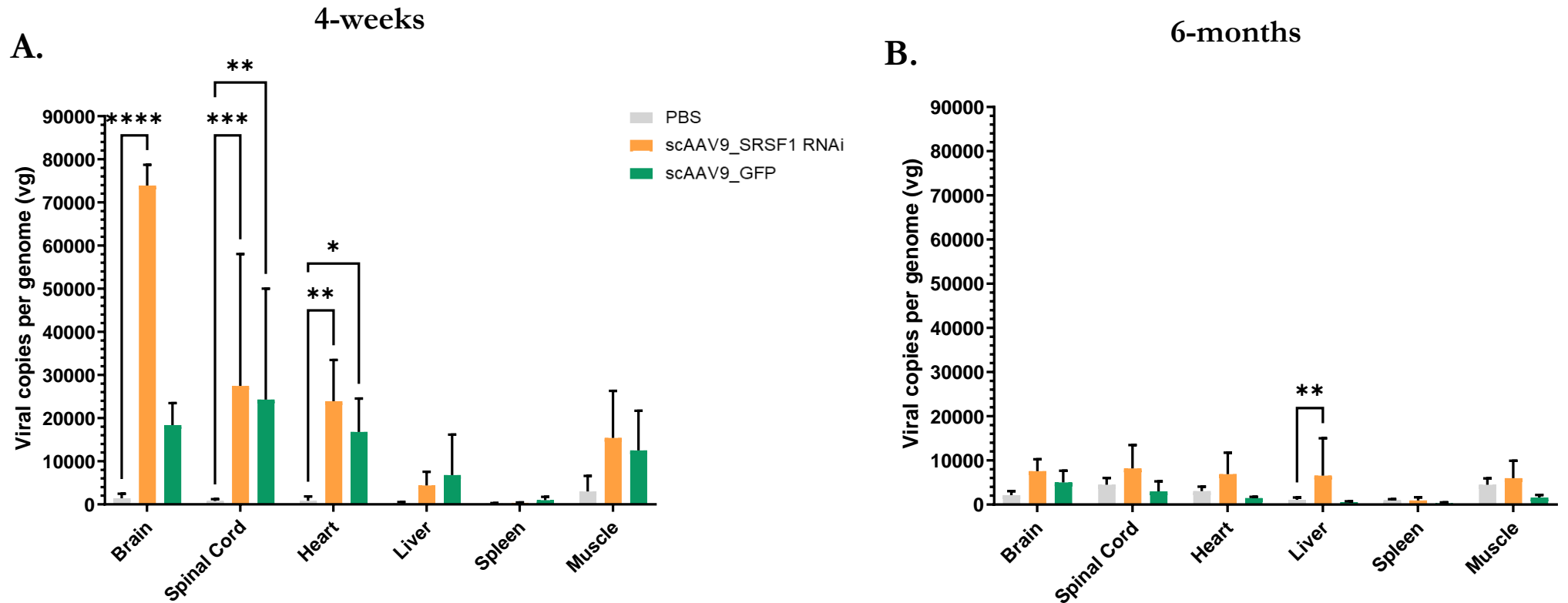


Figure 5. 1 Biodistribution analysis of mice injected with PBS vs scAAV9\_SRSF1-RNAi vs scAAV9\_GFP, sacrificed at 4-weeks (A) and 6-months (B) post injection – Tissue of C57bl/6 mice from 3 of the treatment groups (PBS treated, scAAV9\_SRSF1-RNAi treated and scAAV9\_GFP treated) were assessed via qPCR using primers against GFP to evaluate the biodistribution of the respective viruses (A) in mice sacrificed 4-weeks post cisterna magna injection (n=6) and (B) in mice sacrificed 6-months post cisterna magna injection (n=6, except scAAV9 SRSF1-RNAi n=4). Data analysed by two-way ANOVA followed by post-hoc Dunnett’s multiple comparisons test with respect to PBS treated. Stars indicate  $p < 0.05$  (\*),  $p < 0.01$  (\*\*),  $p < 0.001$  (\*\*\*) and  $p < 0.0001$  (\*\*\*\*).

## **Biodistribution of scAAV9\_SRSF1 m4**

At 4-weeks post-injection the levels of SRSF1 DNA were similar across all tissue types (brain, spinal cord, heart, liver, spleen and muscle) in PBS treated mice (Figure 5. 2). In mice treated with scAAV9\_SRSF1-m4 there was a significant increase in SRSF1 DNA levels in both the brain [ $p < 0.05$  (\*)] and the spinal cord [ $p < 0.0001$  (\*\*\*\*)] in comparison to the other tissue types. There is a small increase in the SRSF1 DNA levels in mice treated with the scAAV9\_SRSF1-m4 virus in the heart compared with PBS treated mice. The tropism of scAAV9 predicts that the target tissue would be the CNS and the heart which aligns with these results. The fact that other organs do not have increased SRSF1 DNA levels indicates that the scAAV9\_SRSF1-m4 virus has reduced distribution outside of the brain, spinal cord and heart and is mainly distributed within the CNS, which was the intended organ system.

The 6-month biodistribution data (Figure 5. 2) indicate that SRSF1 DNA levels across tissue types in PBS treated mice was much more variable, with no significant difference in SRSF1 levels between PBS treated and scAAV9\_SRSF1-m4 treated mice with decreased levels found in both the brain and liver of PBS treated mice. Mice that were treated with the scAAV9\_SRSF1-m4 virus also have a very similar DNA expression to the PBS treated mice. However, the observed increase in SRSF1 DNA levels (Figure 5. 2) in the spinal cord suggests that the virus is still present, but that it has been cleared from both the heart and the brain between 4-weeks and 6-months post injection. There is also an elevated level of SRSF1 DNA seen in the spleen (Figure 5. 2) which is was not observed in the biodistribution of scAAV9\_GFP and scAAV9\_SRSF1-RNAi. The spleen is mainly involved in the immune response and removes any old or damaged red blood cells by filtering the blood. So, the increased DNA levels of SRSF1 which we believe correspond to the presence of the therapeutic scAAV9\_SRSF1-m4 could be due to a low-level immune response to the SRSF1-m4 protein. An immune response would direct cells that are infected with the scAAV9 virus to the spleen where the blood would be filtered resulting in a build-up of the virus within the splenic tissue.

## Biodistribution of scAAV9\_SRSF1-m4

### 4-weeks vs 6-months

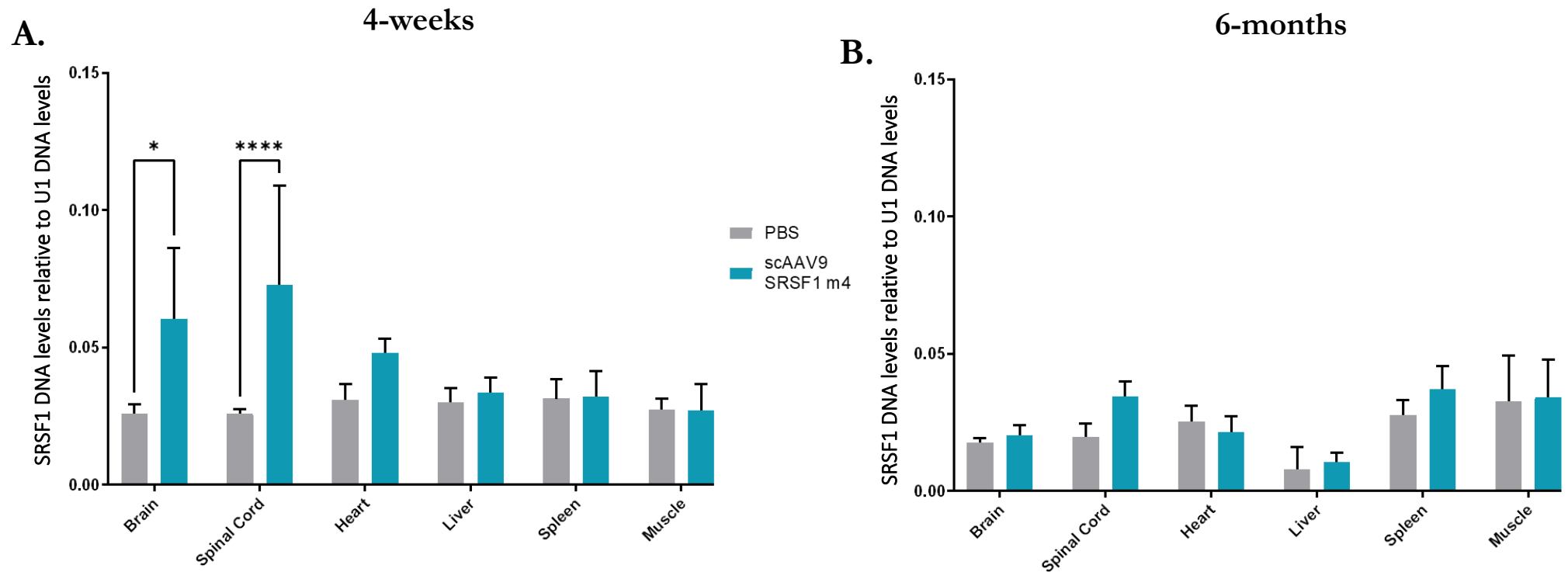


Figure 5. 2 Biodistribution analysis of mice injected with PBS vs scAAV9\_SRSF1-m4 (A) sacrificed 4-weeks post cisterna magna injection and (B) 6-months post cisterna injection – Tissue from PBS treated mice and scAAV9\_SRSF1-m4 treated mice was assessed via qPCR using primers against SRSF1 to evaluate the biodistribution of increased SRSF1 DNA. (A) Mice were sacrificed at 4-weeks post cisterna magna injection (n=6) and (B) mice sacrificed 6-months post cisterna magna injection (PBS n=6 and scAAV9 SRSF1-m4 n=4). Data analysed by two-way ANOVA followed by post-hoc Dunnett's multiple comparisons test with respect to PBS treated. Stars indicate  $p < 0.05$  (\*) and  $p < 0.0001$  (\*\*\*\*).

---

### 5.3.2 Western Blot analysis of protein expression in C57Bl/6J mice 4-weeks and 6-months post injection

---

Following the cisterna magna injection of the 4 treatments, PBS, scAAV9\_GFP, scAAV9\_SRSF1-m4 and scAAV9\_SRSF1-RNAi, the treated mice were sacrificed at either 4-weeks or 6-months. Once sacrificed, the tissue (brain, spinal cord, heart, liver, muscle and spleen) from each animal was harvested for further analysis. The tissue underwent protein extraction (Chapter 2: Materials and Methods) and 40 µg of protein from each organ was analysed via SDS-PAGE and western blot. For this analysis, there were 3 mice in each of the four treatment groups run alongside each other. In each analysis an anti-tubulin antibody was used as the loading control and an SRSF1 antibody was used to assess SRSF1 expression following each treatment at 4-weeks and at 6-months. Anti-GFP and anti-FLAG antibodies were used to ensure that the viruses had successfully transduced into the mouse tissues. GFP expression was expected in mice treated with scAAV9\_GFP and scAAV9\_SRSF1-RNAi as both these viruses contain a GFP transgene and expression of GFP indicates that these viruses were present and functional following viral injection. FLAG expression was expected in mice treated with the scAAV9\_SRSF1-m4 as the virus was tagged with 3 FLAG epitopes (3 X FLAG). The expression of FLAG suggests that the scAAV9\_SRSF1-m4 has successfully transduced the mouse tissue and is functional *in vivo*.

Figure 5. 3A depicts the protein expression observed in the brain cortex of mice 4-weeks post injection. SRSF1 expression indicates that SRSF1 was reduced in brain cortex tissue in mice that were treated with scAAV9\_SRSF1-RNAi 4-weeks post injection. It was also evident that SRSF1-m4 was present in mice treated with scAAV9\_SRSF1-m4 with the presence of a lower band indicating the smaller SRSF1-m4 protein under the endogenous SRSF1 band. There was further evidence that the therapeutic viruses were functional *in vivo* as GFP expression was also present in mice treated with scAAV9\_GFP and in mice treated with scAAV9\_SRSF1-RNAi. All three mice treated with scAAV9\_SRSF1-m4 have bands to indicate FLAG expression suggesting that the virus is also being productive *in vivo*.

The 6-month cohort only has n=3 in each treatment group except the scAAV9\_SRSF1-RNAi group which had n=2 due to a death which was unrelated to the treatment (infected eye). In brain cortex tissue at 6-months post injection (Figure 5. 3B) SRSF1 expression does not follow the same trend as that observed at 4-weeks post injection. There was no obvious reduction in SRSF1 expression in mice treated with scAAV9\_SRSF1-RNAi in comparison to mice treated with PBS. Only one mouse treated with scAAV9\_SRSF1-m4 expressed the

lower weight SRSF1-m4 protein, whereas this band is absent in the brain cortex tissue of the other 2 mice. Mice treated with the control scAAV9\_GFP have reduced SRSF1 expression when compared to the PBS mice which was unexpected. Expression of the GFP protein was still present in the brain cortex of both scAAV9\_SRSF1-RNAi and scAAV9\_GFP treated mice indicating that the virus was still present within the tissue. Those mice treated with scAAV9\_SRSF1-m4 did express the FLAG protein and as expected the mouse that was able to express SRSF1-m4 had increased FLAG expression compared to the other 2 mice in the treatment group.

In the other 4 organs (heart, liver, muscle and spleen) there was no difference between SRSF1 expression and any of the treatments, however, the expression levels were variable across the treatment groups. Overall, there was greater SRSF1 expression in mice 4-weeks post injection versus 6-months post injection in all tissue types. In muscle tissue SRSF1 expression did not appear to have a stable expression across mice at 4-weeks old regardless of treatment. In both liver and spleen, 4-weeks post injection SRSF1 expression appears consistent across treatment groups Figure 5. 3 (C, E, G and I).

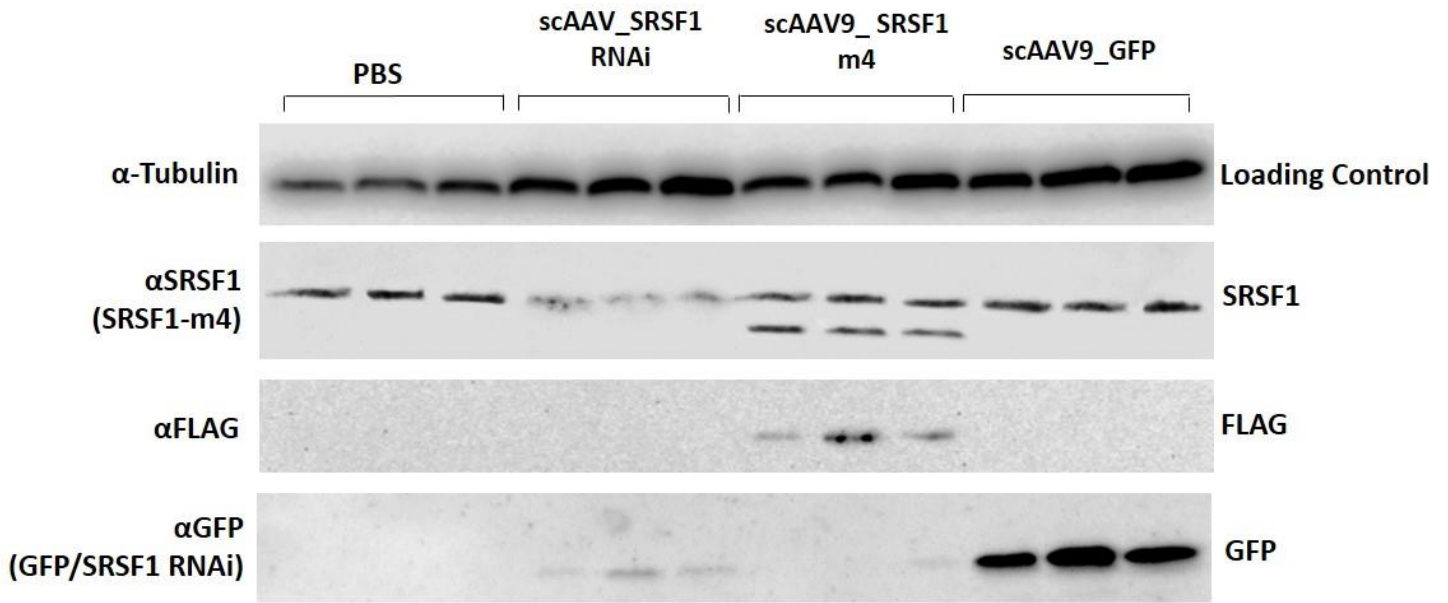
FLAG expression in heart and muscle tissue was evident at 4-weeks post scAAV9\_SRSF1-m4 injection, indicating that the virus had transduced the tissue successfully. However, there was no evidence of SRSF1-m4 expression in either tissue (Figure 5. 3 C and G). GFP expression was observed in the heart tissue at the 4-week time point in mice treated with scAAV9\_GFP yet it was not expressed by mice treated with scAAV9\_SRSF1-RNAi (Figure 5. 3 C). In the muscle tissue, GFP expression was not observed suggesting that the scAAV9\_SRSF1-RNAi and the scAAV9\_GFP virus had not transduced the gastrocnemius muscle (Figure 5. 3 G). FLAG expression was evident at 4-weeks post injection in liver tissue, but again there was no evidence of the lower weight SRSF1-m4 protein. Liver tissue from mice treated with scAAV9\_GFP also expressed GFP, but there was no evidence of GFP expression in liver tissue from mice treated with scAAV9\_SRSF1-RNAi (Figure 5. 3 E). In the spleen tissue from the 4-week time point there was no evidence of either GFP or FLAG expression (Figure 5. 3 I).

In these organs at 6-months SRSF1 expression showed several differences. In the heart and muscle tissue at 6-months post injection (Figure 5. 3 D and H), SRSF1 expression was very variable and, in some mice, it appeared there was no SRSF1 expression within the tissue. SRSF1 expression in the liver at 6-month post injection was mostly consistent. However, 2 mice (one PBS and one scAAV9\_SRSF1-m4 treated mouse) have reduced SRSF1 expression

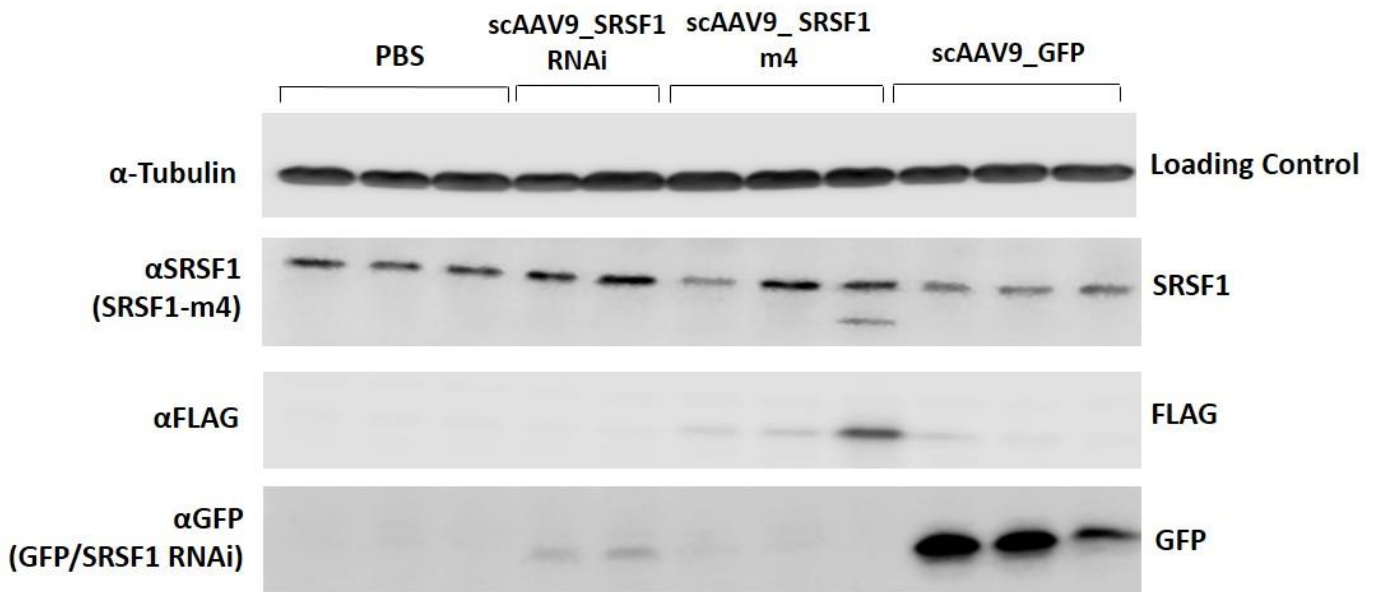
(Figure 5. 3 F). In the spleen, there was no evidence of SRSF1 expression at the 6-month time point which was unexpected (Figure 5. 3 J).

FLAG expression within the heart and muscle tissue at the 6 month time point was still present albeit weaker, especially in the heart tissue, suggesting that the scAAV9\_SRSF1-m4 treatment had circulated to these areas and was able to transduce the cells but there was no evidence of SRSF1-m4 protein expression in the western blot analysis (Figure 5. 3 D and H). FLAG expression was also evident in the liver tissue at 6-months post injection. However, in 2/3 of the scAAV9\_SRSF1-m4 treated mice FLAG expression was increased in comparison to 4-weeks post injection (Figure 5. 3 F). GFP expression was evident in both the heart and liver tissue in mice treated with scAAV9\_GFP at 6-months however expression was no longer evident in mice treated with scAAV9\_SRSF1-RNAi (Figure 5. 3 D and F). In muscle tissue, no GFP expression was apparent in any of the treatment groups (Figure 5. 3 H). At 6-months post injection the spleen tissue showed no evidence of GFP or FLAG expression (Figure 5. 3 J).

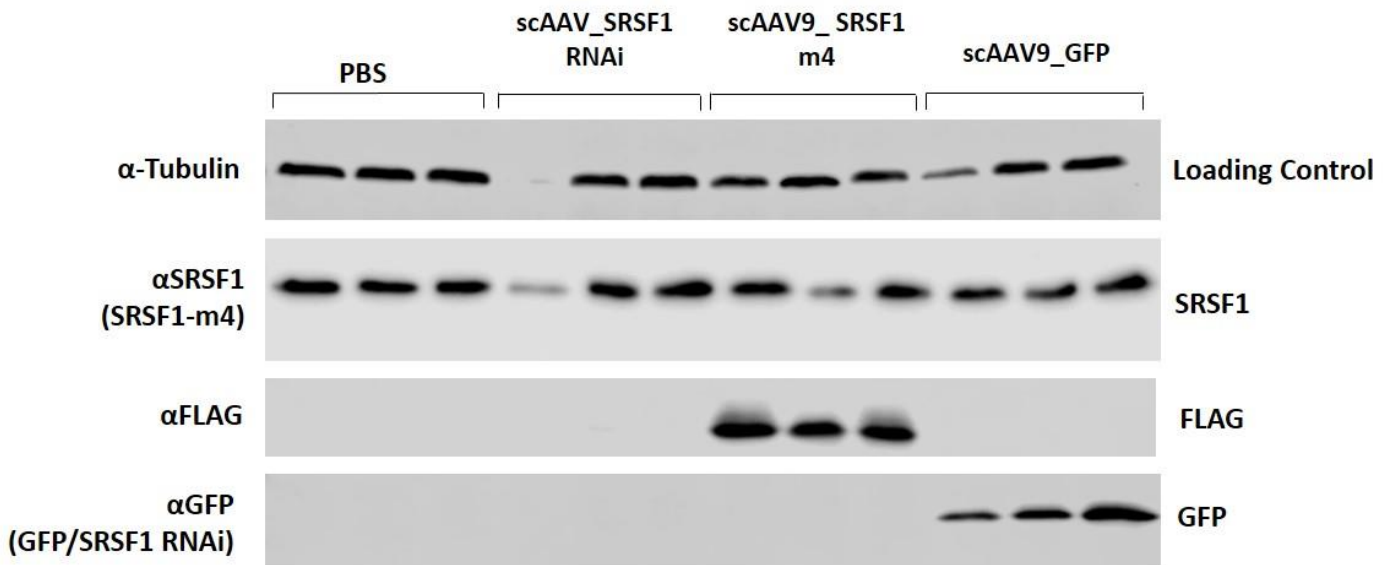
### A. Brain Tissue - 4 weeks post injection



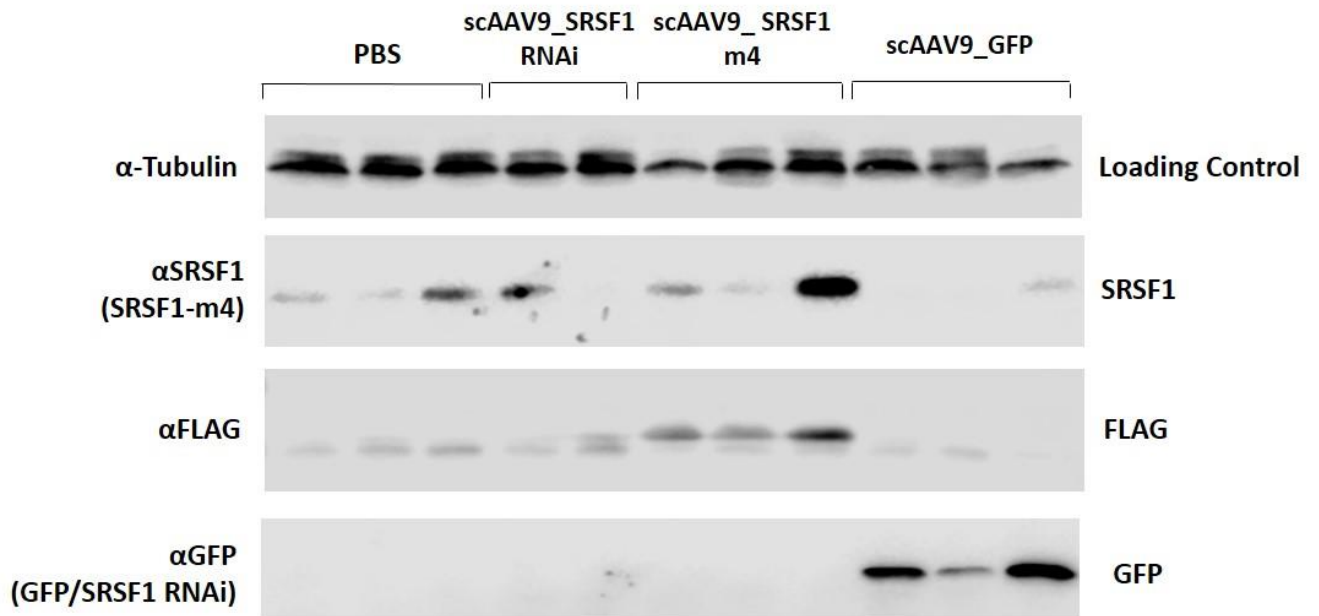
### B. Brain Tissue - 6 months post injection



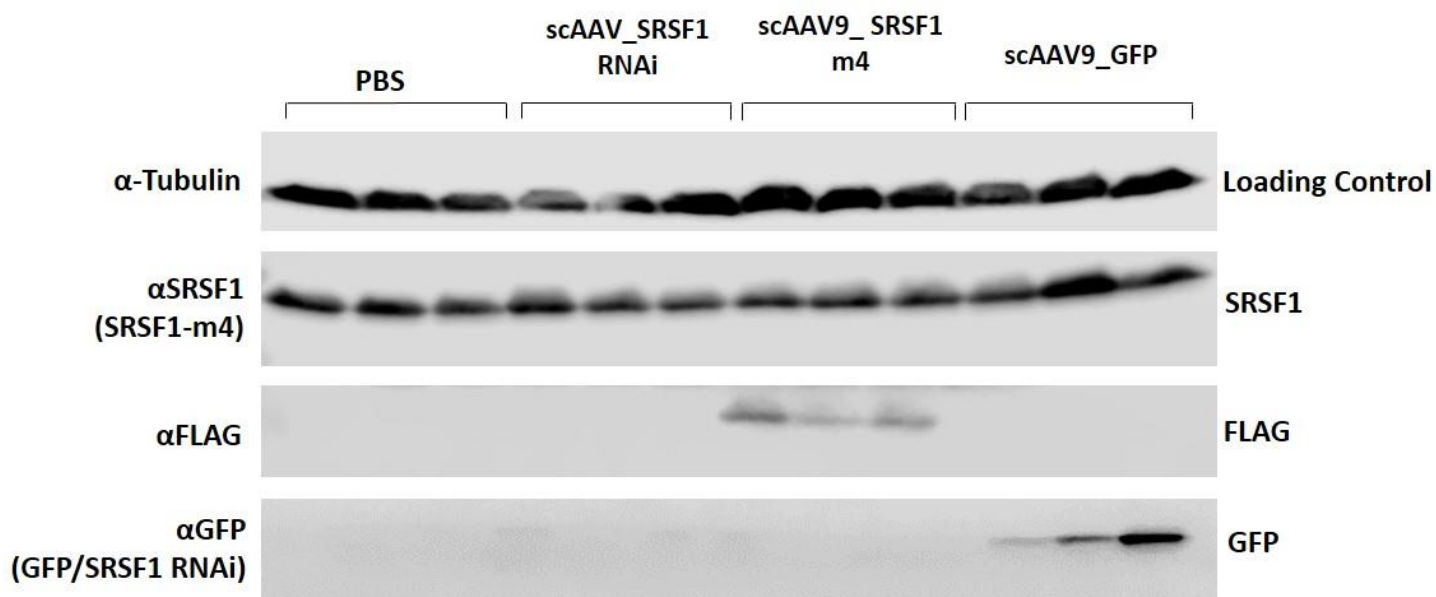
### C. Heart Tissue - 4 weeks post injection



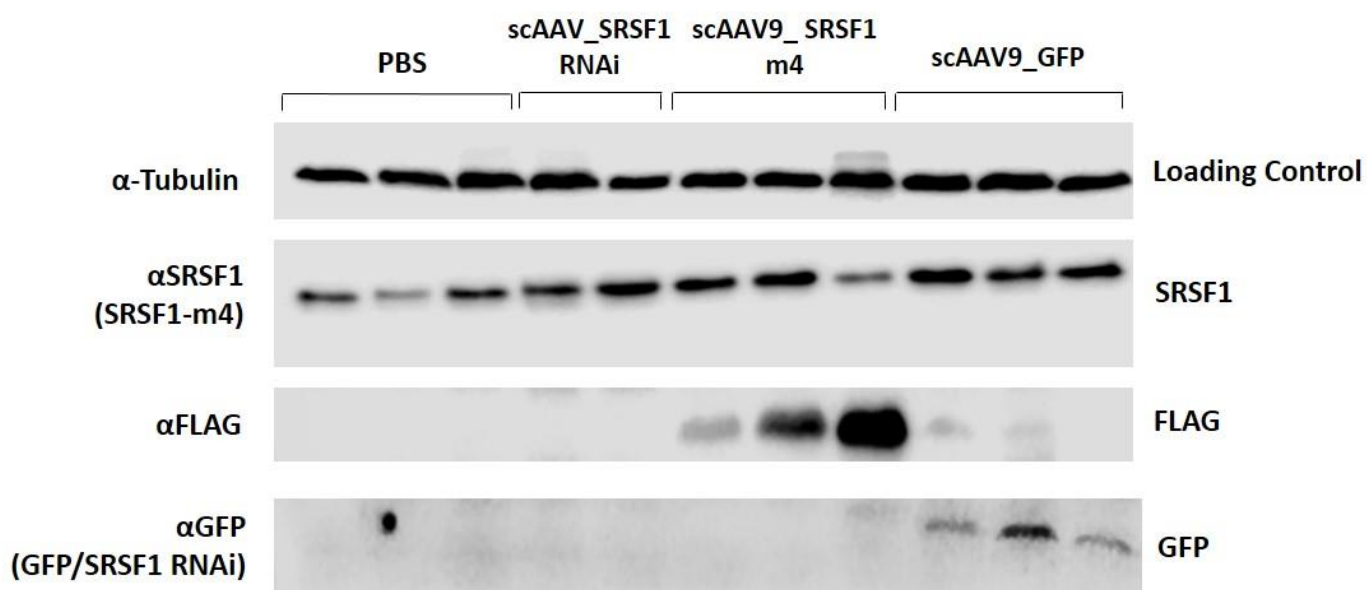
### D. Heart Tissue - 6 months post injection



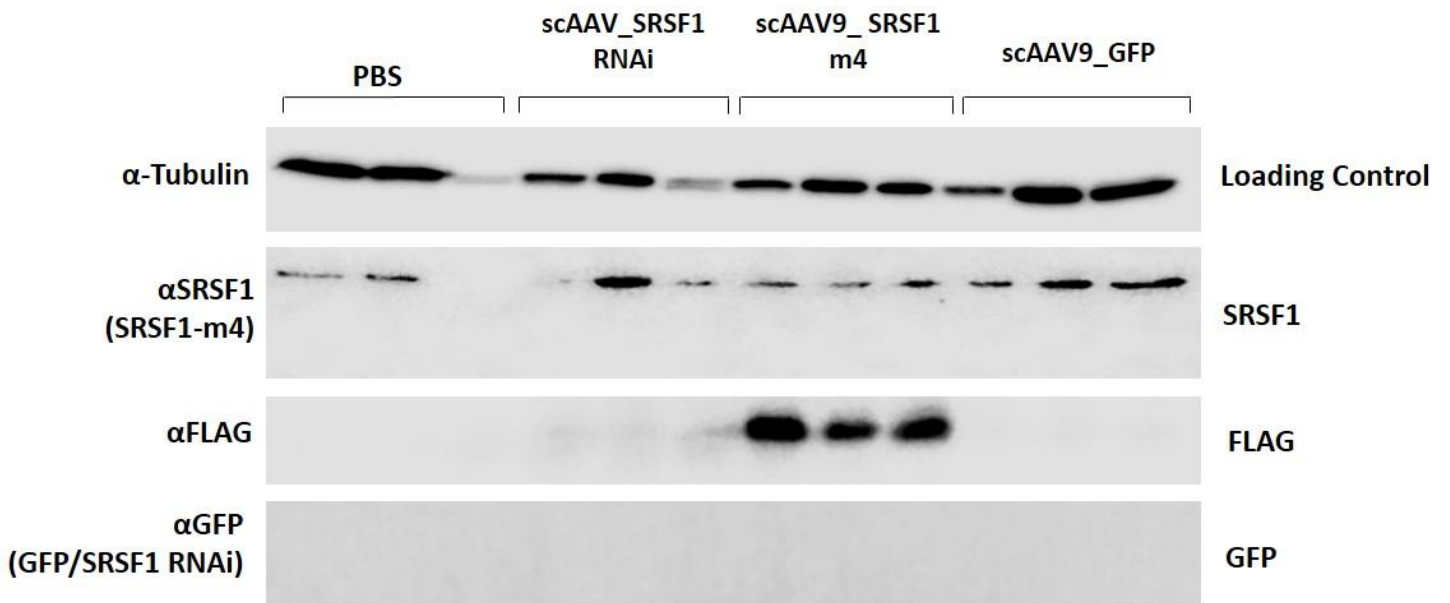
### E. Liver Tissue - 4 weeks post injection



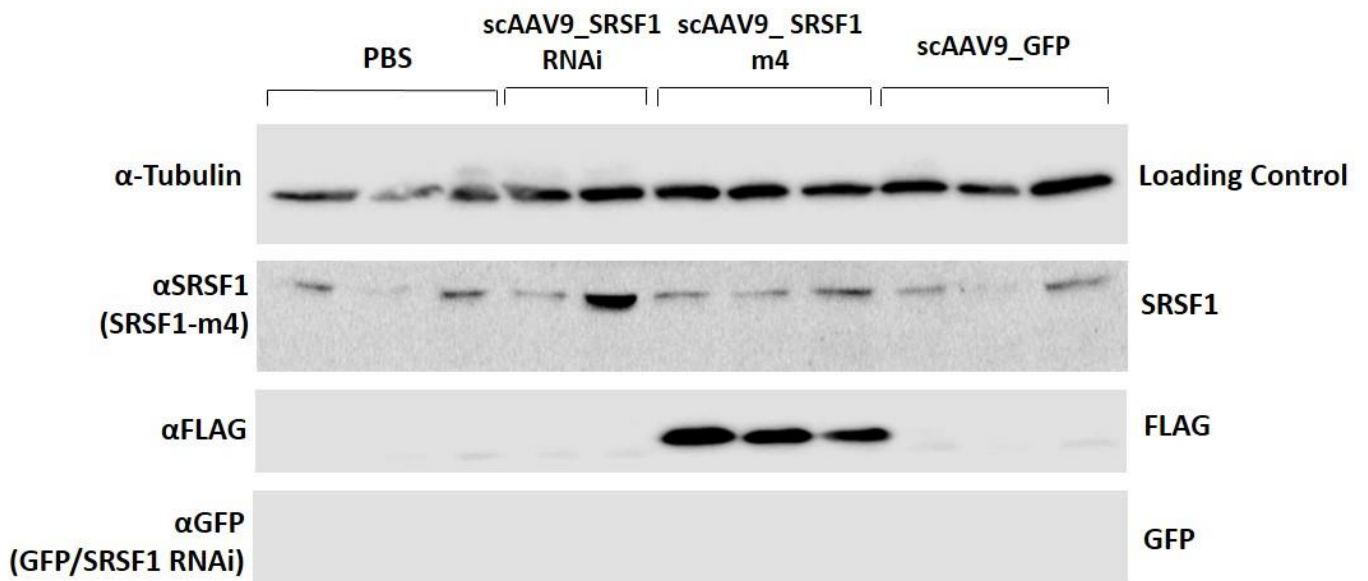
### F. Liver Tissue - 6 months post injection



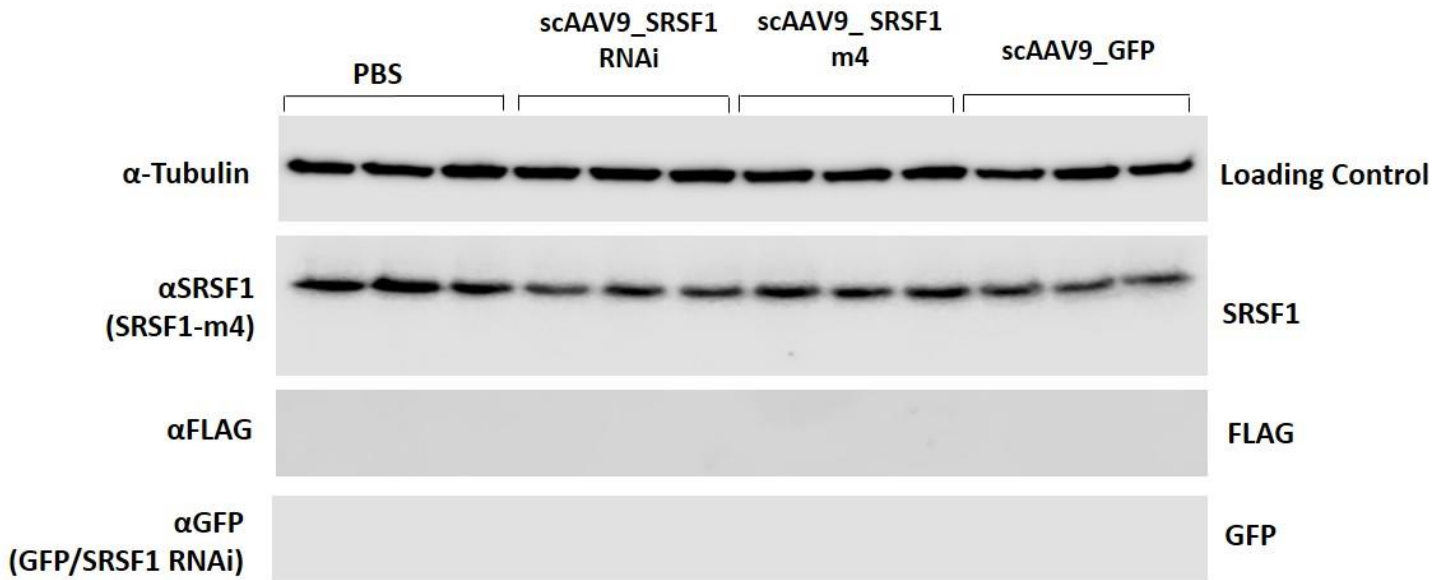
### G. Muscle Tissue - 4 weeks post injection



### H. Muscle Tissue - 6 months post injection



## I. Spleen Tissue - 4 weeks post injection



## J. Spleen Tissue - 6 months post injection

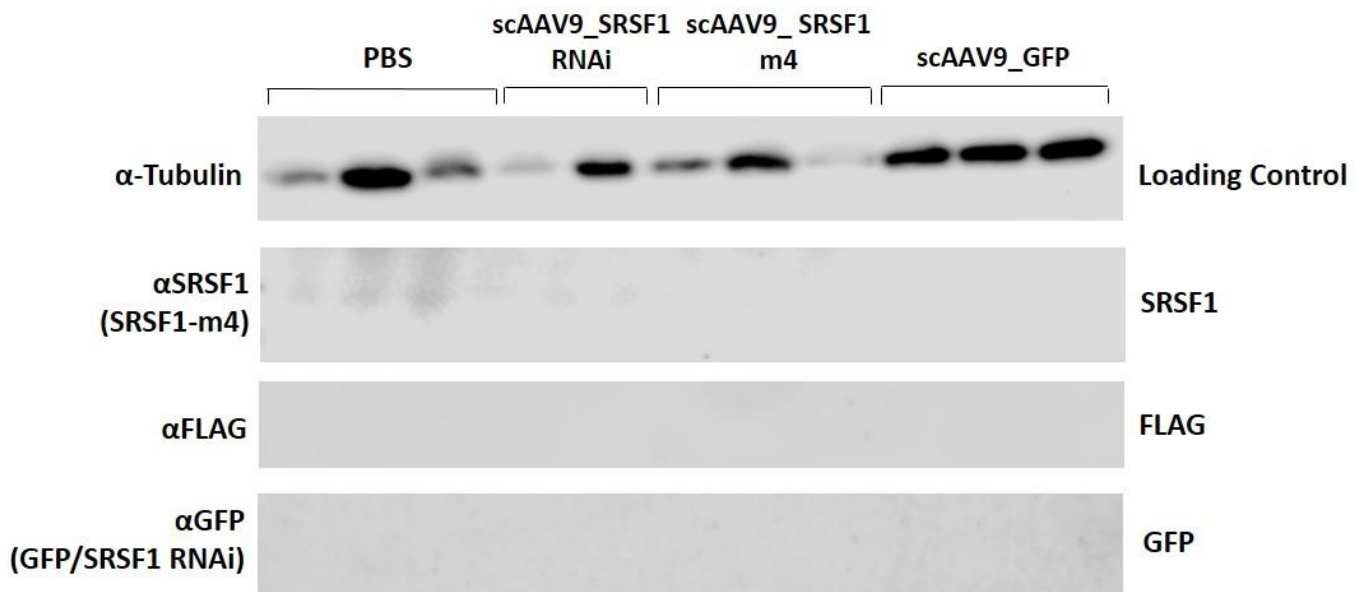


Figure 5. 3 Western blot analysis of brain (A and B), heart (C and D), liver (E and F), muscle (G and H), spleen (I and J) in C57bl/6 mice sacrificed 4-weeks post injection and 6-months post injection— various tissues from mice from each treatment group (PBS, scAAV9\_GFP, scAAV9\_SRSF1-RNAi and scAAV9\_SRSF1-m4) were assessed via Western blot analysis. Tubulin was used as the loading control. FLAG expression was used to view the scAAV9\_SRSF1-m4 - flag tagged virus *in vivo*. A GFP antibody was used view both scAAV9\_SRSF1-RNAi and scAAV9\_GFP by visualising GFP expression. An SRSF1 antibody was used to assess the effect of our gene therapy strategies on SRSF1 expression both at 4-weeks and 6-months post cisterna magna injection. [ $\alpha$ Tubulin = 55 kDa,  $\alpha$ SRSF1 = 33 kDa,  $\alpha$ FLAG = 27 kDa,  $\alpha$ GFP = 24kDa].

---

### 5.3.3 Body weight analysis in wild type C57Bl/6J mice 4-weeks post injection vs mice 6-months post injection

---

Mice in the 4-week cohort were weighed at 3 weeks and at 4 weeks only due to the reduced time between the start and end points of the study. At the 4-week time point there is no significant difference in bodyweight between the 4 treatment groups (Figure 5. 4 A). This could be because there were not enough time points to see any minor fluctuations in weight. It could be that pups could lose a significant amount of weight immediately following the treatment and then gain the weight back, however, it would be difficult to weigh the mice at such a young age as handling them at this critical age could impact on their survival. Any handling of the pups may cause distress to the mother potentially resulting in the death of the pups. It is clear from Figure 5. 4 (A) that there was no significant weight loss or gain that could contribute to reduced survival between 0 and 4-weeks. The overall condition of the pups until 4-weeks was considered normal and no major side effects from the treatments were evident. One mouse was sacrificed early due to the excessive growth of incisors, but this is considered a common ailment in C57Bl/6J mice, with 0.05% of mice of this strain developing this problem (Garcia-Arocena, 2016). The mouse in question was very small in comparison to its siblings and we hypothesise that this was due to the difficulty in eating due to the excessive growth of teeth.

Mice in the 4-week cohort were sacrificed and perfused under terminal anaesthesia at the 4-week time point, and tissue samples were collected for analysis. The brain and the cervical spinal cord from 3 out of the 6 mice, in each treatment group, was collected and prepared for histological analysis and post fixed in 4% paraformaldehyde, followed by sucrose solution and then imbedded in OCT. All other tissue was flash frozen in liquid nitrogen.

Mice in the 6-month cohort were weighed and observed weekly throughout the study. Figure 5. 4 (B) indicates there is no significant difference between the bodyweights between any of the 4 treatment groups. From observation, it could be suggested that animals that were treated with a vector with a CBh promoter had a minor increase in bodyweight compared to PBS treated mice. However, to assess whether this was the case, an area under the curve (AUC) graph was also produced for the 6-month weight data which indicates that there were no significant differences between the weights of mice from each of the 4 treatment groups.

The average weight gain across the experiment was also plotted and an AUC graph was produced from these data. The results from the AUC graphs (Figure 5. 4 D and E) suggest

that there were no significant differences between each of the treatment groups at both 4-weeks and 6-months.

An issue that was a concern, when reviewing the weight data, was that although we used both females and males in each of the treatment groups, each treatment group did not have the same distribution of genders. Male mice generally weigh more than females and there were more males to females in both the scAAV9\_SRSF1-m4 and the scAAV9\_GFP treatment groups in comparison to the scAAV9\_SRSF1-RNAi and PBS treatment groups. The distribution of genders was different between treatment groups because we were injecting mice at post-natal day 1, meaning that sexing pups by observation was difficult and due to the colour of the mice we had limited days to which we would be able to see the cisterna magna through the skull. As this was a safety study and we were interested in the response in both sexes, we decided not to genotype as it would be too time consuming and would potentially waste mouse pups.

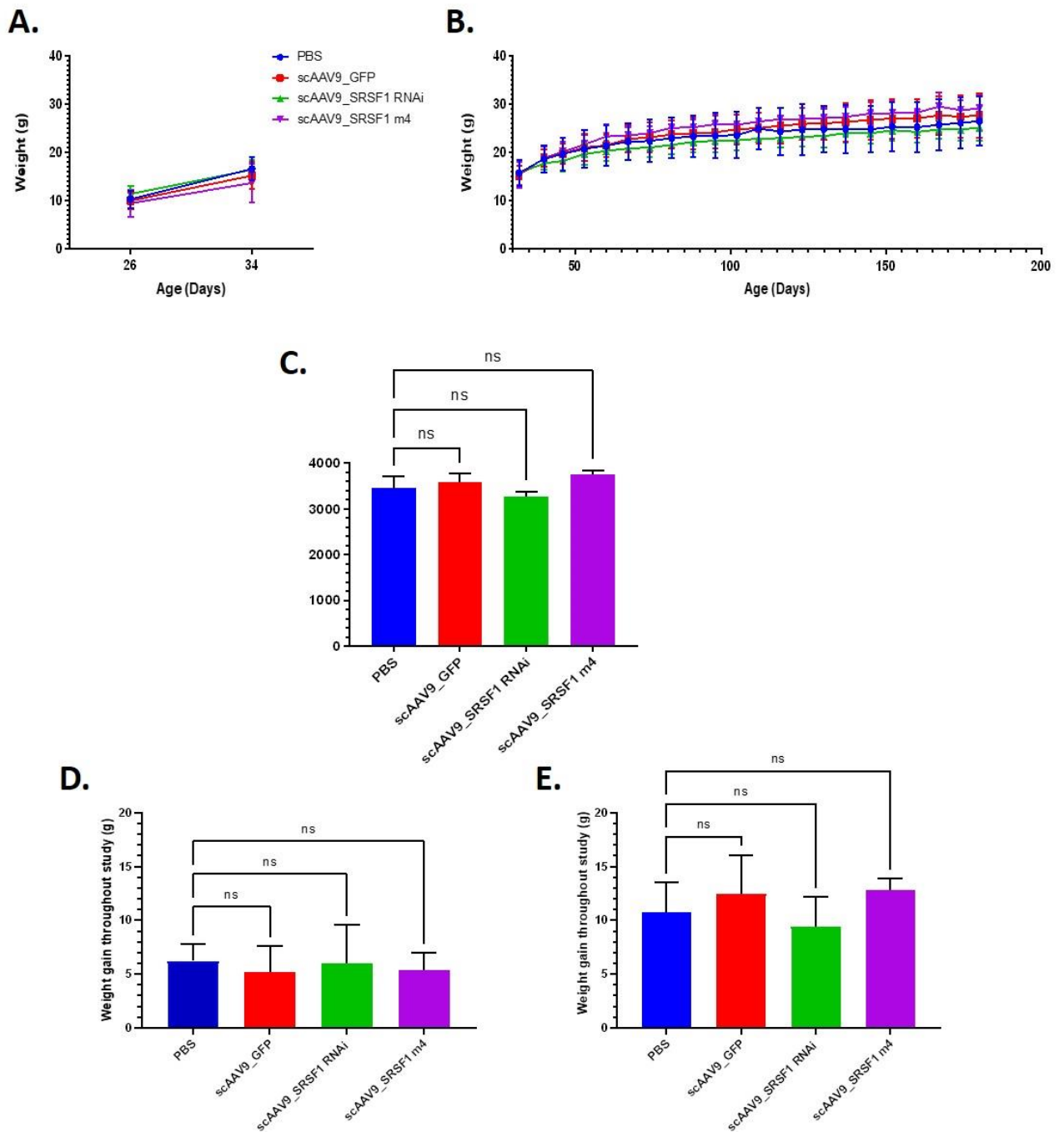


**Figure 5. 4 Cisterna magna delivery of scAAV9\_SRSF1-RNAi and scAAV9\_SRSF1-m4 at post-natal day 1 (P1) results in no significant difference in weight gain** – Mice from the 4 week cohort treated with each of the four treatment groups (PBS, scAAV9\_GFP, scAAV9\_SRSF1-RNAi and scAAV9\_SRSF1-m4) were weighed at 26 and 34 days ( $n=6$ ) (A). Mice were not weighed before 26 days as they had not been weaned and removed from their mothers. Mice in the 6-month cohort were weighed weekly from P30 until the study end (B). An area under the curve (AUC) graph of the 6-month weight data (C). One-way ANOVA of AUC data showed no significant difference in weight data between treatment groups  $p > 0.1$  (ns). Graphs showing the overall weight gain across the study in both the 4-week cohort (D) and the 6-month cohort (E) (4 week cohort  $n=6$ , 6 month cohort  $n=6$  except scAAV9\_SRSF1-RNAi and scAAV9\_SRSF1-m4  $n=4$ ). When comparing the overall weight gain across the study there is no significant difference between the treatment groups. Data analysed by one-way ANOVA followed by post-hoc Dunnett's multiple comparisons test with respect to PBS  $P > 0.05$  (ns).

---

### 5.3.4 Overall Condition and Survival in C57Bl/6J mice

---

Throughout the 6-months of the study there were no observable major side effects relating to any of the 4 treatments (PBS, scAAV9\_GFP, scAAV9\_SRSF1-RNAi and scAAV9\_SRSF1-m4). However, there were several unexplained deaths. All the affected mice appeared to have normal behaviour and there were no warning signs before being found dead. Two scAAV9\_SRSF1-RNAi treated mice were found dead, one at 11 weeks and one at 8 weeks old along with an scAAV9\_SRSF1-m4 treated mouse found dead at 8 weeks old. There was also an scAAV9\_SRSF1-m4 treated mouse that was observed to have neurological deficits. The mouse had very little fear response and was not afraid of people or the prospect of falling. The mouse had an unusual gait compared to neurotypical mice and did not react when objects were placed near its face and eyes, suggesting potential blindness. These traits were likely due to the injection process and we hypothesise that the cisterna magna injection may not have been placed in the correct position and could have damaged the surrounding brain tissue accounting for the unusual behaviour. Although, we are not able to confirm that these deficits were due to the treatment, we would expect if the treatment was to blame we would have seen a similar response in other treated mice, especially if it was related to an inflammatory response. If the treatment was involved, we would have also expected that the neurological deficits would get worse over time. Instead the issues remained the same throughout the 6-month study. Another mouse injected with the scAAV9\_SRSF1-m4 also became sick with a chronic eye infection which eventually led to the mouse being sacrificed early due to welfare concerns. Eye infections in C57Bl/6J mice are again a common ailment and as such this illness is unlikely to be related to the therapeutic treatment.

Overall, the study used 48 C57Bl/6J mice and only 3 mice were observed to have premature deaths, therefore this study has an 93.75% survival rate up to 6-months post injection, which is as expected, as an average C57bl/6 mouse colony has a 90% survival rate for mice aged up to 18 months old (Turturro *et al.*, 1999). The 4 -week cohort had a 100% survival rate up until 4 weeks and the 6-month cohort had an 87.5% survival rate up until 6-months.

---

### 5.3.5 Rotarod Analysis in C57Bl/6J mice

---

At post-natal day 70, mice in the 6-month cohort underwent the rotarod behavioural test every 2 weeks until 6-months of age. Mice were placed on the rotarod for up to 5 mins as the machine accelerated from 3 to 37 revolutions per minute. In C57Bl/6J mice we would expect no motor deficits at this age, and we would expect the mice to remain on the rotarod for the entire program.

From observation, there appeared to be no behavioural differences between the 4 treatment groups whilst the mice were undergoing the rotarod behavioural test. Figure 5. 5A indicates that there were no significant differences between the four treatment groups and the amount of time spent running on the rotarod. An area under the curve graph (Figure 5. 5B) was also used to assess whether there were any differences between the 4 treatment groups, and again it confirms that there were no significant differences in motor performance between the treatment groups. However, it is indicated that animals treated with the scAAV9\_SRSF1-RNAi were the most consistent and remained on the rotarod the whole 5 minutes during every session. This may have been due to coincidence or the treatment may have provided a very slight improvement in motor performance. The overall results suggest that none of the interventions have significant side effects involving the motor function between 70 and 180 days, which is a positive outcome.

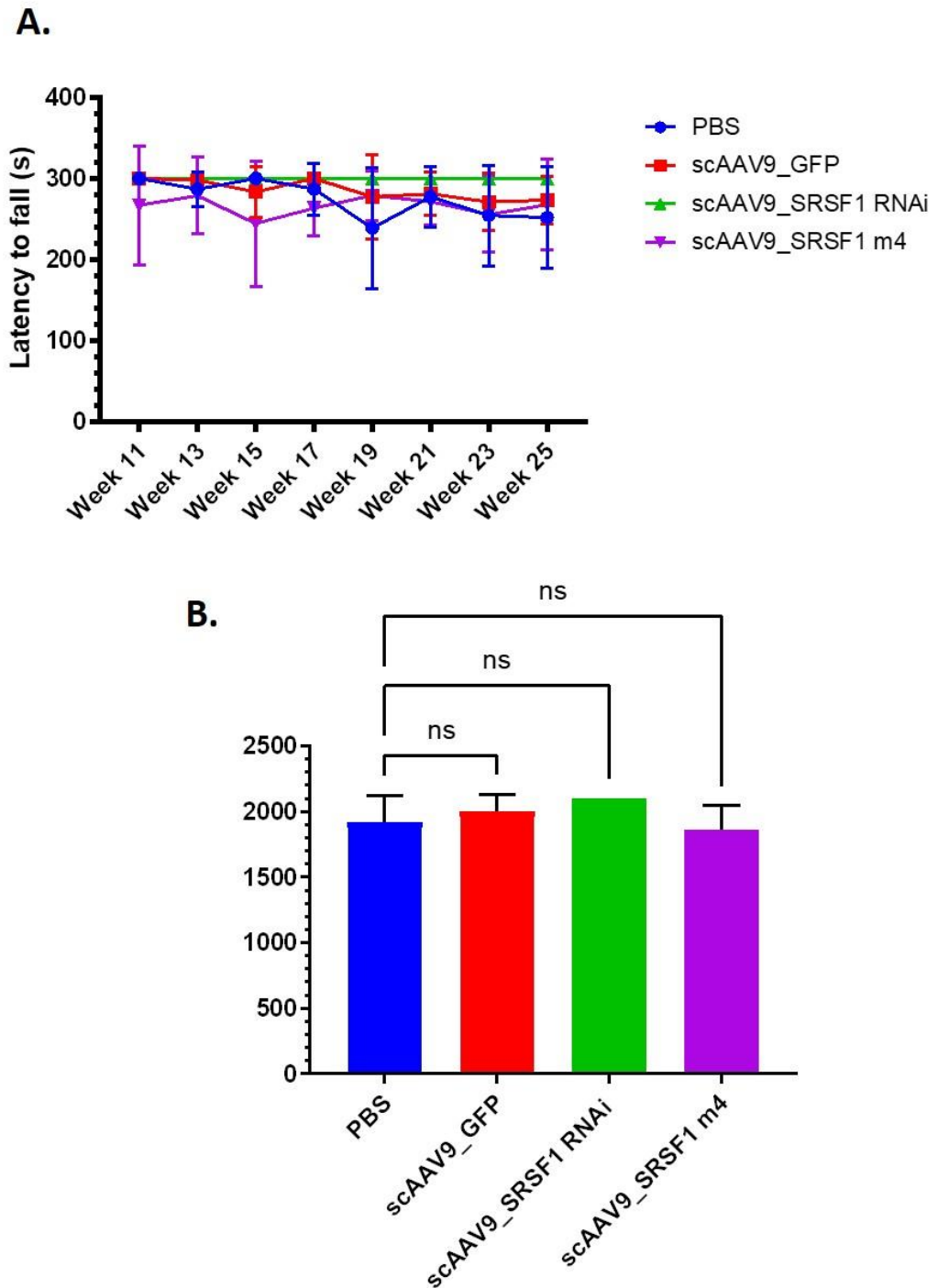


Figure 5. 5 Cisterna magna delivery of scAAV9\_SRSF1-RNAi and scAAV9\_SRSF1-m4 at post-natal day 1 (P1) results in no significant difference in rotarod performance – Rotarod performance was assessed in the 6 month cohort using mice from each treatment group (PBS, scAAV9\_GFP, scAAV9\_SRSF1-RNAi, scAAV9\_SRSF1-m4) every two weeks from week 11 to week 25. Graphs showing rotarod performance measured as time to fall in seconds against age in days (**A**) and area under the (AUC) of rotarod performance (**B**) n=6 except scAAV9 SRSF1-RNAi and scAAV9 SRSF1-m4 n=4. AUC data analysed by one-way ANOVA followed by post-hoc Dunnett's multiple comparisons test with respect to PBS (ns)  $P > 0.05$ .

## 5.4 Histological analysis of the gene therapy interventions

### 5.4.1 The effect of the therapeutic viruses on motor neuron cell count

In MND, loss of the motor neurons is what inevitably causes the death of afflicted individuals. In this part of the study, the effect of the treatments on the number of motor neurons was assessed. To date, there has been no previous published research to review the effect SRSF1 manipulation may have on the motor neuron survival. It was hypothesised that because the mice had no disease phenotype, then the SRSF1 treatments would have no obvious effect on motor neuron survival. It is expected that the motor neurons of these wild-type mice should have healthy motor neurons with no evident motor neuron degeneration.

The cervical spinal cord which had been imbedded into OCT was processed using the cryostat and sectioned into a 5-slide series with 6 sections per slide. One slide per series underwent Nissl staining. Nissl is a stain that labels RNA and DNA and allows for the identification of neuronal structures. In this case it allowed us to identify motor neurons within the cervical spinal cords of the treated mice. The following criteria were used to confirm that a cell was a motor neuron: the cell body must be 25 $\mu$ m or greater, must have 3 or more major dendrites, the nucleus must be in focus and the nucleolus must be visible within it (Figure 5. 6). Figure 5. 9 indicates that there was more variability in motor neuron cell count between treatment groups in mice at 4-weeks. In the 4-week cohort, the average number of motor neurons per ventral horn was very similar suggesting that there were no significant differences in the number of motor neurons in each treatment group. Figure 5. 7 displays a representative image of the 4-week Nissl staining and no obvious difference between the number of motor neurons in the four treatment groups is evident. At 6-months the variability between treatment groups had decreased, but at least 2 of the treatment groups had an n=2 due to unexpected deaths (Figure 5. 9). Again, looking at the microscopic images from the four treatment groups (Figure 5. 8) no obvious difference in the number of ventral horn motor neurons was observed.

## Motor Neuron cell counting

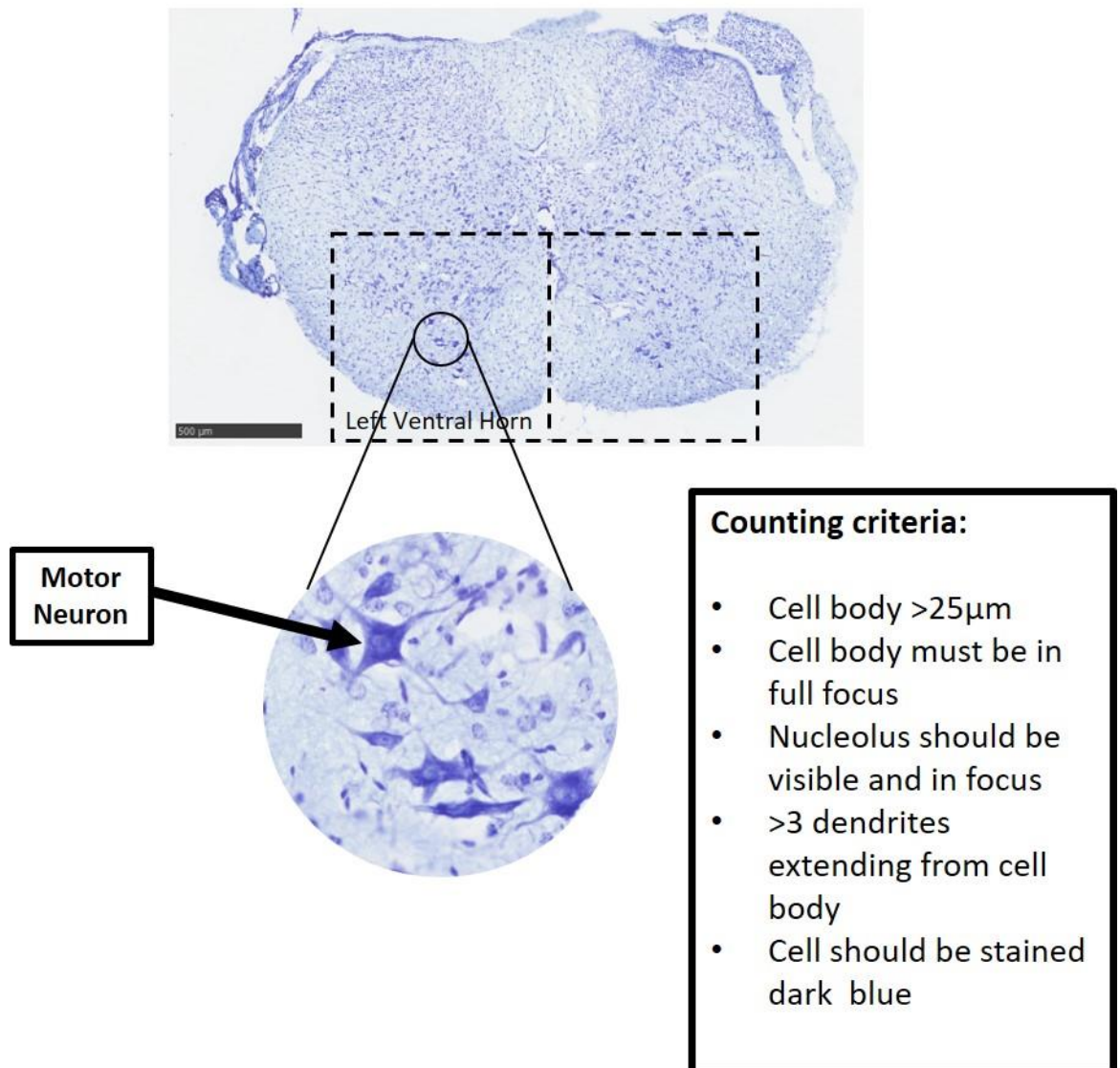


**Figure 5. 6 Counting motor neurons in Nissl stained cervical spinal cord sections** – Spinal cord tissue underwent Nissl staining and was scanned using the NanoZoomer S60 digital slide scanner. The NanoZoomer software was then used to count the motor neurons in both the left and right ventral horns of each section. The overall average of motor neurons per ventral horn was then calculated for each treatment group. The criteria used to count the motor neurons are described above. Scale bar = 500  $\mu$ m.

## Nissl Staining at 4 weeks post injection

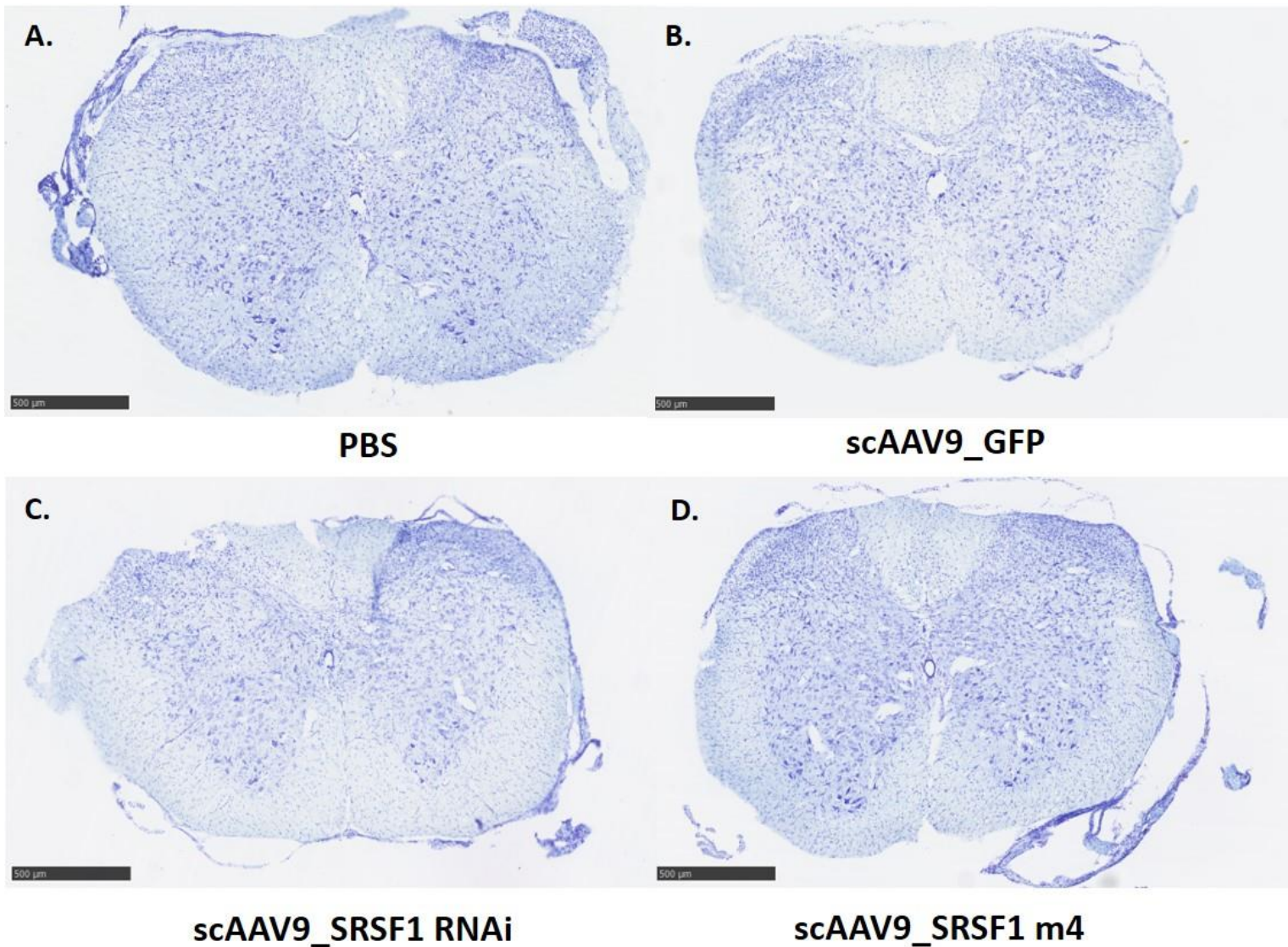
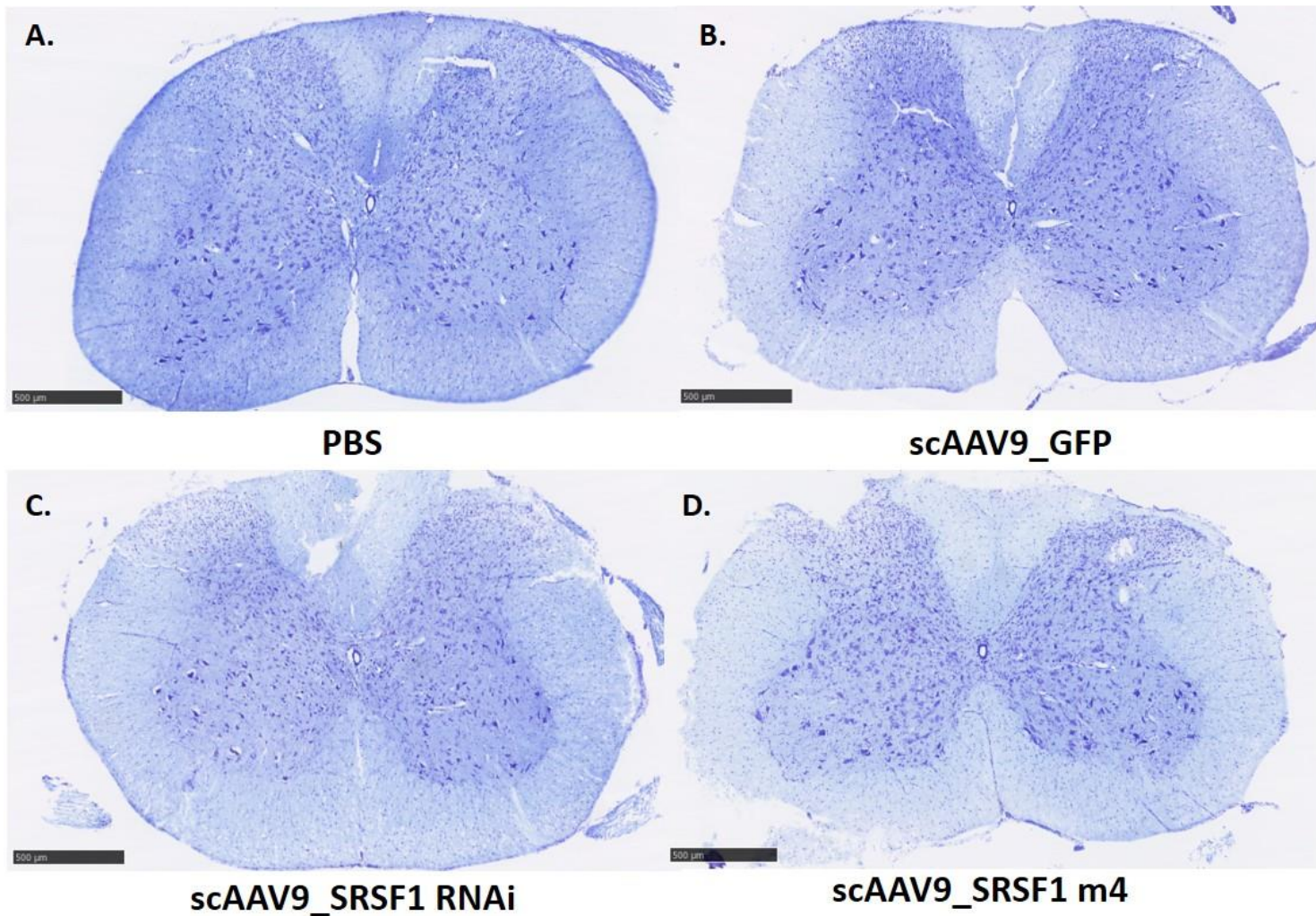


Figure 5. 7 Nissl stained cervical spinal cord sections 4-weeks post cisterna magna injection – Spinal cord tissue harvested 4-weeks post injection from C57bl/6 mice treated with (A) PBS, (B) scAAV9\_GFP, (C) scAAV9\_SRSF1-RNAi and (D) scAAV9\_SRSF1-m4 that has undergone nissl staining to allow for the counting of motor neurons. The average number of motor neurons per ventral horn was compared between all 4 of the treatment groups. Scale bar = 500 µm.

## Nissl Staining at 6 months post injection



**Figure 5. 8** Nissl stained cervical spinal cord sections 6-months post cisterna injection – Spinal cord tissue harvested 6-months post injection from C57bl/6 mice treated with (A) PBS, (B) scAAV9\_GFP, (C) scAAV9\_SRSF1-RNAi and (D) scAAV9\_SRSF1-m4 that has undergone nissl staining to allow for the counting of motor neurons. The average number of motor neurons per ventral horn was compared between all 4 of the treatment groups. Scale bar = 500 µm.

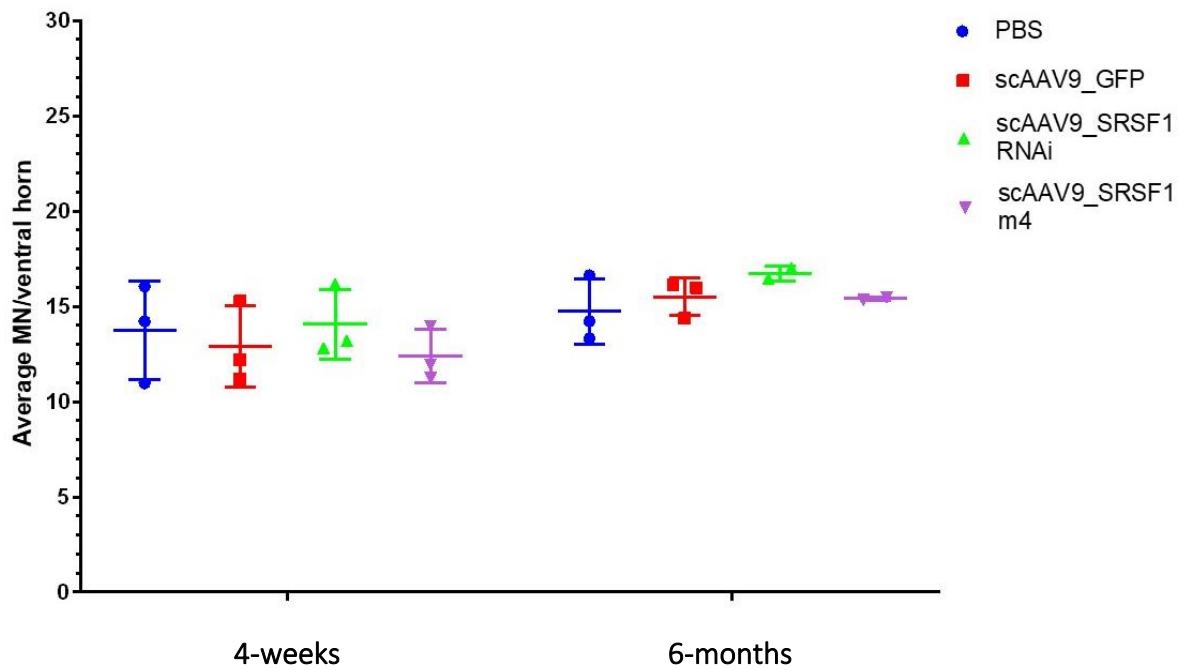


Figure 5. 9 Cisterna magna delivery of scAAV9 SRSF1-RNAi and scAAV9 SRSF1-m4 at post-natal day 1 (P1) results in no significant difference in the average number of motor neurons per ventral horn at both 4-weeks and 6-months – Spinal cord tissue taken from mice treated with PBS, scAAV9 CBh\_GFP, scAAV9\_SRSF1-RNAi and scAAV9\_SRSF1-m4 underwent Nissl staining to review the number of motor neurons present in the ventral horn of the spinal cord. The graph depicts the average number of motor neurons per ventral horn throughout the cervical spinal cord at 4-weeks and 6-month post cisterna magna injection. Each set of data has been counted by two separate investigators (4-weeks = Charlotte Mason and Eloise Sowter, 6-months = Charlotte Mason and Aytac Gul). There is no significant difference in the average number of motor neurons per ventral horn between treatment groups at both 4-weeks and 6months post cisterna magna injection. The mean of the 2 investigator’s data was calculated and plotted onto this graph. Data analysed by two-way ANOVA followed by post-hoc Dunnett’s multiple comparisons test with respect to PBS treated (4-week cohort n=6, 6 month cohort n=6 except scAAV9 SRSF1-RNAi and scAAV9 SRSF1-m4 n=4) with  $p > 0.05$  (ns).

---

#### 5.4.2 The effect of the therapeutic viruses on SRSF1 expression in the spinal cord

---

Neurodegeneration of the motor neurons is the main cause of MND symptoms and the process that inevitably causes the death of patients. This part of the study was designed to assess the effect of the treatments (PBS, scAAV9 CBh\_GFP, scAAV9\_SRSF1-RNAi and scAAV9\_SRSF1-m4) on SRSF1 expression in the spinal cord using DAB staining against SRSF1. To date, there has been no previous published research to review SRSF1 manipulation in the spinal cord. It was hypothesised that, because the mice had no disease phenotype, the scAAV9\_SRSF1-RNAi treatment would reduce SRSF1 expression and that the scAAV9\_SRSF1-m4 treatment would also cause some alteration in the level of SRSF1 expression in the spinal cord.

Figure 5. 10 shows spinal cord sections from each of the 4 treatment groups 4-weeks post injection: negative control (A), PBS (B), scAAV9\_GFP (C), scAAV9\_SRSF1-RNAi (D) and scAAV9\_SRSF1-m4 (E). The amount of SRSF1 staining in each mouse was not accurately quantified due to study time restraints and difficulty of quantifying such easily-saturated staining. However, from observation of Figure 5. 10 and reviewing all images across the spinal cord, the SRSF1 staining is less intense and there are less SRSF1 positive cells in scAAV9\_SRSF1-RNAi treated mice at 4-weeks post injection. There is no obvious visible difference in SRSF1 expression between the other three treatments (PBS, scAAV9\_GFP and scAAV9\_SRSF1-m4) at 4-weeks post injection.

At 6 months post injection (Figure 5. 11) there are no observable differences between the 4 treatment groups (A-E) and the additional microscopy images from the SRSF1 DAB staining.

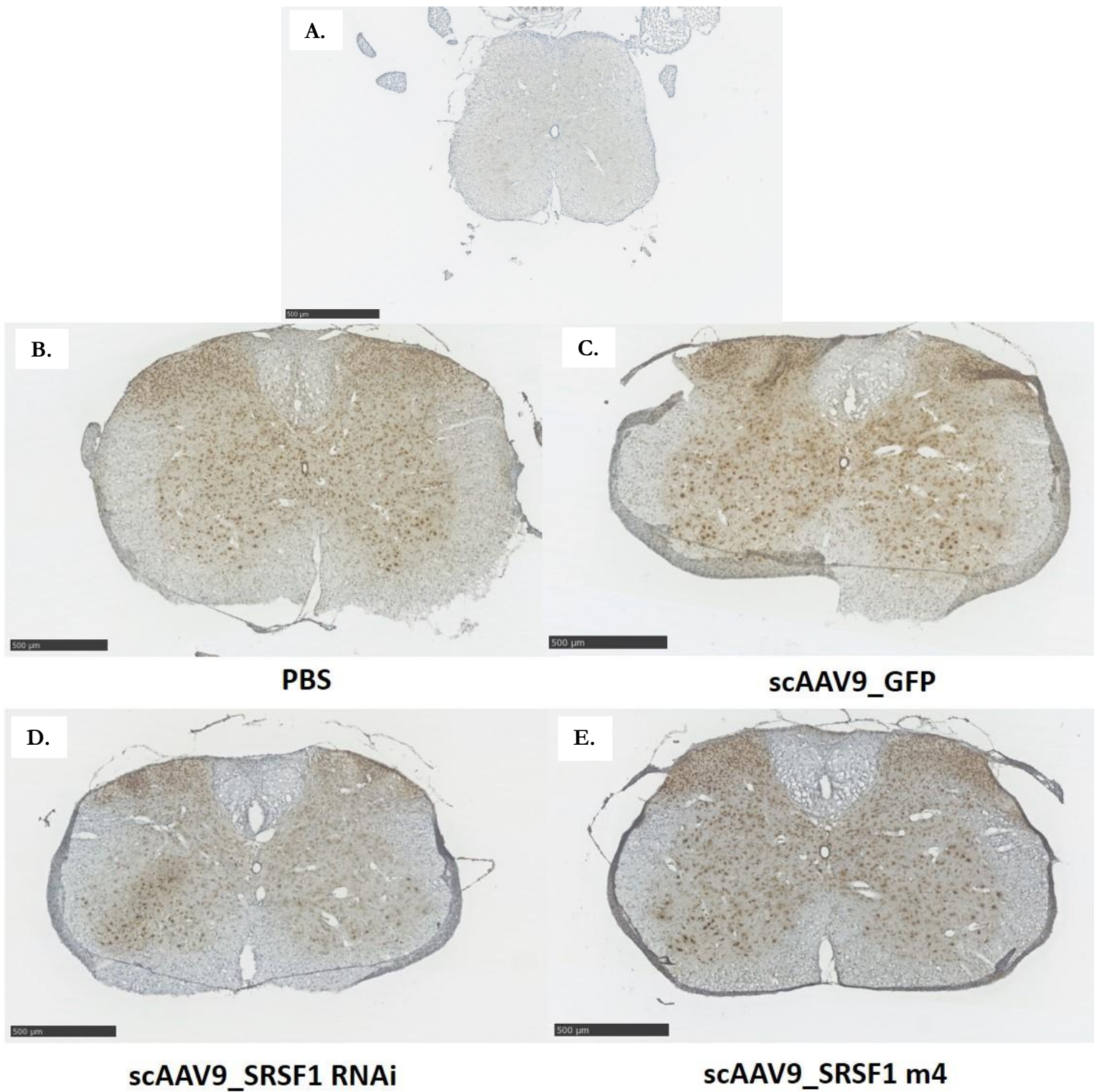
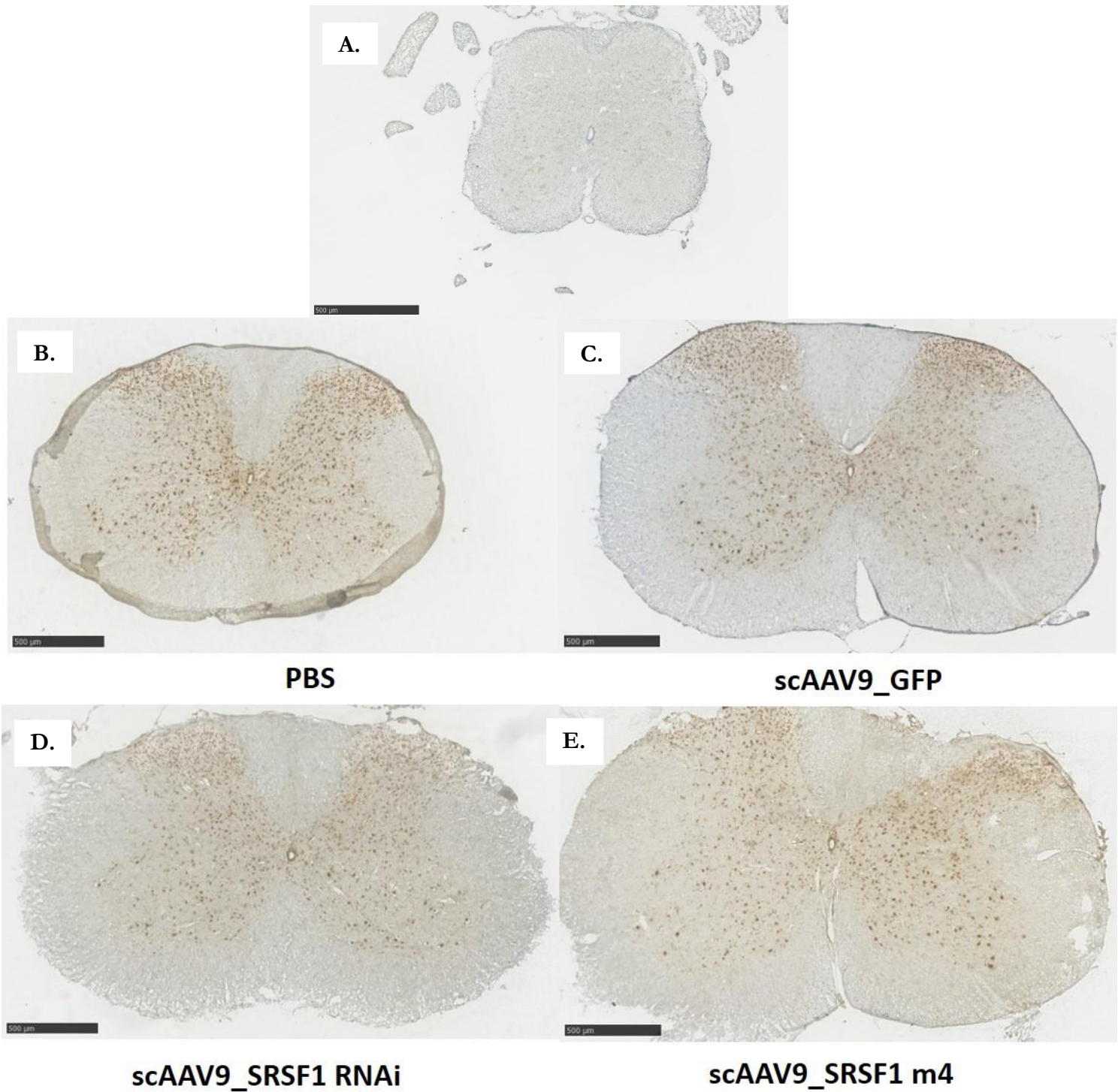


Figure 5. 10 SRSF1 DAB stained cervical spinal cord sections 4-weeks post cisterna magna injection – Spinal cord tissue harvested 4-weeks post cisterna magna injection from C57bl/6 mice treated with (A) negative control, (B) PBS, (C) scAAV9\_GFP, (D) scAAV9\_SRSF1-RNAi and (E) scAAV9\_SRSF1-m4 that has undergone SRSF1 DAB staining to allow for the visualisation of SRSF1 expression in the spinal cord. Scale bar = 500 µm.



**Figure 5.11 SRSF1 DAB stained cervical spinal cord sections 6-months post cisterna magna injection** – Spinal cord tissue harvested 6-months post cisterna magna injection from C57bl/6 mice treated with **(A)** negative control, **(B)** PBS, **(C)** scAAV9\_GFP, **(D)** scAAV9\_SRSF1-RNAi and **(E)** scAAV9\_SRSF1-m4 that has undergone SRSF1 DAB staining to allow for the visualisation of SRSF1 expression in the spinal cord. Scale bar = 500 µm.

## 5.5 *In vivo* testing of the therapeutic scAAV9 viral vectors in a C9ORF72 ALS/FTD mouse model

For this study, the *C9ORF72*-ALS/FTD mouse model developed by the Ranum lab was used to assess the effect of our designed therapeutic constructs on the production of toxic dipeptide repeat proteins (DPRs). In this experiment we used a different control virus, scAAV9\_scrambled-RNAi, which had been developed and used as a control in Scarrott, 2019. The scAAV9\_scrambled-RNAi had the same backbone as the scAAV9\_SRSF1-RNAi, but instead of an RNAi against SRSF1 it had a scrambled sequence that would not produce an RNAi against any sequence and was essentially a stuffer sequence.

The original design was to have 4 experimental groups: Non-Transgenic untreated, Transgenic untreated, Transgenic scAAV9\_scrambled-RNAi treated and Transgenic scAAV9\_SRSF1-RNAi treated with 10 female mice per group. The mice were injected via the cisterna magna between post-natal day 1 and post-natal day 2 with 5  $\mu$ l of virus/treatment at a rate of 1  $\mu$ l per minute at a dosage of  $1.18 \times 10^{10}$  vg/ $\mu$ l (scAAV9\_scrambled-RNAi) and  $1.98 \times 10^9$  vg/ $\mu$ l (scAAV9\_SRSF1-RNAi). The total dosage was  $5.9 \times 10^{13}$  vg/kg for scAAV9\_SRSF1-RNAi treated mice and  $1 \times 10^{13}$  vg/kg for scAAV9\_SRSF1-m4. The viral vectors were buffer exchanged into a vehicle solution of sterile phosphate-buffered saline plus 35 mM sodium chloride (PBS + 35 mM NaCl) to avoid a reaction to the remaining serum free media following administration. The untreated animals did not undergo any injection or anaesthesia. The end time-point for this study would be 4 months post-injection to review the DPR production in the mouse tissue following treatment.

Each of the mouse litters consisted of a mixture of both control and virus treated pups to account for litter differences and environment. The mice were observed daily for the first week to ensure that their condition was stable and then every few days thereafter. Body weight measurement was performed weekly, starting from 35 days old and rotarod was assessed using a forward/reverse rotarod programme (described in Chapter 2 - Material and Methods). The study was designed to assess for hindlimb claspings, involving mice being suspended from their tail at 20 cm from procedure surface for 15 s. They would be considered to have a claspings phenotype if one or both hindlimbs were retracted and touched the abdomen for 3s. This procedure was ideally performed weekly following body weight assessment. Open field testing to review general locomotor activity levels and anxiety and

willingness to explore was planned as was the object recognition test to evaluate cognition, particularly recognition memory.

Unfortunately, due to the COVID-19 pandemic which commenced in February 2020, this planned study was severely impacted mid recruitment. The animal facility was shut down to essential animal maintenance staff from March 2020, meaning that no more animals could be recruited to our study and any mice currently within the study could not undergo any testing or analysis. The facility only allowed us to enter to sacrifice any remaining mice, but at certain time points only meaning that many of the mice were not sacrificed at our suggested time point of 4 months post injection. The tissue of the recruited mice was harvested, flash frozen in liquid nitrogen and stored for future analysis.

The protein was extracted from the tissue and was used in an MSD assay to assess the DPR levels in the 6 tissue types of each experimental group: brain, spinal cord, heart, liver, spleen and muscle (Figure 5. 12). The MSD assay specifically evaluated the levels of the poly-GP species of DPR. The abnormal RAN translation of the *C9ORF72* repeat transcripts results in the production of 5 different DPRs (poly-GA, poly-GR, poly-PA, poly-PR and poly-GP) within the cytoplasm. Significant poly-GP levels have been detected in the CSF of asymptomatic *C9ORF72* mutation carriers in comparison to healthy controls and even patients with other neurodegenerative diseases. The poly-GP DPR levels have been found to be similar in both asymptomatic carriers and symptomatic *C9ORF72*-ALS/FTD cases. It has been suggested that pre-symptomatic expression of poly-GP and likely other DPR species may contribute to disease onset and thus represents a potential biomarker of disease (Lehmer, C. *et al*, 2017).

As expected, transgenic *C9ORF72* ALS/FTD BAC 500 mice show significant expression levels of poly-GP DPRs in comparison to their non-transgenic counterparts. Overall, the results suggested that there was no significant difference between the transgenic untreated, scAAV9\_scrambled RNAi and scAAV9\_SRSF1-RNAi treatment groups across tissue types except in the liver. A significant increase in DPR levels was observed in the liver of animals treated with scAAV9\_scrambled-RNAi vs transgenic untreated animals. Due to the significant disruption of the pandemic to this experiment we did not want to draw any conclusions from these results until we had repeated the experiment in more appropriate conditions.

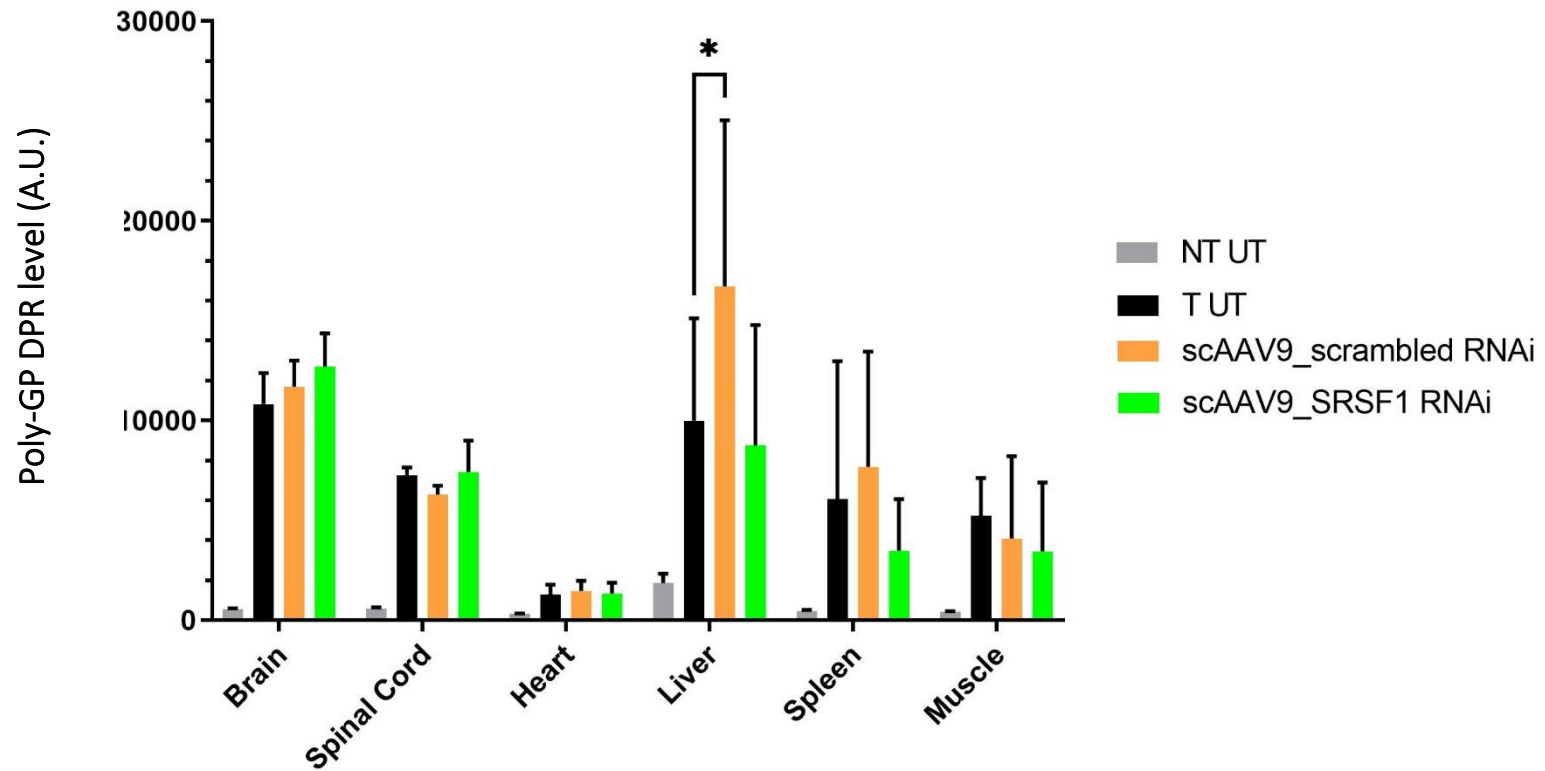


Figure 5. 12 Poly-GP MSD assay to assess the effect of scAAV9\_SRSF1-RNAi on the expression of poly-GP DPRs in various tissue types (experiment adversely affected by COVID-19). DPR expression in 6 types of C9ORF72 ALS/FTD mouse tissue: brain, spinal cord, liver, spleen, heart and muscle. Mice were sacrificed between 3-month and 4-month post cisterna magna injection (NT UT and T UT n=5 and scAAV9 scrambled and scAAV9\_SRSF1-RNAi n=4). Data analysed by two-way ANOVA followed by post-hoc Dunnett's multiple comparisons test with respect to transgenic untreated (T UT). Stars indicate  $p < 0.05$  (\*).

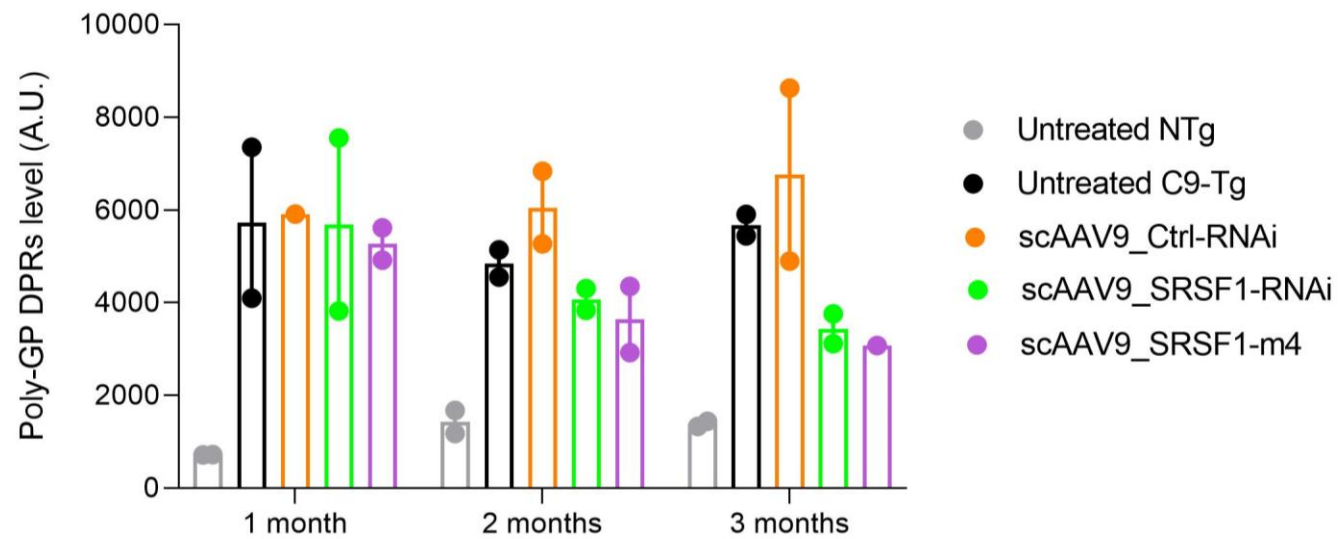
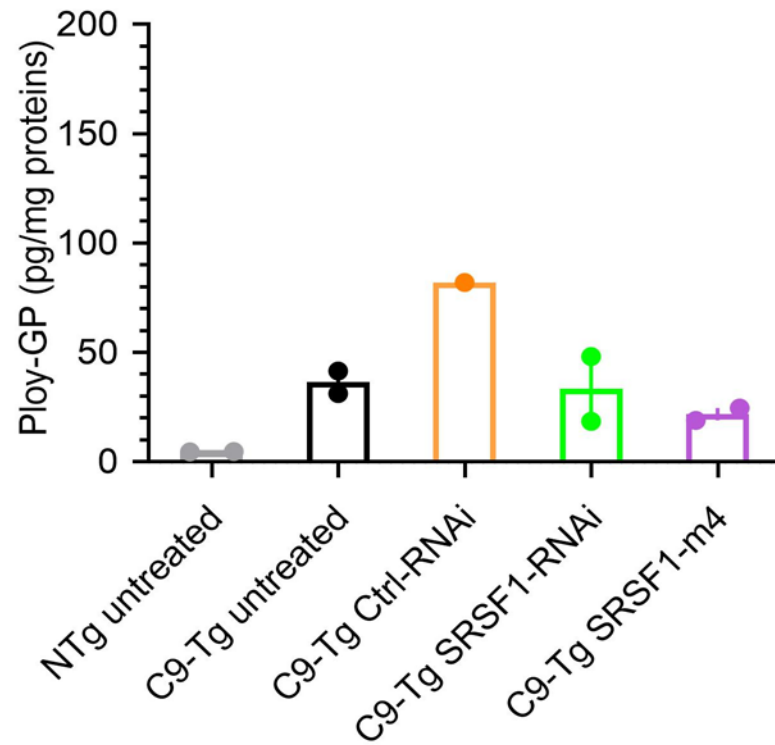


Figure 5. 13 Poly-GP MSD Assay to assess the effect of scAAV9\_SRSF1-RNAi or scAAV9\_SRSF1-m4 on toxic DPR levels in the brain cortex (experiment unaffected by COVID-19). Expression of Poly-GP DPR levels in brain cortex tissue of C9ORF72 ALS/FTD. Mice were sacrificed at 1 month, 2 months and 3 months post cisterna magna injection (n=2).

A. 2 months post-injection



B. 3 months post-injection

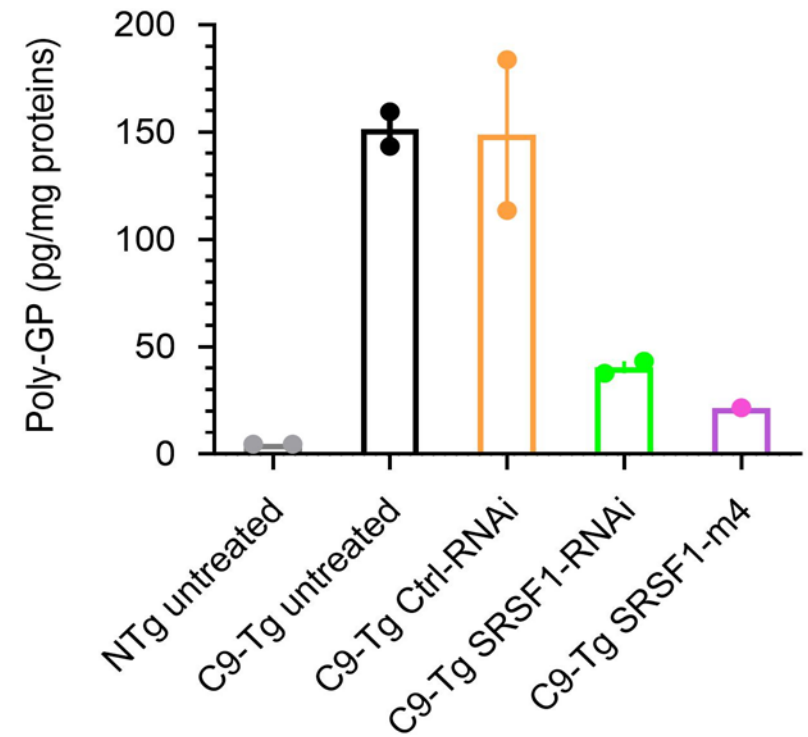


Figure 5. 14 Poly-GP MSD Assay (normalised to a standard curve) to assess the effect of SRSF1 depletion or the expression of SRSF1-m4 on toxic DPR levels in the brain cortex (experiment unaffected by COVID-19). Expression of Poly-GP DPR levels in the brain cortex tissue of C9ORF72 ALS/FTD (A) in mice sacrificed at 1-month (ns between any of the groups) and (B) mice sacrificed at 2 months post cisterna magna injection (n=2).

This study was affected by Covid-19 related closure of the University and working in shift pattern for the following year. Non-transgenic untreated, transgenic untreated, transgenic scAAV9\_scrambled RNAi treated (dosage of  $1.13 \times 10^{10}$  vg/ $\mu$ l), transgenic scAAV9\_SRSF1-RNAi treated (dosage of  $1.18 \times 10^{10}$ vg/ $\mu$ l) and transgenic scAAV9\_SRSF1-m4 treated (dosage of  $2 \times 10^9$  vg/ $\mu$ l) with 10 female mice per group. In the initial study it was decided that there would not be an scAAV9\_SRSF1-m4 treatment group due to limited stocks of the scAAV9\_SRSF1-m4 virus. However, as pandemic restrictions lifted, new scAAV9\_SRSF1-m4 stocks were produced and were available, before mouse work was able to continue meaning that viral stocks were replenished for the start of the new study.

The new study was intended to start as soon as the COVID-19 restrictions allowed. However, the animals were severely stressed due to the change in routine and staff member turnover, resulting in months of breeding issues. Eventually recruitment resumed in March 2021 but is still ongoing with 31 out of 50 mice recruited. The study was designed so that 2 mice from each treatment group would be sacrificed at 1 month, 2 months and 3 months, whilst 4 mice from each treatment group would be sacrificed at 4 months.

Despite the challenges, this pilot proof-of-concept data promisingly suggests that partial depletion of SRSF1 or expression of the SRSF1-m4 mutant lead to successful inhibition of DPR expression in the brain of 3-month old C9ORF72-ALS/FTD mice. Figure 5. 13 depicts the DPR levels in the cortex tissue of the brain at each of the 3 timepoints in the 5 treatment groups. The DPR levels in the non-transgenic mice are considerably lower than those seen in the four transgenic C9ORF72 ALS/FTD mice. At one-month post injection the DPR levels across the transgenic treatment groups appear similar. However, at 2 months and 3 months post treatment the data trend suggests that mice treated with scAAV9\_SRSF1-RNAi and scAAV9\_SRSF1-m4 have reduced DPR levels compared with transgenic untreated mice and scAAV9\_Ctrl-RNAi treated mice. To reassess these data and to reaffirm the data we have previously observed, the MSD assay was redone but this time comparing the brain samples against a Poly-GP antibody standard curve.

Figure 5. 14 shows the 2 month and 3-month poly-GP DPR levels post treatment against the standard curve. The trend remains the same as described above - the scAAV9\_SRSF1-RNAi and scAAV9\_SRSF1-m4 treated mice have reduced poly-GP DPR levels compared to the untreated and scAAV9\_Cntrl-RNAi treated mice at 2 months. At 3 months the reduced poly-GP DPR trend in scAAV9\_SRSF1-RNAi and scAAV9\_SRSF1-m4 treated mice becomes significant compared to the DPR levels in untreated transgenic mice. Overall, this reduction in poly-GP DPR level is very encouraging for progressing with SRSF1

manipulation gene therapy strategies. However, due to low n numbers, very few robust conclusions can be drawn from these data until the study can be completed with the planned n numbers.

## 5.6 Discussion

In this section the aim is to provide a full discussion of the results described in chapter 5 (Investigating the effects of the viral-mediated therapeutic SRSF1 manipulation *in vivo*). In Chapter 4, the successful packaging of scAAV\_SRSF1-RNAi, scAAV\_SRSF1-m4 and scAAV\_GFP (Production of Functional Large-Scale SRSF1-Targeting Gene Therapy Viruses for Subsequent Investigation in Mouse Studies) into scAAV9 adeno-associated viruses was described and discussed. The 4 viruses were then tested *in vivo*, in both a wild-type C57bl/6 mouse model and a C9ORF72 ALS/FTD BAC 500 mouse model (Liu *et al.*, 2016). The first *in vivo* study assessed the safety and efficacy of the SRSF1 manipulating viruses, scAAV9\_SRSF1-RNAi and scAAV9\_SRSF1-m4, using the C57bl/6 mouse model. Following this initial study, the effect of scAAV9\_SRSF1-RNAi and scAAV9\_SRSF1-m4 on DPR levels in a diseased mouse model was evaluated.

The four treatments (PBS, scAAV9\_GFP, scAAV9\_SRSF1-RNAi and scAAV9\_SRSF1-m4) were injected into the cisterna magna of postnatal day 1 mouse pups and, the weights, motor performance and general survival were tracked in both experimental groups (4 week and 6 month cohorts). Neither control group, PBS or scAAV9\_GFP, or either SRSF1 viruses produced any severe side effects that resulted in abnormal growth or development in the C57bl/6 mouse model. The lack of weight differences between the PBS group and the experimental groups suggests that the administration route had no significant impact on the mice. Due to the different experimental groups incorporating different ratios of males: females – this might have resulted in significant weight differences between groups, but this does not appear to have been the case. However, in future experiments only female mice will be used to avoid this potential issue (The Jackson Laboratory). The reason that a specific sex was not chosen for this study was that we were injecting post-natal day 1 and the sex is not immediately obvious without the use of a sexing PCR test. To ensure that we did not waste any animals or resources unnecessarily it was decided sex would not be inclusion criterion for the purposes of this study. However, when reviewing the results, there was an awareness that there may be sex-related differences between treatment groups, but the comparison between sexes was not an aim of this study.

Throughout the study, several mice suffered eye infections which has been prevalent in other studies with scAAV9 (Scarrott, 2019), but it is also a common ailment amongst C57bl/6 mice. Published studies suggest that ophthalmic abnormalities in C57bl/6 inbred mice vary from 4.4% (Chase, 1942) to 10% (Kalter, 1968). Mice that are affected by these ophthalmic

abnormalities often develop recurrent ocular infections, resulting from the small or absent eyes, with consequent poor tear and debris drainage, rather than being due to poor animal husbandry (Smith, Roderick and Sundberg, 1994). It is reasonable to conclude that the recurrent eye infections in these mice is likely unrelated to the cisterna magna injection or a result of the scAAV9 viral administration.

During the study one mouse treated with scAAV9\_SRSF1-m4 had neurological issues that were attributed to the intrathecal administration process potentially causing brain damage due to misplacement of the needle. The mouse had an unusual gait, with a reduced fear response in comparison to its cage mates. However, this may have been due to significant issues with its vision. The assumption is that the needle may have been misplaced and caused significant brain damage. It is unlikely that the scAAV9\_SRSF1-m4 treatment was the cause of these deficits, as over the course of several studies, 32 animals have been injected with scAAV9\_SRSF1-m4 with no similar side-effects. The potential to misplace the needle does highlight the issue with the invasive method of administration, although, in humans a stereotaxic setup and extensive imaging methods would be available to guide the treatments into the CSF successfully and also in humans intrathecal delivery can be undertaken via lumbar puncture rather than via the cisterna magna route.

Overall, survival rate of the mice in the study was as expected, with a 93.75% survival rate by 6 months, in comparison to the average of 90% survival rate at 18 months described by the National Institute of Aging strain survival information. The survival data therefore indicate that none of the treatments (PBS, scAAV9\_GFP, scAAV9\_SRSF1-RNAi or scAAV9\_SRSF1-m4) affect the overall survival of C57bl/6 mice. The rotarod data confirm that the treatments had no significant adverse effect on the motor function of the mice, suggesting that the virus distributed in the muscles did not contribute to any motor function deficits. scAAV9\_SRSF1-RNAi treated mice had a higher and more consistent rotarod score than any other group, suggesting that this treatment could increase motor function, but the data was not significantly different to the other treatment groups. Further research into motor function following SRSF1 manipulation will be required in the future but it would be a beneficial off-target effect if the reduction of SRSF1 could increase motor function in patients with ALS.

One of the key aims of the safety and efficacy study in C57bl/6 mice was to assess the biodistribution of the scAAV9 viruses. qPCR with primers targeting the eGFP DNA was used to observe the biodistribution of scAAV9\_GFP and scAAV9\_SRSF1-RNAi across 6 tissue types: brain, spinal cord, heart, liver, spleen and muscle. The scAAV9\_SRSF1-RNAi

biodistribution results show a dramatic increase in GFP DNA in the brain and spinal cord 4-weeks post injection, suggesting that the virus is able to enter and remain within the tissue of interest for at least 1 month. Unfortunately, there was a higher distribution of scAAV9\_SRSF1-RNAi in the heart than we had anticipated. SRSF1 is essential for the development of the heart during the embryonic stage, yet SRSF1 requirement is unclear in young animals but it is known that homozygous SRSF1 knockout mice do have embryonic lethal phenotypes due to SRSF1 regulated CaMKII $\delta$  alternative splicing in cardiac muscle (Xu, Yang, J. H. Ding, *et al.*, 2005; Lee *et al.*, 2016). Research from this study therefore suggests that although the SRSF1 reducing scAAV9 DNA is present within the heart, it does not impact on the overall survival of developing mice or produce any obvious cardiac related side-effects. On the whole, the scAAV9\_SRSF1-RNAi treatment is targeting the CNS. Off-target distribution of scAAV9 was found in the muscle but could be beneficial in motor neuron disease patients potentially helping to preserve the health of the neuromuscular junction.

The biodistribution analysis of scAAV9\_GFP showed a substantial increase in distribution in the CNS, but this was much lower than that observed in animals treated with scAAV9\_SRSF1-RNAi. The strong promoter CBh promoter driving the expression of eGFP could be causing toxic build-up of GFP in transduced cells resulting in cell death (Ansari *et al.*, 2016; Khabou *et al.*, 2018). The degradation and removal of the GFP positive cells would explain the lower GFP DNA present within the CNS. Although we cannot comment directly on whether GFP toxicity was a result of GFP protein accumulation or an anti-GFP immune response, the observation of potential toxicity raises concerns over the use of scAAV9 with eGFP to transduce the CNS. Promising developments in other fluorescent tracking methods suggest that new fluorescent proteins could be engineered to track vectors without causing toxicity (Gray *et al.*, 2011).

In the 4 week mouse brain western blot analysis, there is a high expression of the GFP protein in mice treated with scAAV9\_GFP in comparison to the mice treated with scAAV9\_SRSF1-RNAi. Low DNA level combined with a high protein expression level indicates that less scAAV9\_GFP is required to create higher levels of GFP protein expression. The CBh promoter is likely causing this scenario. It is a much stronger promoter than the H1 promoter in scAAV9\_SRSF1-RNAi and recent studies have indicated that GFP expression greatly depends on the promoter within the AAV (although this research did not directly compare H1 with CBh promoters) even with equal dosage (Damdindorj *et al.*, 2014; Nieuwenhuis *et al.*, 2021).

By 6-months post injection there was a much lower distribution across tissues of both scAAV9\_SRSF1-RNAi and scAAV9\_GFP viruses compared with at 4-weeks post injection. The high genome copies of GFP observed in the CNS in scAAV9\_SRSF1-RNAi treated mice was no longer evident suggesting that the virus had been lost. Initially it was suggested that dosage may be a contributing factor. It could be that the dosage of scAAV9 was too low to create a sustainable reduction in SRSF1 expression across the 6 month study. Previous AAV9 treatments in our lab had used an approximate dosage of  $5 - 9 \times 10^{12}$  vg/kg depending on the weight of the treated mouse at P40 (Scarrott, 2019). This is almost 5 times less than the dosage given to mice in this study at P1 however, the biodistribution of the viruses used in Scarrott 2019 was not assessed, but the AAV9 shRNA against SOD1 was still effective after 3 - 5 months. Armbruster *et al* 2016 used scAAV9 to correct SMN1 levels and found that the optimal dosage was  $3 \times 10^{13}$  vg/kg which is over 10 times more than the dosage that was used in the C57 safety study. Again, the biodistribution data from Armbruster *et al* 2016 was only reviewed at one time point of 3 months and so it is unknown whether the biodistribution had decreased between injection and sacrifice. Previous scAAV9 biodistribution studies have indicated that the biodistribution has reduced in particular tissues but the therapeutic effect of the virus is still apparent even in the presence of this reduction (Bobo *et al.*, 2020). Bobo *et al* used an scAAV9 virus to treat mucopolysaccharidosis (MPS) IIIA, a devastating lysosomal storage disease (LSD) resulting in severe neuronopathy. MPS IIIA is caused by autosomal recessive mutations in N-sulfoglucosamine sulfohydrolase (SGSH), a lysosomal enzyme that is essential for the degradation of a class of biologically important glycosaminoglycans (GAGs). The group used an scAAV9 virus to replace the SGSH gene. Unlike our study, they used IV as their method of administration at multiple dosages, but in keeping with this safety study they assessed the biodistribution at several time points (2 months, 8 months and at the endpoint of the study). It was concluded that mice treated with  $2.5 \times 10^{12}$  vg/kg had a maintained biodistribution in the brain yet showed a reduced distribution over time in the liver, spleen, kidney and lung. In contrast, mice treated with a 2 times higher dosage  $5 \times 10^{12}$  vg/kg had an increasing distribution over time in the brain, kidney, heart and muscle. Although the administration varied, the results indicate that dosage plays a key role in how scAAV9 distributes itself across tissue over time. Although these results provide evidence that the biodistribution of scAAV9 can reduce over time, it still gives us no indication on the optimum cisterna magna dosage to maintain biodistribution in the long-term. The mechanism by which scAAV9 is removed from tissue has yet to be elucidated, with further research required.

From the biodistribution data, increased GFP DNA was observed in PBS treated animals at 6-months post injection, which was an unexpected finding. Contamination of samples via the surgical equipment was the first potential explanation, however the same method was used at 4-weeks and 6-months post cisterna magna injection and therefore GFP would have been expected at similar levels in the 4 week distribution, this was not the case. Contamination during the qPCR experimental stage and/or during protein extraction was also considered as a potential cause but the samples were rerun using UV to sterilise qPCR plates and pipettes between treatment groups with little effect on the GFP genome copies. AAV shedding was considered to be the most likely scenario. To ensure that litter variation was taken into account in this study, at least one mouse from each litter was given each treatment depending on litter size. However, this also meant that mice with different treatments were housed together. Even after weaning age, the mice remained in same sex cages with mice from different treatment groups. In hindsight splitting the mice into one treatment per cage would have avoided any shedding issues after 3 weeks of age. Had scAAV9 shedding been an issue within the first 4-weeks it would be expected to be observed in the 4-week distribution data. However, very little GFP DNA signal was found in the control group of mice.

Previous studies have researched shedding of AAV in sheep models, but the shedding was dose dependent and was only evident within the first 48 to 72 hours in the urine and faeces. Functional vector shedding was more prevalent in the faeces than other excreta of treated animals (Farraha *et al.*, 2019). Other studies of AAV shedding in mouse models have suggested that the functional vector shedding of AAV is present in urine up to day 37 and in faeces up to day 14 (Ferla *et al.*, 2017). However, these studies used AAV2/8 as their therapeutic virus. Had scAAV9\_SRSF1-RNAi or scAAV9\_GFP been excreted via urine, faeces or saliva and there had been functional vectors remaining in these excreta, this could have been ingested by other mice in the cage resulting in GFP DNA entering PBS treated animals. Two of the treatments, scAAV9\_GFP and scAAV9\_SRSF1-RNAi, expressed GFP, but this study only tested the comparison between PBS treated and GFP treated mice. Had there been more time, the hypothesis of AAV shedding could have been investigated by testing scAAV9\_SRSF1-m4 treated tissue for GFP DNA. If there had been AAV shedding it is unlikely to be of functional vectors as the western blot results do not indicate any GFP expression in tissue of any of the 6-month cohort PBS treated mice. Unfortunately, there is very little research about AAV shedding, especially for timepoints more than one week post treatment. Had the C9ORF72 mouse study gone ahead as planned, the collection of urine

and faeces from each mouse was considered to confirm whether AAV shedding was the culprit for the detection of GFP DNA in the PBS mice.

When assessing the biodistribution of scAAV's in the same study, the same qPCR primers should be used to be able to directly compare the biodistribution of each treatment. As discussed in chapter 4, finding qPCR primers that would specifically target the scAAV's DNA was more difficult than anticipated. Previously, it has been revealed that quantitative PCR (qPCR) can underestimate AAV titre due to inverted terminal repeats (ITR) that exist in all AAV vectors. ITRs are the only remaining element from the wild genome that form high structural conformations which interfere with qPCR titration (Fagone *et al.*, 2012). To titre scAAV there are a number of targets within the scAAV sequence of the vector that can be utilised depending on the design of the vector e.g. the eGFP, Poly-A site or the promoter/CMV enhancer regions. It would have been advantageous if there had been the same target available in each of the three vectors used to produce the viruses, but this was not the case. This resulted in eGFP primers being used for the biodistribution of scAAV9\_SRSF1-RNAi and scAAV9\_GFP whilst primers against SRSF1 were used against scAAV9\_SRSF1-m4. CMV and Poly A primers were designed for scAAV9\_SRSF1-m4. However, several sets of primers designed to bind to these targets were nonspecific and unsuccessful. Primers designed against the promoter were not desirable as the CBh promoter was too GC rich. DNA templates with high GC content can reduce the efficiency of PCR due to the tendency of these templates to fold into complex secondary structures. This occurs due to increased hydrogen bonding between guanine and cytosine bases, which can cause the DNA to be resistant to melting in the PCR process. The biodistribution of scAAV9\_SRSF1-m4 therefore had to be calculated by assuming that the SRSF1 DNA levels of PBS mice was the baseline and any increase in SRSF1 DNA observed in scAAV9\_SRSF1-m4 treated mice was due to the presence of the virus in tissue. Although this method of biodistribution was effective, in the future it would be advisable to design plasmids, including control treatments, to have the same primer targets to ensure that the biodistribution can be directly compared across treatments.

The biodistribution of the scAAV9\_SRSF1-m4 was observed across 6 tissue types: brain, spinal cord, heart, liver, spleen and muscle. As previously stated, primers targeting SRSF1 DNA were used. As previously observed in the biodistribution of scAAV9\_SRSF1-RNAi, there was a significant increase in SRSF1 DNA levels in the CNS of mice treated with scAAV9\_SRSF1-m4, which was expected. The assumption is that the increase in SRSF1 DNA levels is attributed to the inserted SRSF1-m4 virus. Results from this biodistribution

study indicate that scAAV9\_SRSF1-m4 has very few off-target distributions except in the heart where an increase was present, but at a level not considered significant. The advantage of using SRSF1 primers was that endogenous SRSF1 DNA levels in PBS treated mice could be observed and compared at both 4-weeks and at 6-months. SRSF1 DNA levels appear stable and constant across tissue at 4-weeks. However, at 6-months levels appear to drop in the brain, spinal cord, heart and liver, whereas levels in the spleen and muscle remain unchanged. Combining the SRSF1 DNA level data with the SRSF1 protein expression data from the western blot analysis will give a clearer picture regarding SRSF1 levels in mouse tissue at different ages. There has been very little research that compares SRSF1 expression and DNA levels across healthy mouse tissue. Wagner *et al* 2019 did review SRSF1 expression using DAB immunohistochemistry staining in healthy mouse tissue, but levels of SRSF1 were not analysed using other methods.

The biodistribution data in the wild type mice have raised a number of further research questions. Why and how is the virus being removed from the mouse tissue? In future experiments it would be beneficial to have additional timepoints between 4-weeks and 6-months to review whether the virus is lost gradually across months. Answering this particular question will lead to an understanding of how to keep the scAAV9 treatments within the CNS for a more beneficial time period. Age may change the outcome of distribution studies. For example, injecting via the cisterna magna at different ages would be an interesting topic of future research. Although, injecting at P1 is beneficial it does not mimic human disease. It is unlikely that C9ORF72 ALS/FTD would be diagnosed at birth without a stringent screening process and so in humans the earliest administration of treatment would be middle age which is not reflected in our current P1 treatment *in vivo* model.

Western blot analysis was undertaken from freshly prepared protein extracts. However, the protein extracts tend to degrade quickly, even following the use of a protease inhibitor cocktail in an attempt to protect the samples. Therefore, the quality of the samples rapidly declined meaning that the first run via SDS-PAGE was the best western blot image. When trying to repeat the western blot for clearer images or to check a result, the degradation of the samples was immediately evident. Images in Figure 5. 3 (2A) depicting tubulin expression in the heart tissue 4-weeks post injection, show an unexpected reduced expression of tubulin in scAAV9\_SRSF1-RNAi mouse #1, 4-weeks post injection. Further reruns of the western blot were completed, but with each new repeat the expression of tubulin became unstable as the proteins degraded over time.

Western blot analysis has shown SRSF1 depletion is evident at 4-weeks post injection, indicating that scAAV9\_SRSF1-RNAi successfully reduces the expression of SRSF1 *in vivo* in the brain. This supports our aim to assess the ability of scAAV9\_SRSF1-RNAi to mediate short-term transgene expression in the central nervous system (CNS) of wild type mice after injection via the cisterna magna. Although the expression of SRSF1 was not quantified, visually it was clear that the reduction is not 100% as the band is still present. The study indicates that the partial reduction of SRSF1 in the brain does not cause a reduction in survival after 4-weeks. This is advantageous because we do not want to completely knockdown SRSF1 as this has been shown to be lethal in knock-out mice, yet the total knockdown of SRSF1 in adult mice has yet to be studied.

However, there is no evidence that reduced SRSF1 expression is maintained in the brains of scAAV9\_SRSF1-RNAi treated mice at 6-months post injection. Therefore, it cannot be confirmed whether the treatment can mediate long-term transgene expression. Combined with the 6 month biodistribution data this suggests that the loss of virus results in a return to normal levels of SRSF1 expression in the brain.

Due to the amount of tissue available there was not a sufficient amount of spinal cord protein available for western blot analysis and so comparison of DNA levels vs protein expression was not available for this tissue type.

Across other tissue types at 4-weeks SRSF1 expression appears consistent across tissue and treatment groups apart from the muscle tissue where expression levels appear variable and unstable. The control protein, tubulin, was also considerably variable in expression suggesting that tubulin is not expressed consistently in this tissue type. Previous studies (Lewis, Lee and Cowan, 1985; Jee et al, 2009) have shown that  $\alpha$ -tubulin expression is low in muscle tissue and in hindsight  $\alpha$ -tubulin should not have been used as the loading control protein. The SDS-PAGE was also conducted using a GAPDH antibody as the control which is expressed consistently in muscle tissue, but this would not allow us to compare between tissue types. Unfortunately, due to alpha tubulin expression levels in the muscle tissue this study is limited as SRSF1 expression cannot be compared to tubulin expression in muscle tissue. Therefore, no conclusions can be drawn as to whether SRSF1 expression has been reduced in the muscles of scAAV9\_SRSF1-RNAi treated mice. In fact, very few conclusions about SRSF1 expression can be drawn since tubulin appears to be inconsistent in muscle tissue, therefore, SRSF1 expression cannot be deduced in the absence of a robust normalisation method. Across other tissue types at 4-weeks SRSF1 expression appears consistent across tissue and treatment groups apart from the muscle tissue where expression

levels appear variable and unstable. The control protein, tubulin, was also considerably variable in expression suggesting that tubulin is not expressed consistently in this tissue type. Previous studies (Lewis, Lee and Cowan, 1985; Jee *et al.*, 2009) have shown that  $\alpha$ -tubulin expression is low in muscle tissue and in hindsight  $\alpha$ -tubulin should not have been used as the loading control protein. The SDS-PAGE was also conducted using a GAPDH antibody as the control which is expressed consistently in muscle tissue but this would not allow us to compare between tissue types. Unfortunately, due to alpha tubulin expression levels in the muscle tissue this study is limited as SRSF1 expression cannot be compared to tubulin expression in muscle tissue. Therefore, no conclusions can be drawn as to whether SRSF1 expression has been reduced in the muscles of scAAV9\_SRSF1-RNAi treated mice. In fact, very few conclusions about SRSF1 expression can be drawn since tubulin appears to be inconsistent in muscle tissue, therefore, SRSF1 expression cannot be deduced in the absence of a robust normalisation method.

At 6-months, in all mice, SRSF1 expression is variable across tissue types. In all tissue types there is an observable reduction of SRSF1 expression at 6-months in comparison to mice at 4-weeks post injection. This could provide further evidence that SRSF1 plays a greater role in early development especially in the muscle and heart tissue, where the difference between time-points is most obvious. Previous research has confirmed that nuclear SRSF1 is essential for normal embryonic development (Lin *et al.*, 2005; Xu *et al.*, 2005; Haward *et al.*, 2021). It could be speculated that once past the initial embryonic development, that SRSF1 expression is reduced due to reduced requirement, but further research is required to confirm this hypothesis.

SRSF1 expression in the liver between the two time points appears to have consistent expression across the four treatments suggesting an abundance of SRSF1 in liver tissue at both ages. Waqar Arif's thesis reviewed the role of SRSF1 in liver physiology by using both a knockout mouse model, designed to knock down only SRSF1 in the liver, and by knocking down SRSF1 in the liver with an AAV mRNA with a hepatocyte specific promoter. The AAV8 against SRSF1 was injected via the tail vein into 8 weeks old mice and tissue was harvested at 2- and 4- weeks post injection. The results indicated that 2 weeks post AAV injection showed the greatest reduction in SRSF1 but by 4-weeks the liver had started to regenerate itself and produce hepatocytes capable of generating SRSF1, confirmed using immunofluorescent staining. It could be hypothesized that any knockdown of SRSF1 that may have occurred following scAAV9\_SRSF1-RNAi injection would have been masked by the regeneration of the liver of hepatocytes able to express normal levels of SRSF1 (Arif,

2020). To confirm that this was the case, harvesting tissue at a closer time-point, before 2 weeks post injection, would likely give us a clearer answer. This research could also explain why SRSF1-m4 may not be expressed in the liver. If the liver cells are rapidly regenerating in response to the scAAV9\_SRSF1-m4 virus, any hepatocytes expressing the SRSF1-m4 protein will be in the minority. Without staining the liver tissue, it is difficult to assess the distribution of the virus across the whole organ. Equally the biodistribution data suggest that there is very little distribution of scAAV9\_SRSF1-RNAi in the liver and so it is likely that any knock-down within the tissue would be minimal.

The western blot analysis on the C57bl/6 mouse tissue has shown that SRSF1-m4 is expressed in the brain cortex tissue 4-weeks post injection, again supporting our aim to assess the ability of scAAV9\_SRSF1-m4 to mediate short-term transgene expression in the central nervous system (CNS) of wild type mice after injection via the cisterna magna. But again, there is little evidence to suggest that scAAV9\_SRSF1-m4 is mediating long-term transgene expression. 2 of 3 the scAAV9\_SRSF1-m4 treated mice do not express the SRSF1-m4 protein 6-months post injection. The mouse that has a band to indicate SRSF1-m4 expression was sacrificed one month early due to repeated eye infections which were affecting its welfare. This mouse was only 5 months old rather than 6-months old, but this gives a rough estimate as to when transgene expression may cease following cisterna magna injection. Further experiments, with several more time points between 4-weeks and 6-months would be beneficial to review when m4 expression declines. The administration efficiency could also be an issue. It could be that only one of the 3 injections was successfully administered, resulting in scAAV9\_SRSF1-m4 #1 and #2 having reduced m4 expression. FLAG expression was much lower in mouse #1 and #2 in the brain, heart and liver in comparison to mouse #3. However there appears to be a similar expression in all 3 mice in the muscle tissue suggesting the biodistribution could be slightly different between the mice. Had the injection not successfully entered the cisterna magna this could account for these differences. It could be that a second dosage would be beneficial but further research would be required to address the question.

The study has confirmed that both scAAV9\_SRSF1-RNAi (GFP) and scAAV9\_SRSF1-m4 (FLAG-tagged) are able to successfully transduce the brain enabling cells to express the GFP and FLAG genes. scAAV9\_SRSF1-RNAi does not show GFP expression at 4-weeks post injection in any tissue except brain cortex tissue which could indicate that the virus has not transduced the cells of other tissue types even if DNA is present (Figure 5. 2). This is a positive outcome as it would be advantageous for the treatment to only remain within the

CNS and would prevent any potential off-target effects in non-CNS tissues. The weaker H1 promoter could be the cause of reduced GFP expression in tissue. It is already known from Chapter 3 “Designing and developing viral vectors for SRSF1-targeted gene therapy approaches in mice” that the treatment of scAAV9\_SRSF1-RNAi in cells results in lower GFP expression than the treatment of scAAV9\_GFP, we would also expect this to be the case *in vivo*.

In scAAV9\_SRSF1-RNAi treated mice, at 6-months there is still GFP expression in the brain cortex. Although the GFP expression is still evident, reduced SRSF1 expression is no longer present 6-months post injection in mice treated with scAAV9\_SRSF1-RNAi. This suggests that cells that were transduced at the beginning of the study are still expressing GFP but that the transduced cells no longer have lower levels of SRSF1, this is in keeping with the biodistribution data which show that by 6-months the virus is no longer detectable.

The control scAAV9\_GFP virus expresses GFP at both time points in the brain, heart and liver tissue. This suggests that the distribution of AAV9 with a CBH promoter does reach these three tissue types, which is supported by the fact that FLAG is expressed at a similar level in each tissue. It is interesting that FLAG is expressed well in the muscle tissue however GFP is not indicating that scAAV9\_SRSF1-m4 is able to transduce the muscle well but scAAV9\_GFP is not. The only difference between these two viruses is the transgene, indicating either SRSF1-m4 is responsible for this effect or there is GFP toxicity in the muscle tissue. However, had it been due to GFP toxicity in muscle we might have expected a detrimental effect on the motor function of the mice which was not detected.

In the biodistribution data there is a low level of scAAV9\_GFP DNA across the tissue types. However, the reverse effect is observed in the western blot analysis, with high expression of the GFP protein in the tissue. It is anticipated that the strong CBh promoter is responsible for this effect. Less GFP DNA is required to produce a high expression of protein when a stronger promoter is driving expression (Gerdes, Castro and Löwenstein, 2000).

An interesting observation was the fact that none of the three viruses successfully transduced the spleen. Very low levels of viral DNA are present in the biodistribution data at both timepoints and there is no evidence of the expression of GFP or FLAG in the western blot data. There was also no evidence of SRSF1 expression in the spleen at 6-months which was unexpected. SRSF1 is known to be expressed in blood cells. However, having perfused the spleen and removing the majority of the blood it is unknown whether the structural cells of the spleen express SRSF1. There are minimal data on SRSF1 expression in the spleen, especially data using a perfused spleen. The human protein atlas suggests that there is strong

SRSF1 expression in the human spleen. However, it is unknown whether this tissue was perfused or not before processing for histology and so without this confirmation no conclusions can be drawn.

Previous research conducted by the lab assessed the effect of SRSF1 depletion on patient derived neurons to investigate their survival. These experiments compared the SRSF1 expression of control and *C9ORF72* ALS/FTD patient neurons, confirming that SRSF1 expression is present and variable in human neurons depending on pathology (Hautbergue *et al.*, 2017). Nissl staining of the spinal cord confirmed that none of the four treatments (PBS, scAAV9\_GFP, scAAV9\_SRSF1-RNAi or scAAV9\_SRSF1-m4) impact motor cell count in the cervical spinal cord. There is no observable difference between the histopathology images or in the quantification data. As C57bl/6 mice are healthy with no motor neuron disease, a difference between the four treatment groups was not expected. In a mouse model of motor neuron disease, we would expect reduced or damaged motor neurons within the spinal cord. The treatments had not been designed to increase the number of motor neurons but merely to protect motor neurons that were already present. Overall, the results suggest that the therapeutic viruses do not cause adverse effects, affect the number of motor neurons or cause neurodegeneration following administration. It also confirms that at 4-weeks the reduction of SRSF1 or the expression of SRSF1-m4 in the brain does not interfere with motor neuron survival.

Unfortunately, due to COVID-19 there were certain limitations in assessing SRSF1 expression in the brain via histopathology. Due to COVID-19 restrictions, there was not enough time to quantify the SRSF1 staining in the spinal cord. The observable differences in SRSF1 expression between the treatment groups was instead reviewed following immunostaining. Visually there appears to be a reduction in SRSF1 staining at 4-weeks in mice treated with scAAV9\_SRSF1-RNAi. However, we are unable to confirm this finding without staining quantification. The SRSF1 staining indicates that by 6-months post cisterna magna injection there were no visual differences between the treatment groups. The staining confirmed that SRSF1 is expressed within the nucleus of motor neurons. Ideally, spinal cord tissue could have been used to conduct a western blot to confirm the histopathological outcome, however, the spinal cord does not provide enough protein to load 40 mg into 2 western cassettes which was the reason a western analysis was not carried out on the spinal cord tissue.

Following the safety and efficacy study using C57bl/6 mice the scAAV9\_SRSF1-RNAi and scAAV9\_SRSF1-m4 was tested in a *C9ORF72*-ALS/FTD mouse model (Liu *et al.*, 2016)

have been reported designed to produce the toxic dipeptide repeat proteins. In this particular study only female mice were used as Liu *et al.*, 2016 suggested that females had more robust disease phenotype. The aim of the study was to assess the effect of the SRSF1 manipulating viruses on DPR levels in the *C9ORF72*-ALS/FTD mouse model. An exciting new development from Adrian Isaacs laboratory found that DPR level can be assessed using an MSD assay with an anti-Poly-GP antibody to review the levels of the Poly-GP DPR in half a mouse brain cortex (Quaegbeur *et al.*, 2020). As time was limited for this final *C9ORF72* ALS/FTD mouse model, this new method of measuring DPR level was more effective and less time consuming than traditional western blot analysis. The study was limited by its low n numbers and as such we are unable to confirm whether our hypothesis of whether our 2 SRSF1 manipulating gene therapies reduce DPR levels. The trend of the collected data suggests that there is an observable reduction. It is disappointing that after all the hard work over the last four years we are still not able to report the solid confirmation that these therapeutic strategies effectively reduce DPR levels in a mouse model of *C9ORF72*-ALS/FTD. Although the treatments show a trend towards reducing DPRs in the C500 mouse brain, the effect that each of the treatments has on SRSF1 or SRSF1-m4 expression has not been investigated in this mouse model due to time constraints. We therefore cannot at this stage confirm whether the reduction in DPR expression is caused by the manipulation of SRSF1 and therefore further research is necessary to confirm the overall hypothesis of this project. The results thus far indicate a trend for Poly-GP DPR level reduction in the cortex, at least 3 months post scAAV9\_SRSF1-RNAi or scAAV9\_SRSF1-m4 cisterna magna injection. The untreated transgenic mouse data from this study also establishes the DPR levels of this mouse model between the ages 1 and 3 months, which indicates an increasing trend over time. These data give us a greater understanding as to when DPR levels may peak which will allow for the calculation of the most effective time-point to manipulate SRSF1 for the most effective treatment approach. Despite the challenges, this pilot proof-of-concept data promisingly suggests that partial depletion of SRSF1 or expression of the SRSF1-m4 mutant lead to successful inhibition of DPR expression in the brain of 3-month old *C9ORF72*-ALS/FTD mice (Figure 5. 13).

The current *C9ORF72* ALS/FTD mouse model from Jackson Laboratories is only effective to observe the DPR levels of the disease model. The behavioural phenotype suggested by Ranum (Liu *et al.*, 2016) appeared to be unreliable once the model had been replicated in Jackson FVB-BAC mice (Mordes *et al.*, 2020; JAX stock #029099). Further research will include using *C9ORF72* ALS/FTD mice with a known behavioural phenotype of *C9ORF72* ALS/FTD (Nguyen *et al.*, 2020) for which the colony is currently being expanded at The

University of Sheffield, using FBV mice from Janvier rather than JAX, as in the Ranum and Saxena labs. The study will include greater n numbers and a variety of behavioural tests (including marble burying, reverse rotarod and open field) that have not shown disease-related phenotypes in the current Jackson C9 BAC 500 colony. It would also be beneficial to optimise the MSD assay to assess DPR levels in living mice, for example using peripheral blood or CSF. This could allow for constant DPR level tracking throughout a study without the requirement of sacrificing the mouse to harvest CNS tissue. Unfortunately, harvesting the CSF from a mouse is a difficult procedure which may not result in a usable amount of CSF 100% of the time which would be necessary during a study. Currently, harvesting mouse CSF still requires the death of the animal. DPR levels can be measured in human CSF samples (Lehmer *et al.*, 2017) which will provide a pharmacodynamic biomarker in human genetic therapy trials for C9-ALS.

The first aim of this chapter was to assess biodistribution and the ability of scAAV9\_GFP, scAAV9\_SRSF1-RNAi and scAAV9\_SRSF1-m4 to mediate short and long-term transgene expression and stability in the CNS of wild-type C57bl/6 mice after cisterna magna injection. Several key findings have been made. The results of this study give an overall understanding of the biodistribution of these viruses 4-weeks and 6-months post cisterna magna injection. There is DNA evidence that scAAV9\_SRSF1-RNAi and scAAV9\_SRSF1-m4 remain in the CNS in the short-term (at least 4-weeks post injection) but their distribution in the CNS reduces to baseline levels by 6-months, suggesting that increased dosage or further virus development will be required for successful long-term transgene stability. Western blot analysis has confirmed that scAAV9\_SRSF1-RNAi is able to deplete SRSF1 in the brain of a C57bl/6 mouse model 4-weeks post injection, and that scAAV9\_SRSF1-m4 is able to express SRSF1-m4 4-weeks post injection in the brain of a C57bl/6 mouse model. These findings suggest that the 2 SRSF1 manipulating viruses can mediate short-term transgene expression successfully. Histology data indicate that from a visual perspective there could also be reduced SRSF1 expression in the spinal cords of scAAV9\_SRSF1-RNAi treated mice at 4-weeks post cisterna magna injection in comparison to the other 3 treatment groups. To confirm this finding quantification of SRSF1 staining will be required in the future.

Long-term transgene expression has not been confirmed via this study as there was no evidence of SRSF1 depletion in scAAV9\_SRSF1-RNAi treated mice at 6-months and only 1 scAAV9\_SRSF1-m4 treated mouse was able to express SRSF1-m4 6-months post injection. Also, at 6-months, SRSF1 expression is more variable across tissues at 6-months compared

to 4-weeks suggesting that SRSF1 expression levels fluctuate during different periods of development.

Most importantly the experiments discussed in this chapter indicate that there were no significant off-target effects resulting in reduced survival or severe motor impairments. Neither scAAV9\_SRSF1-RNAi or scAAV9\_SRSF1-m4 administration result in weight loss, weight gain or have any major effect on weight maintenance. The novel gene therapies have neither a positive nor negative toxic effect on motor neuron cell counts.

The next aim, and overall aim, of the entire project was to assess whether the therapeutic viruses were able to reduce DPR levels in a mouse model that expresses *C9ORF72* sense transcripts and upregulated antisense transcripts and produces DPRs. The initial MDS assay results from this study indicate that both scAAV9\_SRSF1-RNAi and scAAV9\_SRSF1-m4 can reduce DPR levels in a diseased mouse model, which supports the original hypothesis. Although these are promising data, low n numbers mean that future work is required before confirming that these therapeutic strategies do in fact robustly reduce DPR levels in a *C9ORF72* mammalian disease model.

Polymorphic hexanucleotide expansions of over 30 repeats in the *C9ORF72* gene are the most commonly known genetic cause of amyotrophic lateral sclerosis (ALS) and frontotemporal dementia (FTD), linking these two disorders at each ends of a spectrum. ALS is an adult onset disease characterised by selective death of motor neurons, leading to progressive paralysis and eventually death within approximately 2-3 years. Pathological *C9ORF72* repeat expansions are also often associated with frontotemporal dementia, which is a brain disorder caused by the degeneration of the frontal and/or temporal lobes of the brain and leading to altered cognitive and personality features. Recent studies have identified the mechanism which selectively drives the nuclear export of the pathological *C9ORF72* repeat transcripts, resulting in the production and build-up of toxic dipeptide repeat proteins within the cytoplasm.

As of yet, there are no specific treatments that are able target and treat *C9ORF72*-ALS/FTD and other forms of ALS/FTD. There are 2 licensed drugs available that manage or minimally slow ALS symptoms; the standard of care being Riluzole (Bensimon, Lacomblez and Meininger, 1994) and Edaravone (Berry *et al.*, 2021). The overall goal for ALS research as a whole is to develop an effective treatment or cure to increase survival time and prevent the fatality of the disease. The focus of the present study is to manipulate the nuclear export factor SRSF1, which has been reported to reduce neurotoxicity in *in vivo* models of *C9ORF72*-ALS/FTD. Partial depletion of the nuclear export factor SRSF1 or the expression of an engineered protein, SRSF1-m4, which specifically blocks the nuclear export of repeat transcripts (a point mutant of SRSF1 which does not interact with the nuclear export machinery but retains the ability to bind pathological repeat transcripts) was shown to prevent neurodegeneration and rescue locomotor deficits *in vivo* in *C9ORF72*-ALS *Drosophila*. This intervention also promotes the survival of motor neurons in a patient-derived co-culture system (Hautbergue *et al.*, 2017).

At the start of the project, two hypotheses were formulated. Firstly, it was hypothesised that partial depletion of SRSF1 within a mouse brain would lead to the reduction and sequestration of SRSF1 onto the sense and antisense pathological *C9ORF72* repeat transcripts. This would therefore inhibit the interaction of the transcripts with the nuclear export machinery of the cell, resulting in decreased dipeptide repeat protein (DPR) production in the cytoplasm, decreased protein aggregation and consequently decreased neurotoxicity. The second hypothesis speculated that the expression of the mutant SRSF1

m4 protein, which had been designed to interact with *C9ORF72* repeat expansions but lacks the ability to interact with the export machinery of the cell. This would prevent the RNA export of the toxic repeat transcripts out of the cell and also prevent the formation of DPRs in the cytoplasm of the cell; again, this would result in decreased DPR aggregation and overall neurotoxicity. This project expands on previous work (Hautbergue et al, 2017; Castelli et al, 2021) by evaluating the safety and efficacy of SRSF1 depletion and SRSF1-m4 expression therapeutic vectors in *in vivo* mouse models.

The results obtained indicate that both therapeutic vectors may be effective in reducing DPR production in both *in vitro* and in a *C9ORF72*-ALS/FTD mouse model. The *in vitro* results of this study provide evidence that partial scAAV-mediated depletion of SRSF1 and expression of SRSF1-m4 expression does result in a reduction in DPR production in both human HEK cell and mouse N2A cell models, indicating that the engineered plasmids and the newly designed SRSF1-shRNA are functional. This was expected as scAAV9\_SRSF1-RNAi was engineered to: (i) target mouse, rat, non-human primate and human SRSF1 to prevent the need to change the shRNA cassette along the translational path to clinical trial, and (ii) to limit genome-wide off target effects by using an off-target predicting software, siPOTR, in the design period.

As the study progressed on its translational path into a wild type C57Bl/6 mouse model, the evidence indicated that partial SRSF1 depletion does occur and SRSF1-m4 is expressed at 1 month post-injection of the corresponding AAV9. It is important to consider that this mouse model was not a *C9ORF72*-ALS/FTD disease model and so does not naturally produce neurotoxic DPRs. A wild type mouse model was used first to comply with the 3R design of this project to ensure as little suffering as possible occurred. The study shows that the delivery of AAV9-mediated SRSF1 manipulation via cisterna magna injection results in no obvious off-target behavioural or biological effects stemming from the use of RNAi against SRSF1 or the expression of SRSF1-m4. This provides confidence that, at the dosages used, these vectors can be deemed safe. Once it was evident that the strategies caused no severe life limiting effects in wild type mice with no disease phenotype, we were able to move on and test the treatments in a *C9ORF72* mouse model. Further clarification as to whether these treatments affect DPR production was required, and to do this a mouse model that produces DPRs was required and in this case we used *C9ORF72*-ALS/FTD Ranum mice (Liu *et al*, 2016; Nguyen *et al.*, 2020). During this study, only female C9-500 mice were used, as male mice with the *C9ORF72* expansions do not show decreased survival compared to non-transgenic males following 1 year. However, a large proportion of male mice do develop

disease phenotypes, like those found in slow progressive female mice by 1 year of age, although this has no effect on their survival compared to non-transgenic male mice. The effects of scAAV9-SRSF1-shRNA and SRSF1-m4 on the DPR expression levels were quantified. However, unfortunately, due to the Covid-19 pandemic, the longer subsequent *in vivo* behavioural study in this mouse model could not be conducted. Evidence suggests that SRSF1 manipulation is able to significantly reduce DPR production 3 months after virus administration in a limited number of *C9ORF72*-ALS/FTD mice. Due to time constraints imposed by Covid, SRSF1 expression levels could not be rigorously confirmed.

The results of this study show that a CSF delivery route is effective at targeting the CNS and remaining within it for at least 1 month post-injection. CSF delivery is easily translatable to human clinical trials with the use of intrathecal injection. This route of administration was chosen based on previous studies undertaken within our department, and their collaborators, to develop an AAV gene therapy-based treatment for SOD1 ALS. It was found that a dosage of  $5 \times 10^{10}$  vg/g was effective to reduce the expression of SOD1 by 27 % and 32 % in the brainstem and cerebellum respectively, and prolonged survival by up to 42% in a SOD1 mouse model. This SRSF1 manipulation project used a similar strategy to that of (Scarrott, 2019). In which an RNAi against the SOD1 protein was designed and inserted into an AAV virus and tested *in vivo*. This strategy had been shown to be very successful which is why it was used as a basis for this study.

Cisterna magna injection of an scAAV9 expressing a SOD1-shRNA was previously used as the route of administration and was tolerated well in both P1 and P40 mice, with no serious adverse effects (Iannitti *et al.*, 2018). This research into SRSF1 manipulation has further shown that this route of administration is well tolerated in mice at P1. It has confirmed that depletion of SRSF1 by up to 70% and the expression of SRSF1-m4 is well tolerated in mice at P1. However, in further work, it would be advisable to review the outcome when the treatments are administered at different age groups. In humans, *C9ORF72*-ALS/FTD is usually diagnosed later in life and it would be beneficial for *in vivo* studies to reflect that time point. The expression of a foreign/human protein (human-SRSF1) in a mouse model had not been previously undertaken in adult mice. Therefore 3 mice were injected with scAAV9\_SRSF1-m4 at P40. Unfortunately, the adult mice reacted badly to the virus and had to be culled <7days following administration. Due to the nature of the severe effects observed not all the mouse tissue could be collected and analysed. However, we predict that these fatal side effects were due to an immune response in adult mice to the human-SRSF1 protein. To confirm this prediction further analysis would be required but due to the 3Rs *in*

*in vivo* study design framework, it was judged unethical due to unnecessary suffering of the animals to repeat the experiment at the P40 time-point.

SRSF1-m4 protein expression could only be detected at 4 weeks post injection and was no longer expressed at 6 months, suggesting that scAAV9 SRSF1-m4 had been degraded and/or diluted within the organs. Previous research has indicated that following newborn administration of AAV, there is a high transduction rate within the first 4 weeks. However, as rapid growth of the animal occurs, organs and blood vessels increase in size, which results in dilution of the vector due to increased proliferation of cells. A number of studies have suggested that delaying administration could prevent dilution of successfully transduced cells and result in a more stable long-term gene expression (Cunningham *et al.*, 2008; Wang *et al.*, 2012). These studies were undertaken in the liver, but this research indicates that this could also be the case when reviewing transduction in the brain. Further research into this area will be required to confirm whether this is the case.

This project has succeeded in a number of areas. Firstly, the premise of SRSF1 manipulation is promising, since the results did not suggest that SRSF1 was not therapeutic or unsafe. Indeed, the fact that healthy mice can have both therapeutic vectors administered with no adverse effect upon survival or quality of life suggests that if this treatment were administered to a healthy subject, it would not result in an adverse effect. These experiments have also proven that SRSF1 manipulation can be tolerated *in vivo*. This knowledge could be utilised in combating other SRSF1-dependent diseases, perhaps even using modalities such as small molecule drugs, peptides and other gene therapy vectors. Secondly, making viruses in-house allowed us to make changes to plasmids and modify them with a reduced cost, but it was difficult to ensure that the viruses had the same titre without processing through a GMP facility. Furthermore, the study has provided evidence that both of these treatments are able to target both DPR production and the target tissues *i.e.* the CNS.

However, the project also has limitations. For example, it does not consider how different manufacturing methods could change the outcome, depending on purity and/or concentration of the virus. At no point during this study were the empty capsid ratios of the scAAV9 treatments analysed. Therefore, it is unclear how pure the viruses were. Had there been a large ratio of empty capsid to functional virus, this could have dramatically affected the overall transduction efficiency of the scAAV9 treatments. Results from this study suggest that the virus only appears to be active and present for 1 month post-injection, therefore an increase in dosage may be required for a longer term effect. In the C57bl/6 *in vivo* study

(Chapter 4 - Production of Functional Large-Scale SRSF1-Targeting Gene Therapy Viruses for Subsequent Investigation in Mouse Studies) there were only two time points and so it is unclear at what point between 1 and 6 months that the SRSF1-m4 expression levels and the knockdown effect of SRSF1-RNAi started to decline. Further *in vivo* experiments to assess more time points would be beneficial to answer this crucial question. Once it is clear when the virus starts to be cleared from the body it will be much easier to assess whether an increased dosage is required to prolong the therapeutic effect of the scAAV9. Ideally these viruses would only be administered to a patient once, to prevent any immune response from being mounted following multiple doses. It may also be that a larger dose of therapeutic virus is required to maintain a therapeutic effect.

Sex differences should also be considered in future studies. During the first efficacy *in vivo* study (described in chapter 4) AAV9\_SRSF1-RNAi and scAAV9\_SRSF1-m4 were administered into C57bl6 mice of both sexes. Although this study has suggested that administration of scAAV9\_SRSF1-RNAi and scAAV9\_SRSF1-m4 was deemed safe in both sexes, previously it has been reported that there are significant sex differences in AAV transduction, depending on the target organ. To save time and to reduce the wastage of animals, it was decided to use both males and females for the safety and efficacy study; this meant that data were not separated by sex, and it is therefore unknown whether sex played a role in the overall results. Davidoff et al, 2003, found that the administration of AAV8 via liver-targeted delivery resulted in significantly higher transgene expression in male mice versus female mice, irrespective of promoter type. Castration of male mice showed a reduction of AAV transgene expression in males compared to the levels observed in female mice, whereas transient exposure of female mice to dihydrotestosterone (DHT) prior to administration of rAAV vector improved stable hepatocyte genes compared to the transfer levels observed in males. This suggests that androgens may be responsible for enhanced gene transfer (Davidoff *et al.*, 2003). Although this study did not find any significant difference between transduction rates in other non-hepatic organs, few other studies have investigated whether sex could affect the transduction and overall efficiency of AAV treatments. This may be due to differences in AAV clearance between the sexes, but to date very few studies have investigated this question. Systemic administration of AAV9-Fluc into C57bl6 and nude mice has also been shown to have significantly higher transduction of the brain in female mice in comparison to male mice (Maguire *et al.*, 2013). It would be interesting to clarify whether this is due to increased transduction efficiency or if it is related to viral clearance or metabolism. Again, several studies have suggested sex transduction differences, but there is

a paucity of robust published; it is vital that these differences are pursued in future research to develop the field. This is because it is likely that AAV gene therapy would need to be modified in terms of dose to ensure that transduction efficiency is optimal in both sexes.

From the study, it is now known that a partial knockdown of SRSF1 using AAV is not lethal *in vivo* and creates no serious off-target effects at least over a 6 month period. However, the study has not considered potential sex differences in SRSF1 expression. SRSF1 is implicated in many pathways, some of which have not been fully investigated. For example, it has been suggested that SRSF1 is implicated in T-cell gene regulation and function (Moulton *et al.*, 2015). Cravens *et al* have followed on from this research and have confirmed that oestrogen can modulate SRSF1 expression and down-regulate protein levels via post transcriptional mechanisms in T lymphocytes, revealing a potential molecular link between hormones, immune cells and autoimmune disease (Cravens *et al.*, 2017; Ramanujan *et al.*, 2021). Previous studies in the Hautbergue lab, including the present study, have shown that reducing SRSF1 confers neuroprotection in a human *C9ORF72* cell model and in *Drosophila* and mouse models (Hautbergue *et al.*, 2017), but if endogenous oestrogen is also able to reduce SRSF1 protein levels, then it may be that reproductive females are at an advantage over males in terms of ALS disease onset and survival.

Sex is a crucial factor in the *C9ORF72*-linked ALS, since *C9ORF72* expansion negatively impacts on survival time in men compared to women: fALS male patients carrying the *C9ORF72* expansion characterized by spinal onset have a reduced survival rate compared to females with the same type of onset (Rooney *et al.*, 2017). Unfortunately, the effect of hormones, including oestrogen, and overall sex differences in ALS is also an underdeveloped area of research. If there is in fact a relationship between oestrogen levels and SRSF1 protein levels, the use of female C9-500 mice could be an issue. Female mice have steady oestrogen levels across their lifespan, whereas in human's oestrogen levels drop following the menopause, which is usually around the time of onset of *C9ORF72*-ALS symptoms. The reduction in oestrogen may potentially lead to an increase in SRSF1 protein levels, resulting in the increase of pre-mRNA export of the *C9ORF72* repeat transcripts, thereby increasing DPR production in the cytoplasm and leading to motor neuron injury. However, this suggestion is merely speculative and would require extensive future research.

An additional variable to consider is the strain of mice used. For example, it has been demonstrated that in C57bl/6 mice SRSF1 knockdown no longer occurs at 6 months, whereas in C9-500 mice, DPR levels are reduced at 3 months. Indeed, He *et al.*, 2019, have

suggested that treatment outcomes may differ between different strains of mice, and especially between FVB mice and C57bl/6 mice. Other research has shown that FVB mice may be more susceptible to GFP toxicity compared to C57bl/6 mice. This is why this study did not use the scAAV9\_GFP control virus but instead used untreated and scAAV9\_scrambled as controls in the C9ORF72 Ranum mouse model (FVB background). Ideally, in future research, wild-type mice of the same background strain should be used in the safety and efficacy studies, in order to control for any strain differences in which might affect the gene therapy approach.

The project results indicate novel progress in translational neuroscience, in that this is the first study to evaluate SRSF1 manipulation in the treatment of ALS. Following the promising results suggested by this study a collaboration with *LifeArc* and the MND Association is being undertaken. The charities have funded a 3 year project to investigate the optimal intrathecal route of administration and the dose of scAAV9-SRSF1-RNAi virus prior to evaluating the neuroprotective potential of the gene therapy in a 12-month study that will assess both motor and cognitive behaviours as well as molecular outcomes in the C9ORF72-ALS/FTD mice. This study will also review for the first time the behavioural effects of the treatments following administration that was unable to take place in the present study during the Covid pandemic.

As for future work, there are several avenues that can be taken to further our understanding of this specific field. During the C57bl/6 mouse experiments, there was evidence of GFP DNA and expression in the PBS treated mice. GFP was found in both qPCR data when reviewing viral DNA distribution and using immunofluorescence staining. Originally it was thought that the GFP DNA could be from contamination during the qPCR procedure. Yet the experiment was repeated following a full decontamination protocol but GFP DNA was still present, albeit at lower levels. Due to this issue the scAAV9\_GFP control virus was discontinued for subsequent *in vivo* work. In the future experiments to rule out shedding would be beneficial. This can be before sacrifice from the start of the experiment by taking faecal and urinary samples and using qPCR to assess viral DNA levels at successive time points. It is currently unknown whether viruses that are administered are shed in the faeces and urine and if so for how long. Could there be any live virus that could be taken up by other animals in the cage? If this could be the case in mice, it is reasonable to assume that shedding could occur in humans and reasonable precautions may be required for health staff and immediate family members following gene therapy. Further development in this area is important especially as gene therapy becomes increasingly popular as a treatment option.

Despite the large number of unanswered questions arising from this project, it is important to highlight that this project has led to interesting findings and significance that will contribute to the developments of new therapeutic avenues for *C9ORF72*-ALS/FTD treatment and other SRSF1-dependent diseases. To summarize, the project has confirmed that SRSF1 manipulation is safe in a wild-type mouse model up to 6 months post administration. The research has also confirmed that there is at least a correlation between SRSF1 depletion and SRSF1-m4 expression and the reduction of DPR levels in the cerebral cortex. Not only has this project discovered that SRSF1 manipulation is a viable treatment option in an animal model, now it is known that SRSF1 depletion and SRSF1-m4 expression can be beneficial in treating *C9ORF72*-ALS/FTD. Considering the effects following the administration of scAAV9\_SRSF1-m4 in mice at P40, the preferable strategy following this study to progress with would be scAAV9\_SRSF1-RNAi. This is further verified by recent work by Castelli *et al*, 2021, who have recently investigated the genome-wide RNA changes in *C9ORF72*-ALS/FTD patient-derived neurons and *Drosophila*, and the neuroprotection conferred by SRSF1-RNAi gene therapy approach which specifically inhibits the SRSF1-dependent nuclear export of pathological *C9ORF72*-repeat transcripts. Their results indicate that SRSF1 partial depletion only leads to expression changes in a small proportion of *C9ORF72*-ALS/FTD disease-altered transcripts, which suggests not all these RNA alterations need to be normalized and that the gene therapeutic approach is safe as it does not disrupt global gene expression. The authors have found that the efficacy of this intervention is also validated at genome-wide level with transcripts modulated in the vast majority of biological processes affected in *C9ORF72*-ALS which gives further confidence in the conclusions suggested from the results of this study (Castelli *et al*, 2021). This work from the host laboratory gives us greater confidence in the clinical cassette generated in the present project that could be used as a gene therapy and tested in humans. The cassette would require minor modification, such as the replacement of GFP with a stuffer sequence as well as GMP manufacture. Other modalities that can mimic SRSF1 depletion mechanisms can now be developed and compared with gene therapy e.g. small molecules, peptides, other gene therapy vectors etc.

## REFERENCES

- 2020, C. and G. T. C. A. clinical trials report (2020) *Cell and Gene Therapy Catapult ATMP clinical trials report 2020*. Available at: <http://alliancerm.org/wp-content/uploads/2021/01/SOTTI-2021-pdf.pdf> (Accessed: 14 December 2021).
- 2020, M. T. P. press release J. 16 (2020) ‘As the First ALS Treatment in Indonesia RADICAVA has been approved first in ASEAN countries’, pp. 1–2.
- A. C. Ludolph and J. Brettschneider (2015) ‘TDP-43 in amyotrophic lateral sclerosis – is it a prion disease?’, *European Journal of Neurology*, 22(5), pp. 753–761. Available at: <https://onlinelibrary.wiley.com/doi/10.1111/ene.12706>.
- Abbas, A. R. *et al.* (2009) ‘Deconvolution of Blood Microarray Data Identifies Cellular Activation Patterns in Systemic Lupus Erythematosus’, *PLoS ONE*, 4(7), p. 6098. doi: 10.1371/journal.pone.0006098.
- Akache, B. *et al.* (2006) ‘The 37/67-Kilodalton Laminin Receptor Is a Receptor for Adeno-Associated Virus Serotypes 8, 2, 3, and 9’, *Journal of Virology*, 80(19), pp. 9831–9836. doi: 10.1128/jvi.00878-06.
- Akdim, F. *et al.* (2011) ‘Efficacy of apolipoprotein B synthesis inhibition in subjects with mild-to-moderate hyperlipidaemia’, *European Heart Journal*, 32(21), pp. 2650–2659. doi: 10.1093/eurheartj/ehr148.
- Al-Chalabi, A. *et al.* (2017) ‘ENCALS statement on edaravone’, in *Amyotrophic Lateral Sclerosis and Frontotemporal Degeneration*. Taylor and Francis, pp. 471–474. Available at: <https://helda.helsinki.fi/bitstream/handle/10138/229608/21678421.2017.pdf?sequence=1> (Accessed: 9 January 2018).
- Alami, N. H. *et al.* (2014) ‘Axonal Transport of TDP-43 mRNA Granules Is Impaired by ALS-Causing Mutations’, *Neuron*. Cell Press, 81(3), pp. 536–543. doi: 10.1016/J.NEURON.2013.12.018.
- ALSoD (2011) *ALSoD: Amyotrophic Lateral Sclerosis Online Genetics Database, Amyotrophic Lateral Sclerosis*. Available at: <http://alsod.iop.kcl.ac.uk/home.aspx> (Accessed: 24 January 2018).

- An, H. *et al.* (2019) 'ALS-linked FUS mutations confer loss and gain of function in the nucleus by promoting excessive formation of dysfunctional paraspeckles', *Acta Neuropathologica Communications*, 7(1), p. 7. doi: 10.1186/s40478-019-0658-x.
- Anczuków, O. *et al.* (2012) 'The splicing factor SRSF1 regulates apoptosis and proliferation to promote mammary epithelial cell transformation', *Nature Structural & Molecular Biology*, 19(2), pp. 220–228. doi: 10.1038/nsmb.2207.
- Anczuków, O. *et al.* (2015) 'SRSF1-Regulated Alternative Splicing in Breast Cancer', *Molecular Cell*. Elsevier, 60(1), pp. 105–117. doi: 10.1016/j.molcel.2015.09.005.
- Andrews, J. A. *et al.* (2020) 'Real-world evidence of riluzole effectiveness in treating amyotrophic lateral sclerosis', *Amyotrophic Lateral Sclerosis and Frontotemporal Degeneration*, 21(7–8), pp. 509–518. doi: 10.1080/21678421.2020.1771734.
- Ansari, A. M. *et al.* (2016) 'Cellular GFP Toxicity and Immunogenicity: Potential Confounders in in Vivo Cell Tracking Experiments', *Stem Cell Reviews and Reports*, 12(5), pp. 553–559. doi: 10.1007/s12015-016-9670-8.
- Aoki, Y. *et al.* (2017) 'C9orf72 and RAB7L1 regulate vesicle trafficking in amyotrophic lateral sclerosis and frontotemporal dementia', *Brain*, 140(4), pp. 887–897. doi: 10.1093/brain/awx024.
- Arif, W. (2020) *Elucidating the role of SRSF1, a prototypical splicing factor, in liver physiology*.
- Armbruster, N. *et al.* (2016) 'Efficacy and biodistribution analysis of intracerebroventricular administration of an optimized scAAV9-SMN1 vector in a mouse model of spinal muscular atrophy', *Molecular Therapy - Methods & Clinical Development*, 3, p. 16060. doi: 10.1038/mtm.2016.60.
- Armstrong, R. A. (2017) 'Neuronal cytoplasmic inclusions in tau, TDP-43, and FUS molecular subtypes of frontotemporal lobar degeneration share similar spatial patterns', *Folia Neuropathologica*, 55(3), pp. 185–192. doi: 10.5114/fn.2017.70482.
- Arnold, E. S. *et al.* (2013) 'ALS-linked TDP-43 mutations produce aberrant RNA splicing and adult-onset motor neuron disease without aggregation or loss of nuclear TDP-43', *Proceedings of the National Academy of Sciences*, 110(8), pp. E736–E745. doi: 10.1073/pnas.1222809110.

- Ash, P. E. A. *et al.* (2013) 'Unconventional Translation of C9ORF72 GGGGCC Expansion Generates Insoluble Polypeptides Specific to c9FTD/ALS', *Neuron*, 77(4), pp. 639–646. doi: 10.1016/j.neuron.2013.02.004.
- Atanasio, A. *et al.* (2016) 'C9orf72 ablation causes immune dysregulation characterized by leukocyte expansion, autoantibody production and glomerulonephropathy in mice', *Scientific Reports*, 6(1), p. 23204. doi: 10.1038/srep23204.
- Atkinson, R. A. K. *et al.* (2015) 'C9ORF72 expression and cellular localization over mouse development', *Acta Neuropathologica Communications*, 3(1), p. 59. doi: 10.1186/s40478-015-0238-7.
- Azzouz, M. *et al.* (2004) 'VEGF delivery with retrogradely transported lentivector prolongs survival in a mouse ALS model', *Nature*, 429(6990), pp. 413–417. doi: 10.1038/nature02544.
- Bang, J., Spina, S. and Miller, B. L. (2015) 'Frontotemporal dementia', *The Lancet*. Elsevier Ltd, 386(10004), pp. 1672–1682. doi: 10.1016/S0140-6736(15)00461-4.
- Beck, J. *et al.* (2013) 'Large C9orf72 Hexanucleotide Repeat Expansions Are Seen in Multiple Neurodegenerative Syndromes and Are More Frequent Than Expected in the UK Population', *The American Journal of Human Genetics*. Cell Press, 92(3), pp. 345–353. doi: 10.1016/J.AJHG.2013.01.011.
- Bell, C. L. *et al.* (2012) 'Identification of the Galactose Binding Domain of the Adeno-Associated Virus Serotype 9 Capsid', *Journal of Virology*, 86(13), pp. 7326–7333. doi: 10.1128/JVI.00448-12.
- Bennett, C. F. *et al.* (2017) 'Pharmacology of Antisense Drugs', *Annual Review of Pharmacology and Toxicology*, 57(1), pp. 81–105. doi: 10.1146/annurev-pharmtox-010716-104846.
- Bensimon, G., Lacomblez, L. and Meininger, V. (1994) 'A Controlled Trial of Riluzole in Amyotrophic Lateral Sclerosis', *New England Journal of Medicine*, 330(9), pp. 585–591. doi: 10.1056/NEJM199403033300901.
- Berry, J. *et al.* (2021) 'Radicava/Edaravone Findings in Biomarkers From Amyotrophic Lateral Sclerosis (REFINE-ALS)', *Neurology: Clinical Practice*, 11(4), pp. e472–e479. doi: 10.1212/CPJ.0000000000000968.

- Bevan, A. K. *et al.* (2011) ‘Systemic Gene Delivery in Large Species for Targeting Spinal Cord, Brain, and Peripheral Tissues for Pediatric Disorders’, *Molecular Therapy*, 19(11), pp. 1971–1980. doi: 10.1038/mt.2011.157.
- Bey, K. *et al.* (2017) ‘Efficient CNS targeting in adult mice by intrathecal infusion of single-stranded AAV9-GFP for gene therapy of neurological disorders’, *Gene Therapy*, 24(5), pp. 325–332. doi: 10.1038/gt.2017.18.
- Bey, K. *et al.* (2020) ‘Intra-CSF AAV9 and AAVrh10 Administration in Nonhuman Primates: Promising Routes and Vectors for Which Neurological Diseases?’, *Molecular Therapy - Methods & Clinical Development*, 17, pp. 771–784. doi: 10.1016/j.omtm.2020.04.001.
- Van Blitterswijk, M. *et al.* (2015) ‘Novel clinical associations with specific C9ORF72 transcripts in patients with repeat expansions in C9ORF72’, *Acta Neuropathol*, 3, pp. 863–876. doi: 10.1007/s00401-015-1480-6.
- Bobo, T. A. *et al.* (2020) ‘Targeting the Root Cause of Mucopolysaccharidosis IIIA with a New scAAV9 Gene Replacement Vector’, *Molecular Therapy - Methods & Clinical Development*, 19, pp. 474–485. doi: 10.1016/j.omtm.2020.10.014.
- Bodansky, A. *et al.* (2010) ‘TDP-43 and ubiquitinated cytoplasmic aggregates in sporadic ALS are low frequency and widely distributed in the lower motor neuron columns independent of disease spread’, *Amyotrophic Lateral Sclerosis*, 11, pp. 321–327. doi: 10.3109/17482961003602363.
- Van Den Bosch, L. and Robberecht, W. (2000) ‘Different receptors mediate motor neuron death induced by short and long exposures to excitotoxicity’, *Brain Research Bulletin*, 53(4), pp. 383–388. doi: 10.1016/S0361-9230(00)00371-3.
- Boudreau, R. L. *et al.* (2013) ‘siSPOTR: a tool for designing highly specific and potent siRNAs for human and mouse’, *Nucleic Acids Research*, 41(1), pp. e9–e9. doi: 10.1093/nar/gks797.
- Vanden Broeck, L. *et al.* (2015) ‘Functional complementation in *Drosophila* to predict the pathogenicity of TARDBP variants: evidence for a loss-of-function mechanism’, *Neurobiology of Aging*, 36(2), pp. 1121–1129. doi: 10.1016/j.neurobiolaging.2014.09.001.
- Vanden Broeck, L., Callaerts, P. and Dermaut, B. (2014) ‘TDP-43-mediated neurodegeneration: towards a loss-of-function hypothesis?’, *Trends in Molecular Medicine*, 20(2),

pp. 66–71. doi: 10.1016/j.molmed.2013.11.003.

Bruijn, L. I. *et al.* (1997) ‘ALS-linked SOD1 mutant G85R mediates damage to astrocytes and promotes rapidly progressive disease with SOD1-containing inclusions.’, *Neuron*, 18(2), pp. 327–38. Available at: <http://www.ncbi.nlm.nih.gov/pubmed/9052802> (Accessed: 4 January 2018).

Büning, H. *et al.* (2015) ‘Engineering the AAV capsid to optimize vector–host-interactions’, *Current Opinion in Pharmacology*, 24, pp. 94–104. doi: 10.1016/j.coph.2015.08.002.

Bunton-Stasyshyn, R. K. A. *et al.* (2015) ‘SOD1 Function and Its Implications for Amyotrophic Lateral Sclerosis Pathology’, *The Neuroscientist*, 21(5), pp. 519–529. doi: 10.1177/1073858414561795.

Buratti, E. *et al.* (2005) ‘TDP-43 Binds Heterogeneous Nuclear Ribonucleoprotein A/B through Its C-terminal Tail’, *Journal of Biological Chemistry*, 280(45), pp. 37572–37584. doi: 10.1074/jbc.M505557200.

Byrne, S. *et al.* (2014) ‘Intermediate repeat expansion length in C9orf72 may be pathological in amyotrophic lateral sclerosis’, *Amyotrophic Lateral Sclerosis and Frontotemporal Degeneration*, 15(1–2), pp. 148–150. doi: 10.3109/21678421.2013.838586.

Cáceres, J. F. and Krainer, A. R. (1993) ‘Functional analysis of pre-mRNA splicing factor SF2/ASF structural domains.’, *The EMBO journal*, 12(12), pp. 4715–26. Available at: <http://www.ncbi.nlm.nih.gov/pubmed/8223480> (Accessed: 13 December 2017).

Calcedo, R. *et al.* (2011) ‘Adeno-Associated Virus Antibody Profiles in Newborns, Children, and Adolescents’, *Clinical and Vaccine Immunology*. American Society for Microbiology (ASM), 18(9), pp. 1586–1588. doi: 10.1128/CVI.05107-11.

Campbell, S. and Vogt, V. M. (1997) ‘In vitro assembly of virus-like particles with Rous sarcoma virus Gag deletion mutants: identification of the p10 domain as a morphological determinant in the formation of spherical particles’, *Journal of Virology*, 71(6), pp. 4425–4435. doi: 10.1128/jvi.71.6.4425-4435.1997.

Castelli, L. M. *et al.* (2018) ‘SRSF1-dependent nuclear export of C9ORF72 repeat transcripts: targeting toxic gain-of-functions induced by protein sequestration as a selective therapeutic strategy for neuroprotection’, *Therapeutic Targets for Neurological Diseases*, pp. 1–10. doi:

10.14800/ttnd.1619.

Castelli, L. M. *et al.* (2021) ‘SRSF1-dependent inhibition of C9ORF72-repeat RNA nuclear export: genome-wide mechanisms for neuroprotection in amyotrophic lateral sclerosis’, *Molecular Neurodegeneration*, 16(1), p. 53. doi: 10.1186/s13024-021-00475-y.

Castle, M. J. *et al.* (2016) ‘Controlling AAV Tropism in the Nervous System with Natural and Engineered Capsids’, in *Methods in Molecular Biology*, pp. 133–149. doi: 10.1007/978-1-4939-3271-9\_10.

Chadeuf, G. *et al.* (2005) ‘Evidence for Encapsulation of Prokaryotic Sequences during Recombinant Adeno-Associated Virus Production and Their in Vivo Persistence after Vector Delivery’, *Molecular Therapy*, 12(4), pp. 744–753. doi: 10.1016/j.ymthe.2005.06.003.

Chase, H. B. (1942) ‘Studies on an Anophthalmic Strain of Mice. III. Results of Crosses with Other Strains.’, *Genetics*, 27(3), pp. 339–48. doi: 10.1093/genetics/27.3.339.

Chew, J. *et al.* (2015) ‘Neurodegeneration. C9ORF72 repeat expansions in mice cause TDP-43 pathology, neuronal loss, and behavioral deficits.’, *Science (New York, N.Y.)*. NIH Public Access, 348(6239), pp. 1151–4. doi: 10.1126/science.aaa9344.

Choi, V. W., McCarty, D. M. and Samulski, R. J. (2006) ‘Host Cell DNA Repair Pathways in Adeno-Associated Viral Genome Processing’, *Journal of Virology*. American Society for Microbiology (ASM), 80(21), pp. 10346–10356. doi: 10.1128/JVI.00841-06.

Chou, C.-C. *et al.* (2018) ‘TDP-43 pathology disrupts nuclear pore complexes and nucleocytoplasmic transport in ALS/FTD’, *Nature Neuroscience*. Nature Publishing Group, p. 1. doi: 10.1038/s41593-017-0047-3.

Choudhury, S. R. *et al.* (2017) ‘Viral vectors for therapy of neurologic diseases’, *Neuropharmacology*, 120, pp. 63–80. doi: 10.1016/j.neuropharm.2016.02.013.

Ciura, S. *et al.* (2013) ‘Loss of function of C9orf72 causes motor deficits in a zebrafish model of Amyotrophic Lateral Sclerosis’, *Annals of Neurology*, 74(2), p. n/a-n/a. doi: 10.1002/ana.23946.

Cooper-Knock, J. *et al.* (2013) ‘C9ORF72 transcription in a frontotemporal dementia case with two expanded alleles’, *Neurology*, 81(19), pp. 1719–1721. doi:

10.1212/01.wnl.0000435295.41974.2e.

Cooper-Knock, J. *et al.* (2014) 'Sequestration of multiple RNA recognition motif-containing proteins by C9orf72 repeat expansions', *Brain*. Oxford University Press, 137(7), pp. 2040–2051. doi: 10.1093/brain/awu120.

Cravens, E. N. *et al.* (2017) 'Estrogen downregulates the expression of serine arginine splicing factor 1 (SRSF1) in human t lymphocytes', in *Arthritis and Rheumatology*. Available at: <http://ovidsp.ovid.com/ovidweb.cgi?T=JS&PAGE=reference&D=emed18&NEWS=N&AN=618916741>.

Cunningham, S. C. *et al.* (2008) 'Gene Delivery to the Juvenile Mouse Liver Using AAV2/8 Vectors', *Molecular Therapy*, 16(6), pp. 1081–1088. doi: 10.1038/mt.2008.72.

D'Erchia, A. M. *et al.* (2017) 'Massive transcriptome sequencing of human spinal cord tissues provides new insights into motor neuron degeneration in ALS', *Scientific Reports*, 7(1), p. 10046. doi: 10.1038/s41598-017-10488-7.

Damdindorj, L. *et al.* (2014) 'A Comparative Analysis of Constitutive Promoters Located in Adeno-Associated Viral Vectors', *PLoS ONE*. Edited by J. Prata, 9(8), p. e106472. doi: 10.1371/journal.pone.0106472.

Das, S. and Krainer, A. R. (2014) 'Emerging Functions of SRSF1, Splicing Factor and Oncoprotein, in RNA Metabolism and Cancer', *Molecular Cancer Research*. NIH Public Access, 12(9), pp. 1195–1204. doi: 10.1158/1541-7786.MCR-14-0131.

Davidoff, A. M. *et al.* (2003) 'Sex significantly influences transduction of murine liver by recombinant adeno-associated viral vectors through an androgen-dependent pathway', *Blood*, 102(2), pp. 480–488. doi: 10.1182/blood-2002-09-2889.

Davidson, Y. *et al.* (2007) 'Ubiquitinated pathological lesions in frontotemporal lobar degeneration contain the TAR DNA-binding protein, TDP-43', *Acta Neuropathologica*, 113(5), pp. 521–533. doi: 10.1007/s00401-006-0189-y.

Daya, S. and Berns, K. I. (2008) 'Gene therapy using adeno-associated virus vectors', *Clinical Microbiology Reviews*, 21(4), pp. 583–593. doi: 10.1128/CMR.00008-08.

Dejesus-Hernandez, M. *et al.* (2017) 'In-depth clinico-pathological examination of RNA foci

in a large cohort of C9ORF72 expansion carriers', *Acta Neuropathol*, 3, pp. 255–269. doi: 10.1007/s00401-017-1725-7.

DeJesus-Hernandez, M. *et al.* (2011) 'Expanded GGGGCC Hexanucleotide Repeat in Noncoding Region of C9ORF72 Causes Chromosome 9p-Linked FTD and ALS', *Neuron*, 72(2), pp. 245–256. doi: 10.1016/j.neuron.2011.09.011.

Detrait, E. R. *et al.* (2002) 'Reporter Gene Transfer Induces Apoptosis in Primary Cortical Neurons', *Molecular Therapy*, 5(6), pp. 723–730. doi: 10.1006/mthe.2002.0609.

Donnelly, C. J. *et al.* (2013) 'RNA Toxicity from the ALS/FTD C9ORF72 Expansion Is Mitigated by Antisense Intervention', *Neuron*. Cell Press, 80(2), pp. 415–428. doi: 10.1016/J.NEURON.2013.10.015.

Dull, T. *et al.* (1998) 'A Third-Generation Lentivirus Vector with a Conditional Packaging System', *Journal of Virology*, 72(11), pp. 8463–8471. doi: 10.1128/JVI.72.11.8463-8471.1998.

Ederle, H. and Dormann, D. (2017) 'TDP-43 and FUS en route from the nucleus to the cytoplasm', *FEBS Letters*, 591(11), pp. 1489–1507. doi: 10.1002/1873-3468.12646.

Fagone, P. *et al.* (2012) 'Systemic Errors in Quantitative Polymerase Chain Reaction Titration of Self-Complementary Adeno-Associated Viral Vectors and Improved Alternative Methods', *Human Gene Therapy Methods*, 23(1), pp. 1–7. doi: 10.1089/hgtb.2011.104.

Farg, M. A. *et al.* (2014) 'C9ORF72, implicated in amyotrophic lateral sclerosis and frontotemporal dementia, regulates endosomal trafficking', *Human Molecular Genetics*, 23(13), pp. 3579–3595. doi: 10.1093/hmg/ddu068.

Farraha, M. *et al.* (2019) 'Analysis of recombinant adeno-associated viral vector shedding in sheep following intracoronary delivery', *Gene Therapy*, 26(9), pp. 399–406. doi: 10.1038/s41434-019-0097-0.

Federici, T. *et al.* (2012) 'Robust spinal motor neuron transduction following intrathecal delivery of AAV9 in pigs', *Gene Therapy*, 19, pp. 852–859. doi: 10.1038/gt.2011.130.

Ferguson, R., Serafeimidou-Pouliou, E. and Subramanian, V. (2016) 'Dynamic expression of the mouse orthologue of the human amyotrophic lateral sclerosis associated gene C9orf72 during central nervous system development and neuronal differentiation', *Journal of Anatomy*,

229(6), pp. 871–891. doi: 10.1111/joa.12526.

Ferla, R. *et al.* (2017) ‘Non-clinical Safety and Efficacy of an AAV2/8 Vector Administered Intravenously for Treatment of Mucopolysaccharidosis Type VI’, *Molecular Therapy - Methods & Clinical Development*, 6, pp. 143–158. doi: 10.1016/j.omtm.2017.07.004.

Flotte, T. R. C. B. J. (1995) ‘Adeno-associated virus vectors for gene therapy’, *Gene Therapy*, 2(6), pp. 357–362. Available at: <https://europepmc.org/article/med/7584109>.

Food and Drug Administration (2016) *Recommendations for Microbial Vectors Used for Gene Therapy, Guidance for Industry*. Available at: <http://www.fda.gov/BiologicsBloodVaccines/GuidanceComplianceRegulatoryInformation/Guidances/default.htm>.

Foust, K. D. *et al.* (2009) ‘Intravascular AAV9 preferentially targets neonatal neurons and adult astrocytes’, *Nature Biotechnology*, 27(1), pp. 59–65. doi: 10.1038/nbt.1515.

Foust, K. D. *et al.* (2013) ‘Therapeutic AAV9-mediated Suppression of Mutant SOD1 Slows Disease Progression and Extends Survival in Models of Inherited ALS’, *Molecular Therapy*. Elsevier, 21(12), pp. 2148–2159. doi: 10.1038/mt.2013.211.

François, A. *et al.* (2018) ‘Accurate Titration of Infectious AAV Particles Requires Measurement of Biologically Active Vector Genomes and Suitable Controls’. doi: 10.1016/j.omtm.2018.07.004.

Fratta, P. *et al.* (2012) ‘C9orf72 hexanucleotide repeat associated with amyotrophic lateral sclerosis and frontotemporal dementia forms RNA G-quadruplexes’, *Scientific Reports*, 2(1), p. 1016. doi: 10.1038/srep01016.

Freibaum, B. D. *et al.* (2015) ‘GGGGCC repeat expansion in C9orf72 compromises nucleocytoplasmic transport’, *Nature*, 525(7567), pp. 129–133. doi: 10.1038/nature14974.

Freibaum, B. D. and Taylor, J. P. (2017) ‘The Role of Dipeptide Repeats in C9ORF72-Related ALS-FTD’, *Frontiers in Molecular Neuroscience*. Frontiers Media SA, 10, p. 35. doi: 10.3389/fnmol.2017.00035.

Frick, P. *et al.* (2018) ‘Novel antibodies reveal presynaptic localization of C9orf72 protein and reduced protein levels in C9orf72 mutation carriers’, *Acta Neuropathologica Communications*,

6(1), p. 72. doi: 10.1186/s40478-018-0579-0.

Gao, G. *et al.* (2004) 'Clades of Adeno-Associated Viruses Are Widely Disseminated in Human Tissues', *Journal of Virology*, 78(12), pp. 6381–6388. doi: 10.1128/JVI.78.12.6381-6388.2004.

Garcia-Arocena, D. (2016) *How to Spot and Manage Malocclusion in Research Mice, The Jackson Laboratory*. Available at: <https://www.jax.org/news-and-insights/jax-blog/2016/july/how-to-spot-malocclusion-in-research-mice#:~:text=When the malocclusion is later,a provision of powdered diet.>

Gendron, T. F. *et al.* (2013) 'Antisense transcripts of the expanded C9ORF72 hexanucleotide repeat form nuclear RNA foci and undergo repeat-associated non-ATG translation in c9FTD/ALS', *Acta Neuropathol*, 3, pp. 829–844. doi: 10.1007/s00401-013-1192-8.

George, L. A. *et al.* (2017) 'Hemophilia B Gene Therapy with a High-Specific-Activity Factor IX Variant', *New England Journal of Medicine*, 377(23), pp. 2215–2227. doi: 10.1056/NEJMoa1708538.

Gerdes, C. A., Castro, M. G. and Löwenstein, P. R. (2000) 'Strong Promoters Are the Key to Highly Efficient, Noninflammatory and Noncytotoxic Adenoviral-Mediated Transgene Delivery into the Brain in Vivo', *Molecular Therapy*. Cell Press, 2(4), pp. 330–338. doi: 10.1006/MTHE.2000.0140.

Gómez-Tortosa, E. *et al.* (2013) 'C9ORF72 hexanucleotide expansions of 20-22 repeats are associated with frontotemporal deterioration.', *Neurology*. American Academy of Neurology, 80(4), pp. 366–70. doi: 10.1212/WNL.0b013e31827f08ea.

Govindasamy, L. *et al.* (2006) 'Structurally Mapping the Diverse Phenotype of Adeno-Associated Virus Serotype 4', *Journal of Virology*, 80(23), pp. 11556–11570. doi: 10.1128/JVI.01536-06.

Gray, S. J. *et al.* (2011) 'Optimizing promoters for recombinant adeno-associated virus-mediated gene expression in the peripheral and central nervous system using self-complementary vectors', *Human Gene Therapy*, 22(9), pp. 1143–1153. doi: 10.1089/hum.2010.245.

Gray, S. J. *et al.* (2013) 'Global CNS gene delivery and evasion of anti-AAV-neutralizing

antibodies by intrathecal AAV administration in non-human primates', *Gene Therapy*, 20(4), pp. 450–459. doi: 10.1038/gt.2012.101.

Grimm, D. *et al.* (1998) 'Novel Tools for Production and Purification of Recombinant Adenoassociated Virus Vectors', *Human Gene Therapy*, 9(18), pp. 2745–2760. doi: 10.1089/hum.1998.9.18-2745.

Gros-Louis, F., Gaspar, C. and Rouleau, G. A. (2006) 'Genetics of familial and sporadic amyotrophic lateral sclerosis', *Biochimica et Biophysica Acta - Molecular Basis of Disease*, 1762(11–12), pp. 956–972. doi: 10.1016/J.BBADIS.2006.01.004.

Gurney, M. E. *et al.* (1994) 'Motor neuron degeneration in mice that express a human Cu,Zn superoxide dismutase mutation.', *Science (New York, N.Y.)*, 264(5166), pp. 1772–5. Available at: <http://www.ncbi.nlm.nih.gov/pubmed/8209258> (Accessed: 4 January 2018).

Haeusler, A. R. *et al.* (2014) 'C9orf72 nucleotide repeat structures initiate molecular cascades of disease', *Nature*, 507(7491), pp. 195–200. doi: 10.1038/nature13124.

Haidet-Phillips, A. M. *et al.* (2011) 'Astrocytes from familial and sporadic ALS patients are toxic to motor neurons', *Nature Biotechnology*, 29(9), pp. 824–828. doi: 10.1038/nbt.1957.

Halbert, C. L. *et al.* (2011) 'Capsid-expressing DNA in AAV vectors and its elimination by use of an oversize capsid gene for vector production', *Gene Therapy*, 18(4), pp. 411–417. doi: 10.1038/gt.2010.167.

Halbert, C. L., Allen, J. M. and Miller, A. D. (2001) 'Adeno-Associated Virus Type 6 (AAV6) Vectors Mediate Efficient Transduction of Airway Epithelial Cells in Mouse Lungs Compared to That of AAV2 Vectors', *Journal of Virology*, 75(14), pp. 6615–6624. doi: 10.1128/JVI.75.14.6615-6624.2001.

Hammond, S. L. *et al.* (2017) 'Cellular selectivity of AAV serotypes for gene delivery in neurons and astrocytes by neonatal intracerebroventricular injection', *PLOS ONE*. Edited by J. Qiu, 12(12), p. e0188830. doi: 10.1371/journal.pone.0188830.

Hao, Z. *et al.* (2019) 'Motor dysfunction and neurodegeneration in a C9orf72 mouse line expressing poly-PR', *Nature Communications*, 10(1), p. 2906. doi: 10.1038/s41467-019-10956-w.

- Hardiman, O. *et al.* (2017) ‘Amyotrophic lateral sclerosis’, *Nature Reviews Disease Primers*. Macmillan Publishers Limited, 3, pp. 1–18. doi: 10.1038/nrdp.2017.71.
- Hardiman, O., van den Berg, L. H. and Kiernan, M. C. (2011) ‘Clinical diagnosis and management of amyotrophic lateral sclerosis’, *Nature Reviews Neurology*, 7(11), pp. 639–649. doi: 10.1038/nrneurol.2011.153.
- Harms, M. *et al.* (2013) ‘C9orf72 Hexanucleotide Repeat Expansions in Clinical Alzheimer Disease’, *JAMA Neurology*, 70(6), p. 736. doi: 10.1001/2013.jamaneurol.537.
- Harms, M. B. *et al.* (2013) ‘Lack of C9ORF72 coding mutations supports a gain of function for repeat expansions in amyotrophic lateral sclerosis’, *Neurobiology of Aging*, 34(9), pp. 2234.e13–2234.e19. doi: 10.1016/j.neurobiolaging.2013.03.006.
- Hautbergue, G. M. *et al.* (2008) ‘Mutually exclusive interactions drive handover of mRNA from export adaptors to TAP’, *Proceedings of the National Academy of Sciences*, 105(13), pp. 5154–5159. doi: 10.1073/pnas.0709167105.
- Hautbergue, G. M. (2017) *Personalised Medicine*. Edited by S. El-Khamisy. Cham: Springer International Publishing (Advances in Experimental Medicine and Biology). doi: 10.1007/978-3-319-60733-7.
- Hautbergue, G. M. *et al.* (2017) ‘SRSF1-dependent nuclear export inhibition of C9ORF72 repeat transcripts prevents neurodegeneration and associated motor deficits’, *Nature Communications*. Nature Publishing Group, 8, p. 16063. doi: 10.1038/ncomms16063.
- Haward, F. *et al.* (2021) ‘Nucleo-cytoplasmic shuttling of splicing factor SRSF1 is required for development and cilia function’, *eLife*, 10. doi: 10.7554/eLife.65104.
- Hinderer, C. *et al.* (2018) ‘Severe Toxicity in Nonhuman Primates and Piglets Following High-Dose Intravenous Administration of an Adeno-Associated Virus Vector Expressing Human SMN’, *Human Gene Therapy*, 29(3), pp. 285–298. doi: 10.1089/hum.2018.015.
- Hocquemiller, M. *et al.* (2016) ‘Adeno-Associated Virus-Based Gene Therapy for CNS Diseases’, *Human Gene Therapy*, 27(7), pp. 478–496. doi: 10.1089/hum.2016.087.
- Home - *ClinicalTrials.gov* (no date). Available at: <https://www.clinicaltrials.gov/ct2/home> (Accessed: 9 January 2018).

Honda, D. *et al.* (2014) ‘The ALS/FTLD-related RNA-binding proteins TDP-43 and FUS have common downstream RNA targets in cortical neurons’, *FEBS Open Bio*. No longer published by Elsevier, 4, pp. 1–10. doi: 10.1016/J.FOB.2013.11.001.

Hottinger, A. F. *et al.* (2000) ‘Complete and Long-Term Rescue of Lesioned Adult Motoneurons by Lentiviral-Mediated Expression of Glial Cell Line-Derived Neurotrophic Factor in the Facial Nucleus’, *The Journal of Neuroscience*, 20(15), pp. 5587–5593. doi: 10.1523/JNEUROSCI.20-15-05587.2000.

Howard, D. B. *et al.* (2008) ‘Tropism and toxicity of adeno-associated viral vector serotypes 1, 2, 5, 6, 7, 8, and 9 in rat neurons and glia in vitro’, *Virology*, 372(1), pp. 24–34. doi: 10.1016/j.virol.2007.10.007.

Hui, D. J. *et al.* (2015) ‘AAV capsid CD8+ T-cell epitopes are highly conserved across AAV serotypes’, *Molecular Therapy - Methods & Clinical Development*, 2, p. 15029. doi: 10.1038/mtm.2015.29.

Iannitti, T. *et al.* (2018) ‘Translating SOD1 Gene Silencing toward the Clinic: A Highly Efficacious, Off-Target-free, and Biomarker-Supported Strategy for fALS’, *Molecular Therapy - Nucleic Acids*. Cell Press, 12, pp. 75–88. doi: 10.1016/J.OMTN.2018.04.015.

*Invitrogen Block-it RNAi designer* (2021) *ThermoFisher*. Available at: <https://rnaidesigner.thermofisher.com/rnaiexpress/> (Accessed: 16 December 2021).

Ishigaki, S. and Sobue, G. (2018) ‘Importance of Functional Loss of FUS in FTLD’, *ALS. Front. Mol. Biosci*, 5, p. 44. doi: 10.3389/fmolb.2018.00044.

Ishihara, N. *et al.* (2005) ‘Inhibition of apoptosis-inducing factor translocation is involved in protective effects of hepatocyte growth factor against excitotoxic cell death in cultured hippocampal neurons’, *Journal of Neurochemistry*, 95(5), pp. 1277–1286. doi: 10.1111/j.1471-4159.2005.03446.x.

Ito, Hidefumi *et al.* (2008) ‘Treatment with edaravone, initiated at symptom onset, slows motor decline and decreases SOD1 deposition in ALS mice’, *Experimental Neurology*, 213(2), pp. 448–455. doi: 10.1016/j.expneurol.2008.07.017.

Jee, H. *et al.* (2009) ‘Significant roles of microtubules in mature striated muscle deduced from the correlation between tubulin and its molecular chaperone  $\alpha$ B-crystallin in rat muscles’, *The*

*Journal of Physiological Sciences*, 59(3), pp. 149–155. doi: 10.1007/s12576-008-0014-6.

Ji, A.-L. *et al.* (2017) ‘Genetics insight into the amyotrophic lateral sclerosis/frontotemporal dementia spectrum’, *Journal of Medical Genetics*, 54(3), pp. 145–154. doi: 10.1136/jmedgenet-2016-104271.

Ji, X. *et al.* (2013) ‘SR Proteins Collaborate with 7SK and Promoter-Associated Nascent RNA to Release Paused Polymerase’, *Cell*. Elsevier Inc., 153(4), pp. 855–868. doi: 10.1016/j.cell.2013.04.028.

Jiang, J. *et al.* (2016) ‘Gain of Toxicity from ALS/FTD-Linked Repeat Expansions in C9ORF72 Is Alleviated by Antisense Oligonucleotides Targeting GGGGCC-Containing RNAs.’, *Neuron*. NIH Public Access, 90(3), pp. 535–50. doi: 10.1016/j.neuron.2016.04.006.

Kaczmarek, J. C., Kowalski, P. S. and Anderson, D. G. (2017) ‘Advances in the delivery of RNA therapeutics: from concept to clinical reality’, *Genome Medicine*, 9(1), p. 60. doi: 10.1186/s13073-017-0450-0.

Kalter, H. (1968) ‘Sporadic congenital malformations of newborn inbred mice’, *Teratology*, 1(2), pp. 193–199. doi: 10.1002/tera.1420010208.

Karni, R. *et al.* (2007) ‘The gene encoding the splicing factor SF2/ASF is a proto-oncogene’, *Nature Structural & Molecular Biology*, 14(3), pp. 185–193. doi: 10.1038/nsmb1209.

Kastelein, J. J. P. *et al.* (2006) ‘Potent Reduction of Apolipoprotein B and Low-Density Lipoprotein Cholesterol by Short-Term Administration of an Antisense Inhibitor of Apolipoprotein B’, *Circulation*, 114(16), pp. 1729–1735. doi: 10.1161/CIRCULATIONAHA.105.606442.

Kawahara, Y. and Mieda-Sato, A. (2012) ‘TDP-43 promotes microRNA biogenesis as a component of the Drosha and Dicer complexes.’, *Proceedings of the National Academy of Sciences of the United States of America*. National Academy of Sciences, 109(9), pp. 3347–52. doi: 10.1073/pnas.1112427109.

Khabou, H. *et al.* (2018) ‘Dosage Thresholds and Influence of Transgene Cassette in Adeno-Associated Virus-Related Toxicity’, *Human Gene Therapy*, 29(11), pp. 1235–1241. doi: 10.1089/hum.2018.144.

- Kiernan, M. C. *et al.* (2011) 'Amyotrophic lateral sclerosis', *The Lancet*, 377(9769), pp. 942–955. doi: 10.1016/S0140-6736(10)61156-7.
- Kilkenny, C. *et al.* (2013) 'Improving bioscience research reporting: The ARRIVE guidelines for reporting animal research', *Animals*. Public Library of Science, 4(1), pp. 35–44. doi: 10.3390/ani4010035.
- Koppers, M. *et al.* (2015) 'C9orf72 ablation in mice does not cause motor neuron degeneration or motor deficits', *Annals of Neurology*, 78(3), pp. 426–438. doi: 10.1002/ana.24453.
- Kotterman, M. A. *et al.* (2015) 'Antibody neutralization poses a barrier to intravitreal adeno-associated viral vector gene delivery to non-human primates', *Gene Therapy*, 22(2), pp. 116–126. doi: 10.1038/gt.2014.115.
- Kumar, D. R. *et al.* (2011) 'Jean-Martin Charcot: the father of neurology.', *Clinical medicine & research*. Marshfield Clinic, 9(1), pp. 46–9. doi: 10.3121/cmr.2009.883.
- Kvamme, E., Torgner, I. A. and Roberg, B. (1991) 'Evidence indicating that pig renal phosphate-activated glutaminase has a functionally predominant external localization in the inner mitochondrial membrane.', *The Journal of biological chemistry*, 266(20), pp. 13185–92. Available at: <http://www.ncbi.nlm.nih.gov/pubmed/2071598>.
- Kwiatkowski, T. J. *et al.* (2009) 'Mutations in the FUS/TLS Gene on Chromosome 16 Cause Familial Amyotrophic Lateral Sclerosis', *Science*, 323(5918), pp. 1205–1208. doi: 10.1126/science.1166066.
- Kwon, I. *et al.* (2014) 'Poly-dipeptides encoded by the C9orf72 repeats bind nucleoli, impede RNA biogenesis, and kill cells', *Science*, 345(6201), pp. 1139–1145. doi: 10.1126/science.1254917.
- Kwon, I. and Schaffer, D. V (2007) 'Expert Review Designer Gene Delivery Vectors: Molecular Engineering and Evolution of Adeno-Associated Viral Vectors for Enhanced Gene Transfer'. doi: 10.1007/s11095-007-9431-0.
- Lacomblez, L. *et al.* (1996) 'Dose-ranging study of riluzole in amyotrophic lateral sclerosis. Amyotrophic Lateral Sclerosis/Riluzole Study Group II.', *Lancet (London, England)*. Elsevier, 347(9013), pp. 1425–31. doi: 10.5555/URI:PII:S0140673696916803.

- Laflamme, C. *et al.* (2019) 'Implementation of an antibody characterization procedure and application to the major ALS/FTD disease gene C9ORF72', *eLife*, 8. doi: 10.7554/eLife.48363.
- Lagier-Tourenne, C. *et al.* (2012) 'Divergent roles of ALS-linked proteins FUS/TLS and TDP-43 intersect in processing long pre-mRNAs', *Nature Neuroscience*. NIH Public Access, 15(11), pp. 1488–1497. doi: 10.1038/nn.3230.
- Lagier-Tourenne, C. *et al.* (2013) 'Targeted degradation of sense and antisense C9orf72 RNA foci as therapy for ALS and frontotemporal degeneration', *Proceedings of the National Academy of Sciences*, 110(47), pp. E4530–E4539. doi: 10.1073/pnas.1318835110.
- Lagier-Tourenne, C. and Cleveland, D. W. (2009) 'Rethinking ALS: The FUS about TDP-43', *Cell*, 136(6), pp. 1001–1004. doi: 10.1016/j.cell.2009.03.006.
- Lattante, S., Rouleau, G. A. and Kabashi, E. (2013) 'TARDBP and FUS Mutations Associated with Amyotrophic Lateral Sclerosis: Summary and Update', *Human Mutation*, 34(6), pp. 812–826. doi: 10.1002/humu.22319.
- Lee, S.-H. *et al.* (2016) 'The splicing factor SRSF1 modulates pattern formation by inhibiting transcription of tissue specific genes during embryogenesis', *Biochemical and Biophysical Research Communications*, 477(4), pp. 1011–1016. doi: 10.1016/j.bbrc.2016.07.021.
- Lee, Y.-B. *et al.* (2013) 'Hexanucleotide Repeats in ALS/FTD Form Length-Dependent RNA Foci, Sequester RNA Binding Proteins, and Are Neurotoxic', *Cell Reports*. Elsevier, 5(5), pp. 1178–1186. doi: 10.1016/j.celrep.2013.10.049.
- Lehmer, C. *et al.* (2017) 'Poly- <scp>GP</scp> in cerebrospinal fluid links C9orf72 - associated dipeptide repeat expression to the asymptomatic phase of <scp>ALS</scp> / <scp>FTD</scp>', *EMBO Molecular Medicine*, 9(7), pp. 859–868. doi: 10.15252/emmm.201607486.
- Leone, P. *et al.* (2012) 'Long-Term Follow-Up After Gene Therapy for Canavan Disease', *Science Translational Medicine*, 4(165). doi: 10.1126/scitranslmed.3003454.
- Lewis, S. A., Lee, M. G. and Cowan, N. J. (1985) 'Five mouse tubulin isotypes and their regulated expression during development.', *The Journal of Cell Biology*, 101(3), pp. 852–861. doi: 10.1083/jcb.101.3.852.

- Li, Chengwan. *et al.* (2009) 'Cellular immune response to cryptic epitopes during therapeutic gene transfer', *Proceedings of the National Academy of Sciences*, 106(26), pp. 10770–10774. doi: 10.1073/pnas.0902269106.
- Li, Chengwen *et al.* (2009) 'Cytotoxic-T-Lymphocyte-Mediated Elimination of Target Cells Transduced with Engineered Adeno-Associated Virus Type 2 Vector In Vivo', *Journal of Virology*, 83(13), pp. 6817–6824. doi: 10.1128/JVI.00278-09.
- Lin, S. *et al.* (2005) 'Dephosphorylation-Dependent Sorting of SR Splicing Factors during mRNP Maturation', *Molecular Cell*, 20(3), pp. 413–425. doi: 10.1016/j.molcel.2005.09.015.
- Ling, S.-C. *et al.* (2010) 'ALS-associated mutations in TDP-43 increase its stability and promote TDP-43 complexes with FUS/TLS.', *Proceedings of the National Academy of Sciences of the United States of America*. National Academy of Sciences, 107(30), pp. 13318–23. doi: 10.1073/pnas.1008227107.
- Liu-Yesucevitz, L. *et al.* (2014) 'ALS-Linked Mutations Enlarge TDP-43-Enriched Neuronal RNA Granules in the Dendritic Arbor', *Journal of Neuroscience*, 34(12), pp. 4167–4174. doi: 10.1523/JNEUROSCI.2350-13.2014.
- Liu, E. Y. *et al.* (2014) 'C9orf72 hypermethylation protects against repeat expansion-associated pathology in ALS/FTD', *Acta Neuropathol*, 3, pp. 525–541. doi: 10.1007/s00401-014-1286-y.
- Liu, H.-S. *et al.* (1999) 'Is Green Fluorescent Protein Toxic to the Living Cells?', *Biochemical and Biophysical Research Communications*, 260(3), pp. 712–717. doi: 10.1006/bbrc.1999.0954.
- Liu, Y., Pattamatta, A., Zu, T., Borchelt, D. R., *et al.* (2016) 'C9orf72 BAC Mouse Model with Motor Deficits and Article C9orf72 BAC Mouse Model with Motor Deficits and Neurodegenerative Features of ALS/FTD', *Neuron*, 90(3), pp. 521–34. doi: 10.1016/j.neuron.2016.04.005.
- Liu, Y., Pattamatta, A., Zu, T., Reid, T., Bardhi, O., Borchelt, David R., *et al.* (2016) 'C9orf72 BAC Mouse Model with Motor Deficits and Neurodegenerative Features of ALS/FTD', *Neuron*, 90(3), pp. 521–534. doi: 10.1016/j.neuron.2016.04.005.
- Liu, Y., Pattamatta, A., Zu, T., Reid, T., Bardhi, O., Borchelt, David R., *et al.* (2016) 'C9orf72 BAC Mouse Model with Motor Deficits and Neurodegenerative Features of ALS/FTD',

*Neuron*. Elsevier Inc., 90(3), pp. 521–534. doi: 10.1016/j.neuron.2016.04.005.

Liu, Y. *et al.* (2021) ‘Variant-selective stereopure oligonucleotides protect against pathologies associated with C9orf72-repeat expansion in preclinical models’, *Nature Communications*, 12(1), p. 847. doi: 10.1038/s41467-021-21112-8.

Lock, M. *et al.* (2010) ‘Characterization of a Recombinant Adeno-Associated Virus Type 2 Reference Standard Material’, *Human Gene Therapy*, 21(10), pp. 1273–1285. doi: 10.1089/hum.2009.223.

Long, J. C. and Caceres, J. F. (2009) ‘The SR protein family of splicing factors: master regulators of gene expression’, *Biochemical Journal*, 417(1), pp. 15–27. doi: 10.1042/BJ20081501.

Lu, L. *et al.* (2009) ‘Amyotrophic Lateral Sclerosis-linked Mutant SOD1 Sequesters Hu Antigen R (HuR) and TIA-1-related Protein (TIAR)’, *Journal of Biological Chemistry*, 284(49), pp. 33989–33998. doi: 10.1074/jbc.M109.067918.

Lukashchuk, V. *et al.* (2016) ‘AAV9-mediated central nervous system–targeted gene delivery via cisterna magna route in mice’, *Molecular Therapy - Methods & Clinical Development*, 3(July 2015), p. 15055. doi: 10.1038/mtm.2015.55.

Mackenzie, I. R. A., Rademakers, R. and Neumann, M. (2010) ‘TDP-43 and FUS in amyotrophic lateral sclerosis and frontotemporal dementia’, *The Lancet Neurology*. Elsevier, 9(10), pp. 995–1007. doi: 10.1016/S1474-4422(10)70195-2.

Mackenzie, I. R. and Rademakers, R. (2008) ‘The role of transactive response DNA-binding protein-43 in amyotrophic lateral sclerosis and frontotemporal dementia’, *Current Opinion in Neurology*. NIH Public Access, 21(6), pp. 693–700. doi: 10.1097/WCO.0b013e3283168d1d.

Maguire, C. A. *et al.* (2013) ‘Mouse Gender Influences Brain Transduction by Intravascularly Administered AAV9’, *Molecular Therapy*, 21(8), pp. 1470–1471. doi: 10.1038/mt.2013.95.

Majounie, E., Renton, A. E., *et al.* (2012) ‘Frequency of the C9orf72 hexanucleotide repeat expansion in patients with amyotrophic lateral sclerosis and frontotemporal dementia: a cross-sectional study’, *The Lancet Neurology*, 11(4), pp. 323–330. doi: 10.1016/S1474-4422(12)70043-1.

- Majounie, E., Abramzon, Y., *et al.* (2012) 'Repeat Expansion in C9ORF72 in Alzheimer's Disease', *New England Journal of Medicine*, 366(3), pp. 283–284. doi: 10.1056/NEJMc1113592.
- Masrori, P. and Van Damme, P. (2020) 'Amyotrophic Lateral Sclerosis: A Clinical Review', *European Journal of Neurology*, 10, pp. 1918-1929. doi: 10.1111/ene.14393
- Mara Gaudette, Makito Hirano, Teepu Siddique (2000) 'Current status of SOD1 mutations in familial amyotrophic lateral sclerosis', *Amyotrophic Lateral Sclerosis and Other Motor Neuron Disorders*. Taylor & Francis, 1(2), pp. 83–89. doi: 10.1080/14660820050515377.
- Martin, J. *et al.* (2013) 'Generation and Characterization of Adeno-Associated Virus Producer Cell Lines for Research and Preclinical Vector Production', *Human Gene Therapy Methods*, 24(4), pp. 253–269. doi: 10.1089/hgtb.2013.046.
- McCarty, D. *et al.* (2003) 'Adeno-associated virus terminal repeat (TR) mutant generates self-complementary vectors to overcome the rate-limiting step to transduction in vivo', *Gene Therapy*, 10, pp. 2112–2118. doi: 10.1038/sj.gt.3302134.
- McCarty, D. M. (2008) 'Self-complementary AAV Vectors; Advances and Applications', *Molecular Therapy*. Cell Press, 16(10), pp. 1648–1656. doi: 10.1038/MT.2008.171.
- McCarty, D., Monahan, P. and Samulski, R. (2001) 'Self-complementary recombinant adeno-associated virus (scAAV) vectors promote efficient transduction independently of DNA synthesis', *Gene Therapy*. Nature Publishing Group, 8(16), pp. 1248–1254. doi: 10.1038/sj.gt.3301514.
- McDermott, C. J. and Shaw, P. J. (2008) 'Diagnosis and management of motor neurone disease.', *BMJ (Clinical research ed.)*. BMJ Publishing Group, 336(7645), pp. 658–62. doi: 10.1136/bmj.39493.511759.BE.
- Mendell, J. R. *et al.* (2017) 'Single-Dose Gene-Replacement Therapy for Spinal Muscular Atrophy', *New England Journal of Medicine*, 377(18), pp. 1713–1722. doi: 10.1056/NEJMoa1706198.
- Miller, T. *et al.* (2020) 'Phase 1–2 Trial of Antisense Oligonucleotide Tofersen for SOD1 ALS', *New England Journal of Medicine*, 383(2), pp. 109–119. doi: 10.1056/NEJMoa2003715.
- Miller, T. M. *et al.* (2013) 'An antisense oligonucleotide against SOD1 delivered intrathecally

for patients with SOD1 familial amyotrophic lateral sclerosis: A phase 1, randomised, first-in-man study', *The Lancet Neurology*, 12(5), pp. 435–442. doi: 10.1016/S1474-4422(13)70061-9.

Mitchell, J. C. *et al.* (2013) 'Overexpression of human wild-type FUS causes progressive motor neuron degeneration in an age- and dose-dependent fashion', *Acta Neuropathologica*, 125(2), pp. 273–288. doi: 10.1007/s00401-012-1043-z.

Mizielinska, S. *et al.* (2013) 'C9orf72 frontotemporal lobar degeneration is characterised by frequent neuronal sense and antisense RNA foci', *Acta Neuropathol*, 3, pp. 845–857. doi: 10.1007/s00401-013-1200-z.

Mizielinska, S. *et al.* (2014) 'C9orf72 repeat expansions cause neurodegeneration in *Drosophila* through arginine-rich proteins', *Science*, 345(6201), pp. 1192–1194. doi: 10.1126/science.1256800.

Moiani, A. *et al.* (2012) 'Lentiviral vector integration in the human genome induces alternative splicing and generates aberrant transcripts', *Journal of Clinical Investigation*, 122(5), pp. 1653–1666. doi: 10.1172/JCI61852.

Mordes, D. A. *et al.* (2020) 'Absence of Survival and Motor Deficits in 500 Repeat C9ORF72 BAC Mice', *Neuron*, 108(4), pp. 775-783.e4. doi: 10.1016/j.neuron.2020.08.009.

Mori, Kohji, Arzberger, T., *et al.* (2013) 'Bidirectional transcripts of the expanded C9orf72 hexanucleotide repeat are translated into aggregating dipeptide repeat proteins', *Acta Neuropathologica*, 126(6), pp. 881–893. doi: 10.1007/s00401-013-1189-3.

Mori, Kohji, Weng, S.-M., *et al.* (2013) 'The C9orf72 GGGGCC repeat is translated into aggregating dipeptide-repeat proteins in FTLD/ALS.', *Science (New York, N.Y.)*. American Association for the Advancement of Science, 339(6125), pp. 1335–8. doi: 10.1126/science.1232927.

Mori, K. *et al.* (2013) 'The C9orf72 GGGGCC Repeat Is Translated into Aggregating Dipeptide-Repeat Proteins in FTLD/ALS', *Science*, 339(6125), pp. 1335–1338. doi: 10.1126/science.1232927.

Mori, S. *et al.* (2008) 'Brief Report Tissue distribution of cynomolgus adeno-associated viruses AAV10, AAV11, and AAVcy.7 in naturally infected monkeys', *Arch Virol*, 153, pp.

375–380. doi: 10.1007/s00705-007-1097-8.

Morlando, M. *et al.* (2012) ‘FUS stimulates microRNA biogenesis by facilitating co-transcriptional Drosha recruitment’, *The EMBO Journal*, 31(24), pp. 4502–4510. doi: 10.1038/emboj.2012.319.

Van Mossevelde, S. *et al.* (2017) ‘Relationship between C9orf72 repeat size and clinical phenotype’, *Current Opinion in Genetics & Development*. Elsevier Current Trends, 44, pp. 117–124. doi: 10.1016/J.GDE.2017.02.008.

Moulton, V. R. *et al.* (2015) ‘Serine Arginine-Rich Splicing Factor 1 (SRSF1) Contributes to the Transcriptional Activation of CD3 $\zeta$  in Human T Cells’, *PLOS ONE*. Edited by S.-N. Liossis, 10(7), p. e0131073. doi: 10.1371/journal.pone.0131073.

Mueller, C. *et al.* (2020) ‘SOD1 Suppression with Adeno-Associated Virus and MicroRNA in Familial ALS’, *New England Journal of Medicine*, 383(2), pp. 151–158. doi: 10.1056/NEJMoa2005056.

Müller-Mcnicoll, M. *et al.* (2016) ‘SR proteins are NXF1 adaptors that link alternative RNA processing to mRNA export’. doi: 10.1101/gad.276477.

Murphy, S. L. *et al.* (2009) ‘Diverse IgG Subclass Responses to Adeno-Associated Virus Infection and Vector Administration’, *Journal of Medical Virology*, 81, pp. 65–74. doi: 10.1002/jmv.21360.

Nakaya, T. *et al.* (2013) ‘FUS regulates genes coding for RNA-binding proteins in neurons by binding to their highly conserved introns’, *RNA*, 19(4), pp. 498–509. doi: 10.1261/rna.037804.112.

Naldini, L. *et al.* (1996) ‘In Vivo Gene Delivery and Stable Transduction of Nondividing Cells by a Lentiviral Vector’, *Science*, 272(5259), pp. 263–267. doi: 10.1126/science.272.5259.263.

Nathwani, A. C. *et al.* (2011) ‘Adenovirus-Associated Virus Vector–Mediated Gene Transfer in Hemophilia B’, *New England Journal of Medicine*, 365(25), pp. 2357–2365. doi: 10.1056/NEJMoa1108046.

Nathwani, A. C. *et al.* (2014a) ‘Long-Term Safety and Efficacy of Factor IX Gene Therapy in Hemophilia B’, *New England Journal of Medicine*. NIH Public Access, 371(21), pp. 1994–

2004. doi: 10.1056/NEJMoa1407309.

Nathwani, A. C. *et al.* (2014b) ‘Long-Term Safety and Efficacy of Factor IX Gene Therapy in Hemophilia B’, *New England Journal of Medicine*, 371(21), pp. 1994–2004. doi: 10.1056/NEJMoa1407309.

Neumann, M. *et al.* (2006) ‘Ubiquitinated TDP-43 in frontotemporal lobar degeneration and amyotrophic lateral sclerosis.’, *Science (New York, N.Y.)*. American Association for the Advancement of Science, 314(5796), pp. 130–3. doi: 10.1126/science.1134108.

Nguyen, L. *et al.* (2020) ‘Survival and Motor Phenotypes in FVB C9-500 ALS/FTD BAC Transgenic Mice Reproduced by Multiple Labs’, *Neuron*, 108(4), pp. 784-796.e3. doi: 10.1016/j.neuron.2020.09.009.

NICE (2018) *Final evaluation determination – Strimvelis for treating adenosine deaminase deficiency–severe combined immunodeficiency Strimvelis for treating adenosine deaminase deficiency–severe combined immunodeficiency 1 Recommendations*. Available at: <https://www.nice.org.uk/guidance/gid-hst10005/documents/final-evaluation-determination-document> (Accessed: 12 January 2018).

Nieuwenhuis, B. *et al.* (2021) ‘Optimization of adeno-associated viral vector-mediated transduction of the corticospinal tract: comparison of four promoters’, *Gene Therapy*, 28(1–2), pp. 56–74. doi: 10.1038/s41434-020-0169-1.

Nonaka, T. *et al.* (2013) ‘Prion-like Properties of Pathological TDP-43 Aggregates from Diseased Brains’, *Cell Reports*, 4(1), pp. 124–134. doi: 10.1016/j.celrep.2013.06.007.

O’Rourke, J. G. *et al.* (2015) ‘C9orf72 BAC Transgenic Mice Display Typical Pathologic Features of ALS/FTD.’, *Neuron*. NIH Public Access, 88(5), pp. 892–901. doi: 10.1016/j.neuron.2015.10.027.

O’Rourke, J. G. *et al.* (2016) ‘C9orf72 is required for proper macrophage and microglial function in mice’, *Science*, 351(6279), pp. 1324–1329. doi: 10.1126/science.aaf1064.

ORourke, J. G. *et al.* (2016) ‘C9orf72 is required for proper macrophage and microglial function in mice’, *Science*, 351(6279), pp. 1324–1329. doi: 10.1126/science.aaf1064.

Palaschak, B. *et al.* (2017) ‘An Immune-Competent Murine Model to Study Elimination of

AAV-Transduced Hepatocytes by Capsid-Specific CD8+ T Cells', *Molecular Therapy - Methods and Clinical Development*. Elsevier Ltd., 5(June), pp. 142–152. doi: 10.1016/j.omtm.2017.04.004.

Parone, P. A. *et al.* (2013) 'Enhancing Mitochondrial Calcium Buffering Capacity Reduces Aggregation of Misfolded SOD1 and Motor Neuron Cell Death without Extending Survival in Mouse Models of Inherited Amyotrophic Lateral Sclerosis', *Journal of Neuroscience*, 33(11), pp. 4657–4671. doi: 10.1523/JNEUROSCI.1119-12.2013.

Pasinelli, P. *et al.* (1998) 'Caspase-1 is activated in neural cells and tissue with amyotrophic lateral sclerosis-associated mutations in copper-zinc superoxide dismutase.', *Proceedings of the National Academy of Sciences of the United States of America*, 95(26), pp. 15763–8. Available at: <http://www.ncbi.nlm.nih.gov/pubmed/9861044> (Accessed: 14 December 2017).

Peters, O. M. *et al.* (2015) 'Human C9ORF72 Hexanucleotide Expansion Reproduces RNA Foci and Dipeptide Repeat Proteins but Not Neurodegeneration in BAC Transgenic Mice', *Neuron*, 88(5), pp. 902–909. doi: 10.1016/j.neuron.2015.11.018.

Pien, G. C. *et al.* (2009) 'Capsid antigen presentation flags human hepatocytes for destruction after transduction by adeno-associated viral vectors', *Journal of Clinical Investigation*, 119(6), pp. 1688–1695. doi: 10.1172/JCI36891.

Pillay, S. *et al.* (2017) 'Adeno-associated Virus (AAV) Serotypes Have Distinctive Interactions with Domains of the Cellular AAV Receptor', *Journal of Virology*. Edited by L. Banks. American Society for Microbiology (ASM), 91(18). doi: 10.1128/JVI.00391-17.

Prudencio, M. *et al.* (2015) 'Distinct brain transcriptome profiles in C9orf72-associated and sporadic ALS', *Nature Neuroscience*, 18(8), pp. 1175–1182. doi: 10.1038/nn.4065.

Quaegebeur, A. *et al.* (2020) 'Soluble and insoluble dipeptide repeat protein measurements in C9orf72-frontotemporal dementia brains show regional differential solubility and correlation of poly-GR with clinical severity', *Acta Neuropathologica Communications*, 8(1), p. 184. doi: 10.1186/s40478-020-01036-y.

Ralph, G. S. *et al.* (2005) 'Silencing mutant SOD1 using RNAi protects against neurodegeneration and extends survival in an ALS model', *Nature Medicine*, 11(43), pp. 429–433. doi: 10.1038/nm1205.

- Ramanujan, S. A. *et al.* (2021) 'Estrogen-Induced hsa-miR-10b-5p Is Elevated in T Cells From Patients With Systemic Lupus Erythematosus and Down-Regulates Serine/Arginine-Rich Splicing Factor 1', *Arthritis and Rheumatology*, 73(11), pp. 2052–2058. doi: 10.1002/art.41787.
- Raoul, C. *et al.* (2005) 'Lentiviral-mediated silencing of SOD1 through RNA interference retards disease onset and progression in a mouse model of ALS', *Nature Medicine*, 11(43), pp. 423–428. doi: 10.1038/nm1207.
- Reddy, K. *et al.* (2013) 'The Disease-associated r(GGGGCC)<sub>n</sub> Repeat from the *C9orf72* Gene Forms Tract Length-dependent Uni- and Multimolecular RNA G-quadruplex Structures', *Journal of Biological Chemistry*, 288(14), pp. 9860–9866. doi: 10.1074/jbc.C113.452532.
- Renton, Alan E. *et al.* (2011a) 'A hexanucleotide repeat expansion in C9ORF72 is the cause of chromosome 9p21-linked ALS-FTD.', *Neuron*. NIH Public Access, 72(2), pp. 257–68. doi: 10.1016/j.neuron.2011.09.010.
- Renton, Alan E. *et al.* (2011) 'A Hexanucleotide Repeat Expansion in C9ORF72 Is the Cause of Chromosome 9p21-Linked ALS-FTD', *Neuron*, 72(2), pp. 257–268. doi: 10.1016/j.neuron.2011.09.010.
- Renton, Alan E. *et al.* (2011b) 'A Hexanucleotide Repeat Expansion in C9ORF72 Is the Cause of Chromosome 9p21-Linked ALS-FTD', *Neuron*, 72(2), pp. 257–268. doi: 10.1016/j.neuron.2011.09.010.
- Ringholz, G. M. *et al.* (2005) 'Prevalence and patterns of cognitive impairment in sporadic ALS', *Neurology*, 65(4), pp. 586–590. doi: 10.1212/01.wnl.0000172911.39167.b6.
- Rogelj, B. *et al.* (2012) 'Widespread binding of FUS along nascent RNA regulates alternative splicing in the brain', *Scientific Reports*. Nature Publishing Group, 2(1), p. 603. doi: 10.1038/srep00603.
- Rogers, G. L. *et al.* (2017) 'Plasmacytoid and conventional dendritic cells cooperate in crosspriming AAV capsid-specific CD8+ T cells', *Blood*, 129(24), pp. 3184–3195. doi: 10.1182/blood-2016-11-751040.
- Rohr, U.-P. *et al.* (2002) 'Fast and reliable titration of recombinant adeno-associated virus

type-2 using quantitative real-time PCR', *Journal of Virological Methods*, 106(1), pp. 81–88. doi: 10.1016/S0166-0934(02)00138-6.

Rohr, U. P. *et al.* (2002) 'Fast and reliable titration of recombinant adeno-associated virus type-2 using quantitative real-time PCR', *Journal of Virological Methods*. Elsevier, 106(1), pp. 81–88. doi: 10.1016/S0166-0934(02)00138-6.

Rohrer, J. D. *et al.* (2015) 'C9orf72 expansions in frontotemporal dementia and amyotrophic lateral sclerosis.', *The Lancet. Neurology*. Elsevier, 14(3), pp. 291–301. doi: 10.1016/S1474-4422(14)70233-9.

Rooney, J. *et al.* (2017) 'C9orf72 expansion differentially affects males with spinal onset amyotrophic lateral sclerosis', *Journal of Neurology, Neurosurgery & Psychiatry*, 88(4), pp. 281.1-281. doi: 10.1136/jnnp-2016-314093.

Rosen, D. R. *et al.* (1993) 'Mutations in Cu/Zn superoxide dismutase gene are associated with familial amyotrophic lateral sclerosis', *Nature*, 362(6415), pp. 59–62. doi: 10.1038/362059a0.

Rothstein, J. D. (2017) 'Edaravone: A new drug approved for ALS', *Cell*. Cell Press, 171(4), p. 725. doi: 10.1016/J.CELL.2017.10.011.

Rutherford, N. J. *et al.* (2012) 'Negative results Length of normal alleles of C9ORF72 GGGGCC repeat do not influence disease phenotype', *Neurobiology of Aging*, 33, p. 2950. doi: 10.1016/j.neurobiolaging.2012.07.005.

Samulski, R. J. and Muzyczka, N. (2014) 'AAV-Mediated Gene Therapy for Research and Therapeutic Purposes', *Annual Review of Virology*. doi: 10.1146/annurev-virology-031413-085355.

Saraiva, J., Nobre, R. J. and Pereira de Almeida, L. (2016) 'Gene therapy for the CNS using AAVs: The impact of systemic delivery by AAV9', *Journal of Controlled Release*. Elsevier, 241, pp. 94–109. doi: 10.1016/J.JCONREL.2016.09.011.

Sareen, D. *et al.* (2013) 'Targeting RNA Foci in iPSC-Derived Motor Neurons from ALS Patients with a C9ORF72 Repeat Expansion', *Science Translational Medicine*. NIH Public Access, 5(208), p. 208ra149. doi: 10.1126/scitranslmed.3007529.

Sawada, H. (2017) 'Clinical efficacy of edaravone for the treatment of amyotrophic lateral

sclerosis', *Expert Opinion on Pharmacotherapy*. Taylor & Francis, 18(7), pp. 735–738. doi: 10.1080/14656566.2017.1319937.

Scarrott, J. (2019) *Investigating The Specificity of RNAi Molecules in Human Gene Therapy for SOD1-Linked Familial Amyotrophic lateral sclerosis*. The University of Sheffield.

Schnödt, M. *et al.* (2016) 'DNA Minicircle Technology Improves Purity of Adeno-associated Viral Vector Preparations', *Molecular Therapy - Nucleic Acids*, 5, p. e355. doi: 10.1038/mtna.2016.60.

Scotter, E. L., Chen, H.-J. and Shaw, C. E. (2015) 'TDP-43 Proteinopathy and ALS: Insights into Disease Mechanisms and Therapeutic Targets', *Neurotherapeutics*, 12(2), pp. 352–363. doi: 10.1007/s13311-015-0338-x.

Sellier, C. *et al.* (2016) 'Loss of C9ORF72 impairs autophagy and synergizes with polyQ Ataxin-2 to induce motor neuron dysfunction and cell death', *The EMBO Journal*, 35, pp. 1276–1297. doi: 10.15252/emj.201593350.

Shang, Y. and Huang, E. J. (2016) 'Mechanisms of FUS mutations in familial amyotrophic lateral sclerosis', *Brain Research*. Elsevier, 1647, pp. 65–78. doi: 10.1016/J.BRAINRES.2016.03.036.

Shen, S. *et al.* (2011) 'Terminal N-Linked Galactose Is the Primary Receptor for Adeno-associated Virus 9', *Journal of Biological Chemistry*, 286(15), pp. 13532–13540. doi: 10.1074/jbc.M110.210922.

Shirley, J. L. *et al.* (2020) 'Type I IFN Sensing by cDCs and CD4+ T Cell Help Are Both Requisite for Cross-Priming of AAV Capsid-Specific CD8+ T Cells', *Molecular Therapy*, 28(3), pp. 758–770. doi: 10.1016/j.ymthe.2019.11.011.

Siddique, T. and Ajroud-Driss, S. (2011) 'Familial amyotrophic lateral sclerosis, a historical perspective.', *Acta Myologica*. Pacini Editore, 30(2), pp. 117–20. Available at: <http://www.ncbi.nlm.nih.gov/pubmed/22106714> (Accessed: 27 December 2017).

Sinangil, F., Loyter, A. and Volsky, D. J. (1988) 'Quantitative measurement of fusion between human immunodeficiency virus and cultured cells using membrane fluorescence dequenching', *Elsevier Science Publishers (Biomedical Division)*, 239(1), pp. 88–92.

Smith, R. S., Roderick, T. H. and Sundberg, J. P. (1994) 'Microphthalmia and associated abnormalities in inbred black mice.', *Laboratory Animal Science*, 44(6), pp. 551–60. Available at: <http://www.ncbi.nlm.nih.gov/pubmed/7898027>.

Sreedharan, J. *et al.* (2008) 'TDP-43 Mutations in Familial and Sporadic Amyotrophic Lateral Sclerosis', *Science*, 319(5870), pp. 1668–1672. doi: 10.1126/science.1154584.

Srinivasan, E. and Rajasekaran, R. (2020) 'A Systematic and Comprehensive Review on Disease-Causing Genes in Amyotrophic Lateral Sclerosis', *Journal of Molecular Neuroscience*, 70(11), pp. 1742–1770. doi: 10.1007/s12031-020-01569-w.

Srivastava, A., Lusby, E. W. and Berns, K. I. (1983) 'Nucleotide sequence and organization of the adeno-associated virus 2 genome', *Journal of Virology*. American Society for Microbiology (ASM), 45(2), pp. 555–564. doi: 10.1128/jvi.45.2.555-564.1983.

Stein, B. S. *et al.* (1987) 'pH-independent HIV entry into CD4-positive T cells via virus envelope fusion to the plasma membrane', *Cell*, 49(5), pp. 659–668. doi: 10.1016/0092-8674(87)90542-3.

Stender, S. *et al.* (2007) 'Adeno-associated viral vector transduction of human mesenchymal stem cells', *European Cells and Materials*, 13, pp. 93–99. doi: 10.22203/eCM.v013a10.

Storkebaum, E. *et al.* (2011) 'Cerebrovascular disorders: molecular insights and therapeutic opportunities', *Nature Neuroscience*, 14(11), pp. 1390–1397. doi: 10.1038/nn.2947.

Sufit, R. L. *et al.* (2017) 'Open label study to assess the safety of VM202 in subjects with amyotrophic lateral sclerosis', *Amyotrophic Lateral Sclerosis and Frontotemporal Degeneration*, 18(3–4), pp. 269–278. doi: 10.1080/21678421.2016.1259334.

Taniue, K. and Akimitsu, N. (2021) 'The Functions and Unique Features of LncRNAs in Cancer Development and Tumorigenesis', *International Journal of Molecular Sciences*, 22(2), p. 632. doi: 10.3390/ijms22020632.

Tao, Z. *et al.* (2015) 'Nucleolar stress and impaired stress granule formation contribute to C9orf72 RAN translation-induced cytotoxicity', *Human Molecular Genetics*, 24(9), pp. 2426–2441. doi: 10.1093/hmg/ddv005.

Tardieu, M. *et al.* (2014) 'Intracerebral Administration of Adeno-Associated Viral Vector

- Serotype rh.10 Carrying Human SGSH and SUMF1 cDNAs in Children with Mucopolysaccharidosis Type IIIA Disease: Results of a Phase I/II Trial', *Human Gene Therapy*, 25(6), pp. 506–516. doi: 10.1089/hum.2013.238.
- Thomsen, G. M. *et al.* (2014) 'Delayed Disease Onset and Extended Survival in the SOD1G93A Rat Model of Amyotrophic Lateral Sclerosis after Suppression of Mutant SOD1 in the Motor Cortex', *Journal of Neuroscience*, 34(47), pp. 15587–15600. doi: 10.1523/JNEUROSCI.2037-14.2014.
- Tintaru, A. M. *et al.* (2007) 'Structural and functional analysis of RNA and TAP binding to SF2/ASF', *EMBO Reports*, 8(8), pp. 756–762. doi: 10.1038/sj.embor.7401031.
- Tran, H. *et al.* (2015) 'Differential Toxicity of Nuclear RNA Foci versus Dipeptide Repeat Proteins in a Drosophila Model of C9ORF72 FTD/ALS', *Neuron*. Elsevier, 87(6), pp. 1207–1214. doi: 10.1016/j.neuron.2015.09.015.
- Trias, E. *et al.* (2016) 'Post-paralysis tyrosine kinase inhibition with masitinib abrogates neuroinflammation and slows disease progression in inherited amyotrophic lateral sclerosis', *Journal of Neuroinflammation*, 13(1), p. 177. doi: 10.1186/s12974-016-0620-9.
- Trinchieri, G. (2007) 'Interleukin-10 production by effector T cells: Th1 cells show self control', *Journal of Experimental Medicine*, 204(2), pp. 239–243. doi: 10.1084/jem.20070104.
- Turturro, A. *et al.* (1999) 'Growth Curves and Survival Characteristics of the Animals Used in the Biomarkers of Aging Program', *The Journals of Gerontology Series A: Biological Sciences and Medical Sciences*, 54(11), pp. B492–B501. doi: 10.1093/gerona/54.11.B492.
- Vance, C. *et al.* (2009) 'Mutations in FUS, an RNA Processing Protein, Cause Familial Amyotrophic Lateral Sclerosis Type 6', *Science*, 323(5918), pp. 1208–1211. doi: 10.1126/science.1165942.
- Vanoni, C. *et al.* (2004) 'Increased internalisation and degradation of GLT-1 glial glutamate transporter in a cell model for familial amyotrophic lateral sclerosis (ALS)', *Journal of Cell Science*, 117(22), pp. 5417–5426. doi: 10.1242/jcs.01411.
- Viphakone, N. *et al.* (2012) 'TREX exposes the Rna-binding domain of nxf1 to enable mRna export'. doi: 10.1038/ncomms2005.

- Wagner, K.-D. *et al.* (2019) ‘Altered VEGF Splicing Isoform Balance in Tumor Endothelium Involves Activation of Splicing Factors Srpk1 and Srsf1 by the Wilms’ Tumor Suppressor Wt1’, *Cells*, 8(1), p. 41. doi: 10.3390/cells8010041.
- Walker, A. K. *et al.* (2013) ‘ALS-Associated TDP-43 Induces Endoplasmic Reticulum Stress, Which Drives Cytoplasmic TDP-43 Accumulation and Stress Granule Formation’, *PLoS ONE*. Edited by W. Le, 8(11), p. e81170. doi: 10.1371/journal.pone.0081170.
- Walsh, M. J. *et al.* (2015) ‘Invited Review: Decoding the pathophysiological mechanisms that underlie RNA dysregulation in neurodegenerative disorders: a review of the current state of the art’, *Neuropathology and Applied Neurobiology*, 41(2), pp. 109–134. doi: 10.1111/nan.12187.
- Wang, L. *et al.* (2007) ‘Cross-Presentation of Adeno-Associated Virus Serotype 2 Capsids Activates Cytotoxic T Cells But Does Not Render Hepatocytes Effective Cytolytic Targets’, *Human Gene Therapy*, 18(3), pp. 185–194. doi: 10.1089/hum.2007.001.
- Wang, L. *et al.* (2010) ‘The Pleiotropic Effects of Natural AAV Infections on Liver-directed Gene Transfer in Macaques’, *Molecular Therapy*, 18(1), pp. 126–134. doi: 10.1038/mt.2009.245.
- Wang, L. *et al.* (2012) ‘Hepatic Gene Transfer in Neonatal Mice by Adeno-Associated Virus Serotype 8 Vector’, *Human Gene Therapy*, 23(5), pp. 533–539. doi: 10.1089/hum.2011.183.
- Webster, C. P. *et al.* (2016) ‘The C9orf72 protein interacts with Rab1a and the ULK1 complex to regulate initiation of autophagy’, *The EMBO Journal*, 35(15), pp. 1656–1676. doi: 10.15252/emj.201694401.
- Wen, X. *et al.* (2014) ‘Antisense Proline-Arginine RAN Dipeptides Linked to C9ORF72-ALS/FTD Form Toxic Nuclear Aggregates that Initiate In Vitro and In Vivo Neuronal Death’, *Neuron*. Cell Press, 84(6), pp. 1213–1225. doi: 10.1016/J.NEURON.2014.12.010.
- Wong, P. C. *et al.* (1995) ‘An adverse property of a familial ALS-linked SOD1 mutation causes motor neuron disease characterized by vacuolar degeneration of mitochondria.’, *Neuron*, 14(6), pp. 1105–16. Available at: <http://www.ncbi.nlm.nih.gov/pubmed/7605627> (Accessed: 4 January 2018).
- Wright, J. F. and Zelenia, O. (2011) ‘Vector Characterization Methods for Quality Control Testing of Recombinant Adeno-Associated Viruses’, in *Viral Vectors for Gene Therapy*, pp.

247–278. doi: 10.1007/978-1-61779-095-9\_11.

Wu, H. *et al.* (2010) ‘A Splicing-Independent Function of SF2/ASF in MicroRNA Processing’, *Molecular Cell*, 38(1), pp. 67–77. doi: 10.1016/j.molcel.2010.02.021.

Xi, Z. *et al.* (2013) ‘Hypermethylation of the CpG Island Near the G4C2 Repeat in ALS with a C9orf72 Expansion’, *The American Journal of Human Genetics*, 92(6), pp. 981–989. doi: 10.1016/j.ajhg.2013.04.017.

Xi, Z. *et al.* (2014) ‘Hypermethylation of the CpG-island near the C9orf72 G4C2-repeat expansion in FTLN patients’, *Human Molecular Genetics*, 23(21), pp. 5630–5637. doi: 10.1093/hmg/ddu279.

Xiao, S. *et al.* (2015) ‘Isoform-specific antibodies reveal distinct subcellular localizations of <scp>C</scp> 9orf72 in amyotrophic lateral sclerosis’, *Annals of Neurology*, 78(4), pp. 568–583. doi: 10.1002/ana.24469.

Xie, Q. *et al.* (2002) ‘The atomic structure of adeno-associated virus (AAV-2), a vector for human gene therapy’, *Proceedings of the National Academy of Sciences*, 99(16), pp. 10405–10410. doi: 10.1073/pnas.162250899.

Xu, X., Yang, D., Ding, J. H., *et al.* (2005) ‘ASF/SF2-Regulated CaMKII $\delta$  Alternative Splicing Temporally Reprograms Excitation-Contraction Coupling in Cardiac Muscle’, *Cell*. Cell Press, 120(1), pp. 59–72. doi: 10.1016/J.CELL.2004.11.036.

Xu, X., Yang, D., Ding, J.-H., *et al.* (2005a) ‘ASF/SF2-Regulated CaMKII $\delta$  Alternative Splicing Temporally Reprograms Excitation-Contraction Coupling in Cardiac Muscle’, *Cell*, 120(1), pp. 59–72. doi: 10.1016/j.cell.2004.11.036.

Xu, X., Yang, D., Ding, J.-H., *et al.* (2005b) ‘ASF/SF2-Regulated CaMKII $\delta$  Alternative Splicing Temporally Reprograms Excitation-Contraction Coupling in Cardiac Muscle’, *Cell*. Cell Press, 120(1), pp. 59–72. doi: 10.1016/J.CELL.2004.11.036.

Yokoi, K. *et al.* (2007) ‘Ocular Gene Transfer with Self-Complementary AAV Vectors’, *Investigative Ophthalmology & Visual Science*, 48(7), p. 3324. doi: 10.1167/iovs.06-1306.

Yoshimura, A. *et al.* (2006) ‘Myosin-Va Facilitates the Accumulation of mRNA/Protein Complex in Dendritic Spines’, *Current Biology*, 16(23), pp. 2345–2351. doi:

10.1016/j.cub.2006.10.024.

Yoshino, H. and Kimura, A. (2006) 'Investigation of the therapeutic effects of edaravone, a free radical scavenger, on amyotrophic lateral sclerosis (Phase II study)', *Amyotrophic Lateral Sclerosis*, 7(4), pp. 247–251. doi: 10.1080/17482960600881870.

van der Zee, J. *et al.* (2013) 'A pan-European study of the C9orf72 repeat associated with FTLD: geographic prevalence, genomic instability, and intermediate repeats.', *Human Mutation*. Wiley-Blackwell, 34(2), pp. 363–73. doi: 10.1002/humu.22244.

Zhang, K. *et al.* (2015) 'The C9orf72 repeat expansion disrupts nucleocytoplasmic transport', *Nature*, 525(7567), pp. 56–61. doi: 10.1038/nature14973.

Zhang, Z. and Krainer, A. R. (2004) 'Involvement of SR Proteins in mRNA Surveillance', *Molecular Cell*. Cell Press, 16(4), pp. 597–607. doi: 10.1016/J.MOLCEL.2004.10.031.

Zheng, C. and Baum, B. J. (2008) 'Evaluation of Promoters for Use in Tissue-Specific Gene Delivery', in *Gene Therapy Protocols*. Totowa, NJ: Humana Press, pp. 205–219. doi: 10.1007/978-1-60327-248-3\_13.

Zou, Z.-Y. *et al.* (2017) 'Genetic epidemiology of amyotrophic lateral sclerosis: a systematic review and meta-analysis', *J Neurol Neurosurg Psychiatry* ., 88(7), pp. 540–549. doi: 10.1136/jnnp-2016-315018.

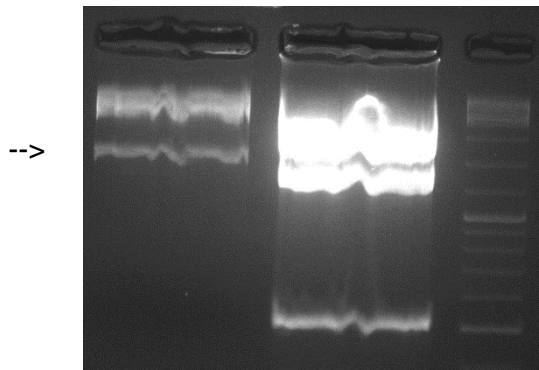
Zu, T. *et al.* (2013) 'RAN proteins and RNA foci from antisense transcripts in C9ORF72 ALS and frontotemporal dementia', *Proceedings of the National Academy of Sciences*, 110(51), pp. E4968–E4977. doi: 10.1073/pnas.1315438110.

Zufferey, R. *et al.* (1997) 'Multiply attenuated lentiviral vector achieves efficient gene delivery in vivo', *Nature Biotechnology*, 15(9), pp. 871–875. doi: 10.1038/nbt0997-871.

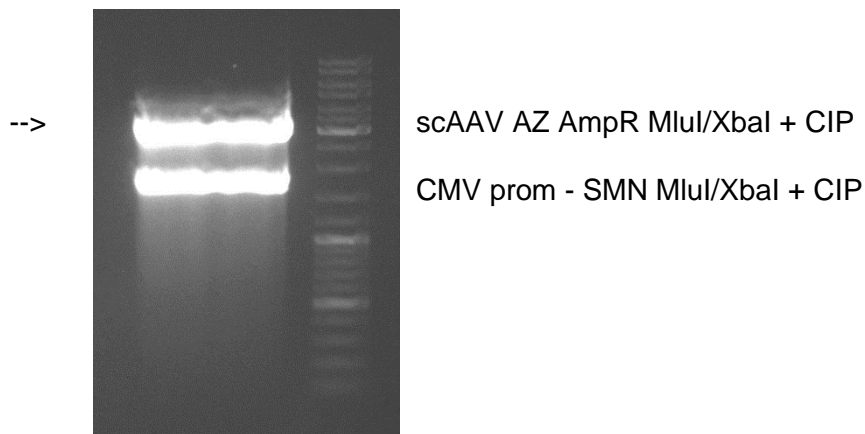
## Appendix - Cloning Strategies

### 1. Cloning Strategy of scAAV AZ AmpR / CBh prom - GFP

**1.1.** Insert preparation: CBh prom - GFP MluI/XbaI was restricted from pAAV AZ AmpR / CBh prom - GFP and extracted from a 1.5% agarose gel



**1.2.** Vector preparation: the plasmid scAAV AZ AmpR / CMV prom - SMN was digested with MluI/XbaI and treated with CIP and the restricted vector band corresponding to scAAV AZ AmpR MluI/XbaI + CIP was extracted from a 1% agarose gel



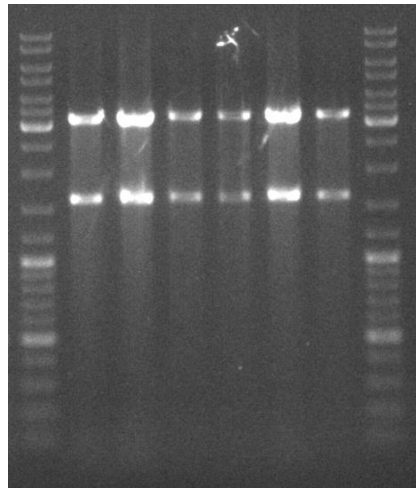
**1.3.** CBh prom - GFP MluI/XbaI was ligated into scAAV AZ AmpR MluI/XbaI + CIP to generate scAAV AZ AmpR / CBh prom - GFP

MluI / XbaI digest was run on 1% agarose gel to check for cloning of CBh prom - GFP insert

Expected sizes:  
3217 bp + 1603 bp

3217bp

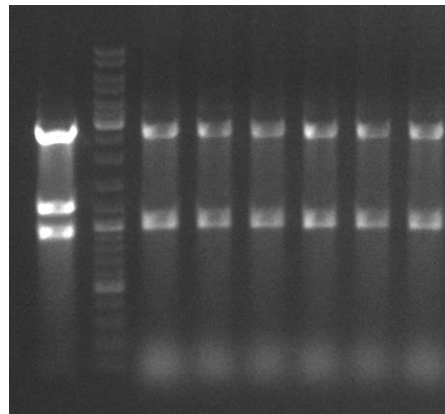
1603bp



SmaI digest was then run to test for integrity of ITRs

Expected sizes:  
2724bp + 1000bp + 997bp  
+77bp + 11bp + 11bp

Left Column  
scAAV / CMV prom - SMN  
One extra insert as it  
contains an extra SmaI site  
in CMV promoter



2724bp

1000+997bp

Clone 1 was selected for a midi-prep

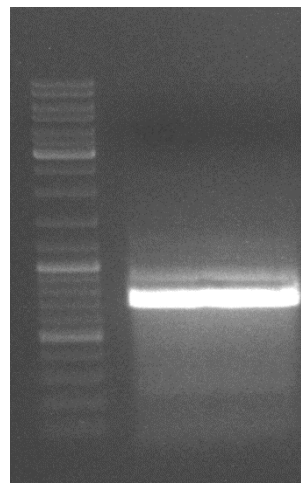
## 2. Cloning of scAAV AZ AmpR / CBh prom - 3x FLAG SRSF1 11-196 m4

SRSF1 m4 mutation locations: R90, 93, 117,118A

CBh promoter cannot be efficiently amplified by PCR as it contains a pure GC rich region. Subcloning is therefore needed as previously described for scAAV - CBh GFP

### 2.1. Cloning of pAAV AZ AmpR / CBh prom - 3xFLAG SRSF1 11-196 m4

**2.1.1.** Insert preparation: Accuzyme PCR to amplify 3x FLAG SRSF1 11-196 m4 from p3X-FLAG / SRSF1 11-196 m4 using primers with 5' EcoRI and 3' XbaI sites. Run a 1.5% agarose gel and gel extract.



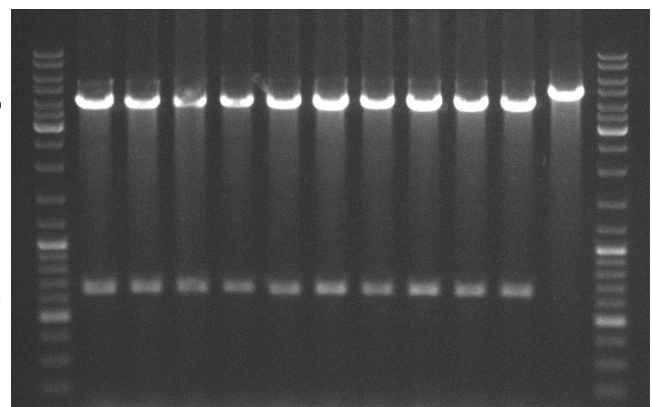
**2.1.2.** Vector preparation: Digest pAAV AZ AmpR CBh prom by EcoRI and XbaI + CIP. Phenol precipitate and resuspend dried pellet.

**2.1.3.** 3xFLAG SRSF1 11-196 m4 EcoRI/XbaI ligated into pAAV AZ AmpR CBh prom EcoRI/XbaI + CIP to obtain pAAV AZ AmpR / CBh prom - 3xFLAG SRSF1 11-196 m4. EcoRI/XbaI digest run on 1% agarose gel

Expected sizes:  
4278bp + 672 bp

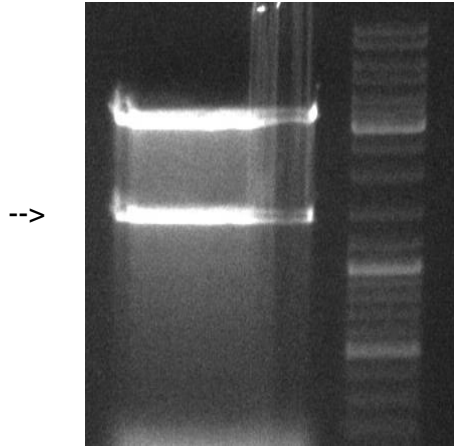
4278bp

672bp



## 2.2. Cloning of scAAV AZ AmpR / CBh prom - SRSF1 11-196 m4

2.2.1. Insert preparation: CBh prom - 3x FLAG SRSF1 11-196 m4 fragment was digested from pAAV AZ AmpR / CBh prom - 3xFLAG SRSF1 11-196 m4 using MluI and XbaI and extracted from a 1% preparative agarose gel.



2.2.2. Vector prep: use scAAV AZ AmpR MluI/XbaI + CIP prepared above in 1.2.

2.2.3. CBh prom - 3x FLAG SRSF1 11-196 m4 MluI/XbaI ligated into scAAV AZ AmpR MluI/XbaI+CIP to obtain scAAV AZ AmpR / CBh prom - 3x FLAG SRSF1 11-196 m4

MluI / XbaI digest run on 1% agarose gel to check for cloning of CBh prom - 3x FLAG SRSF1 11-196 m4 insert

Expected sizes:

3217bp + 1493bp

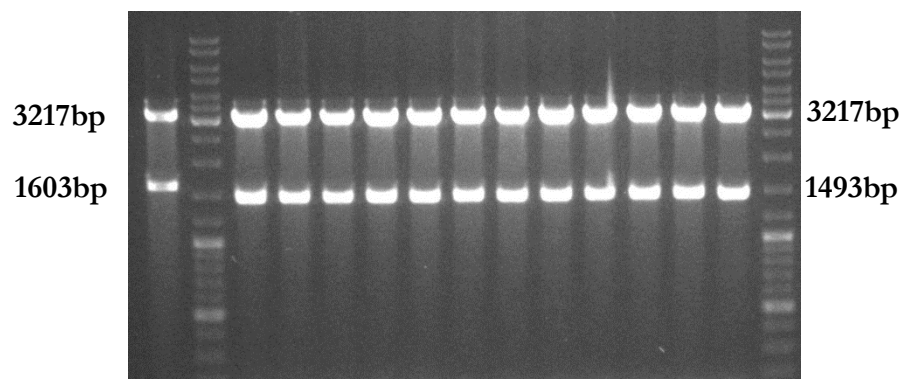
All clones are correct

Left column is a control

scAAV / CBh prom - GFP

Expected sizes:

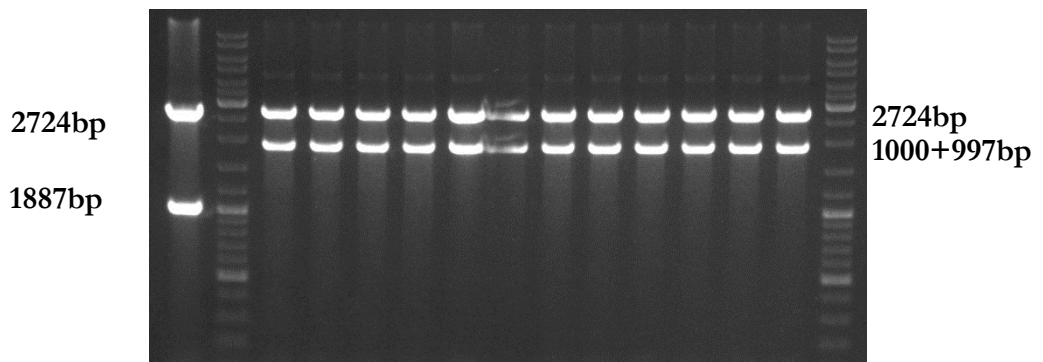
3217 bp + 1603 bp



An SmaI digest was run to test the integrity of the ITRs.

Expected sizes:  
2724bp + 1887bp  
+ 77bp + 11bp + 11bp

Left line is control  
scAAV / CBh prom - GFP  
2724bp + 1000bp + 997bp  
+77bp + 11bp + 11bp



scAAV AZ AmpR / CBh prom - 3x FLAG SRSF1 11-196 m4 clone 1 was selected for a midiprep and checked using an MluI /XbaI digest and an SmaI digest and was deemed correct with bands of expected size as below.

